Vol. 282, No. 2, October 20, 1993 ISSN 0003-2670

INCLUDING PAPERS PRESENTED
IN HONOUR OF PROFESSOR ERNÖ PUNGOR

ANALYTICA CHIMICA ACTA

An international journal devoted to all branches of analytical chemistry

ELSEVIER

ANALYTICA CHIMICA ACTA

Scope. *Analytica Chimica Acta* publishes original papers, preliminary communications and reviews dealing with every aspect of modern analytical chemistry. Reviews are normally written by invitation of the editors, who welcome suggestions for subjects. Preliminary communications of important urgent work can be printed within four months of submission, if the authors are prepared to forego proofs.

Submission of Papers

Americas

Prof. Harry L. Pardue
Department of Chemistry
1393 BRWN Bldg, Purdue University
West Lafayette, IN 47907-1393
USA

Tel:(+1-317) 494 5320
Fax:(+1-317) 496 1200

Computer Techniques

Prof. J.T. Clerc
Universität Bern
Pharmazeutisches Institut
Baltzerstrasse 5, CH-3012 Bern
Switzerland

Tel:(+41-31) 654171
Fax:(+41-31) 654198

Prof. Sarah C. Rutan
Department of Chemistry
Virginia Commonwealth University
P.O. Box 2006
Richmond, VA 23284-2006
USA
Tel:(+1-804) 367 1298
Fax:(+1-804) 367 8599

Other Papers

Prof. Alan Townshend
Department of Chemistry
The University
Hull HU6 7RX
Great Britain

Tel:(+44-482) 465027
Fax:(+44-482) 466410

Prof. Willem E. van der Linden
Laboratory for Chemical Analysis
Department of Chemical Technology
Twente University of Technology
P.O. Box 217, 7500 AE Enschede
The Netherlands
Tel:(+31-53) 892629
Fax:(+31-53) 356024

Prof. Paul Worsfold
Dept. of Environmental Sciences
University of Plymouth
Plymouth PL4 8AA
Great Britain

Tel:(+44-752) 233006
Fax:(+44-752) 233009

Submission of an article is understood to imply that the article is original and unpublished and is not being considered for publication elsewhere. *Anal. Chim. Acta* accepts papers in English only. There are no page charges. Manuscripts should conform in layout and style to the papers published in this issue. See inside back cover for "Information for Authors".

Publication. *Analytica Chimica Acta* appears in 16 volumes in 1994 (Vols. 281–296). *Vibrational Spectroscopy* appears in 2 volumes in 1994 (Vols. 6 and 7). Subscriptions are accepted on a prepaid basis only, unless different terms have been previously agreed upon. It is possible to order a combined subscription (*Anal. Chim. Acta* **and** *Vib. Spectrosc.*).
Our p.p.h. (postage, packing and handling) charge includes surface delivery of all issues, except to subscribers in the U.S.A., Canada, Australia, New Zealand, China, India, Israel, South Africa, Malaysia, Thailand, Singapore, South Korea, Taiwan, Pakistan, Hong Kong, Brazil, Argentina and Mexico, who receive all issues by air delivery (S.A.L.–Surface Air Lifted) at no extra cost. For Japan, air delivery requires 25% additional charge of the normal postage and handling charge; for all other countries airmail and S.A.L. charges are available upon request.

Subscription orders. Subscription prices are available upon request from the publisher. Subscription orders can be entered only by calendar year and should be sent to: Elsevier Science Publishers B.V., Journals Department, P.O. Box 211, 1000 AE Amsterdam, The Netherlands. Tel: (+31-20) 5803 642, Telex: 18582, Telefax: (+31-20) 5803598, to which requests for sample copies can also be sent. Claims for issues not received should be made within six months of publication of the issues. If not they cannot be honoured free of charge. Readers in the U.S.A. and Canada can contact the following address: Elsevier Science Publishing Co. Inc., Journal Information Center, 655 Avenue of the Americas, New York, NY 10010, U.S.A. Tel: (+1-212) 6333750, Telefax: (+1-212) 6333990, for further information, or a free sample copy of this or any other Elsevier Science Publishers journal.
Advertisements. Advertisement rates are available from the publisher on request.

US mailing notice – Analytica Chimica Acta (ISSN 0003-2670) is published biweekly by Elsevier Science Publishers (Molenwerf 1, Postbus 211, 1000 AE Amsterdam). Annual subscription price in the USA US$ 3035.75 (subject to change), including air speed delivery. Second class postage paid at Jamaica, NY 11431. *USA Postmasters*: Send address changes to Anal. Chim. Acta, Publications Expediting, Inc., 200 Meacham Av., Elmont, NY 11003. Airfreight and mailing in the USA by Publication Expediting.

ANALYTICA CHIMICA ACTA

An international journal devoted to all branches of analytical chemistry

(Full texts are incorporated in CJELSEVIER, a file in the Chemical Journals Online database available on STN International; Abstracted, indexed in: Aluminum Abstracts; Anal. Abstr.; Biol. Abstr.; BIOSIS; Chem. Abstr.; Curr. Contents Phys. Chem. Earth Sci.; Engineered Materials Abstracts; Excerpta Medica; Index Med.; Life Sci.; Mass Spectrom. Bull.; Material Business Alerts; Metals Abstracts; Sci. Citation Index)

VOL. 282 NO. 2 CONTENTS OCTOBER 20, 1993

Papers honouring Professor Ernö Pungor

Laudatio
(by Dr. H. Malissa) 227

Enzymatic biosensor for urea based on an ammonium ion-selective bulk optode membrane
C. Stamm, K. Seiler and W. Simon (Zürich, Switzerland) 229
Investigation of silver iodide-based ion-selective membranes by scanning electrochemical microscopy
K. Tóth, G. Nagy (Budapest, Hungary), B.R. Horrocks and A.J. Bard (Austin, TX, USA) 239
Cation permselectivity in the phase boundary of ionophore-incorporated solvent polymeric membranes as studied by Fourier transform infrared attenuated total reflection spectrometry
K. Umezawa (Tokyo, Japan), X.M. Lin (Sapporo, Japan), S. Nishizawa, M. Sugawara and Y. Umezawa (Tokyo, Japan) 247
Selectivity of plasticized poly(vinyl chloride)-based ion-selective electrodes
V. Horváth and G. Horvai (Budapest, Hungary) 259
Detection limit of ion-selective bulk optodes and corresponding electrodes
E. Bakker, M. Willer and E. Pretsch (Zürich, Switzerland) 265
Anion effects on Donnan failure of aminated-poly(vinyl chloride)-based and neutral-carrier-based pH sensors
R.P. Buck, V.V. Cosofret and E. Lindner (Chapel Hill, NC, USA) 273
Prediction of the equilibrium value of a potentiometric signal. Application of the measuring technique to molecule-sensitive sensors
J. Havas, L. Kecskés and E. Rohonczy-Boksay (Budapest, Hungary) 283
Electrochemical oxidation of lysergic acid-type ergot alkaloids in acetonitrile. Part 1. Stoichiometry of the anodic oxidation electrode reaction
T. Dankházi, É. Fekete, K. Paál and G. Farsang (Budapest, Hungary) 289
Liposome immunomigration field assay device for Alachlor determination
S.T.A. Siebert, S.G. Reeves and R.A. Durst (Geneva, NY, USA) 297
Flow-injection study of inhibition and reactivation of immobilized acetylcholinesterase: determination of the pesticides paraoxon and carbamoylcholine
I.A. Takruni, A.M. Almuaibed and A. Townshend (Hull, UK) 307
Determination of the degree of substitution of hydroxypropylated β-cyclodextrins by differential scanning calorimetry
Cs. Novák, G. Pokol, J. Sztatisz, L. Szente and J. Szejtli (Budapest, Hungary) 313

Regular Papers

Electroanalytical Chemistry and Sensors
Bioelectrocatalysis of a water-soluble tetrathiafulvalene–2-hydroxypropyl-β-cyclodextrin complex
S. Zhao and J.H.T. Luong (Montreal, Canada) 319
Adsorptive stripping voltammetry of trace thallium
J. Wang and J. Lu (Las Cruces, NM, USA) 329
Chemically and mechanically resistant carbon dioxide optrode based on a covalently immobilized pH indicator
B.H. Weigl, A. Holobar, N.V. Rodriguez and O.S. Wolfbeis (Graz, Austria) 335
Potentiometric phosphate selective electrode based on a multidendate–tin(IV) carrier
N.A. Chaniotakis (Irakleon, Greece), K. Jurkschat and A. Rühlemann (Halle/S., Germany) 345

(Continued overleaf)

Contents (continued)

Enzymatic Techniques

A mediated amperometric enzyme electrode using tetrathiafulvalene and L-glutamate oxidase for the determination of L-glutamic acid
N.F. Almeida and A.K. Mulchandani (Riverside, CA, USA) 353

Enzyme-based chemically amplified flow-injection determination of catechol and catecholamines using an immobilized tyrosinase reactor and L-ascorbic acid
Y. Hasebe, K. Takamori and S. Uchiyama (Saitama, Japan) 363

Flow Analysis

Enhanced selectivity in flow-injection analysis for L-amino acids using electrodialysis with amino acid oxidation
J.C. Cooper, J. Danzer and H.-L. Schmidt (Freising-Weihenstephan, Germany) 369

Dual flow-injection analysis system for determining bromide and reactive phosphorus in natural waters
P.R. Freeman, B.T. Hart and I.D. McKelvie (Caulfield East, Australia) 379

Flow system based on sequential delivery of air-sandwiched solutions into a micro cell for spectrophotometric catalytic analysis
S. Kawakubo, M. Iwatsuki and T. Fukasawa (Kofu-shi, Japan) 389

Volumetric triangle-programmed flow titrations based on precisely generated concentration gradients
B. Fuhrmann and U. Spohn (Halle, Germany) 397

Chemometrics

Neural networks for interpretation of infrared spectra using extremely reduced spectral data
M. Meyer, K. Meyer and H. Hobert (Jena, Germany) 407

Hypertext tools for the selection of dissolution methods prior to the atomic absorption analysis of pharmaca
W. Penninckx, J. Smeyers-Verbeke, D.L. Massart (Brussels, Belgium), L.G.C.W. Spanjers and F.A. Maris (Oss, Netherlands) 417

Optimization by mathematical procedures of two dynamic headspace techniques for quantifying virgin olive oil volatiles
M.T. Morales and R. Aparicio (Seville, Spain) 423

Environmental Analysis

Use of hydrogen in electrothermal atomic absorption spectrometry to decrease the background signal arising from environmental slurry samples
L. Ebdon, A.S. Fisher and S.J. Hill (Plymouth, UK) 433

Determination of trace metal ions in water samples by on-line preconcentration and inductively coupled plasma mass spectrometry
H.-J. Yang, K.-S. Huang, S.-J. Jiang, C.-C. Wu and C.-H. Chou (Kaohsiung, Taiwan) 437

Determination of morestan residues in waters by solid-phase spectrofluorimetry
J.L. Vilchez, R. Avidad, J. Rohand, A. Navalón and L.F. Capitán-Vallvey (Granada, Spain) 445

Gas Chromatography

Solvent venting technique for gas chromatography with microwave-induced plasma atomic emission spectroscopy
M.E. Birch (Cincinnati, OH, USA) 451

PAPERS PRESENTED IN HONOUR OF PROFESSOR ERNŐ PUNGOR

Analytica Chimica Acta, 282 (1993) 227–228
Elsevier Science Publishers B.V., Amsterdam

Laudatio for Dr. Dr. h.c.(mult.) Ernő Pungor

Ernő Pungor was born on 30th October 1923 in Vasszécsény, near Savaria (Szombathely = Steinamanger), the old Roman capital of Pannonia, in a country where every single place is breathing ancient culture and civilization, but at a time when the shadows of the lost World War I darkened daily life.

His childhood was governed by the love of his family and the fruitfulness and the beauty of the wide Hungarian plains decorated with famous old churches, palaces and castles. So, no wonder that the excellent primary education of young Ernő in a convent school raised him to become an outstanding young man with a broad humanistic background, coupled with all the realism needed to withstand the dangers of military service during World War II and the times thereafter.

In 1948 he graduated in chemistry from the Pázmány Péter University in Budapest to become, after obtaining a PhD in 1949, Assistant Professor at the Institute for Inorganic and Analytical Chemistry (under Elemér Schulek). Here he started his analytical career with the first paper on dyestuffs: "Experimental data on the theory of adsorption indicators" (1949). In addition to research in titrimetric chemical analysis, he started work on flame photometry and gas analysis. Looking at the some 30 papers produced in that period with different co-authors we can well imagine Ernő Pungor's eagerness and devotion to do research work in analytical chemistry. Until 1962 he remained in Budapest, being promoted by the Hungarian Academy of Sciences to Candidate of Chemical Science (1952), DSc (1956), corresponding member (1967) and finally to full member in 1976.

His autonomous work started in 1962 as Professor and Director of the Department of Analytical Chemistry at the University for Chemical Industries at Veszprém, where he remained until 1970. In this most fruitful period he not only continued the work on titrimetric analysis but also built up a school of analytical chemists that rapidly gained international recognition. Even in the period when the establishment of joint ventures with Western universities was difficult, Pungor managed to achieve close cooperation with the Technical University of Vienna (1962), the University of Birmingham (1964), ETH Zürich (1968) and many others.

In 1970 he was offered the Chair at the Insitute for General and Analytical Chemistry at the Technical University of Budapest (as successor to the late László Erdey), which he held for 20 years until 1990, when he became President of the Hungarian National Committee for Technical Development and Minister without Portfolio.

We now see in Ernő Pungor who greatly broadened his research base, especially to include ion selective electrodes, flow-injection methods

and automation, the promoter of analytical chemistry with special attention to the education of analysts. He described his research philosophy (1983) in an interesting paper: "How did research into ion-selective electrodes came into being?" In giving full credit to his forerunners and coworkers, he ended:"... the individual cannot emancipate himself from his earlier experiences since these would exert an effect upon him even in topics which are seemingly far from the original one. But this is perfectly right. Perhaps therefore it is unfavourable if the researcher works and acquires experience in a very narrow field because in this case for the solution of the problem he would be able to consider the question only in a narrow horizon." How true!

In 1975 Pungor was the chairman of Euroanalysis II, held in Budapest and showing the great interest of European analytical chemists in collaboration. During his chairmanship of the WPAC/FECS, a very specific task was started, namely assessing the situation of teaching analytical chemistry in 130 universities, demonstrating the need for separate Chairs for analytical chemistry and establishing a unified basic curriculum to be used in respect of the ongoing European unification and for the sake of mobility of students.

Not only have some 350 scientific papers and 15 books made him famous around the world, but his outstanding and friendly personality has made him one of the most popular leaders in the international analytical community. He was president of the Association of Editors of European Chemical Journals in 1977, a member of the International Federation of the Scientific Editors Association in 1981, Chairman of the Working Party on Analytical Chemistry of FECS from 1981 to 1987, a member of IUPAC from 1977 to 1987, of its Analytical Chemistry Division Committee from 1977 to 1981 and of its Electroanalytical Committee from 1981 to 1987, Chairman of the Analytical Division of the Hungarian Chemical Society and Head of the Analytical Group of the Hungarian Academy of Sciences since 1970, and a member of many Hungarian scientific committees.

Many scientific awards have been made to him, including honorary member of the Chemical Section of the Czechoslovak Academy of Sciences in 1968, honorary Doctor (Dr.techn.h.c.) of the Technical University of Vienna, 1983, and of the Technical University of Bratislava, 1985, honorary member of the Egyptian Pharmaceutical Society in 1973, of the Austrian Analytical and Microanalytical Society in 1977, of the Chemical Society of Finland in 1979, of the Analytical Chemical Society Japan in 1981, and of the Technical Society of Finland in 1990; Honorary Professor at the Árpád Academy, Honorary Professor of the Agricultural University of Lima, Peru, in 1973, recipient of the Robert Boyle Gold Medal of the Royal Society of Chemistry in 1986, recipient of the Talanta Gold Medal in 1987, Gold Medal of the Hungarian Academy of the Sciences in 1988 and Gold Medal of the Institute of Analytical Chemistry of the Technical University of Vienna in 1988.

Every one of his huge number of friends and colleagues is fascinated by his intellect and charm and also by his classical–humanistic education and reliability – and *amicus certus in re incerta cernitur*. And so we wish him from all our hearts: *ad multos annos*

H. Malissa, sen.

Analytica Chimica Acta, 282 (1993) 229–237
Elsevier Science Publishers B.V., Amsterdam

Enzymatic biosensor for urea based on an ammonium ion-selective bulk optode membrane

Christine Stamm, Kurt Seiler and Wilhelm Simon [1]

Department of Organic Chemistry, Swiss Federal Institute of Technology (ETH), Universitätstr. 16, CH-8092 Zürich (Switzerland)

(Received 6th May 1993)

Abstract

A urea biosensor with the enzyme urease entrapped in a photo-cross-linked polymer is described. The enzyme layer is placed on top of an NH_4^+-selective optode membrane incorporating the ionophore nonactin and a hydrogen ion-selective chromoionophore. The immobilization was carried out under very mild conditions, so that the properties of the optode membrane remained unchanged. The short-term repeatability, dynamic response, selectivity and the long-term stability of the sensor and the influence of the buffer concentration are discussed.

Keywords: Biosensors; Enzymatic methods; Ion-selective electrodes; Ammonium; Enzyme electrodes; Membrane electrodes; Urea

Over the years there has been a steady growth in the use of enzymes as selective and sensitive biotransducers and despite their inherent instability there is a wide field of possible applications [1]. Among the enzymes that have been used in analytical systems, urease is one of the best known, and it has been extensively studied [2–4]. Being a model enzyme for a great variety of new immobilization techniques, it has been combined with many different types of transducing elements. Very often, the enzymatically generated products have been detected with ion-selective sensors for NH_4^+ [5,6] or pH [7,8], or with gas-sensing devices for NH_3 [9–14] or CO_2 [15].

In addition to potentiometric transduction [7,9,12–15] there has been an ever increasing number of attempts to construct sensors with optical transduction. Among other advantages, they can be combined with modern waveguide technology, which opens up the possibilities of miniaturization and of remote sensing. They are free from electrical interference and optical detection is highly compatible with the instrumentation in clinical laboratories. Optical biosensors for several species and applications have been presented, including sensors for glucose [16], cholesterol [17] and ethanol [18].

A promising approach has been used for the immobilization of urease on a fibre-optic sensor, based on the measurement of microenvironmental pH changes [8]. Another fibre-optic urea sensor, based on NH_3 detection, has been presented [11] but lacks sufficient long term stability. Fluorescence biosensors for the detection of urea and for the determination of urease activity have been described recently [19,20].

A wide variety of reversible bulk optodes for cations, anions, neutral species and gases have been developed [21,22]. Recently, many specially designed carriers that bind neutral species based on a molecular recognition process have been

Correspondence to: C. Stamm, Department of Organic Chemistry, Swiss Federal Institute of Technology (ETH), Universitätstr. 16, CH-8092 Zürich (Switzerland).

[1] Deceased on 17th November, 1992.

used as selective components in optical sensors [23–25]. Another approach involves the use of enzymes that are highly specific for certain uncharged species and the subsequent detection of the generated products by an optode, which opens up the possibility of detecting a great variety of neutral species with only a limited number of carriers.

It has been recognized that appropriate immobilization of enzymes will not only allow their repeated use but also often increases their stability [1,26]. Although most enzymatic urea sensors have been constructed by entrapping urease in different gels [5,27], covalent attachment [14,28] and cross-linking [11,13,29] have also been described. Unfortunately, many of these methods include chemicals that are liable to inactivate the biocatalyst. In contrast, Fukui et al. [30] have reported on photo-cross-linkable prepolymers that allow the entrapment of enzymes under very mild conditions. These prepolymers have been used for the immobilization of a great variety of enzymes, microbial cells and organelles [31–33].

The aim of this work was to demonstrate that plasticized poly(vinyl chloride) membranes, incorporating ion-selective carriers and hydrogen ion-selective chromoionophores, can be used for the design of enzyme-based optical sensors. For this purpose an ion-selective optode with nonactin as carrier was chosen, and it could be shown that bulk optodes are well suited for the construction of biosensors. Special attention was paid to the immobilization method so that the enzyme activity was not affected and the function of the optode membrane was not disturbed. The hydrophilic photo-cross-linkable prepolymers described by Fukui et al. [30] were found to fulfil both requirements.

EXPERIMENTAL

Reagents

All salts and the starter for the polymerization, benzoin ethyl ether, were of highest purity available (Fluka, Buchs, Switzerland). For the preparation of optode membranes, poly(vinyl chloride) (PVC; high molecular weight), nonactin, sodium tetrakis[3,5-bis(trifluoromethyl)phenyl]borate [$NaTm(CF_3)_2PB$], 2-nitrophenyl octyl ether (o-NPOE) and tetrahydrofuran (THF) were used (Fluka). The synthesis of the chromoionophore *N*,*N*-(diethyl)-5-[(2-octyldecyl)imino]-5*H*-benzo-[*a*]phenoxazin-9-amine (ETH 5350) was described previously [34]. The enzyme urease (urea aminohydrolase, EC 3.5.1.5, from jack beans, Type IX, 61 000 U g^{-1}) was used (Sigma). The photo-cross-linkable prepolymer ENT-4000 for the preparation of the enzyme layer was kindly supplied by Takuo Kawamoto of Department of Industrial Chemistry, Kyoto University.

Apparatus

UV–visible absorption measurements were carried out with a Uvikon Model 810 double-beam spectrophotometer (Kontron, Zürich). For flow-through measurements, a Perista Minipump Model SJ-1211 (Atto, Tokyo) and silicon tubes of 1 mm i.d. (Sikolit; Angst & Pfister, Zürich) were used. The pH values were measured with a Ross Model 8103 glass electrode (Orion Research, Ütikon am See, Switzerland). For UV irradiation of the photo-cross-linkable prepolymers a Camag UV lamp (Camag, Muttenz, Switzerland) was used. An Olympus BH-2 microscope (Olympus Optical, Volketswil, Switzerland) was used to determine the thickness of the enzyme layer.

Standard solutions and buffers

All aqueous solutions were prepared with doubly quartz-distilled water. Urea solutions were prepared daily, phosphate buffers monthly and all solutions were stored at room temperature. Sodium phosphate (NaH_2PO_4–NaOH) and magnesium acetate [$Mg(OAc)_2$–HOAc] buffers were prepared according to [35]. For details, see Result and Discussion.

Preparation of optode membranes

Membrane components were weighed and dissolved in 1 ml of freshly distilled tetrahydrofuran. The compositions of the membranes are given in Table 1. Using a spin-on device [36], two identical membranes of about 4 μm thickness were cast on glass plates.

TABLE 1

Compositions of the optode membranes

Component	Amount (mg)			
	I	II	III	IV
ETH 5350	0.9	1.1	1.1	1.1
Nonactin	1.3	1.5	1.3	1.2
$NaTm(CF_3)_2PB$	1.8	1.8	1.5	1.5
o-NPOE	168.9	164.0	168.9	168.4
PVC	82.0	81.9	86.7	82.0

Preparation of the enzyme layer

The photo-cross-linkable prepolymer ENT-4000 [main chain, poly(ethylene glycol), molecular weight ca. 4000] (0.5 g) and the starter benzoin ethyl ether (5 mg) were weighed and melted in a water-bath at 80°C [30]. Urease (40 mg) was dissolved in 0.3 ml of water. Of this enzyme solution, 0.2 ml was added to the molten polymer with subsequent stirring. The mixture was stored at 4°C (up to 1 month). For membrane preparation, the mixture was spread on a glass plate, covered with a polyethylene foil and irradiated at 366 nm for 3 min. Prior to use, the enzyme membrane was soaked in the phosphate buffer solution. After marking the membranes on the top and bottom, their thickness was obtained by focusing the two marks under a light microscope [37]. For the determination of the thickness of the wet enzyme layer, the swelling of the polymerized gel posed a problem, because it varied with the water content. The layer thickness was reproducible within the range ± 20 μm for wet membranes.

Procedures

The wet enzyme layer was placed on top of the optode membrane, fixed with O-rings and then two such enzyme optode membranes were mounted in a flow-through cell [36] with an inner volume of about 600 μl (Fig. 1). During experiments, the flow-rate was kept constant at about 2 ml/min with a peristaltic pump. For absorption measurements the cell was mounted in the spectrophotometer. No reference cell was used. All measurements were performed in the transmittance mode, at the wavelength of maximum absorption (655 nm) of the protonated form of the chromoionophore. The limiting absorbance values, A_{min} and A_{max}, were determined with dilute solutions of NaOH and HCl, respectively.

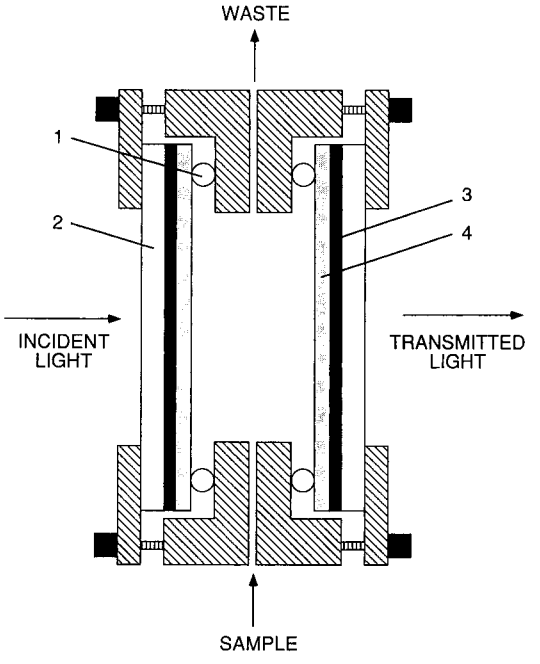

Fig. 1. Schematic diagram of the experimental set-up. 1 = O-ring; 2 = glass plate; 3 = optode membrane; 4 = enzyme layer.

Calculations

Activity coefficients were calculated according to the Debye–Hückel formalism with parameters given in [38].

The pH of a phosphate buffer solution after the hydrolysis of urea can be determined by calculating the pH of a solution with given concentrations of ammonium carbonate and buffer ions, as the dissolution of ammonium carbonate yields the same products as the hydrolysis of urea:

hydrolysis of urea:

$$CO(NH_2)_2 + 2H_2O + H^+ \xrightarrow{\text{urease}} 2NH_4^+ + HCO_3^- \quad (1)$$

dissolution of ammonium carbonate:

$$(NH_4^+)_2(CO_3^{2-}) + H^+ \longrightarrow 2NH_4^+ + HCO_3^- \quad (2)$$

A formalism described by Keller-Lehmann [39]

was used for the calculation. The given equations for the equilibria of a buffered solution of $NaHCO_3$ were modified for phosphate buffers and extended by an additional equilibrium for the deprotonation of NH_4^+. The pH values of the buffered ammonium carbonate solutions were calculated iteratively and the original buffer pH was used as the starting value.

The selectivity coefficients for sodium and potassium were determined by the separate solution method [40]. The constants of the respective single-ion response curves were fitted to the experimental data by changing the corresponding K_{exch} values.

THEORY

The urea optode consists of two layers (Fig. 2). The substrate urea diffuses into the hydrophilic enzyme layer where urease catalyses its hydrolysis. The NH_4^+ ions produced and the change in pH are sensed by the ion-selective optode membrane.

The description of the working principle of this type of optode membrane and its characterization has been given elsewhere in detail [21]. The membrane contains a neutral NH_4^+-selective ionophore L (nonactin) and a neutral H^+ ion-selective chromoionophore C (ETH 5350), forming the charged complexes LNH_4^+ and CH^+, respectively. The addition of the sodium salt of a lipophilic counter ion R^- [$NaTm(CF_3)_2PB$], defines the total concentration of the positively charged species in the membrane. The overall ion-exchange equilibrium constant is given by [21,41]

$$K_{exch}^{LNH_4^+} = \frac{a_{H^+}}{a_{NH_4^+}} \cdot \frac{[C]}{[CH^+]} \cdot \frac{[LNH_4^+]}{[L]} \qquad (3)$$

The activity symbols refer to species in the aqueous phase and brackets refer to components in the organic membrane phase (where activity coefficients are assumed to be constant). This optode membrane responds to the ratio of the H^+ activity to the NH_4^+ activity (or formally to NH_3 gas). The absorbance of the optode membrane is related to the degree of protonation of the chromoionophore, which is defined as $1-\alpha$, and thus α is the ratio of deprotonated to total chromoionophore concentration:

$$\alpha = \frac{C}{C_{tot}} = \frac{A_{prot} - A}{A_{prot} - A_{deprot}} \qquad (4)$$

where A_{prot} and A_{deprot} are the absorbance values when the chromoionophore is fully protonated and fully deprotonated, respectively, and A is the absorbance for a given equilibrium.

The following equation describes the response curve of an NH_4^+-selective optode if a singly charged interfering ion J^+ is present and if all relevant species form 1:1 complexes [40]:

$$a_{NH_4^+} + k_{NH_4^+,J^+}^{opt} \cdot a_{J^+} = \frac{a_{H^+}}{K_{exch}^{LNH_4^+}} \cdot f(\alpha) \qquad (5)$$

where the selectivity coefficient $k_{NH_4^+,J^+}^{opt}$ is expressed by the ratio of the two exchange constants for NH_4^+ and H^+ [40], and

$$f(\alpha) = \frac{\alpha}{1-\alpha} \frac{[R_{tot}^-] - (1-\alpha)[C_{tot}]}{[L_{tot}] - \{[R_{tot}^-] - (1-\alpha)[C_{tot}]\}}$$

The total concentrations of the respective species are described by L_{tot}, C_{tot} and R_{tot}^-. If log $a_{NH_4^+}$ is plotted versus the degree of protonation at constant pH, a sigmoid curve is obtained [21].

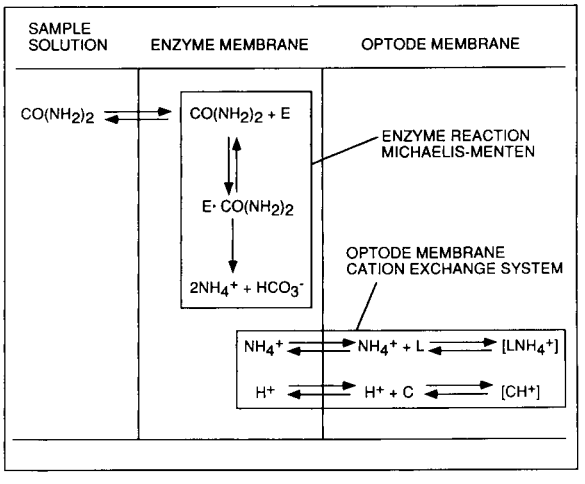

Fig. 2. Scheme of the enzyme optode consisting of the optode membrane and the enzyme layer directly attached to it. E = enzyme; L = ammonium ion-selective ionophore; C = hydrogen ion-selective chromoionophore.

Assuming that the whole system is perfectly pH buffered, the activity of the enzymatically produced NH_4^+ is proportional to the concentration of urea. With Eqn. 5, this leads to the following relationship:

$$[\text{urea}] \propto \frac{a_{H^+}}{K^{LNH_4^+}_{exch}} \cdot f(\alpha) - \left(k^{opt}_{NH_4^+,J} + a_{J^+}\right) \qquad (6)$$

However, if the solution is only weakly buffered, the pH will rise during substrate conversion. Consequently, the resulting degree of protonation of the chromoionophore is lower. Unfortunately, the final pH is not known but it can be iteratively calculated for a known buffer composition (see *Calculations*). The calculated pH value is inserted into Eqn. 6 and so the expected degree of protonation for a given urea concentration can be obtained as shown in Fig. 3. The calculation was carried out for 1×10^{-5} M–0.1 M urea solutions in phosphate buffers of four different concentrations. The lower the buffer capacity, the lower is the degree of protonation. The effect is small for low urea concentrations (10^{-5} M). The fact that the calculated degree of protonation of the highly buffered solutions at 10^{-5} M urea is lower than expected can be explained by the interference with sodium ions from the buffer. The largest difference between the buffers is seen for concentrations of about 10^{-3} M, because in this concentration range the pH changes drastically as the buffer capacity is insufficient. At high urea concentrations (0.1 M), a high pH value is calculated for all described buffers and therefore the resulting degrees of protonation are comparable. The influence of buffer concentration is confirmed by experimental data, as will be shown below (see Results and Discussion).

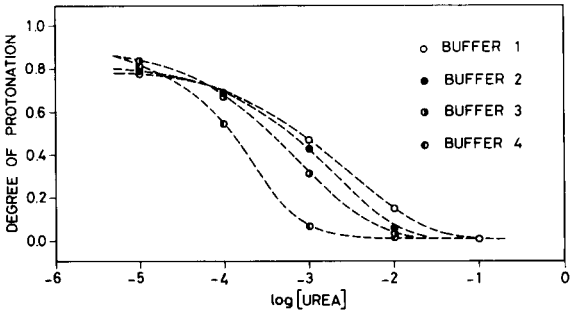

Fig. 3. Calculated response for five different urea concentrations in various buffer concentrations according to Eqn. 6. Each value was corrected with the calculated pH (see *Calculations*). (○) Buffer 1 = 0.029 M NaOH–0.05 M NaH_2PO_4; buffers (●) 2, (◑) 3 and (◐) 4 = 2-, 10- and 100-fold dilutions of buffer 1, respectively.

RESULTS AND DISCUSSION

Membrane composition and measuring range

The first cation-selective bulk optode [21] was selective for NH_4^+ and incorporated nonactin as ionophore and ETH 5294 as chromoionophore. It had a measuring range for NH_4^+ from 10^{-5} to 10^{-2} M at pH 7.35. For better solubility of nonactin, the plasticizer o-NPOE was chosen in this work and the chromoionophore ETH 5350 was used because of its higher molar absorptivity and basicity [37]. This optode (composition I, see Table 1) had a measuring range for NH_4^+ of about 10^{-4}–0.1 M at pH 7.0. The possibility of shifting the measuring range by using chromoionophores with different pK_a values is of great importance for the design of such an enzymatic sensor. It allows the sample pH to be adjusted to the value required by the enzyme.

Enzyme layer

For the construction of a biosensor, special attention has to be paid to the enzyme immobilization. First, the method has to be mild enough so that the biocatalyst is not deactivated. Second, the fragile optode membrane should not be affected and its function should not be hampered. The water-soluble prepolymer ENT-4000 of Fukui et al. [30] fulfils both requirements.

The thickness of the enzyme layers was measured with a light microscope and ranged from 30 to 40 μm for dry membranes and from 60 to 100 μm for wet membranes.

Absorption spectra

For urea measurements, an enzyme optode with composition I was used. Phosphate buffers of pH 7.0 were chosen to ensure favourable conditions for the function of the enzyme [2]. Figure

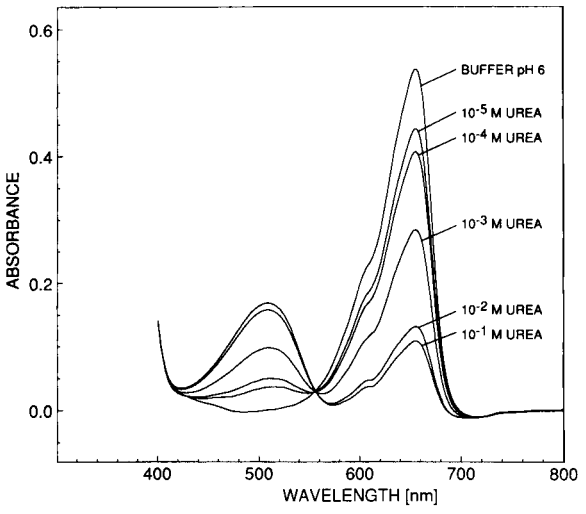

Fig. 4. Absorption spectra of an enzyme optode with composition I. Measurements with 1×10^{-5}–0.1 M urea solutions in phosphate buffer of pH 7.0 (0.029 M NaOH–0.05 M NaH_2PO_4) were performed, going from diluted to concentrated solutions. A phosphate buffer of pH 6.0 (0.028 M NaOH–0.025 M NaH_2PO_4) was used. The spectra were recorded after the steady state had been reached.

4 shows the absorption spectra of such an enzyme optode when exposed to different urea solutions.

Selectivity

Selectivities towards the singly charged cations sodium and potassium were determined for an optode membrane (composition IV) with and without the enzyme layer. It was shown that the addition of the enzyme layer did not adversely affect the selectivity behaviour.

The determined selectivity coefficients agree well with the corresponding values published earlier [21] and with the potentiometric selectivity coefficients of ion-selective electrodes based on nonactin [42] (see Table 2). If the analyte and the interferent have the same charge, the selectivity coefficients for optodes and for electrodes are formally equal and can be compared directly [40].

To exclude interfering cations from the optode membrane, a small amount of fixed cationic sites [poly(ethylene glycol) prepolymers with quaternary ammonium groups] was added to the photocross-linkable prepolymer. Unfortunately, the membrane became turbid and the expected effect could not be observed, although it has been shown that the use of ionomer membranes can improve the selectivity [43].

TABLE 2

Selectivity coefficients of the enzyme optode for the interfering ions K^+ and Na^+, and comparison with an NH_4^+ optode [21] and corresponding potentiometric selectivity coefficients [42]

Interfering ion J^+	log $k^{opt}_{NH_4^+,J^+}$		Log $k^{pot}_{NH_4^+,J^+}$: NG_4^+ electrode [42]
	Enzyme optode [a] (this work)	NH_4^+ optode [21]	
K^+	−0.9	−1.2	−0.8
Na^+	−2.9	−2.7	−2.9

[a] Enzyme optode (composition IV); measurements of NH_4^+, K^+ and Na^+ in $Mg(OAc)_2$ buffer of pH 5.0 [0.007 M $Mg(OAc)_2$–0.0061 M HOAc].

Dynamic response

All measurements were made in the flow-through mode. The response time was considerably longer if the measurements were carried out in the batch mode, because a stable signal was established only after complete conversion of substrate. The response time ($t_{95\%}$) was 1–4 min for $0.1–1\times10^{-5}$ M urea solutions (see Fig. 5) and 3–6 min for recovery to buffer response. The response time varied with the analyte concentration, the buffer capacity and the thickness of the membrane. The $t_{95\%}$ times for NH_4^+ determinations with an optode membrane having an enzyme layer on top were about three times longer than those without an enzyme layer. The values for NH_4^+ and urea measurements (both with enzyme layer) were comparable. Hence the diffusion through the enzyme layer is assumed to be the rate-limiting step for the dynamic response, as shown in Table 3. The response time of this biosensor is longer than that for normal bulk optodes. Nevertheless the use of thinner enzyme layers would accelerate the response.

Short-term repeatability

For the determination of short-term repeatability, the enzyme optode (composition II) was

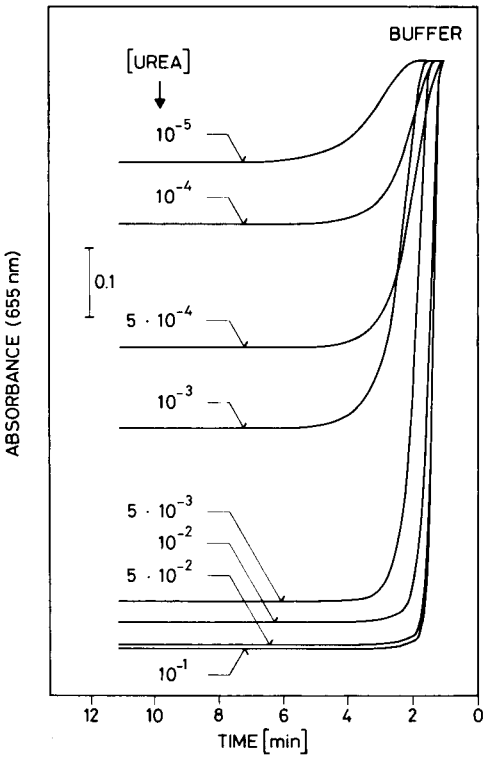

Fig. 5. Dynamic response of an enzyme optode with composition II is shown. Measurements with 1×10^{-5}–0.1 M urea solutions in phosphate buffer of pH 7.0 (0.029 M NaOH–0.05 M NaH_2PO_4) were made, going from diluted to concentrated solutions.

exposed four times to concentration changes between 1×10^{-3} and 5×10^{-3} M urea solutions in a phosphate buffer of pH 7.0 (0.05 M NaH_2PO_4–0.029 M NaOH). Between the concentration changes the membrane was placed in contact with phosphate buffer of pH 6.0 (0.025 M NaH_2PO_4–0.0028 M NaOH) in order to ensure complete and fast recovery of the signal. The mean absorbance values were 0.246 ± 0.005 and 0.068 ± 0.002, which corresponds to concentrations of $1 \times 10^{-3} \pm 5 \times 10^{-5}$ M and $5 \times 10^{-3} \pm 9 \times 10^{-5}$ M. From these values the short-term repeatability was calculated to be 5% and 3% for 1×10^{-3} and 5×10^{-3} M, respectively.

TABLE 3

Response times ($t_{95\%}$) for NH_4^+ measurements with and without enzyme layer and comparison with urea measurements

Concentration [M] [a]	$t_{95\%}$ (min)		
	Urea [b]	NH_4Cl [b]	NH_4Cl [c]
1×10^{-4}	7.0	7.0	2.0
1×10^{-3}	5.0	6.5	1.5
0.01	2.0	4.0	1.0
0.1	1.0	2.0	0.5

[a] Concentration step from the buffer to the respective solution. [b] Optode membrane with enzyme layer. [c] Optode membrane without enzyme layer.

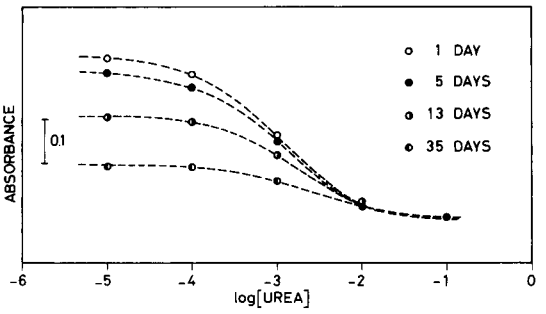

Fig. 6. For the evaluation of the long-term stability, an enzyme optode with composition I was measured (○) 1, (●) 5, (◑) 13 and (◐) 35 days after its preparation. Measurements with 1×10^{-5}–0.1 M urea solutions in phosphate buffer of pH 7.0 (0.029 M NaOH–0.05 M NaH_2PO_4) were made, going from diluted to concentrated solutions. The membrane was stored at room temperature in buffer solution.

Long term stability

The stability of an enzyme optode (composition I) was monitored 1, 5, 13 and 35 days after membrane preparation. In between it was stored at room temperature in buffer solution (drying out would cause crumbling and cracking of the enzyme layer). Figure 6 shows that after 1 month the sensitivity had decreased substantially. This effect was mainly caused by the loss of enzyme activity. As the steady-state response of the sensor is influenced by the enzyme activity, frequent calibration is required for long-term measurements. This disadvantage is inherent with all biocatalysts and is often the limiting factor in the lifetime of the sensor. Washing out of chromoionophore might have had some influence, as the measured absorbance had decreased slightly after 1 month [37].

Influence of buffer capacity

It has been stated above (see Theory, Fig. 3) that the buffer capacity influences the sensor signal. Thus urea solutions (1×10^{-5}–0.1 M) in four different buffers were measured in order to verify the predictions of the theory. Figure 7 shows that the shape of the curves indeed changed with the buffer concentration. For weakly buffered solutions the pH had risen drastically and therefore the degree of protonation was lower than in strongly buffered solutions. In the lower concentration range ($< 10^{-4}$ M) interference with sodium from the buffer observed. This explains the smaller degree of protonation at 1×10^{-5} M urea for the strongly buffered solutions. In Fig. 8 the experimental values are compared with those calculated according to Eqn. 6. When the pH was assumed to be constant, the calculated values deviated from the experimental values. However, good agreement was obtained when the estimated pH (see *Calculations*) was used for the calculation of the theoretical values (while all other parameters of Eqn. 6 remained unchanged). When analysing unknown urea samples, the pH could be evaluated iteratively, using Eqs. 6 and taking the buffer pH as the starting value. However, for practical purposes it would be more suitable to construct calibration graphs in the measurement range.

Conclusions

It has been shown that bulk optodes with incorporated ionophores are suitable for the construction of optical biosensors. The chosen immobilization method with hydrophilic photo-crosslinkable prepolymers is very suitable as it is very mild and does not destroy the optode membrane. Special attention has to be paid to the buffering of the system as the optode responds to the ratio of NH_4^+ and H^+ activities. Hence the need for control of the sample pH places certain limitations with respect to practical applications. The selectivity of the presented system is comparable to that of potentiometric systems that use nonactin as carrier.

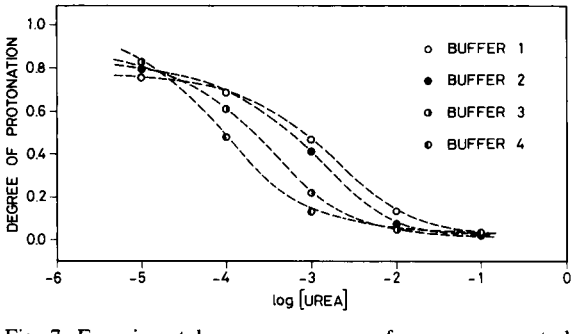

Fig. 7. Experimental response curves of an enzyme optode with composition III. Measurements of 1×10^{-5}–0.1 M urea solutions in four different buffers. (○) Buffer 1 = 0.029 M NaOH–0.05 M NaH_2PO_4; buffers (●) 2, (◑) 3 and (◐) 4 = 2-, 10- and 100-fold dilutions of buffer 1, respectively.

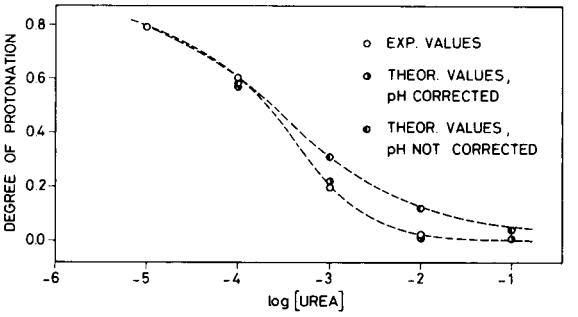

Fig. 8. Comparison between calculated and measured response of an enzyme optode with composition III. Experiments and calculations were made for urea solutions with a phosphate buffer of pH 7.0 (0.00291 M NaOH–0.005 M NaH_2PO_4). The parameters $k^{opt}_{NH_4^+,J^+}$ and $K^{LNH_4^+}_{exch}$ were fitted to the experimental values. ○ = Experimental values; ◑ = theoretical values, pH corrected; ◐ = theoretical values, pH not corrected.

This work was partly supported by the Swiss National Science Foundation. The authors thank Professor Ernö Pretsch for assistance with the manuscript. They also thank Professor Atsuo Tanaka and Dr. Takuo Kawamoto of the Department of Industrial Chemistry, Kyoto University, for supplying the prepolymers.

REFERENCES

1 M.M. Fishmann, Anal. Chem., 52 (1980) 185R.
2 J.B. Sumner and S.F. Howell, J. Biol. Chem., 104 (1934) 619.
3 K.J. Laidler and J.P. Hoare, J. Am. Chem. Soc., 71 (1949) 2699.
4 B.A. Lawton, Z.-H. Lu, R. Pethig and Y. Wei, J. Mol. Liq., 42 (1989) 83.

5 G.G. Guilbault and J.G. Montalvo, J. Am. Chem. Soc., 92 (1970) 2533.
6 G.G. Guilbault, G. Nagy and S.S. Kuan, Anal. Chim. Acta, 67 (1973) 195.
7 R. Koncki, P. Leszczynski, A. Hulanicki and S. Glab, Anal. Chim. Acta, 257 (1992) 67.
8 S. Luo and D.R. Walt, Anal. Chem., 61 (1989) 1069.
9 D.S. Papastathopoulos and G. A. Rechnitz, Anal. Chim. Acta, 79 (1975) 17.
10 G. Johansson and L. Ögren, Anal. Chim. Acta, 84 (1976) 23.
11 T.D. Rhines and M.A. Arnold, Anal. Chim. Acta, 227 (1989) 387.
12 L. Campanella, M.P. Sammartino and M. Tomassetti, Analyst, 115 (1990) 827.
13 G.G. Guilbault and M. Mascini, Anal. Chem. 49 (1977) 795.
14 G.H. Hsiue, Z.S. Chou, N. Yu and K.P. Hsiung, J. Appl. Polym. Sci., 34 (1987) 319.
15 G.G. Guilbault and F.R. Shu, Anal. Chem., 44 (1972) 2161.
16 M.C. Moreno-Bondi, O.S. Wolbeis, M.J.P. Leiner and B.P.H. Schaffar, Anal. Chem., 62 (1990) 2377.
17 A. Krug, A.A. Suleiman and G.G. Guilbault, Anal. Chim. Acta, 256 (1991) 263.
18 O.S. Wolfbeis and H.E. Posch, Fresenius' Z. Anal. Chem., 322 (1988) 255.
19 O.S. Wolfbeis and H. Li, Biosensors Bioelectron., (1993) in press.
20 O.S. Wolfbeis and H. Li, Anal. Chim. Acta, 276 (1993) 115.
21 K. Seiler, W.E. Morf, B. Rusterholz and W. Simon, Anal. Sci., 5 (1989) 557.
22 M. Lerchi, E. Bakker, B. Rusterholz and W. Simon, Anal. Chem., 64 (1992) 1534.
23 K. Seiler, K. Wang, M. Kuratli and W. Simon, Anal. Chim. Acta, 244 (1991) 151.
24 J.-P. Haug, Dissertation, ETH, Zürich, in preparation.
25 P. Bühlmann, M. Badertscher and W. Simon, Tetrahedron, 49 (1993) 595.
26 I. Chibata (Ed.), Immobilized Enzymes, Research and Development, Halstead, New York, 1978.
27 G.G. Guilbault and J. Das, Anal. Biochem., 33 (1970) 341.
28 H.H. Weetall and L.S. Hersh, Biochim. Biophys. Acta, 185 (1969) 464.
29 R. Hintsche, G. Neumann, I. Dransfield, G. Kampfrath, B. Hoffmann and F. Scheller, Anal. Lett., 22 (1989) 2175.
30 S. Fukui and A. Tanaka, Adv. Biochem. Eng. Biotechnol., 29 (1984) 1.
31 S. Fukui, K. Sonomoto, N. Itoh and A. Tanaka, Biochemie, 62 (1980) 381.
32 A. Tanaka, N. Hagi, S. Yasuhara and S. Fukui, J. Ferment, Technol., 56 (1978) 511.
33 A. Tanaka, S. Fukui, T. Iida and E. Hasegawa, FEBS Lett., 66 (1976) 179.
34 T. Rosatzin, P. Holy, K. Seiler, B. Rusterholz and W. Simon, Anal. Chem., 64 (1992) 2029.
35 D.D. Perrin and B. Dempsey, Buffers for pH and Metal Ion Control, Chapman and Hall, London, New York, 1974, pp. 135–139.
36 K. Seiler, Ionenselektive Optodenmembranen, Fluka, Buchs, 1991.
37 E. Bakker, M. Lerchi, T. Rosatzin, B. Rusterholz and W. Simon, Anal. Chim. Acta, (1993) in press.
38 P.C. Meier, Anal. Chim. Acta, 136 (1982) 363.
39 B. Keller-Lehmann, Dissertation, ETH, Zürich, 1990, No. 9255.
40 E. Bakker and W. Simon, Anal. Chem., 64 (1992) 1805.
41 W.E. Morf, K. Seiler and W. Simon, in E. Pungor (Ed.), Ion-Selective Electrodes, Vol. 5, Pergamon Press, Oxford, and Akadémiai Kiadó, Budapest, 1989, p. 141.
42 U. Thanei-Wyss, W.E. Morf, P. Lienemann, Z. Stefanac, I. Mosteret and R. Dörig, Mikrochim. Acta, III (1983) 135.
43 M.E. Meyerhoff, S.A. Rosario and G.S. Cha, Anal. Chem., 62 (1990) 2418.

Analytica Chimica Acta, 282 (1993) 239–246
Elsevier Science Publishers B.V., Amsterdam

Investigation of silver iodide-based ion-selective membranes by scanning electrochemical microscopy

Klára Tóth and Géza Nagy

Institute for General and Analytical Chemistry, Technical Analytical Research Group of the Hungarian Academy of Sciences, Technical University of Budapest, H-1111 Budapest (Hungary)

Benjamin R. Horrocks and Allen J. Bard

Department of Chemistry and Biochemistry, The University of Texas at Austin, Austin, TX 78712 (USA)

(Received 9th August 1993)

Abstract

The proton concentration–distance profile developed at the interface of silver iodide-based solid-state electrodes in corroding cyanide solutions of low buffer capacity has been studied by scanning electrochemical microscopy using a potentiometric tip. The experimental results verified the theory developed earlier for the interpretation of the operation mechanism of "corrosion" type electrodes.

Keywords: Ion-selective membranes; Scanning electron microscopy; Silver iodide

Solid-state ion-selective electrodes based on silver iodide or a mixture of silver iodide and silver sulphide have been widely used to monitor the cyanide ion concentration in different matrices (e.g. [1–4]). The operational model of silver halide electrodes responding to complex forming ligands such as cyanide has been elaborated on the basis of a dissolution or "corrosion" reaction between the silver halide (AgX) and the cyanide and has been discussed in a number of articles [1,2,5–9]. Accordingly the silver halide-based sensors have a cyanide response, through sensing the halide ions generated in a surface reaction such as:

$$AgX + 2CN^- \rightarrow Ag(CN)_2^- + X^- \quad (1)$$

Safety reasons dictate that cyanide measurements should be made in strongly basic solutions (pH > 11), where volatile HCN is not present. However, it is obvious that the pH can affect the potential response of the electrode to cyanide. The electrode potential vs. pH dependence has been studied experimentally and the early observations could be interpreted on the basis of protolytic equilibria and the corrosion reaction [1,2]. For use in monitoring enzyme catalysed processes generating cyanide the pH cannot be selected at random. A pH value providing good stability and high catalytic activity for the enzymatic reaction is a prerequisite. Mascini [10] investigated cyanide-cleaving enzyme reactions with a cyanide ion-selective electrode. The experimental electrode potential vs. pH curves thus recorded in highly buffered cyanide solutions were not in complete agreement with earlier observations [10]. To obtain a better understanding about the mechanism, detailed experimental studies on the pH dependence of the cyanide electrode response were carried out. The results of these experiments

Correspondence to: K. Tóth and A.J. Bard at the above addresses.

revealed that in the pH range 5–9 the potential of the cyanide electrode depends not only on the cyanide ion activity and pH but also strongly on the buffer capacity of the solution [11].

In the early work, surface iodide concentration values were calculated by considering the cyanide concentrations and the dissociation constants of the relevant complex and the weak acid taking part in the corrosion process. By substituting these concentration values into the Nernst equation, the theoretical electrode potential vs. pH curves were calculated [7,10–12]. However, the experimental curves in the case of low buffer capacities showed a poor fit to this curve. This finding could be explained by taking into account the reaction:

$$AgX + 2HCN \rightarrow Ag(CN)_2^- + 2H^+ + X^- \qquad (2)$$

and the generated local concentration profiles [11].

In the lower pH range reaction 2 competes with reaction 1 at the membrane surface and as the "corrosion" dissolution reaction proceeds, the iodide (X^-), the dicyanoargentate and also the hydrogen ion concentrations increase while the cyanide concentration decreases in the vicinity of the electrode membrane–solution interface. A concentration gradient will build up and transport processes driven by it will take place. In quiescent solution the diffusion and natural convection produce the concentration profile, while in stirred solution it is convective diffusion. Under steady state conditions the surface iodide concentration, which is dependent on the bulk cyanide and hydrogen ion concentrations, determines the response function.

When reaction 2 occurs, as discussed above, the solution layer in direct contact with the membrane would be more acidic than the bulk of the solution. The pH difference between the vicinity of the membrane surface and the bulk is naturally buffer-capacity dependent, and becomes larger as the buffer capacity of the solution decreases. Thus, the buffer capacity can influence the surface iodide activity and consequently the potential of the silver iodide electrode. The difference between the measured and the calculated pH–cyanide activity dependent response curves originates from the pH gradient.

Attempts made to verify the above explanation, namely the existence of a local pH gradient at the solution–electrode membrane interface by ordinary chromogenic indicators were successful [13]. The change in pH with distance from the interface under different circumstances, however, could not be measured experimentally.

The processes taking place at the surface of corrosion-type cyanide electrodes have been studied with different surface analytical methods such as photoelectron spectroscopy, scanning electron microscopy and x-ray fluorescence spectrometry [14]. With these methods the surface of the untreated and pretreated and consequently dried membranes could be investigated in a vacuum. Changes in the composition of the solid membrane surfaces caused by treatment such as conditioning in solutions of different compositions for different time periods could be detected. However, no information could be gathered about the concentration profiles at the solution–membrane interface.

With the development of scanning electrochemical microscopy (SECM) employing an ultramicro voltammetric electrode, a new tool has become available to obtain chemical information about conductive and non-conductive substrates, to study electrode surfaces with high spatial resolution and kinetics of surface reactions [15]. Recent progress in the fabrication of a pH-selective potentiometric tip for SECM has provided a new way to investigate local pH effects of different reactions which are not accessible with microvoltammetric tips and amperometric techniques. The smallness of the potentiometric tip allows surfaces to be imaged with high spatial resolution and concentration profiles to be monitored precisely.

In amperometric SECM a precise tip-substrate (target) distance calibration method has been elaborated [16]. It operates by comparing the amperometric signal with a theoretically derived and experimentally well-proved current–distance calibration curve. In the case of SECM with a potentiometric tip, the signal from the tip can not be used for distance calibration. Therefore a separate independent method is needed for the determination of the absolute tip to target surface

distance for the effective use of potentiometric SECM. It has been proved that the antimony microdisc electrode can be used in both amperometric and potentiometric microscopy. In this way the distance calibration can be made in the amperometric mode while the pH imaging can be performed in the potentiometric mode [17].

Antimony pH electrodes are well known and are widely used in different areas when glass electrodes are inappropriate, e.g., in fluoride media or in the food industry. The properties of antimony electrodes have been reviewed recently [18]. The micro versions of antimony pH electrodes, employed mostly in different areas of experimental life sciences, are fabricated as very thin-walled capillaries to facilitate penetration and minimise invasion [19,20]. For microscopy a more durable and polishable design is needed which has a well-defined tip geometry to allow mass transport-based distance calibration. An antimony microdisc electrode for SECM has recently been described [17].

The purpose of the study reported here was to monitor proton concentration profiles in solutions of different buffer capacities generated above an AgI surface by the corrosion reaction and to provide in situ evidence for the assumption given in an earlier publication [11,14] in order to interpret the cyanide electrode response function in weakly buffered media.

EXPERIMENTAL

Instrumentation

A recent, slightly modified version of the basic scanning electrochemical microscope capable of performing both potentiometric and amperometric imaging [17] was used in these investigations.

The instrument used three piezoelectric inchworm motors for high precision three dimensional positioning (Burleigh Instruments, Fishers, NY). Their movement was controlled by a PC via an analog-to-digital converter (ADC). The cell holder contained two inchworm positioners which moved the cell in the horizontal x or y direction, while the measuring tip was mounted on the vertical (z) motor. The amperometric microscopy set used an EI-400 bipotentiostat (Ensman Instrument, Bloomington, IN) as the measuring apparatus. For potentiometric microscopy a homebuilt high-impedance voltmeter was used to measure the potential difference between the tip and a conventional 0.1 M silver/silver chloride reference electrode located in the bulk of the solution. In both operation modes the output of the measuring instrument was fed into one of the channels of the ADC board to allow data acquisition by computer for image formation.

The cell was a shallow conical PTFE cup with a volume of ca. 4 ml. Its wide mouth allowed easy observation during manual approximate positioning of the tip. The narrower cell bottom, which screwed into the cell body, was used as a target holder. The cylindrical sample targets were mounted in the cell by tight fitting into a hole bored through the cell bottom. The auxiliary electrode used for amperometric measurements was a platinum wire of 0.5 mm diameter entering the cell through the PTFE cell wall.

For electrochemical characterisation of antimony electrodes a BAS 100A potentiostat was used. The pH measurements were performed with an Orion pH meter (Model 701A).

Targets

To achieve a true steady state concentration profile around the silver iodide surface in cyanide solutions, glass shield inlaid microdisc silver iodide targets were made. To prepare such targets, glass capillaries were sealed at one end in a flame with slow rotation to achieve a gradual tapering of the capillary bore toward the sealed end. Finely ground, dry silver iodide powder (for preparation see below) was introduced inside the capillary and was compacted by drop hammering inside a guide tube, and subjected to a vacuum. The silver iodide was carefully melted under vacuum by holding the closed end of the tube in a microflame. After letting it cool down slowly, the sealed end was polished to expose a small circular silver iodide disc (diameter 25–120 μm) in the middle of a flat glass surface of ca. 2 mm diameter. After polishing, the microelectrode targets were inserted into the base of the cell as outlined above.

Electrode fabrication

Pressed pellets of silver iodide used to prepare membrane discs (5 mm diam., 6 mm thick) were made of silver iodide precipitate pressed at 10^9 Pa. These pellets were incorporated into Philips solid state electrode bodies. The internal filling solution was 0.1 M KNO_3, 1 mM $AgNO_3$ and the internal reference electrode was a chloride coated silver wire.

The silver iodide used for the preparation of the discs was precipitated by titration of stirred 0.1 M silver nitrate with 0.1 M sodium iodide dropwise under careful potentiometric control. An iodide-selective indicator electrode (Radelkis Type OP-I-7111D) and a silver/silver chloride double junction reference electrode (Radelkis Type OP-8202) was used for end-point detection. The precipitate obtained was aged by standing for 24 h, washed three times with distilled water and dried in an oven at 105°C for 3 h.

The illustrated, step by step procedure for antimony SECM tip fabrication is given elsewhere [17]. Here a short description only is given. Antimony shot (99.999%, Aldrich, Milwaukee, WI) was melted and sucked into a thick-walled Pyrex capillary (outer diameter, 7 mm, inner diameter, 1 mm). With standard glassblowing techniques, antimony-filled capillaries of outside diameter in the 1–2 mm range were pulled manually. It is advisable to heat up the end of the capillary and use tweezers for rapid pulling. In this way the build up of excess pressure in the column of antimony and deformation of the capillary can be avoided. A section of the antimony-filled capillary, about 50 mm long, was carefully selected under optical microscope view. (The antimony fiber inside must be continuous with a diameter of 20–100 μm.) These capillaries were pulled again using the heating coil of a microelectrode puller (Stoelting). A small weight (1–2 g) was attached to one end of the antimony capillary. The voltage applied to the coil was manually controlled observing the extension of the heated section of the capillary. A short tapered section of the capillary obtained was mounted in another glass capillary serving as a holding body. A well-defined disc of antimony was exposed by gently scoring near the end of the capillary and carefully breaking the capillary against a fingertip. Electrical contact was made by mercury introduced through the back of the supporting capillary. The relatively thick glass wall (total diameter to disc diameter ratio = 5 to 10) of these small capillaries allows careful polishing (with MOYCO, Ultralap aluminacoated strips). Electrodes with an antimony disc down to 3 μm diameter were made in this way. For preparation of electrodes with a smaller disc diameter the double pulled glass-coated antimony fibers were sealed under vacuum in low melting point glass, as is commonly done in the preparation of microdisc electrodes from platinum wire [21]. The antimony fiber-containing glass rods prepared in this way can be pulled down for size reduction, bevelled and polished.

RESULTS AND DISCUSSION

Electrode characterisation

The pH function of the shielded microdisc antimony electrodes was carefully studied with different buffer systems. A typical calibration graph obtained for a series of phosphate buffers is linear and has the equation $E = (-108.6 - 45.5$ pH) mV. The diameter of the antimony microdisc was 6 μm and a saturated calomel electrode was used as a reference electrode. The electrode showed no change of potential at pH 7 when changing the phosphate concentration in the range of 1–100 mM. The slopes of the calibration graphs obtained with different electrodes were typically between 40 and 50 mV per pH. This is the usual slope value for a polycrystalline antimony electrode. Different treatments suggested in the literature, such as soaking in oxidising agents (permanganate or dichromate) or anodization under different conditions, were tried in order to improve the slope of the pH function. However, no significant success was achieved. Therefore the antimony tips were used in microscopy without special pretreatment.

It was observed that after voltammetric experiments, especially if the antimony tip was negatively polarised for long times, the pH measuring function was lost (the electrode potential drifted,

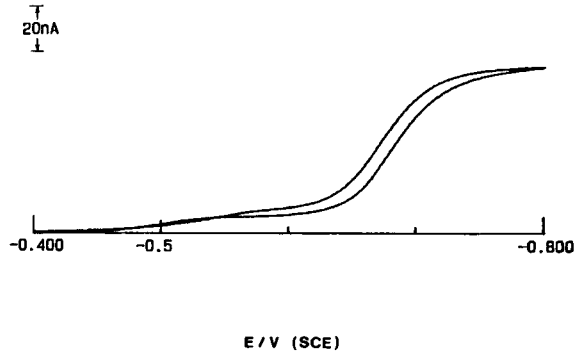

Fig. 1. Cyclic voltammogram of methyl viologen (9.1 mM in argon purged 0.1 M KCl; polarising rate, 10 mV s^{-1}).

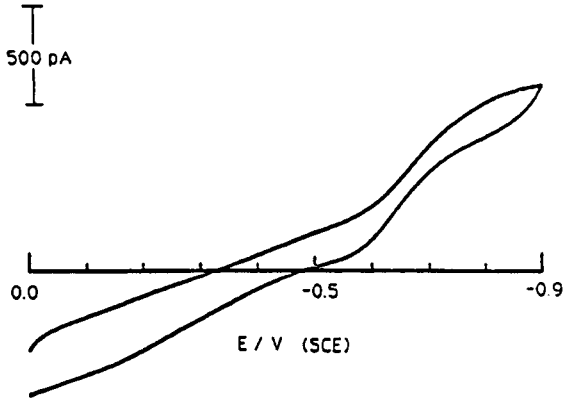

Fig. 2. Cyclic voltammograms of an antimony microelectrode of 3 μm diameter in air-saturated 1 mM (pH 7.0) phosphate buffer containing 0.1 M KCl. Sweep rate: 100 mV s^{-1} [17].

the slope of the pH calibration graph decreased and the reproduction of the potential value became poor). The reason for this is the reduction of the oxide film at the electrode surface. The pH function of the antimony electrode was restored after a few hours in air, or soaking in oxidising solutions. The easiest way to restore the pH function, however, was to polarize the tip for a few seconds to 0 V. After this, the original pH function of the electrode was regained. Reproducible behaviour was observed for any individual microelectrode prepared as described; the calibration points were found to be within a few mV when measured on different days. While the oxygen concentration was changed in the cell by bubbling nitrogen gas, no significant change in the electrode potential was observed.

For tip–substrate distance calibration, amperometric measurements can well be used in scanning electrochemical microscopy [16,17]. To investigate the applicability of the antimony tip in this respect voltammetric measurements were carried out. Fig. 1 shows a cyclic voltammogram of 9.1 mM methylviologen in argon purged 0.1 M KCl at a 25-μm diameter antimony tip. The half-wave potential is in agreement with the formal potential (−0.68 V vs. SCE) and the voltammogram has the characteristic sigmoidal shape expected for a microelectrode. Making several cycles or keeping the electrode potential on the plateau for a longer period did not produce noticeable changes of the electrochemical activity of the electrode surface. This guaranties that the distance calibration can be made with the antimony measuring tip in the amperometric mode.

In order to avoid the need of adding an external redox couple to the sample solution, the use of oxygen reduction for distance calibration was attempted. Fig. 2 [17] shows a cyclic voltammogram prepared in air-saturated phosphate buffer, pH 7.0. The oxygen reduction wave is clearly defined. It was also verified with nitrogen purging. Setting the potential of the microelectrode between −0.7 and −0.9 V a steady state current was obtained which reflected well the oxygen concentration in the solution.

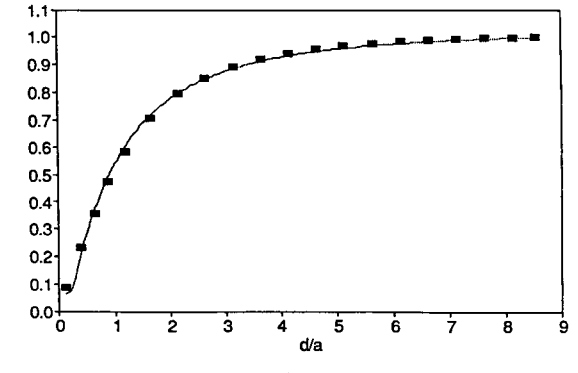

Fig. 3. Current-distance (i_T–d) curve (i_T normalized to $i_{T\infty}$ and d to the radius of the tip, a) for a 4 μm diameter antimony microdisc operating in amperometric mode. The solution was 0.1 M (pH 7.0) phosphate buffer containing 0.1 M KCl, while the sample surface was a PTFE disc. Solid line = experimental data; and ■ = theoretical values [17].

For tip–substrate distance calibration the electrode potential was set to −0.8 V and air-saturated buffer solution was introduced into the PTFE cell. The oxygen reduction current was monitored while the electrode approached the PTFE substrate surface. The experimental current–distance curve is shown in Fig. 3 (solid line) [17]. It can be seen that while the tip is far from the target surface, the current is constant. When it approaches the surface, owing to the irreversible character of oxygen reduction and the blocking or shielding effect ("negative feedback" [15,16]) of the surface on the oxygen diffusion to the electrode, the current decreases. The good fit of the theoretical points to the experimental curve proves that the oxygen reduction curve on the antimony tip allows the measurement of absolute tip–surface distance [17].

The amperometric distance calibration is very advantageous especially if the oxygen reduction current is used. In this case no redox agent addition is necessary. An external additive can easily interfere with the system investigated or with the pH measuring function of the antimony electrode. For the amperometric distance measurement no knowledge of the diffusion coefficient, concentration or stoichiometry of the electrochemical reduction of the material, here the oxygen, is required.

Potentiometric studies with a silver iodide membrane electrode

To investigate the pH dependence of the cyanide electrode function in buffered or unbuffered cyanide solutions, the pH of the test solution was adjusted to high values by adding solid potassium hydroxide. The potential of the silver iodide based cyanide electrode and of a pH measuring glass electrode immersed in the solution were recorded while, by adding portions of nitric acid the pH was gradually decreased. To avoid hydrogen cyanide loss the measurements were performed in a closed cell. The potential of the cyanide electrode was plotted as a function of bulk pH measured. The experimentally observed plots ranged between two limiting cases. In highly buffered media when the cyanide concentration was relatively low the electrode potential–pH

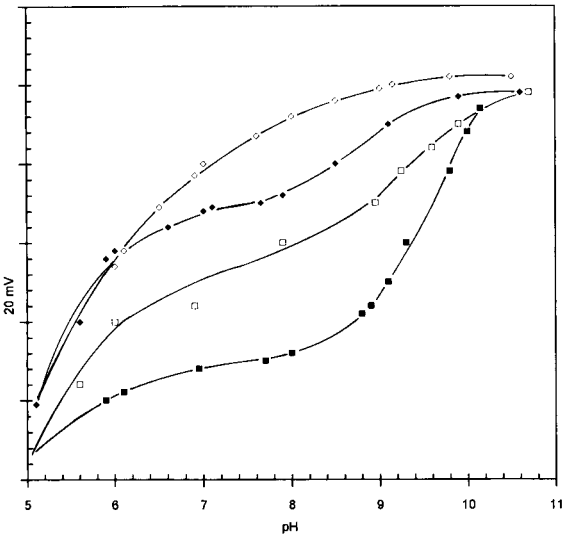

Fig. 4. Electrode potential vs. pH curves for a silver iodide based cyanide electrode in 10^{-3} M KCN solutions of different buffer capacities. ◇, 10^{-1} M Britton Robinson buffer; ◆, 10^{-3} M Britton Robinson buffer; □, 10^{-5} M Britton Robinson buffer; ■, no buffer is added. All solutions contained 0.1 M KCl too. Reference electrode was a double junction Ag/AgCl electrode, Radelkis Type OP-8202.

curve showed theoretical behaviour: that means it could be described by the earlier mentioned equation [10,11], i.e.,

$$E = E_I^0 - S \log \frac{K_{HCN}\sqrt{K}\, a_{CN,t}}{K_{HCN}(2\sqrt{K} + 1) + a_H} \qquad (3)$$

where S is the slope of the cyanide electrode calibration graph, E is the potential of the cyanide electrode, E_I^0 is the standard potential, K_{HCN} is dissociation constant of HCN (4.8×10^{-10} M), K is the equilibrium constant for

$$AgI + 2CN^- \rightleftarrows Ag(CN)_2^- + I^- \qquad (4)$$

the surface reaction ($K = 6.28 \times 10^4$ M), a is the ion activity, t stands for total ($a_{CN,t} = a_{CN^-} + a_{HCN}$).

The other limiting case is obtained in the absence of external buffer. Experimentally obtained electrode potential–pH curves are shown in Fig. 4. As can be seen in the case of the low buffer capacity media in the pH range 5–10 the measured electrode potential is more positive than is expected theoretically or is observed at

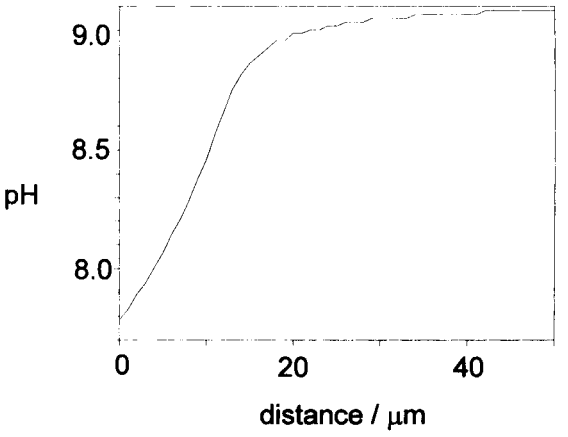

Fig. 5. pH–distance profile over a 40-μm silver iodide target in 1 mM KCN, 0.1 M KCl and 1 mM pH 9.0 phosphate buffer. The tip diameter was 15 μm and the x-axis is the absolute tip-to-surface distance.

higher buffer capacity. This indicates a lower iodide activity at the measuring membrane surface. As was mentioned earlier the anomalous behaviour could be explained by assuming that there is a difference between the bulk pH and the local pH at the electrode membrane surface. The extent of this pH difference could be estimated from the difference between the theoretical and experimental curves.

Scanning electrochemical microscopy with the potentiometric tip

Using scanning electrochemical microscopy with the pH measuring antimony tip, the existence of the local pH gradient was checked. An estimation of the thickness and shape of this diffusion layer was also attempted. An SECM experiment was carried out in the following manner. First the silver iodide target was placed in the cell. The tip was roughly positioned over the target manually, using the x–y piezoelectric motors. A telescopic lens was very helpful for this. (To avoid a major concentration change caused by the corrosion reaction in the small volume cell, small targets (diameter 40–80 μm) were used in these studies). Air-saturated cyanide-free buffer solution (4 ml) was introduced into the cell and using a -0.8 V measuring potential, the tip-target distance was adjusted and determined. As was indicated before, this was accomplished by following the oxygen reduction amperometric current intensity vs. Z direction step, distance curve and fitting it to the theoretical working curve data. To regain its pH measuring function the tip was polarised at 0.0 V for a few seconds. After this the potentiometric measuring mode was installed. Different buffered and unbuffered cyanide solutions were introduced and the microscopic experiments were performed.

Figure 5 shows the pH–distance profile over the centre of a 40-μm diameter silver iodide target. The solution contained 1 mM KCN, 0.1 M KCl and 1 mM pH 9.0 phosphate buffer. The decrease of pH near the silver iodide surface is apparent. Furthermore, the measured surface pH of ca. 7.8 is in reasonable agreement with the value estimated from Fig. 4 by considering the displacement on the pH axis of the E–pH curve in 10^{-3} M buffer from the curve in the most concentrated buffer. The inflection on the pH–distance curve is most likely due to the shielding effect of the tip (15 μm diameter) on the target at small distances. In other words, when the tip approaches too closely it blocks the cyanide transport to the surface so the corrosion process slows down. This steric hindrance affects the cyanide diffusion more than the pH equilibration.

As a control, the pH–distance curves were also recorded in cyanide-free solutions containing 100

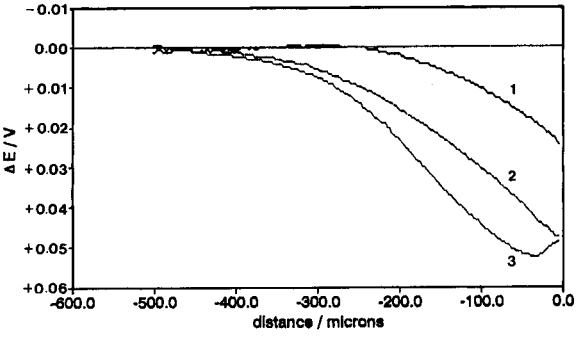

Fig. 6. ΔE–distance profiles over a silver iodide target in 1 mM phosphate buffer (pH 9.0) at different cyanide concentration levels. The antimony tip was 15 μm. The solution contained 0.1 M KCl also. Cyanide concentration: (1) 1 mM; (2) 3 mM; (3) 5 mM.

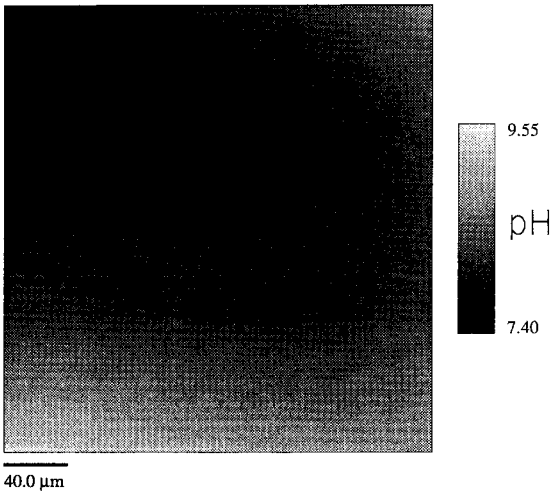

Fig. 7. Image of the pH profile over a 40 μm diameter silver iodide target. The gray scale shows the antimony tip potential corresponding to pH values; white corresponds to higher pH. The tip diameter was 15 μm. The solution contained 0.1 M KCl, 1 mM KCN and 10^{-4} M pH 9.0 phosphate buffer.

mM potassium chloride. No measurable difference could be observed in this experiment between the pH of the bulk solution and at the silver iodide target surface.

Figure 6 exhibits E vs. distance curves recorded over silver iodide surface with SECM incorporating a 2-μm antimony tip in 10^{-3} M phosphate buffer (pH 9) at 1, 3 and 5 mM KCN concentration levels. (The solutions also contained 0.1 M KCl in all cases.) Higher cyanide concentration results in higher corrosion rate which is clearly reflected on the ΔE vs. distance curves. ΔE in relevance to the ΔpH means the difference of the local and bulk electrode potential values of the antimony tip.

The above SECM experiment clearly proves that the corrosion reaction involves an appreciable pH change in the solution adjacent to the silver iodide surface when the buffer capacity is small. This validates the basic assumption made in the earlier explanation for the anomalous pH dependence of the cyanide electrode function observed in unbuffered media.

The SECM can provide a two-dimensional image of the silver iodide disk taking advantage of the pH change caused by the corrosion reaction. Figure 7 shows an image of a 40 μm diameter silver iodide target in 1 mM KCN, 0.1 M KCl and 0.1 mM phosphate buffer (pH 9.0). At the distance measured, the pH is about two units lower than in the bulk solution. The lower near surface pH in this image compared to Fig. 5 is consistent with the lower buffer capacity. The pH–electrode potential curves predict the existence in the case of higher cyanide concentration and unbuffered media of large pH differences (1–3) between the electrode surface and the bulk of the solution.

The support of this work by a grant from the US National Science Foundation (CHE 9214480) and by the Hungarian OTKA 5-346 is gratefully acknowledged.

REFERENCES

1 K. Tóth and E. Pungor, Anal. Chim. Acta, 51 (1970) 221.
2 E. Pungor and K. Tóth, Analyst, 95 (1970) 625.
3 P.L. Bailey, Ion-Selective Electrode Reviews, 1 (1970) 81.
4 I. Sekerka and J.F. Lechner, Water Res., 10 (1976) 479.
5 W.E. Morf, G. Kahr and W. Simon, Anal. Chem., 45 (1974) 1538.
6 D.H. Evans, Anal. Chem., 44 (1972) 875.
7 J. Koryta, Anal. Chim. Acta, 61 (1972) 329.
8 G.P. Bound, B. Fleet, H. von Storp and D.H. Evans, Anal. Chem., 45 (1973) 788.
9 A. Hulanicki and A. Lewenstam, Talanta, 24 (1977) 171.
10 M. Mascini, Anal. Chem., 45 (1973) 614.
11 M. Gratzl, F. Rakiás, G. Horvai, K. Tóth and E. Pungor, Anal. Chim. Acta, 102 (1978) 85.
12 G.A. Rechnitz and L. Lenado, Anal. Chem., 44 (1972) 468.
13 M. Gratzl, PhD Thesis, Budapest, 1984.
14 E. Pungor, M. Gratzl, L. Pólos, K. Tóth, M.F. Ebel, H. Ebel, G. Zuba and J. Wernisch, Anal. Chim. Acta, 156 (1984) 9.
15 A.J. Bard, F.R. Fan, D.T. Pierce, P.R. Unwin, D.O. Wipf, F. Zhou, Science, 254 (1991) 68.
16 J. Kwak and A.J. Bard, Anal. Chem., 61 (1989) 1221.
17 B.R. Horrocks, M.V. Mirkin, D.T. Pierce, A.J. Bard, G. Nagy and K. Tóth, Anal. Chem., 65 (1993) 1213.
18 S. Glab, A. Hulanicki, G. Edwall and F. Ingman, Crit. Rev. Anal. Chem., 21 (1989) 29.
19 H.A. Bicher and S. Onki, Biochim. Biophys. Acta, 255 (1972) 900.
20 Y. Matsumura, K. Kajino and M. Fujimoto, Membr. Biochem., 3 (1980) 99.
21 R.M. Wightman and D.O. Wipf, in A.J. Bard (Ed.), Electroanalytical Chemistry, Marcel Dekker, New York, 1988, Vol. 15.

Analytica Chimica Acta, 282 (1993) 247–257
Elsevier Science Publishers B.V., Amsterdam

Cation permselectivity in the phase boundary of ionophore-incorporated solvent polymeric membranes as studied by Fourier transform infrared attenuated total reflection spectrometry [1]

Kayoko Umezawa

Department of Chemistry, College of Art and Science, University of Tokyo, Komaba, Tokyo 153 (Japan)

Xiao Ming Lin

Division of Environmental Conservation, Graduate School of Environmental Science, Hokkaido University, Sapporo 060 (Japan)

Seiichi Nishizawa, Masao Sugawara and Yoshio Umezawa

Department of Chemistry, School of Science, University of Tokyo, Hongo, Tokyo 113 (Japan)

(Received 7th May, 1993)

Abstract

The behaviour of permselective membrane transport was studied by Fourier transform IR attenuated total reflection spectrometry and potential measurements for the solvent polymeric membranes incorporating several different ionophores. The stoichiometric ratios between the complexed cations and their corresponding counter anions in the phase boundary, 0.31–1.8 μm in depth, of the membrane were determined for each membrane made in contact with various primary ion solutions. When hydrophilic counter anions were used for the primary ion solutions, the IR spectra of the membrane were exclusively those of the complexed cations, and no IR-active anionic peak appeared. The intensity of the former peaks was found to be dependent on an added anionic site, carboxylated poly(vinyl chloride) and a derivative of tetraphenylborate, in the membranes, and also on the penetration depths of the IR beams used. In contrast, when a hydrophobic counter anion, SCN^-, was used for the primary ion solutions, the spectra from both the complexed cation and corresponding counter anion were seen, of which the stoichiometric ratios changed depending on the concentrations of primary ion salts, and on the coexistence of a derivative of tetraphenylborate in the membrane. The results are discussed in terms of the extent of cation permselectivity and its relevance to the potential response of ionophore-incorporated liquid membrane ion-selective electrodes.

Keywords: Infrared spectrometry; Ion-selective electrodes; Attenuated total reflection; Cation permselectivity; Ionophores; Membrane electrodes; Solvent polymeric membranes

Correspondence to: Y. Umezawa, Department of Chemistry, School of Science, University of Tokyo, Hongo, Tokyo 113 (Japan).

[1] Dedicated to Professor Dr Ernö Pungor, who has made major contributions to the field of analytical chemistry, particularly by introducing precipitate-based solid membrane ion-selective electrodes, to commemorate his 70th birthday.

Pungor and co-workers [1–5] investigated by Fourier transform infrared attenuated total reflection (FT-IR-ATR) spectrometry complex formation between a derivative of bis(benzo-15-crown-5) and K^+ in ionophore-incorporated liquid membranes. They found that in the phase boundary of the membranes made in contact with

aqueous KCl, only a small number of the complexes existed; they were easily removed by rinsing with water. In contrast, membranes treated with aqueous KSCN showed a large number of complexes accompanying SCN^- ions, which were not easily removed by rinsing, and the transport rate of the complex into the bulk of the membrane was found to be much slower than the potentiometric response time. From these results, they concluded that the observed potential response was determined essentially at the surface of the membrane rather than in the bulk. Stimulated by the above study, we also measured FT-IR-ATR spectra of bis[(benzo-15-crown-5)-4′-methyl] pimelate and dibenzo-18-crown-6 complexed with K^+ in the phase boundary of poly(vinyl chloride) (PVC) liquid membranes with these ionophores incorporated and obtained essentially the same results [6] as Pungor et al.

From these studies, the complex formation of K^+ with the ionophores in the phase boundary of liquid membranes has been well characterized. However, the behaviour of counter anions, from the viewpoint of cation permselectivity, has not been described with regard to their amount relative to those of the corresponding complexed cations. In other words, the above IR results were not necessarily concerned with the difference between the permselective ionic transport and the bulk solvent extraction into the ionophore-incorporated liquid membranes.

In this study, some unique features of permselective cation transport into the phase boundary of the liquid membranes are discussed in terms of the stoichiometric ratios for counter anions with respect to the complex cations. We investigated in detail by FT-IR-ATR spectrometry the complex formation of K^+ with bis[(benzo-15-crown-5)-4′-methyl] pimelate and valinomycin, of Li^+ with 6,6-dibenzyl-1,4,8,11-tetraoxacyclotetradecane and of Ca^{2+} with *N,N,N′,N′*-tetracyclohexyl-3-oxapentanediamide in the phase boundary (0.31–1.8 μm) of solvent polymeric liquid membranes with these ionophores incorporated. These ionophores were found to exhibit large band shifts or new bands in the IR spectra on complex formation, and we were thereby able to quantitatively measure, using the difference spectrum technique, weak bands from ionophores overlapped with strong absorption bands due to plasticizers and PVC. In addition, we chose IR-active anions, with different extents of hydrophobicity, i.e., SO_4^{2-}, NO_3^- and SCN^-, as counter anion, so as to estimate the amount of the counter anion relative to that of the complexed cation in the membrane surface.

For the generation of cationic membrane potentials at ionophore-incorporated liquid membranes, cation permselectivity is essential [7,8]. Several efforts have been made to characterize the cation permselectivity on the basis of electrodialysis [9–11] and radiotracer methods [9,12–14]. From these studies, the process of permselective ionic transport across the bulk membrane was well established. However, to the best of our knowledge, no study has been reported on the direct spectroscopic observation of cation permselectivity in the phase boundary of liquid membranes, despite its importance for insight at the molecular level into the potential response for ionophore-incorporated liquid membrane ion-selective electrodes (ISEs).

EXPERIMENTAL

Materials

Reagents. Bis[(benzo-15-crown-5)-4′-methyl]-pimelate and, 6,6-dibenzyl-1,4,8,11-tetraoxacyclotetradecane [abbreviated to bis(benzo-15-crown-5) and dibenzyl-14-crown-4, respectively] from Dojindo Laboratories (Kumamoto), valinomycin (VM) from Sigma (St. Louis, MO) and *N,N,N′,N′*-tetracyclohexyl-3-oxapentanediamide (ETH 129) from Fluka (Buchs) were used as ionophores. The structures of these ionophores are shown in Fig. 1. As a source of lipophilic anionic sites, potassium tetrakis(4-chlorophenyl)-borate (KTpClPB) from Dojindo Laboratories was used. 2-Nitrophenyl octyl ether (o-NPOE) from Dojindo Laboratories and bis(2-ethylhexyl) sebacate (DOS) from Tokyo Kasei (Tokyo) were used as plasticizers. Poly(vinyl chloride) (PVC) ($n_{av} \approx$ 1100 from Wako, Osaka, and of high molecular weight from Aldrich, Milwaukee, WI) was used as a polymer matrix. Carboxylated PVC (PVC-

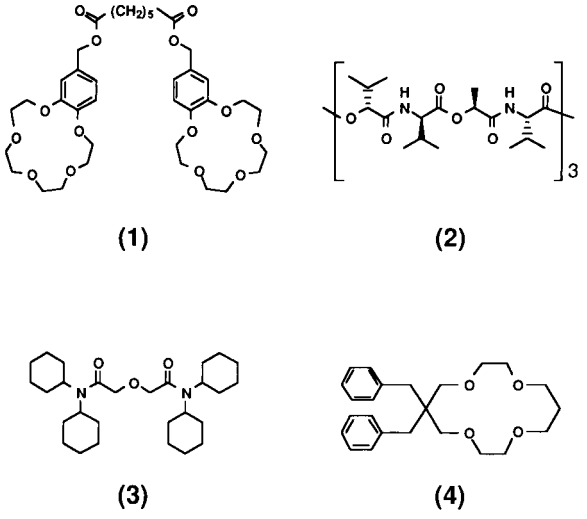

(1) (2) (3) (4)

Fig. 1. Structures of the ionophores used. 1 = bis(benzo-15-crown-5); 2 = VM; 3 = ETH 129; 4 = dibenzyl-14-crown-4; these are ionophores for K^+, K^+, Ca^{2+} and Li^+, respectively.

COOH, carboxy content 1.8%) from Aldrich was also used as a polymer matrix. To eliminate alkali metal cations contained as impurities in the polymer, PVC-COOH was converted into its H-form, washed three times in stirred 0.1 M HCl for several hours each, washed in water several times and dried over silica gel in a desiccator. Tetrahydrofuran (THF) from Wako was freshly distilled from sodium–benzophenone ketyl under an argon atmosphere. All other reagents were of analytical-reagent grade (Wako). Deionized water purified in a Millipore Milli-Q system (17.8 MΩ cm specific resistance) (Japan Millipore) was used throughout.

Preparation of K^+–, Li^+– and Ca^{2+}–ionophore complexes. Several kinds of metal ion–ionophore complexes were prepared and used as references for monitoring the complex formation and for determining the stoichiometric ratios of the complexed cations vs. corresponding counter anions in the phase boundary of the membranes.

{K[bis(benzo-15-crown-5)]}SCN, [K(VM)]SCN, [Ca(ETH 129)$_3$](SCN)$_2$[15,16] and [Li(dibenzyl-14-crown-4)]NO$_3$. A stoichiometric mixture of an ionophore and a metal salt in ethanol or methanol was warmed on a water-bath until the mixture had completely dissolved and then the solution was cooled to room temperature. The complex was obtained by slow evaporation of the solvent [17]. IR (cm^{-1}): {K[bis(benzo-15-crown-5)]}SCN (cast), 2054 (m, sh), 1130 (s, sh), 1106 (w, sh), 1095 (w, sh), 1077 (w, sh), 1046 (w, sh); [K(VM)]SCN (cast), 2054 (m, sh), 1752 (s, sh), 1655 (s, sh) 1194 (s, sh); [Ca(ETH 129)$_3$](SCN)$_2$ (cast), 2054 (m, sh), 1644 (s, sh); [Li(dibenzyl-14-crown-4)]NO$_3$ (cast), 1403 (s, br), 1331 (s, br), 1090 (s, sh).

{K$_2$[bis(benzo-15-crown-5)]$_2$}SO$_4$. An amount of 72 mg (1 mmol) of bis(benzo-15-crown-5) was completely dissolved in 50 ml of THF, then 1 ml of 0.5 M K_2SO_4 solution (0.5 mmol) was gradually added with stirring. An oily complex was obtained by slow evaporation of THF. ^1H NMR (400 MHz, THF-d_8): δ 6.91 (d, $J = 5$ Hz, 2H, arm), 6.84 (dd, $J = 5$ Hz, 2 Hz, 2H, arm), 6.80 (d, $J = 2$ Hz, 2H, arm), 4.45 (s, 2H, Ph–CH_2–O), 4.06–4.02 (m, 8H, Ph–O–CH_2CH$_2$–O), 3.85–3.79 (m, 8H, Ph–O–CH$_2$CH_2–O), 3.68–3.61 (m, 16H, O–CH_2CH_2–O), 2.30–2.23 (m, 4H, COCH_2), 1.63–1.56 (m, 4H, COCH$_2$CH_2), 1.32 ppm (m, $J = 7.3$ Hz, 2H, COCH$_2$CH$_2$CH_2).

Preparation of membranes

Solvent polymeric membranes were prepared as described [18]. THF was added with stirring to dissolve a mixture of a weighed amount of an ionophore, plasticizer and PVC-COOH. This THF solution was poured into a Petri dish, followed by slow evaporation of the THF for 48 h. The membrane thus prepared was cut into 20- and 30-mm diameter circles for IR and potentiometric measurements, respectively. In addition, membranes with [K(VM)]SCN, and [Ca(ETH 129)$_3$](SCN)$_2$ incorporated were prepared as practical stoichiometry standards (see below).

E.m.f. measurements

Each membrane was mounted with PTFE tape on one end of a glass tube (10 mm in diameter and 100 mm in length), in which an appropriate inner reference solution and an Ag/AgCl inner reference electrode were placed. The potentiometric cell assembly was as follows: Ag;AgCl|0.01 M KCl or 0.01 M $CaCl_2$|polymer-supported liq-

uid membrane | sample solution | 1.0 M CH_3CO_2-Li | 3.0 M KCl | AgCl;Ag.

The ionic strength was adjusted with 0.1 M LiCl or 0.1 M KCl. The potentials were measured at 25°C with a Model COM-20R pH–mV meter (Denki Kagaku Keiki, Tokyo).

FT-IR-ATR measurements

FT-IR spectra were recorded under a nitrogen atmosphere with a resolution of either 2 or 4 cm^{-1} on a Model 1720-X (Perkin-Elmer, Norwalk, CT) or a Model FTS-30 FT-IR spectrometer (Bio-Rad, Cambridge, MA) in a room thermostated at 25°C. For ATR measurements, a Perkin-Elmer multiple internal reflection accessory was used with a Ge 45° or ZnSe 45° internal reflection element (IRE) and a wide zone MCT (mercury–cadmium–tellurium) detector operated at liquid nitrogen temperature.

The solvent polymeric membranes were placed in contact, when necessary, with sample solutions prior to the FT-IR-ATR measurements as follows. An ionophore-incorporated membrane was stuck (without glue, of course) on the bottom of a beaker which contained a conditioning solution and soaked (conditioned) for 30 min; the conditioning solution was replaced with a sample solution containing a primary ion salt and the membrane was kept in contact with this solution for a further 30 min with stirring. The membrane thus treated was peeled off the bottom of the beaker and wiped gently with Kimwipe (Wipers S-200, Jujyo-Kimbary, Tokyo) to remove excess of solution visible on the membrane surface. One side of the membrane exposed to the sample solution was stuck on the IRE surface with careful manipulation, avoiding for air bubbles remaining between the IRE and the sample membrane. Reproducible ATR spectra of the membranes were obtained by keeping the above treatment conditions strictly the same, e.g., the same stirring speed and time. Blank membranes having an identical composition of plasticizer and PVC but containing no ionophore were also treated in the same manner and were used for recording the difference spectra as described below.

Well resolved spectra for an ionophore and its complex were obtained by subtracting the spectrum of a blank membrane from that of the corresponding sample membrane (difference spectra), otherwise the large background spectrum arising from PVC and plasticizer would preclude interpretation of the spectrum from the sample membrane of interest.

ATR spectra of ionophores and their complexes in the solid phase (cast films) which were deposited directly on the IRE by allowing their chloroform or methanol solutions to evaporate were also recorded as a reference for use for spectral assignments for the sample membranes.

Calculation of penetration depth of IR beam. The penetration depth d_p of an IR beam into a sample membrane is a function of the refractive indices, n_1 and n_2, of the IRE used and of the membrane, respectively, the angle of incidence, θ, of the IR beam into the IRE, and wavelength, λ, in μm [19]:

$$d_p = \lambda / 2\pi n_1 \left[\sin^2\theta - (n_2/n_1)^2\right]^{-1/2} \quad (1)$$

The value of d_p in this study using the Ge 45° IRE was calculated to be in the range 0.31–0.60 μm, by inserting 4.0 and 1.5 for n_1 and n_2 [20], respectively, 45° for θ and 4.8–9.1 μm for λ (2100–1100 cm^{-1}). Also for the ZnSe 45° IRE ($n_1 = 2.4$), the calculated penetration depths were 1.8 and 1.0 μm, respectively, with 45° and 60° for θ and 9.1 μm (1100 cm^{-1}) for λ.

Determination of a stoichiometry standard of the IR intensity ratio for the counter anions to the complexed cations. As described (see above), a determination was made of a practical stoichiometry standard for the IR intensity ratio that reflects the stoichiometric ratio of the counter anions to the complexed cations which was utilized to discuss the amount of uptake into the membrane of the counter anion relative to that of the complexed cations. For quantitative analysis using IR spectrometry, the peak height is usually measured rather than the band area, assuming that the half band width of each band of the sample has its own value depending on the physical state of the sample (solid, liquid, solution, etc.), and that it does not change as long as the sample is under the same conditions. The latter assumption is valid in the present experimental

TABLE 1

IR peak-height ratios of the anions to the complexed cations transported into the ionophore-incorporated membranes treated by contact with the primary ion solutions [a]

Concentration primary ion salt [b] (M)	$I_{anion}/I_{complexed\ cation} \pm$ S.D. [c]		
	ETH 129+ KTpClPB	ETH 129	VM
1.0×10^{-4}	0	–	–
1.0×10^{-3}	0.22±0.03	0.13±0.01	0.05±0.02
1.0×10^{-2}	–	0.16±0.01	0.13±0.01
1.0×10^{-1}	–	0.18±0.02	0.14±0.01
Stoichiometric standard value [d]	0.76±0.01	0.17±0.01	0.14±0.01

[a] Compositions of each membrane used are the same as those in Table 2. [b] $Ca(SCN)_2$ for ETH 129 and KSCN for VM. [c] Standard deviations for triplicate measurements. The wavenumbers at each key band intensity of which was used for obtaining the $I_{anion}/I_{complexed\ cation}$ are as follows: 2060 cm^{-1} (SCN^-) and 1644 cm^{-1} (C=O) for the ETH 129+KTpClPB-based membrane; 2054 cm^{-1} (SCN^-) and 1644 cm^{-1} (C=O) for the ETH 129-based membrane; 2054 cm^{-1} (SCN^-) and 1740 cm^{-1} (COO) for the VM-based membrane. [d] Obtained with membranes with $[Ca(ETH\ 129)_3](SCN)_2$ or [K(VM)]SCN incorporated (see Experimental for details); their membrane compositions are the same as those in Table 2.

approach performed as follows. Peak heights for the anion- and complex-related bands, I_{anion} and $I_{complexed\ cation}$, respectively, were measured, first, from an ATR difference spectrum for the membrane with a stoichiometric complex salt incorporated, the ratio $I_{anion}/I_{complexed\ cation}$, which reflects the stoichiometry between the complexed cation and corresponding counter anion, was calculated as a practical stoichiometry standard. The stoichiometry standard values thus obtained for some different complex salts are listed in Table 1. A given sample membrane with a given amount of uncomplexed ionophore incorporated under otherwise identical conditions was measured in the same manner after being in contact with an aqueous solution of a primary ion salt. If the $I_{anion}/I_{complexed\ cation}$ ratio for the sample membrane is smaller than the corresponding standard value in Table 1, it may be concluded that the amount of uptake into the membrane of the counter anion is smaller than that of the complexed cation. Likewise, stoichiometric uptake may be concluded when the ratio obtained is equal to a corresponding stoichiometry standard in Table 1.

RESULTS AND DISCUSSION

Complete cation permselectivity: exclusion of counter anions

Figure 2 shows a typical ATR difference spectrum for the bis(benzo-15-crown-5)-incorporated membrane treated by contact with 0.1 M K_2SO_4 [Fig. 2A(a)]. Compared with the same membrane treated with 0.1 M LiCl conditioning solution

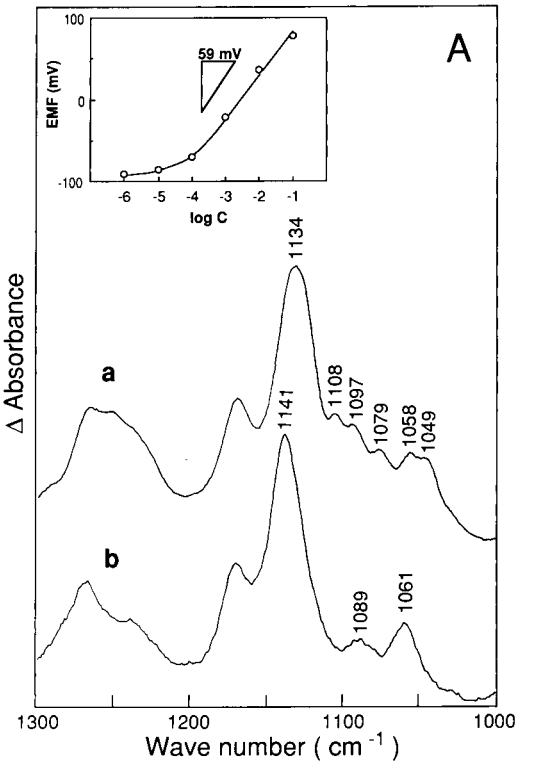

Fig. 2A. ATR difference spectra of (a) a bis(benzo-15-crown-5)-based PVC membrane treated by contact with 0.1 M K_2SO_4 solution for 30 min, and (b) a bis(benzo-15-crown-5)-based PVC membrane itself. Both the membranes were pretreated with 0.1 M LiCl solution for 30 min (conditioning). IRE used, Ge 45°; incidence angle, 45°. Inset: potentiometric response of the bis(benzo-15-crown-5)-based liquid membrane electrode to K_2SO_4 solutions. Ionic strength, 0.1 M (LiCl). Membrane composition (wt.%): bis(benzo-15-crown-5) 2.9, DOS 64.7 and PVC 32.4.

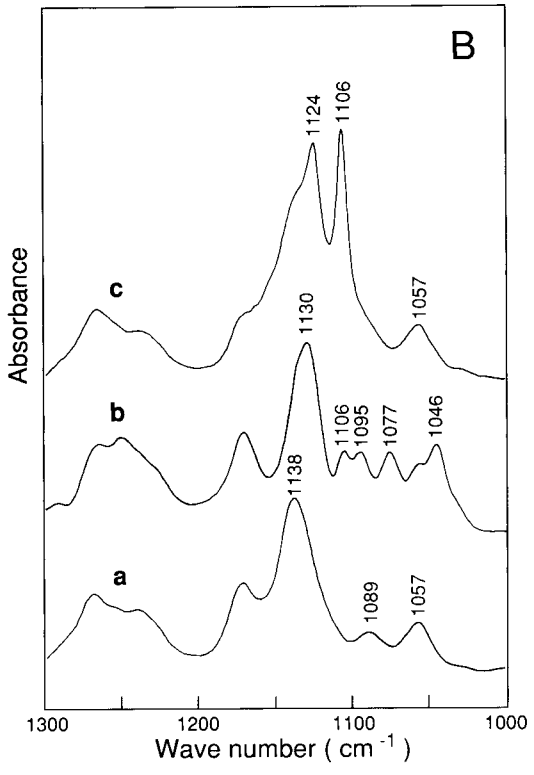

Fig. 2B. ATR spectra of the cast films of (a) bis(benzo-15-crown-5), (b) {K[bis(benzo-15-crown-5)]}SCN and (c) $\{K[bis(benzo\text{-}15\text{-}crown\text{-}5)]\}_2SO_4$. Strong bands at 1106 and 1124 cm^{-1} in (c) are assigned to SO_4^{2-}. IRE used, Ge 45°; incidence angle, 45°.

[Fig. 2A(b)], some clear changes in the spectrum were observed.

On the basis of the cast films of bis(benzo-15-crown-5), {K[bis(benzo-15-crown-5)]}SCN and $\{K[bis(benzo\text{-}15\text{-}crown\text{-}5)]\}_2SO_4$ itself [Fig. 2B(a), (b) and (c), respectively], the above-mentioned changes in the spectra may be ascribed to the formation of the K^+–bis(benzo-15-crown-5) complex in the boundary layer of the membrane. At the same time, importantly, the bands of sulphate, the counter anion, at 1124 and 1106 cm^{-1} [Fig. 2A(a)] were not present, in contrast to the case for the cast film of $\{K[bis(benzo\text{-}15\text{-}crown\text{-}5)]\}_2SO_4$, as shown in Fig. 2B(c). This result indicates that the permselective uptake of K^+ by the membranous bis(benzo-15-crown-5) took place in the surface region of the membrane, leaving the counter anion, SO_4^{2-}, in the adjacent aqueous solution, i.e., $C_{(K^+\text{-crown complex})} \gg C_{(SO_4^{2-})} \approx 0$ (C = concentration).

An ATR spectrum of the dibenzyl-14-crown-4-based membrane treated with 1.0 M $LiNO_3$ solution also showed complex formation with Li^+ without accompanying NO_3^-: the peak at 1090 cm^{-1} responsible for the Li^+–crown complex, but no strong NO_3^- bands at 1403 and 1331 cm^{-1} were found (not shown).

The above FT-IR-ATR data provided clear evidence for complete cation permselectivity: uptake of the primary ion, K^+ or Li^+, into a shallow boundary layer of the membrane, leaving the counter anions, SO_4^{2-} and NO_3^-, in the adjacent aqueous solutions. Also, the potentiometric response curves of these membranes for K_2SO_4 (inset in Fig. 2A) and $LiNO_3$ solutions (not shown) exhibited Nernstian slopes up to 0.1 and 1.0 M K^+ and Li^+, respectively.

Figure 3 shows the effect of the penetration depths on the change in the ATR difference spectra of bis(benzo-15-crown-5)-based liquid membranes in contact with 0.1 M K_2SO_4 solution. On increasing the penetration depth, the IR peak intensity for the K^+–complex cation was found to decrease: the peaks from the complexed cation dominate in spectrum (a), the peaks from both the complexed cation and uncomplexed ionophore in spectrum (b) and only the peaks from the uncomplexed ionophore appeared in spectrum (c). No sulphate bands appeared in any of the above spectra. From these results, there seems to be complete cation permselectivity in the region < 1.8 μm in depth. In other words, the complexed cation does not seem to diffuse deeper than 1.8 μm into the membrane should the corresponding counter anion be sufficiently hydrophilic, such as SO_4^{2-}.

Another interesting example of the penetration depth dependence is demonstrated in the following system. First, the spectral change from Fig. 4a to c for membranes incorporating VM and [K(VM)]SCN, respectively, and the data in Table 2, taken together, demonstrate three key bands for K^+–VM complex formation (see Table 2 and [21]). The spectrum of a VM-incorporated membrane in contact with 0.1 M K_2SO_4 solution was found to exhibit some unique behaviour in each

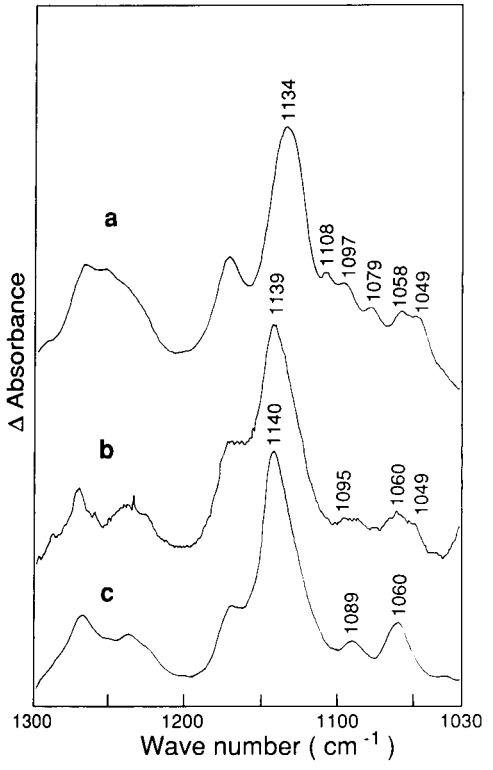

Fig. 3. Effect of the penetration depth, d_p, on ATR difference spectra of bis(benzo-15-crown-5)-based PVC membranes treated by contact with 0.1 M K_2SO_4 solution for 30 min. The penetration depths were calculated at 1100 cm^{-1} (see Experimental) as follows: (a) 0.60 μm (IRE, Ge 45°; incidence angle, 45°); (b) 1.0 μm (IRE, ZnSe 45°; incidence angle, 60°); (c) 1.8 μm (IRE, ZnSe 45°; incidence angle, 45°). Membrane composition (wt.%): bis(benzo-15-crown-5) 2.9, DOS 64.7 and PVC 32.4.

band shift (Fig. 4b): there was a small band at 1743 cm^{-1} ($d_p = 0.38$ μm) for the complexed VM in addition to the band at 1754 cm^{-1} for the uncomplexed VM; there was another band shift from 1662 cm^{-1} for the uncomplexed VM to 1658 cm^{-1} ($d_p = 0.40$ μm) for the mixture of complexed and uncomplexed VM, whereas the band at 1185 cm^{-1} for the uncomplexed VM did not shift to 1195 cm^{-1} ($d_p = 0.55$ μm), assigned to the complexed VM, and sulphate-related bands also did not appear (the calculated penetration depths, d_p, at each corresponding wave number are given hereafter, if necessary in parentheses).

It should be noted that as the penetration depth is dependent on the wavenumber, the location (depth) of each functional group from which the signal arises is different. On the basis of this understanding, the fact that the band shifts were selectively observed only for two (1743 and 1658 cm^{-1}) of the three known key bands for K^+–VM complexation (see above and Table 2) may be used as a sound means of locating the complexed VM in the membrane. These considerations and the above results, taken together, demonstrate again that the complexed cation dominates only near the interface in the membrane, ca. 0.40 μm in this instance, and does not diffuse to a deeper region such as $d_p \approx 0.55$ μm. The difference in the deepest depth observed for cation permselectivity between the K^+–bis(benzo-15-crown-5) and K^+–VM complex cations probably reflects the

TABLE 2

Characteristic bands (cm^{-1}) for the uncomplexed and complexed ionophores dissolved in the solvent polymeric membranes

Uncomplexed ionophore		Complexed ionophore	
VM [a]	1754 (COO)	[K(VM)]SCN [b]	2054 (SCN^-)
	1660 (C=O)		1740 (COO)
	1185 (-C-O-C-)		1654 (C=O)
			1195 (-C-O-C-)
ETH 129 [c]	1648 (C=O)	$[Ca(ETH\ 129)_3](SCN)_2$ [d]	2060 (SCN^-)
(+KTpClPB)		(+KTpClPB)	1644 (C=O)
ETH 129 [e]	1657 (C=O)	$[Ca(ETH\ 129)_3](SCN)_2$ [f]	2054 (SCN^-)
	1642 (C=O)		1644 (C=O)

[a–f] Compositions of each membrane are as follows (wt.%): [a] VM 1.0, o-NPOE 66.0 and PVC 33.0; [b] [K(VM)]SCN 1.0 o-NPOE 66.0 and PVC 33.0; [c] ETH 129 1.0, KTpClPB 0.5, o-NPOE 65.7 and PVC 32.8; [d] $[Ca(ETH\ 129)_3](SCN)_2$ 1.1, KTpClPB 0.5, o-NPOE 65.6 and PVC 32.8; [e] ETH 129 1.0, o-NPOE 66.0 and PVC 33.0; [f] $[Ca(ETH\ 129)_3](SCN)_2$ 1.1, o-NPOE 65.3 and PVC 32.6.

higher hydrophobicity of K^+–bis(benzo-15-crown-5) compared with K^+–VM complex cations. The greatest depths reached by K^+–bis(benzo-15-crown-5) and K^+–VM in the membrane, which was discussed above, were estimated using the respective key bands at 1049 cm^{-1} for K^+–bis(benzo-15-crown-5) (–C–O–C–) and 1195 cm^{-1} for K^+–VM (–C–O–C–). The difference led to an error of only 0.08 μm for the difference between the two depths; the Ge 45° IRE was used with an incidence angle of 45° in this instance. The observed values for the depth were at least 1.0 and 0.4 μm for K^+–bis(benzo-15-crown-5) and K^+–VM complexed cations, respectively, for which the difference is 0.6 μm. The possibility that the difference in the depths between the two systems might originate from the difference in the wavenumbers of the observed key bands is thus precluded.

When PVC-COOH was used instead of PVC as a polymer matrix to test the effect of so-called added anionic sites [22,23], the K^+–VM ion was found to be present deeper in the membrane. The ATR difference spectrum of the VM-based PVC-COOH membranes treated with 0.1 M K_2SO_4 (Fig. 5b) exhibited three typical peaks arising from the K^+–VM complex [1740 cm^{-1} ($d_p = 0.38$ μm), 1655 cm^{-1} ($d_p = 0.40$ μm) and 1194 cm^{-1} ($d_p = 0.55$ μm)] and no peaks appeared from sulphate ions. Permselective cation uptake was again observed, but in this instance the complex cation was found at a penetration depth as great as 0.55 μm. The number of K^+ transported into the PVC-COOH-type membrane would generally be greater than into that of its PVC counterpart (see above). The electrode response to K^+ was improved, probably as a result (see insets in Figs. 4 and 5). A similar result concerning the effect of added anionic sites was also found on comparing the membranes incorporating ETH 129 alone, and both ETH 129 and KTpClPB, in contact with $CaSO_4$ solutions. The increase in the number of K^+ or Ca^{2+} transported into the phase boundary of the PVC-COOH-type or KTpClPB-incorporated membranes discussed above may be relevant to a

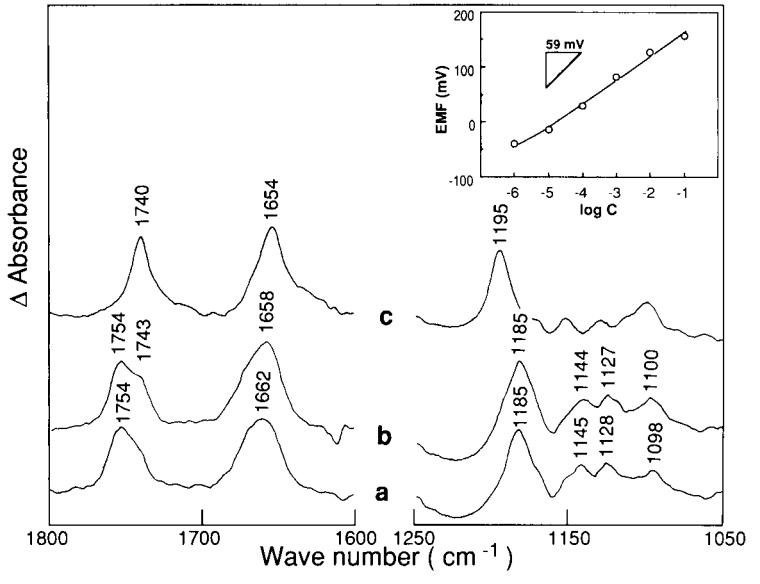

Fig. 4. ATR difference spectra of (a) a VM-based PVC membrane and (b) a VM-based PVC membrane treated by contact with 0.1 M K_2SO_4 solution for 30 min. Both membranes were pretreated with 0.1 M LiCl solution for 30 min (conditioning). An ATR difference spectrum (c) of a [K(VM)]SCN-based PVC membrane is also shown. IRE used, Ge 45°; incidence angle, 45°. Inset: potentiometric response of the VM-based PVC membrane electrode to K_2SO_4 solutions. Ionic strength, 0.1 M (LiCl). Composition of the VM-based membrane (wt.%): VM 1.0, o-NPOE 66.0 and PVC 33.0. Composition of the [K(VM)]SCN-based membrane (wt.%): [K(VM)]SCN 1.0, o-NPOE 66.0 and PVC 33.0.

previous finding that the cation-exchange capacity of a PVC-COOH blank membrane is three times larger than that of a PVC blank membrane [22].

Incomplete cation permselectivity: non-stoichiometric and stoichiometric uptake of cations and counter anions

Although complete cation selectivity was observed for the membrane containing both ETH 129 and KTpClPB treated by contact with $Ca(SCN)_2$ solutions of concentrations $\leqslant 1.0 \times 10^{-4}$ M, this trend did not continue with higher $Ca(SCN)_2$ concentrations. Figure 6 shows ATR difference spectra of the membranes treated with (a) 0.1 M KCl (conditioning) and (b) 1.0×10^{-4} and (c) 1.0×10^{-3} M $Ca(SCN)_2$ solutions. Comparison between spectra (a) and (b) indicates that the band for the complexed ionophore with Ca^{2+}, Ca^{2+}–ETH 129, appeared and the band for the uncomplexed ionophore disappeared, whereas no band from SCN^- appeared, which again reflects that permselective uptake of Ca^{2+} occurred (see Tables 1 and 2). In this concentration range, the

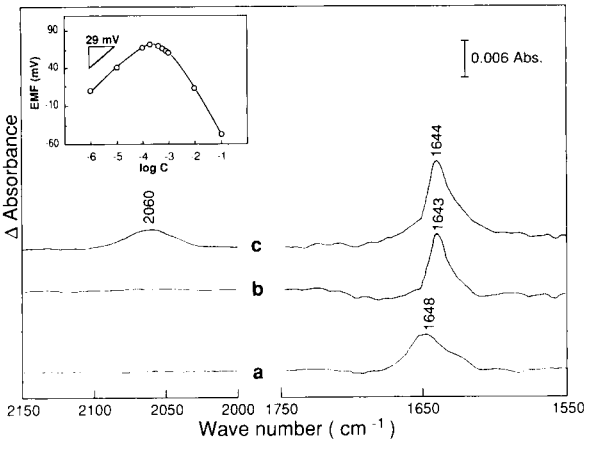

Fig. 6. ATR difference spectra of ETH 129–KTpClPB-based PVC membranes treated by contact with (a) 0.1 M KCl solution for 30 min (conditioning) and (b) 1.0×10^{-4} and (c) 1.0×10^{-3} M $Ca(SCN)_2$ solutions for 30 min. In the last two instances, the membranes were preconditioned with 0.1 M KCl solution for 30 min before treatment with the $Ca(SCN)_2$ solutions. IRE used, Ge 45°; incidence angle, 45°. Inset: potentiometric response of the ETH 129–KTpClPB-based PVC membrane electrode to $Ca(SCN)_2$ solutions. Ionic strength, 0.1 M (KC). Membrane composition (wt.%): ETH 129 1.0, KTpClPB 0.5, o-NPOE 65.7 and PVC 32.8.

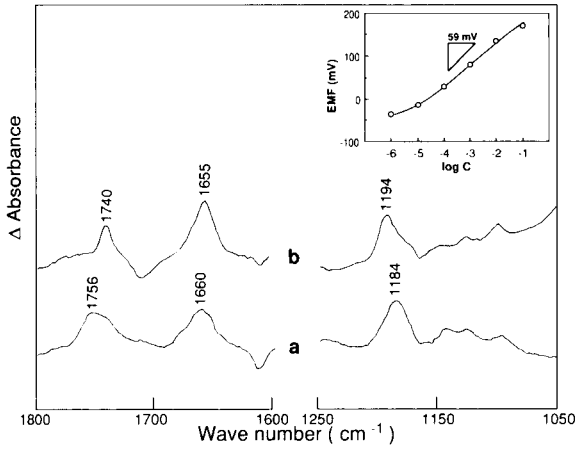

Fig. 5. ATR difference spectra of (a) a VM-based PVC-COOH membrane and (b) a VM-based PVC-COOH membrane treated by contact with 0.1 M K_2SO_4 solution for 30 min. Both membranes were pretreated with 0.1 M LiCl solution for 30 min (conditioning). IRE used, Ge 45°; incidence angle, 45°. Inset: potentiometric response of the VM-based PVC-COOH membrane electrode to K_2SO_4 solutions. Ionic strength, 0.1 M (LiCl). Membrane composition (wt.%): VM 1.0, o-NPOE 66.0 and PVC-COOH 33.0.

electrode response was found to be Nernstian (see inset in Fig. 6). When the same membrane was placed in contact with concentrations of $Ca(SCN)_2 \geqslant 1.0 \times 10^{-3}$ M, spectral bands from both the complexed cation, Ca^{2+}–ETH 129 (1644 cm^{-1}), and SCN^- (2060 cm^{-1}) appeared, reflecting that uptake of SCN^- ions also took place (Fig. 6c). The value of $I_{SCN^-}/I_{Ca^{2+}\ complex}$ obtained in this instance is 0.22 ± 0.03, which is smaller than the corresponding stoichiometric standard of 0.76 ± 0.01 (see Table 1). From this it is concluded that non-stoichiometric uptake of both Ca^{2+} and SCN^-, $C_{Ca^{2+}\ complex} > C_{SCN^-}$, took place in the phase boundary of the membrane. In other words, there is incomplete cation permselectivity in this instance. Also, the slope of the electrode response deviates from Nernstian (see inset in Fig. 6) at this concentration. However, it should be noted that at each concentration above 1.0×10^{-3} M, the observed potential was still more positive than that of the corresponding conditioning potential in 0.1 M KCl solution, which

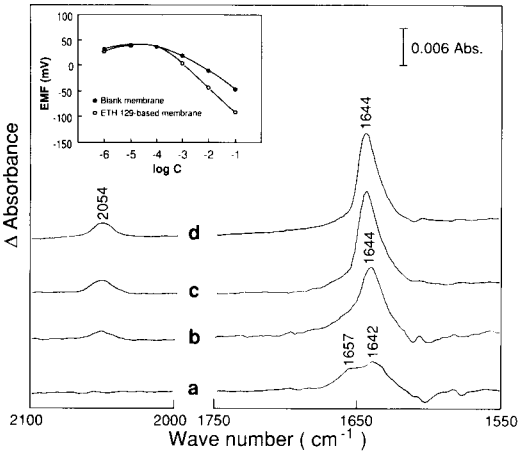

Fig. 7. ATR difference spectra of ETH 129-based PVC membranes treated by contact with (a) 0.1 M KCl solution for 30 min (conditioning) and (b) 1.0×10^{-3} (c) 0.01 and (d) 0.1 M $Ca(SCN)_2$ solutions for 30 min. In the last three instances, the membranes were preconditioned with 0.1 M KCl solution for 30 min before being treated with $Ca(SCN)_2$ solutions. IRE used, Ge 45°; incidence angle, 45°. Inset: potentiometric responses of the ETH 129-based PVC membrane and blank PVC membrane electrodes to $Ca(SCN)_2$ solutions. Ionic strength, 0.1 M (KCl). Composition (wt.%) of the ETH 129-based membrane: ETH 129 1.0, o-NPOE 66.0 and PVC 33.0. Composition of the blank membrane (wt.%): o-NPOE 67.0 and PVC 33.0.

means that the potential is still of cationic origin, although the slope is negative.

Without KTpClPB in the membrane, the uptake of SCN^- ion into the ETH 129-based membrane increased relative to that of the complexed cation, Ca^{2+}–ETH 129. Figure 7 shows ATR difference spectra of the ETH 129-based membranes treated by contact with (a) 0.1 M KCl (conditioning) and (b) 1.0×10^{-3}, (c) 0.01 and (d) 0.1 M $Ca(SCN)_2$ solutions. Uptake of Ca^{2+} by the membranous ETH 129 was revealed by the disappearance of bands for the uncomplexed ETH 129 (1657 and 1642 cm^{-1}) and the appearance of the band for the complexed ETH 129 (1644 cm^{-1}) (see Table 2). A band from SCN^- (2054 cm^{-1}) was also observed for all the membranes treated by contact with $Ca(SCN)_2$ solutions, reflecting the occurrence of SCN^- uptake. The peak-height ratios obtained for the membrane treated with different concentrations of $Ca(SCN)_2$ are listed in Table 1. The value of 0.13 ± 0.01 for $I_{SCN}/I_{Ca^{2+}}$ complex for the membrane treated with 1.0×10^{-3} M $Ca(SCN)_2$ compared with a corresponding stoichiometry standard value of 0.17 ± 0.01 is only slightly smaller, suggesting that cation permselectivity is poorly established in this instance. Further, with increase in $Ca(SCN)_2$ concentration up to and above 0.01 M, there is equal uptake of Ca^{2+} and SCN^- (see Table 1), which may be regarded as complete loss of cation permselectivity.

The ATR results obtained above for the ETH 129-based membranes with and without KTpClPB suggest that KTpClPB resisted and inhibited by as much as 70% the uptake of SCN^- into the membrane phase, which trend is in consistent with many of the previous findings relevant to the so-called anion effect in ionophore-incorporated liquid membrane ISEs [23]. As is well known, the electrode response of the ETH 129-based mem-

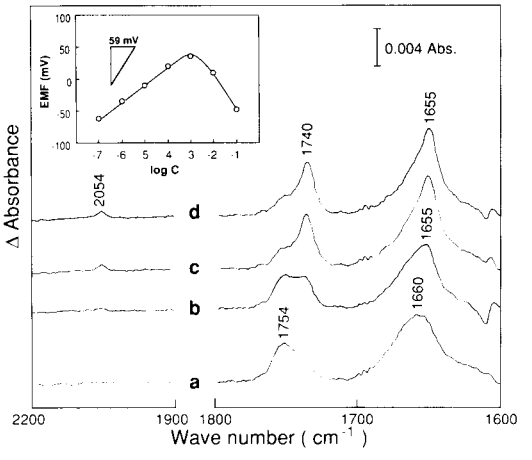

Fig. 8. ATR difference spectra of VM-based PVC membranes treated by contact with (a) 0.1 M LiCl solution for 30 min (conditioning) and (b) 1.0×10^{-3}, (c) 0.01 and (d) 0.1 M KSCN solutions for 30 min. In the last three instances, the membranes were preconditioned with 0.1 M LiCl solution for 30 min before being treated with KSCN solutions. IRE used, Ge 45°; incidence angle, 45°. Inset: potentiometric response of the VM-based PVC membrane electrode to KSCN solutions. Ionic strength, 0.1 M (LiCl). Membrane composition (wt.%): VM 1.0, o-NPOE 66.0 and PVC 33.0.

branes with KTpClPB was superior to that of the ETH129-based membranes without KTpClPB (see insets in Figs. 6 and 7).

The VM-incorporated membranes treated by contact with KSCN solutions also showed both non-stoichiometric and stoichiometric uptake of SCN^- depending on the KSCN concentration, as shown in Fig. 8 and Table 1. Non-stoichiometric uptake of K^+ and SCN^- ions, $C_{K^+ complex} > C_{SCN^-}$, occurred with 1.0×10^{-3} M KSCN solution, whereas higher KSCN concentrations led to complete loss of cation permselectivity.

Conclusions

By observing relatively thin boundary layers, 0.31–1.8 μm, of ionophore-incorporated liquid membranes by FT-IR-ATR spectrometry, it was clearly possible to discriminate between liquid–liquid extraction and permselective ionic transport (charge separation) processes at the aqueous/organic interface.

The depths where complete permselective behaviour for cations was observable with exclusion of counter anions were found to be as great as 1.0 μm. Among factors that govern the magnitude of this depth, the types of ionophores used and the presence of added anionic sites in the membrane were found to be significant.

We thank Professors S. Ikawa and K. Uosaki, Department of Chemistry, Faculty of Science, Hokkaido University, for helpful discussions on IR spectra and for the use of the Model FTS-30 FT-IR spectrometer (Bio-Rad), respectively. Financial support to Y.U. from the Ministry of Education, Science and Culture, Japan, is gratefully acknowledged. The major part of the experimental work presented in this study was performed during the tenure (until March 1993) of Y.U. at the Department of Chemistry, Faculty of Science, Hokkaido University, Sapporo.

REFERENCES

1 R. Kellner, G. Götzinger, E. Pungor, K. Tóth and L. Polos, Fresenius' Z. Anal. Chem., 319 (1984) 839.
2 R. Kellner, G. Götzinger, E. Pungor, K. Tóth and L. Polos, in E. Pungor (Ed.), Ion-Selective Electrodes, Vol. 4, Akadémiai Kiadó, Budapest, 1984, p. 501.
3 R. Kellner, G. Fischbock, G. Götzinger, E. Pungor, K. Tóth, E. Polos and E. Lindner, Fresenius' Z. Anal. Chem., 322 (1985) 151.
4 R. Kellner, E. Zippel, E. Pungor, K. Tóth and E. Lindner, Fresenius' Z. Anal. Chem., 328 (1987) 464.
5 K. Tóth, E. Lindner, E. Pungor, E. Zippel and R. Kellner, Fresenius' Z. Anal. Chem., 331 (1988) 448.
6 M. Sugawara, X.M. Lin, K. Umezawa, S. Nishizawa and Y. Umezawa, in T. Sekine (Ed.), Proc. Int. Solvent Extraction Conf. (ISEC '90), Part B, Elsevier, Amsterdam 1992, 1549.
7 J.H. Boles and R.P. Buck, Anal. Chem., 45 (1973) 2057.
8 W.E. Morf and W. Simon, Helv. Chim. Acta, 69 (1986) 1120, and references cited therein.
9 A.P. Thoma, A. Viviani-Nauer, S. Arvanitis, W.E. Morf and W. Simon Anal. Chem., 49 (1977) 1567.
10 W.E. Morf, P. Wuhrman and W. Simon, Anal. Chem., 48 (1976) 1031.
11 U. Fiedler, Anal. Chim. Acta, 89 (1977) 101.
12 A. Craggs, G.J. Moody, J.D.R. Thomas and A. Willcox, Talanta, 23 (1976) 799.
13 A.M.Y. Jaber, G.J. Moody, J.D.R. Thomas and A. Willcox, Talanta, 24 (1977) 655.
14 B. Doyl, J.G. Moody and J.D.R. Thomas, Talanta, 29 (1982) 257.
15 K. Neupert-Laves and M. Dobler, J. Crystallogr. Spectrosc. Res., 12 (1982) 287.
16 E. Pretsch, D. Ammann, H.F. Osswald, M. Güggi and W. Simon, Helv. Chim. Acta, 63 (1980) 191.
17 C.J. Pederson, J. Am. Chem. Soc., 89 (1967) 7017.
18 G.J. Moody, R.B. Oke and J.D.R. Thomas, Analyst, 95 (1970) 910.
19 N.J. Harrick, Internal Reflection Spectroscopy, Interscience, New York, 1967, p. 30.
20 T. Rosatzin, P. Holy, K. Seiler, B. Rusterholz and W. Simon, Anal. Chem., 64 (1992) 2029.
21 V.A. Howarth, M.C. Petty, G.H. Davies and J. Yarwood, Langmuir, 5 (1989) 330.
22 E. Lindner, E. Gráf, Z. Niegreisz, K. Tóth, E. Pungor and R.P. Buck, Anal. Chem., 60 (1988) 295.
23 D. Ammann, W.E. Morf, P. Anker, P.C. Meier, E. Pretsch and W. Simon, Ion-Sel. Electrode Rev., 5 (1983) 3.

Analytica Chimica Acta, 282 (1993) 259–264
Elsevier Science Publishers B.V., Amsterdam

Selectivity of plasticized poly(vinyl chloride)-based ion-selective electrodes

Viola Horváth and George Horvai

Technical University of Budapest, Institute for General and Analytical Chemistry, Szt. Gellért tér 4, H-1111 Budapest (Hungary)

(Received 6th May 1993)

Abstract

Radiotracer experiments were used to investigate the selectivity of ion-exchange processes of plasticized poly(vinyl chloride)-based ion-selective electrode membranes doped with neutral carrier as the active material. Four different neutral carriers were studied. The ion-exchange selectivity of the membranes was closely correlated with their potentiometric selectivity.

Keywords: Ion-selective electrodes; Potentiometry; Selectivity

One of the most intriguing questions concerning neutral carrier ion-selective membranes is the origin and nature of their potentiometric selectivity. This property of the electrode, i.e., the ability to differentiate potentiometrically between various ions, can be quantified by the well known Nikolsky equation:

$$\Delta\phi_{eq} = \Delta\phi'_{eq} + \frac{RT}{z_M F} \ln\left[a_M + \sum_I k^{pot}_{M-I}(a_I)^{z_M/z_I}\right] \quad (1)$$

where $\Delta\phi_{eq}$ is the equilibrium potential, $\Delta\phi'_{eq}$ is the standard potential, a_M is the activity of the measured ion M, a_I is the activity of the individual interfering ions I, z_M is the "charge" of the measured or primary ion, z_I is the "charge" of the interfering ion and k^{pot}_{M-I} is the potentiometric selectivity coefficient (measured ion/interfering on). The term k^{pot}_{M-I} used to be called the selectivity constant because in many instances it is nearly independent of concentration, but this is not generally true. In addition, this coefficient also depends on the method of determination.

Since the introduction of neutral carrier ion-selective electrodes, it has always been an issue to correlate this empirical coefficient with a physico-chemical property of a plasticized poly(vinyl chloride) (PVC) membrane. Based on theoretical work of Ciani, Eisenmann and Szabo [1] related to bilayer membranes, Morf [2] set up a correlation between the potentiometric selectivity and the stability constants of the different neutral carrier–ion complexes. He deduced the following equation:

$$k^{pot}_{M-I} \approx \beta^{w}_{IS}/\beta^{w}_{MS} \quad (2)$$

where S denotes the neutral carrier, β^{w}_{IS} is the stability constant of the neutral carrier–interfering ion complex in the aqueous phase and, β^{w}_{MS} is the stability constant of the neutral carrier–measured ion complex in the aqueous phase.

This means that the potentiometric selectivity coefficient can be expressed as the ratio of the complex stability constants of MS and IS in the aqueous phase. The experimental verification of

Correspondence to: G. Horvai, Technical University of Budapest, Institute for General and Analytical Chemistry, Szt. Gellért tér 4, H-1111 Budapest (Hungary).

this theory runs into a problem. As the solubility of these complexes in water is very low, it is difficult to find an appropriate analytical technique to provide measurements so that the stability constants β_{IS}^{w} and β_{MS}^{w} can be calculated.

Some workers have tried to overcome this problem by adding an organic solvent (e.g., ethanol) to the aqueous phase, and in some instances this led to acceptable results, i.e., the ratio of the found stability constants correlated well with the potentiometric selectivity constant [3,4]. In other work, k_{M-I}^{pot} was related to the transport selectivity of the PVC membrane [5]. It was proved in electrodialysis experiments that the ratio of cross-membrane transport numbers of different ions was closely related to the potentiometric selectivity.

Cammann [6] and Xie and Cammann [7,8] assumed a kinetic origin of selectivity. They carried out experiments to prove that ion transfer through the membrane/water interface was kinetically more hindered for the interfering ions than for the measured ion. They quantified the kinetic hindrance with the exchange-current density calculated from the charge-transfer resistance and found a fairly good correlation between the potentiometric selectivity and the measured kinetic parameter. Other workers could not support this model on conducting similar experiments [9].

In this paper, experimental evidence is provided that the potentiometric selectivity coefficient of a plasticized PVC-based ion-selective electrode (ISE) membrane can be closely correlated with the selectivity of the ion-exchange processes between the membrane and the bathing solution. Earlier work showed that these membranes behave as low-capacity ion exchangers [10]; the ion-exchange capacity is between 1×10^{-4} and 2×10^{-4} M. Preliminary experiments [11] demonstrated that the ion-exchange process is selective, i.e., the membrane takes up more preferred ion than interfering ion if their concentrations in the aqueous bathing solution are equal. This finding is quantified in this paper by radiotracer experiments conducted with neutral carrier ISE membranes of different types.

EXPERIMENTAL

Chemicals and membrane preparation

The ion-selective electrode membranes were prepared by the method of Craggs et al. [12] by weighing the components into a glass vial, then dissolving them in 2 ml of tetrahydrofuran and casting into a PTFE ring (21 mm diameter). After evaporation of the solvent a thin (100–200 μm) membrane resulted. The compositions of the membranes studied are given in Table 1.

TABLE 1

Compositions of the membranes studied

Selectivity	Weight of PVC (mg)	Plasticizer [a]	Neutral carrier	Salt additive [b]
K^+-selective	50	100 mg DOS	0.75 mg valinomycin	–
K^+-selective	50	100 mg DOS	0.75 mg valinomycin	0.0015 mg KCl
K^+-selective	50	100 mg DOS	0.75 mg valinomycin	0.17 mg KTpClPB
NH_4^+-selective	50	100 mg DOS	0.75 mg nonactin	0.25 mg KTpClPB
Na^+-selective	50	100 mg DOS	0.75 mg Na-II ionophore	–
Ca^{2+}-selective	33	66 mg oNPOE	0.5 mg Ca-I ionophore	0.17 mg KTpClPB

[a] DOS = bis(2-ethylhexyl) sebacate; oNPOE = 2-nitrophenyl octyl ether. [b] KTpClPB = potassium tetrakis(*p*-chlorophenylborate).

The PVC powder was Corvic S704, from ICI. All other chemicals in Table 1 were Fluka products. The chemicals used for making the aqueous solutions were of analytical-reagent grade. Water was doubly distilled in quartz apparatus. To follow the ion-exchange process ^{137}Cs and ^{85}Sr radiotracers were used as aqueous solutions.

Potentiometric behaviour of the membranes

The potentiometric selectivity coefficients were determined by the separate solution method in 0.1 M solutions.

Apparatus

γ-Radiation was measured with an ND 131/F detector (Gamma Works, Budapest). To detect β-radiation an ND 304 scintillation detector (Gamma Works) was used. These detectors were connected to an NK 225/8 nuclear spectrometer (Gamma Works).

Procedure

To study the ion-exchange process, membranes were soaked in the radioactive bathing solutions in a plastic container until no more isotope uptake occurred. This process usually took 2 days. Activity measurements were made after washing the membranes with doubly distilled water and drying with filter-paper. The measured counts were corrected for self-absorption by the membrane.

To study the selectivity of the ion-exchange process, interfering ions were added to the radioactive bathing solution in different concentrations and the radiotracer concentration of the membrane was measured after equilibrium had been reached.

RESULTS AND DISCUSSION

Selectivity of the valinomycin-based K^+-selective membrane

In order to study the effect of interfering ions on the ion-exchange process of a K^+-selective PVC membrane, all of its ion-exchange sites were saturated with $^{137}Cs^+$ ions. Subsequently another salt (KCl, NaCl or NH_4Cl) was added to the bathing solution in increasing amounts. The ^{137}Cs content of the membrane was checked after equilibrium had been reached, i.e., when no further variation in the Cs^+ concentration of the membrane occurred. It was found that the original Cs^+ content of the membrane was partly exchanged by the interfering ions. (In the following experiments the radioactively labelled ion is referred to as the measured ion and all other ions are considered as interfering ions, even if the potentiometric selectivity for a particular ion is better than for the labelled ion.) The results are shown in Fig. 1. The ratio of the Cs^+ concentration to interfering ion concentration in the aqueous phase is plotted on the abscissa on a logarithmic scale. The ordinate shows the percentage of Cs^+ exchanged by the interfering ions. Potassium began to replace Cs^+ at the lowest concentration of all three ions; NH_4^+ was next and Na^+ last. This is in agreement with the potentiometric selectivity order.

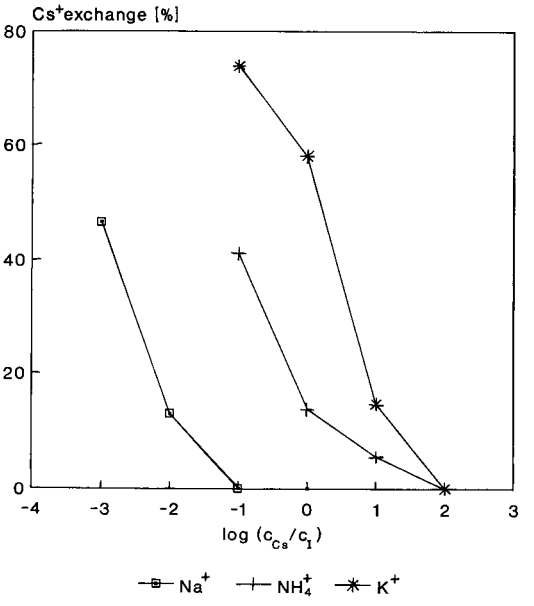

Fig. 1. Variation of the ^{137}Cs content of a valinomycin-containing PVC membrane with the interfering ion concentration of the bathing solution. Logarithm of the ratio of Cs^+ to interfering ion concentration is plotted on the abscissa. □ = Na^+; + = NH_4^+; * = K^+.

TABLE 2

Logarithm of ion-exchange and potentiometric selectivity coefficients for Cs^+ and different interfering ions of K^+-selective membranes with and without salt additives

Membrane	Interfering ion					
	K^+		NH_4^+		Na^+	
	Ion-exchange	Potentiometric	Ion-exchange	Potentiometric	Ion-exchange	Potentiometric
Valinomycin	0.17	0.3	−1.3	−1.5	−3.06	−2.6
Valinomycin + KCl	0.19	0.4	−1.26	−1.5	−2.38	−2.5
Valinomycin + KTpClPB	0.35	0.3	−1.48	−1.5	−2.92	−2.6

The following equation describes the ion-exchange process taking place:

$$I^+(w) + Cs^+(m) = I^+(m) + Cs^+(w)$$

where w and m denote the aqueous and membrane phases, respectively. The equilibrium constant of this process is the selectivity constant of the ion-exchange process:

$$k_{M-I}^{\text{ion-exchange}} = [I^+(m)][Cs^+(w)] / [I^+(w)][Cs^+(m)] \quad (3)$$

Based on this equation, the selectivity constant can be determined provided that the ion concentrations in the appropriate phases are known. In Fig. 1 the abscissa value corresponding to 50% exchange of Cs^+ ions is the logarithm of the selectivity constant, because at this point the concentrations of Cs^+ and interfering ions in the membrane are identical. The approximate values, +0.26 for K^+, −1.35 for NH_4^+, −3.08 for Na^+, are in fairly good agreement with the literature data for potentiometric selectivity coefficients (log k_{Cs-K}^{pot} = + 0.4, log $k_{Cs-NH_4^+}^{pot}$ = − 1.4, log k_{Cs-Na}^{pot} = −2.5 [13]). The determination of the 50% exchange point involves interpolation and it is therefore not highly accurate.

For better measurement of ion-exchange selectivity constants, a slightly different procedure was adopted. From potentiometric selectivity data the concentration of an interfering ion that would cause 50% exchange of Cs^+ ions from the saturated membrane was calculated. Then the calculated amount of the interfering ion was added to the bathing solution. By measuring the actual exchange percentage, the ion-exchange selectivity constant could be calculated using Eqn. 3. The results were compared with measured potentiometric selectivity data and are given in Table 2.

The investigations were extended to hydrophilic and lipophilic salt-containing membranes. In previous work [10] it has been shown that these additives (KCl and KTpClPB) increase the ion-exchange capacity of the PVC membranes. The results can be seen in Table 2. It can be seen that the ion-exchange selectivity constants are well correlated with the potentiometric selectivity coefficients.

TABLE 3

Logarithm of ion-exchange and potentiometric selectivity constants for Cs^+ and different interfering ions for NH_4^+- and Na^+-selective membranes

Neutral carrier	Interfering ion					
	K^+		NH_4^+		Na^+	
	Ion-exchange	Potentiometric	Ion-exchange	Potentiometric	Ion-exchange	Potentiometric
Nonactin	1.50	1.56	2.37	2.40	−0.36	−0.34
Na-II	0.10	0.80	−0.14	0.25	0.26	0.95

TABLE 4

Logarithm of ion-exchange and potentiometric selectivity coefficients for Sr^{2+} and different interfering ions for Ca^{2+}-selective membranes

Neutral carrier	Interfering ion			
	Ca^{2+}		Mg^{2+}	
	Ion-exchange	Potentiometric	Ion-exchange	Potentiometric
Ca-I	2.05	2.56	5.7×10^{-2}	8.7×10^{-2}

Ion-exchange selectivity of other neutral carrier membranes

Similar experiments were carried out with membranes containing neutral carriers other than valinomycin. The results for NH_4^+-, Na^+- and Ca^{2+}-selective membranes are given in Tables 3 and 4. Again good agreement is found between the measured ion-exchange equilibrium constants and the potentiometric selectivity coefficients for NH_4^+ and Ca^{2+} ionophores; the correlation is poorer for the Na^+-selective electrode membrane.

It is interesting that in the radiotracer experiments described here, ion-exchange equilibrium was reached throughout the whole thickness of the membrane and this process typically took 1–2 days. In the potentiometric selectivity measurements, however, the time response was much faster after a solution change, typically within seconds. This shows that for the potentiometric response it may be sufficient that a very thin surface layer of the membrane reaches ion-exchange equilibrium. It is also notable that although the ion exchange proceeds into the membrane interior well after the first few seconds, the e.m.f. reading remains stable.

The results which correlate the potentiometric selectivity with ion-exchange selectivity are not necessarily in contradiction with the kinetic model of selectivity. In cases when the rate of ion exchange at the interface is itself in a functional relationship with the ion-exchange equilibrium constant, one can expect a relationship between exchange rate differences and potentiometric selectivity for different ions. A close relationship between reaction rates and equilibrium constants of similar reactions has often been observed in chemical reactions. If this is also the case here, it appears to be more appropriate to relate the potentiometric selectivity directly to the ion-exchange equilibrium constant than to an ion-exchange rate parameter.

Conclusion

Earlier radiotracer experiments proved that the plasticized PVC-based ion-selective electrode membrane is a small capacity ion-exchanger. The hydrophilic contaminants of PVC behave as cation-exchange sites (probably immobilized in small colloidal droplets of water in the membrane). The ion-exchange process is facilitated by the neutral carrier. As was proposed in preliminary work [11], the equilibrium constant, i.e., the selectivity constant of the ion-exchange process, can be correlated with the potentiometric selectivity of the electrode. This work is an extension of earlier studies in this field. Radioactive tracer uptake was measured in different types of neutral carrier membranes in solutions of different interfering ions in order to determine their ion-exchange selectivity. It was found that a good correlation exists between this physico-chemical parameter and the experimentally determined potentiometric selectivity coefficients.

The authors thank the National Scientific Research Foundation (project numbers OTKA 3113 and OTKA 3116) for financial support.

REFERENCES

1 G. Eisenmann, in R.A. Durst (Ed.), Ion-Selective Electrodes, Special Publication No. 314, National Bureau of Standards, Washington, DC, 1969, p. 1.
2 W.E. Morf, The Principles of Ion-Selective Electrodes and of Membrane Transport, Akadémiai Kiadó, Budapest, 1981.
3 G.A. Rechnitz and E. Eyal, Anal. Chem., 44 (1972) 370.
4 W.E. Morf, D. Ammann, E. Pretsch and W. Simon, Pure Appl. Chem., 36 (1973) 421.
5 W.E. Morf, P. Wuhrmann and W. Simon, Anal. Chem., 48 (1976) 1031.
6 K. Cammann, Anal. Chem., 50 (1978) 936.
7 S. Xie and K. Cammann, J. Electroanal. Chem., 229 (1987) 249.

8 S. Xie and K. Cammann, J. Electroanal. Chem., 245 (1988) 117.
9 R.D. Armstrong, A.K. Covington and G.P. Evans, J. Electroanal. Chem., 159 (1983) 33.
10 G. Horvai, V. Horváth, A. Farkas and E. Pungor, Anal. Lett., 21 (1988) 2165.
11 G. Horvai, V. Horváth, A. Farkas and E. Pungor, Talanta, 36 (1989) 403.
12 A. Craggs, G.J. Moody and J.D.R. Thomas, J. Chem. Educ., 51 (1974) 541.
13 D. Ammann, W.E. Morf, P. Anker, P.C. Meier, E. Pretsch and W. Simon, Ion-Sel. Electrode Rev., 5 (1983) 3.

Analytica Chimica Acta, 282 (1993) 265–271
Elsevier Science Publishers B.V., Amsterdam

Detection limit of ion-selective bulk optodes and corresponding electrodes

Eric Bakker, Michael Willer and Ernö Pretsch

Swiss Federal Institute of Technology (ETH), Department of Organic Chemistry, Universitätstr. 16, CH-8092 Zürich (Switzerland)

(Received 19th April 1993; revised manuscript received 18th May 1993)

Abstract

The detection limit of a highly selective Pb^{2+}-sensitive optode based on a solvent polymeric membrane phase is compared to the corresponding Pb^{2+}-electrode. For this purpose, a practical definition of the detection limit for optodes is presented. Whereas the optode phase has an incorporated Pb^{2+}-selective ionophore and H^+-selective chromoionophore, the ion-selective electrode has no chromoionophore, but otherwise equal composition. It is shown that both optode and electrode are responding to the free ion activity of Pb^{2+} in the sample, which may be buffered by the use of suitable ligands such as NTA and EDTA. The detection limit of the optode ($10^{-13.1}$ M) has been found to be much lower than that of the electrode ($10^{-9.2}$ M), but with sample activities of less than $10^{-11.5}$ M, response times of more than 60 h have been observed with EDTA as metal ion buffer. This is possibly due to a slow decomplexation step of the EDTA–Pb^{2+} complex.

Keywords: Ion-selective electrodes; Lead-sensitive optode

Ion-selective bulk optodes on the basis of solvent polymeric membrane phases have gained considerable interest in the last years. A series of different ion-selective sensors [1–8] (see also [9]), various theoretical treatments on the topic [10–13], and characterization of membrane components [14–16] have been published. The possible use of optical sensors with fibre optic technology, integrated optics and for remote sensing offer in certain cases advantages over the classical ion-selective electrodes. Moreover, an application of optical sensors in clinical mainframe analyzers may contribute to a further standardization of the recognition process. Ion-selective electrodes and optodes are based on similar components, and a thorough comparison of the two measuring principles may lead to a better understanding of both analytical devices.

Ion-selective electrodes are known to respond to the analyte ion activity. This is in contrast to other analytical methods, where usually total concentrations are measured. To avoid analytical artefacts like contaminations by interfering ions, leaching effects from the membrane, and to ensure a defined analyte concentration in the sample, the analyte ion activity may be buffered by selected ligands. Accordingly, clearly better detection limits could be achieved by this approach with silver halide and with solvent polymeric membrane electrodes [17–19]. In the case of ion-selective optodes based on solvent polymeric membranes, the activity of a reference ion (e.g., H^+) has to be kept constant in the sample by a pH buffer. The prerequisite for lowering the practical detection limit by buffering the analyte ion is therefore an excellent selectivity of the

Correspondence to: E. Pretsch, Swiss Federal Institute of Technology (ETH), Department of Organic Chemistry, Universitätstr. 16, CH-8092 Zürich (Switzerland).

sensor with respect to the interfering ions of the pH buffer. Only recently, a Pb^{2+}-selective optode with very high selectivities over Ca^{2+} and Mg^{2+} has been described [7], where the use of metal ion buffered solutions could lead to an improved detection limit.

In this work, a novel description of the detection limit for ion-selective bulk optodes is given, which is related to the definition for ion-selective electrodes according to IUPAC [20]. A comparison of the Pb^{2+}-selective optode described earlier [7] with the corresponding Pb^{2+}-electrode, with respect to detection limit and response to Pb^{2+} buffered solutions, is presented.

EXPERIMENTAL

Aqueous solutions were prepared with doubly quartz distilled water. Buffers and salts of highest quality available were used throughout. For buffer preparation, 3-morpholinopropanesulfonic acid (MOPS), ethylenediaminetetraacetic acid (EDTA) and nitrilotriacetic acid (NTA) were obtained from Fluka (Buchs, Switzerland). For membrane preparation, poly(vinyl chloride) (PVC, high mol. wt.), potassium tetrakis[3,5-bis(trifluoromethyl)phenyl]borate (KTFPB), bis(2-ethylhexyl) sebacate (DOS), and tetrahydrofuran (THF, distilled prior to use) were obtained from Fluka. The Pb^{2+}-selective ionophore *N,N,N′,N′*-tetradodecyl-3,6-dioxaoctanedithioamide (ETH 5435) and the H^+-selective chromoionophore 4-{[9-(dimethylamino)-5*H*-benzo[*a*]phenoxazin-5-ylidene]amino}benzoic acid 11-[(1-butylpentyl)oxy]-11-oxoundecyl ester (ETH 5418) were synthesized in our laboratory and described elsewhere [7,14].

Apparatus

For pH determination, a pH glass electrode (Orion Ross Model 81-02) and pH meter (Orion Model 920A, Orion Research AG, Uetikon am See, Switzerland) were used. Spectrophotometric studies on optode membranes were performed with a specially designed measuring cell [1] mounted in a conventional double-beam spectrophotometer (constant bandwidth, 2 nm; Uvikon 810, Kontron, Zürich, Switzerland). Absorption spectra were recorded between 800 and 400 nm at 25 ± 1°C.

Optode membrane

The optode membrane was prepared from 6.01 mg (27.0 mmol kg^{-1}) of ionophore ETH 5435, 1.54 mg (8.3 mmol kg^{-1}) of chromoionophore ETH 5418, 2.01 mg (8.7 mmol kg^{-1}) of anionic additive KTFPB, 163.0 mg of plasticizer DOS, and 84.0 mg of matrix PVC dissolved in 2.5 ml THF, as described earlier [7].

Ion-selective electrode membranes and EMF measurements

The membranes contained 4.34 mg (27.1 mmol kg^{-1}) of ionophore ETH 5435, 1.44 mg (8.8 mmol kg^{-1}) of anionic additive KTFPB, 116.8 mg of plasticizer DOS, and 58.8 mg of matrix PVC, dissolved in 2 ml of THF. The ion-selective electrode (ISE) assembly and measuring equipment have been described elsewhere [21]. The membranes were conditioned in 4×10^{-3} M $PbCl_2$ over a 48-h period. The EMF values of 3 ion-selective electrodes were measured using the following cell: $Hg|Hg_2Cl_2|KCl$ (sat.)$\|1$ M $NH_4NO_3 \|$ sample $\|\|$ membrane $\|\|4 \times 10^{-3}$ M $PbCl_2|AgCl|Ag$, with a calomel reference electrode of the free-flowing, free-diffusion type [22]. For a different measurement of the detection limit, the inner filling solution was replaced by a Pb^{2+}-buffer (4×10^{-4} M $Pb(NO_3)_2$, 5×10^{-4} M NTA, 1×10^{-2} M MOPS, 3×10^{-3} M $Ca(OH)_2$, 1×10^{-3} M $CaCl_2$ at pH 7.14). Diffusion potentials were corrected according to the Henderson formalism, taking the mobility of *p*-toluenesulfonic acid for the pH buffer MOPS. Activity coefficients for the unbuffered $Pb(NO_3)_2$ solutions were calculated according to [23], whereas activity coefficients in the buffer solutions were assumed to be constant [7] and set to unity. Selectivity coefficients were measured according to the separate solution method [20].

THEORY

Response of ion-selective bulk optodes

As described previously, a cation-selective optode phase usually consists of a $I^{\nu+}$-selective

ionophore L forming positively charged complexes $IL_p^{\nu+}$, a lipophilic anionic additive R^-, and a neutral H^+-selective chromoionophore C forming a positively charged CH^+ and changing its spectral properties upon protonation [12,13]. The following ion-exchange equilibrium is then observed:

$$I^{\nu+}(aq.) + pL(org.) + \nu CH^+(org.) \rightleftharpoons IL_p^{\nu+}(org.) + \nu C(org.) + \nu H^+(aq.) \quad (1)$$

where aq. denotes species in the aqueous phase and org. species in the organic phase. By introducing the ratio of unprotonated to total concentration of chromoionophore, α, as the spectrophotometrically accessible parameter, and the total concentrations of ionophore, L_T, anionic additive, R_T, and chromoionophore, C_T, the response function for such optodes is given as [13]:

$$a_{I^{\nu+}} = \left(K_{exch.}^{IL_p}\right)^{-1}\left(\frac{\alpha a_{H^+}}{1-\alpha}\right)^{\nu} \times \frac{R_T - (1-\alpha)C_T}{\nu\left\{L_T - \frac{p}{\nu}\left[R_T - (1-\alpha)C_T\right]\right\}^{p}} \quad (2)$$

In the case where samples of different pH values must be compared, Eqn. 2 is rewritten:

$$\frac{a_{I^{\nu+}}}{(a_{H^+})^{\nu}} = \left(K_{exch.}^{IL_p}\right)^{-1}\left(\frac{\alpha}{1-\alpha}\right)^{\nu} \times \frac{R_T - (1-\alpha)C_T}{\nu\left\{L_T - \frac{p}{\nu}\left[R_T - (1-\alpha)C_T\right]\right\}^{p}} \quad (3)$$

where $a_{I^{\nu+}}$ and a_{H^+} stand for the free analyte activity of the ions $I^{\nu+}$ and H^+ in the sample, p is the stoichiometric factor of the cation–ionophore complex in the membrane, and $K_{exch.}^{IL_p}$ is the overall equilibrium constant (Eqn. 1). If a constant background of interfering ions J^{z+} is present in the sample, Eqn. 2 is rewritten as [13]:

$$a_{I^{\nu+}} + k_{IJ}^{opt} a_{J^{z+}} = \text{RHS(Eqn. 2)} \quad (4)$$

The definition of the selectivity coefficient $k_{IJ}^{opt.}$ differs from that for an ISE [13]. If the interfering ion has the same charge as the primary ion and forms complexes of the same stoichiometry in the membrane, the selectivity coefficients $k_{IJ}^{opt.}$ should be independent of concentrations in the organic and sample phase.

Detection limit

Midgley [24] introduced a statistical definition of the detection limit for ISEs on the basis of the standard approach for other analytical methods [25]. Some authors used a similar definition for bulk optodes by relating the detection limit to the standard deviation of the background signal [7,12]. Such an approach describes the maximum possible measuring range of an optode, but is poorly comparable with detection limits obtained with ISEs. Therefore, for a stand-alone description of an optode application, the statistical definition may be suitable, but for standardization and comparison purposes, the practical definition given below might be more useful.

The detection limit of a measurement made with an ISE is defined according to IUPAC as the intersection of the two extrapolated linear segments of the calibration graph [20] (see Fig. 1). If the detection limit is given by the interference

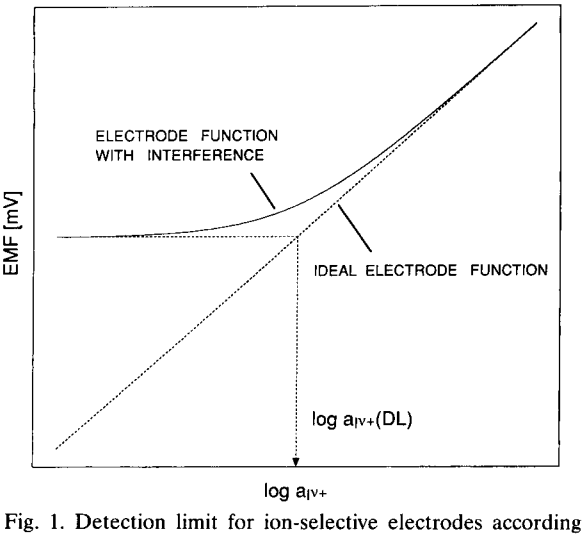

Fig. 1. Detection limit for ion-selective electrodes according to the IUPAC definition [20]. The cross-section of the background signal with the ideal response function according to the Nernst equation is defined as the detection limit.

from a background ion J^{z+}, one can write according to Nicolsky:

$$a_{I^{\nu+}}(DL) = k_{IJ}^{pot} \cdot (a_{J^{z+}})^{\nu/z} \quad (5)$$

A similar approach is presented here for bulk optodes. In this case, the ideal theoretical curve without interfering ions is not linear but describes a sigmoid function (Eqn. 2, Fig. 2). Practically, the detection limit for ion-selective optodes at a certain pH is evaluated by fitting the experimental points with Eqn. 2 (dotted curve in Fig. 2). The intersection of this curve with the horizontal line corresponding to the degree of protonation determined with the pure pH buffer defines the detection limit. If the detection limit $a_{I^{\nu+}}(DL)$ is entirely given by the interference from the buffer background, one can write with Eqn. 4:

$$a_{I^{\nu+}}(DL) = k_{IJ}^{opt} \cdot a_{J^{z+}} \quad (6)$$

If the selectivity coefficient is independent of concentration changes in the sample, the detec-

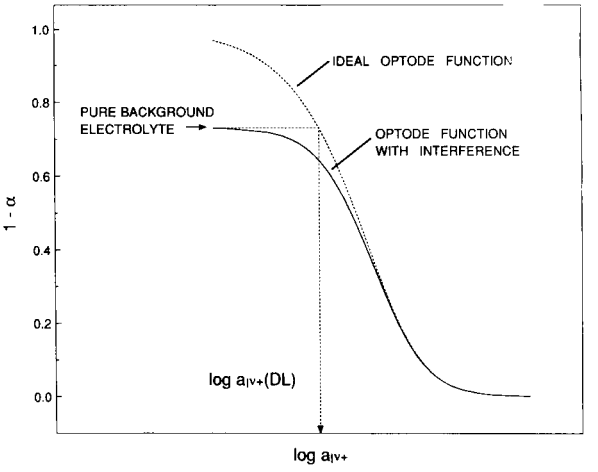

Fig. 2. Detection limit for ion-selective optodes in analogy to the IUPAC definition for ion-selective electrodes (Fig. 1). The cross-section of the background signal with the ideal response function according to Eqn. 2 is defined as the detection limit. If no interference is observed, the experimental conditions (sample pH, pK_a of the chromoionophore) have to be changed in order to determine the detection limit.

TABLE 1

Composition of measuring solutions and response times $t_{95\%}$ observed with the Pb^{2+}-selective bulk optode (membrane thickness: 0.5 μm), with a total concentration of 0.01 M MOPS and 0.5 mM ligand NTA or EDTA in the sample

L [a]	pPb [b]	pCa [c]	pH [d]	$Pb(NO_3)_2$ c_T [M] [e]	$Ca(OH)_2$ c_T [M] [f]	$t_{95\%}$ [h] [g]
NTA	6.85	2.65	6.85	$4 \cdot 10^{-4}$	0.0023	
NTA	7.63	2.69	6.85	$2 \cdot 10^{-4}$	0.0023	
NTA	8.06	2.71	6.85	$1 \cdot 10^{-4}$	0.0023	
NTA	6.87	2.53	7.14	$4 \cdot 10^{-4}$	0.0031	0.08
NTA	7.66	2.56	7.14	$2 \cdot 10^{-4}$	0.0031	0.08
NTA	8.10	2.57	7.14	$1 \cdot 10^{-4}$	0.0031	0.22
NTA	8.57	2.58	7.14	$4 \cdot 10^{-5}$	0.0031	0.27
NTA	9.20	2.59	7.14	$1 \cdot 10^{-5}$	0.0031	0.67
NTA	9.51	2.59	7.14	$5 \cdot 10^{-6}$	0.0031	2.50
NTA	10.21	2.59	7.14	$1 \cdot 10^{-6}$	0.0031	3.00
L	pPb	pMg [h]	pH	$Pb(NO_3)_2$ c_T[M]	$Mg(OH)_2$ c_T[M][i]	$t_{95\%}$ [h]
EDTA	10.74	2.29	7.88	$4 \cdot 10^{-4}$	0.0051	30.0
EDTA	11.52	2.29	7.88	$2 \cdot 10^{-4}$	0.0051	35.0
EDTA	11.94	2.29	7.88	$1 \cdot 10^{-4}$	0.0051	> 60

[a] Metal ion buffer in the sample, NTA (nitrilotriacetic acid) or EDTA (ethylenediaminetetraacetic acid). [b] Free lead ion concentration in the sample, calculated according to complex formation constants given in [27]. [c] Free calcium ion concentration in the sample, calculated according to complex formation constants given in [27]. [d] Adjusted with a pH glass electrode. [e] Total lead concentration in the sample. [f] Total calcium concentration in the sample. [g] Response time of the optode, after which 95% of the equilibrium signal was reached. [h] Free magnesium ion concentration in the sample, calculated according to complex formation constants given in [27]. [i] Total magnesium concentration in the sample.

tion limit is proportional to the activity of the interfering ion in the sample. Interference from acidic samples have usually not to be considered with optodes [13].

For ISEs and optodes with equal selectivity towards the same interfering background, equal detection limits should be obtained. For example, selectivity coefficients towards Na^+ for a K^+-selective optode [3] (log $k^{opt.}_{KNa} = -3.5$) and for the corresponding electrode [26] (log $k^{pot.}_{KNa} = -4.0$) would lead to a detection limit of log $a_{K^+}(DL) = -5.5$ and -6.0, respectively, for a Na^+ background of 0.01 M. The practical definition of the detection limit for optodes is therefore suitable for a direct comparison with ISEs.

RESULTS AND DISCUSSION

Recently, a novel Pb^{2+}-selective bulk optode was described, which is based on the highly selective dithioamide derivative ETH 5435. Very high selectivities over Mg^{2+} and Ca^{2+} (log $k^{opt.}_{PbMg} = -10.9$ and log $k^{opt.}_{PbCa} = -10.8$) had been found [7]. Accordingly, samples could be measured down to a total analyte concentration of 2×10^{-9} M Pb^{2+} at pH 5.7.

It is known that by using metal ion buffers for defining the analyte concentration, the practical detection limit of ISEs can be improved considerably [17]. Therefore, the detection limit was evaluated in this work for the optode and ISE with Pb^{2+}-buffered solutions. The complex stability constants of EDTA and NTA with Pb^{2+}, Ca^{2+} and Mg^{2+} are given in [27] and were used here to calculate the free concentrations of the ions of interest in the sample. The results of the calculations are shown in Table 1. Figure 3 shows the recorded spectra as a function of the Pb^{2+} concentrations in NTA-buffered solutions at pH 7.14. In Fig. 4, calibration graphs at three different pH values for the lead optode with NTA and EDTA in the sample are presented. Figure 5 shows the same experimental data as a function of the ratio $a_{Pb^{2+}}/(a_{H^+})^2$ in the sample solution. All experimental points are given together with the theoretical curves according to Eqns. 2 and 3 and the same overall equilibrium constant log $K^{PbL_2}_{exch.} = -5.5$ (with $p = 2$) presented previously [7]. The experimental points agree well with the theoretical curve, and it can therefore be concluded that ion-selective optodes respond in complete analogy to ISEs to free ion activities in the sample. The detection limit according to the definition given above for the present optode system has been found to be $10^{-13.1}$ M Pb^{2+} at pH 7.88 with 5.1 mM Mg^{2+} as background ion. Owing to the extremely long response times, the lowest concentration giving a stable signal was $10^{-11.5}$ M Pb^{2+} at pH 7.88 (see Table 1). Table 1 shows that response times were especially long with EDTA as metal ion buffer. This may be due to a slow decomplexation of the EDTA–Pb^{2+} complex at higher pH [28].

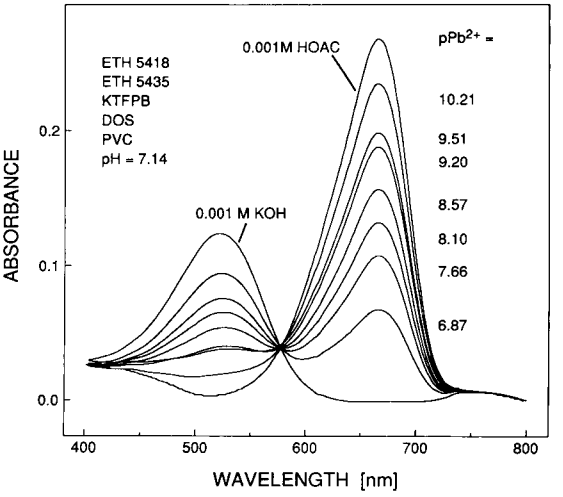

Fig. 3. Recorded spectra of the lead-selective optode as a function of different free lead ion activities in the sample, buffered with NTA as ligand at pH 7.14 (25 ± 1°C). The chromoionophore is subsequently deprotonated with increasing Pb^{2+} concentration in the sample. Absorbance maximum of the protonated form: $\lambda_{max} = 666$ nm.

For a direct comparison, the ISE membrane contained no H^+-selective chromoionophore, but otherwise the same composition as the optode membrane. The electrode showed the expected Nernstian slope for doubly charged Pb^{2+} (see Fig. 6). This is in contrast to earlier findings [29] and is due to the presence of sufficient anionic additive in the membrane [7]. Pure $Pb(NO_3)_2$ solutions and the same NTA buffer solutions at pH 7.14 as for the optode were measured, giving

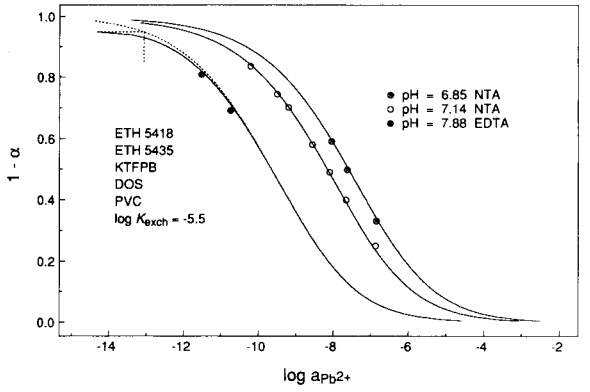

Fig. 4. The degree of protonation of the chromoionophore $(1-\alpha)$ as a function of the free Pb^{2+} activity in the sample with NTA and EDTA as ligands, at different pH values. The theoretical curves were obtained with Eqn. 4. Dotted line for EDTA buffered samples: ideal curve according to Eqn. 2.

a detection limit of $10^{-5.4}$ and $10^{-9.2}$ M Pb^{2+}, respectively. The NTA solutions lead to relatively long acquisition times of up to 70 min. The respective EDTA buffers gave the same detection limits (data not shown). Thus, the detection limit of the ISE is about four orders of magnitude greater than that of the corresponding optode. Since the selectivity of the equally charged ions Pb^{2+}, Ca^{2+} and Mg^{2+} should be equal for optodes and electrodes, the higher detection limit cannot be attributed to interference from the background ions Ca^{2+} or Mg^{2+}. The interference

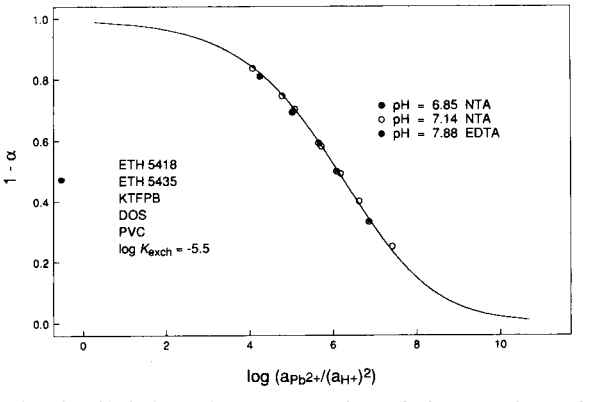

Fig. 5. pH independent presentation of the experimental results according to Eqn. 3. It is shown that all experimental points are well agreeing with the theoretical curve, using the same overall equilibrium constant as described previously [7].

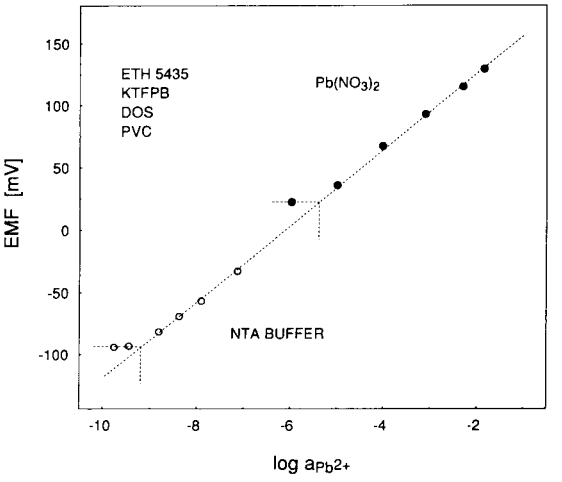

Fig. 6. Response of the lead-selective electrode towards unbuffered $Pb(NO_3)_2$ solutions and the Pb^{2+} buffered samples with NTA at pH 7.14 used for the corresponding optode. The detection limit is lowered with the buffered samples, which however is still much higher than the value obtained with optode measurements. Dotted line with slope of 30.6 mV dec. ($T = 23 \pm 2$°C).

from H^+ would be a possible explanation, since optodes are not sensitive to H^+ interference [13]. However, the experimental selectivity coefficient of log $k^{\text{pot.}}_{\text{PbH}} = -3.6$ would lead to a detection limit of log Pb^{2+}(DL) $= -17.9$ at pH 7.14 according to Eqn. 5, which does not explain the present findings. The replacement of the inner filling electrolyte of the electrode by a solution buffered to 1.3×10^{-7} M Pb^{2+} did not significantly lower the detection limit (data not shown).

The large difference between the detection limits of the Pb^{2+}-selective optode as compared to the corresponding ISE is not fully understood at this point. It could be related to the kinetic limitation imposed by the buffer, since both the optode and the ISE exhibit unusually long response times. Another reason might be caused by the fact that the signal of the ISE is directly dependent on the sample activity near the sample–membrane interface at all times. Traces of undiscriminated interfering ions could have considerable effects on the ISE signal. Since the optode membrane requires approximately 5×10^{-10} mol of analyte ions to enter the organic phase for inducing half protonation of the chro-

moionophore [12], traces of interfering ions may be consumed without having a detectable influence on the signal. Because of their inherently faster response times, ISEs are more sensitive to fast fluctuations of ion activities than optodes. Bulk optodes are in these respects, therefore, obviously more robust systems.

Conclusions

It has been shown that ion-selective bulk optodes, in analogy to ion-selective electrodes, respond to free analyte ion activities, which can be adjusted by metal buffering of the sample. This is in contrast to other analytical techniques, where total analyte concentrations are measured. With the Pb^{2+} optode, much lower detection limits could be observed than with the Pb^{2+}electrode. The practical detection limit for the extremely selective optode was in this case however governed by the response time of the sensor.

This work was supported by the Swiss National Science Foundation and Ciba-Corning Diagnostic Co. The authors thank Markus Lerchi for helpful discussions.

LITERATURE

1 W.E. Morf, K. Seiler, B. Rusterholz and W. Simon, Anal. Chem., 62 (1990) 738.
2 K. Seiler, W.E. Morf, B. Rusterholz and W. Simon, Anal. Sci., 5 (1989) 557.
3 K. Wang, K. Seiler, W.E. Morf, U.E. Spichiger, W. Simon, E. Lindner and E. Pungor, Anal. Sci., 6 (1990) 715.
4 K. Seiler, K. Wang, E. Bakker, W.E. Morf, B. Rusterholz, U.E. Spichiger and W. Simon, Clin. Chem., 37 (1991) 1350.
5 P. Holý, W.E. Morf, K. Seiler, W. Simon and J.-P. Vigneron, Helv. Chim. Acta, 73 (1990) 1171.
6 H. He, G. Uray and O.S. Wolfbeis, Anal. Chim. Acta, 246 (1991) 251.
7 M. Lerchi, E. Bakker, B. Rusterholz and W. Simon, Anal. Chem., 64 (1992) 1534.
8 S.S.S. Tan, P.C. Hauser, K. Wang, K. Fluri, K. Seiler, B. Rusterholz, G. Suter, M. Krüttli, U.E. Spichiger and W. Simon, Anal. Chim. Acta, 255 (1991) 35.
9 M.A. Arnold, Anal. Chem., 64 (1992) 1015A.
10 W.E. Morf, K. Seiler, B. Lehmann, Ch. Behringer, S.S.S. Tan, K. Hartman, P.R. Sørensen and W. Simon, in E. Pungor (Ed.), Ion-Selective Electrodes, Vol. 5, Akadémiai Kiadó, Budapest, 1989, p. 115.
11 W.E. Morf, K. Seiler, P.R. Sørensen and W. Simon, in E. Pungor (Ed.), Ion-Selective Electrodes, Vol. 5, Akadémiai Kiadó, Budapest, 1989, p. 141.
12 K. Seiler and W. Simon, Anal. Chim. Acta, 266 (1992) 73.
13 E. Bakker and W. Simon, Anal. Chem., 64 (1992) 1805.
14 E. Bakker, M. Lerchi, T. Rosatzin, B. Rusterholz and W. Simon, Anal. Chim. Acta, 278 (1993) 211.
15 T. Rosatzin, E. Bakker, K. Suzuki and W. Simon, Anal. Chim. Acta, 280 (1993) 197.
16 O. Dinten, U.E. Spichiger, N. Chaniotakis, P. Gehrig, B. Rusterholz, W.E. Morf and W. Simon, Anal. Chem., 63 (1991) 596.
17 W.E. Morf, The Principles of Ion-Selective Electrodes and of Membrane Transport, Akadémiai Kiadó, Budapest, 1981.
18 J. Ruzicka, E.H. Hansen and C.J. Tjell, Anal. Chim. Acta, 67 (1973) 155.
19 D. Ammann, T. Bührer, U. Schefer, M. Müller and W. Simon, Pflügers Arch., 409 (1987) 223.
20 IUPAC Recommendations for Nomenclature of Ion-Selective Electrodes, Pure Appl. Chem., 48 (1976) 127.
21 Ch. Behringer, B. Lehmann, J.-P. Haug, K. Seiler, W.E. Morf, K. Hartman and W. Simon, Anal. Chim. Acta, 233 (1990) 41.
22 R.E. Dohner, D. Wegmann, W.E. Morf and W. Simon, Anal. Chem., 58 (1986) 2585.
23 P.C. Meier, Anal. Chim. Acta, 136 (1982) 363.
24 D. Midgley, Analyst 104 (1979) 248.
25 D.L. Massart, B.G.M. Vandeginste, S.N. Deming, Y. Michotte and L. Kaufman, Chemometrics: a Textbook, Elsevier, Amsterdam, 1988.
26 D. Ammann, W.E. Morf, P. Anker, P.C. Meier, E. Pretsch and W. Simon, Ion-Sel. Electrode Rev., 5 (1983) 3.
27 A.F. Martell and R.M. Smith, Critical Stability Constants, Vol. 1–6, Plenum Press, New York, London, 1976.
28 A.M. Cook and F.A. Long, J. Am. Chem. Soc., 80 (1958) 33.
29 E. Lindner, T. Tóth, E. Pungor, F. Behm, P. Oggenfuss, D.H. Welti, D. Ammann, W.E. Morf, E. Pretsch and W. Simon, Anal. Chem., 56 (1984) 1127.

Analytica Chimica Acta, 282 (1993) 273–281
Elsevier Science Publishers B.V., Amsterdam

Anion effects on Donnan failure of aminated-poly(vinyl chloride)-based and neutral-carrier-based pH sensors

Richard P. Buck, Vasile V. Cosofret and Erno Lindner [1]

Department of Chemistry, University of North Carolina, Chapel Hill, NC 27599-3290 (USA)

(Received 28th April 1993)

Abstract

Aminated poly(vinyl chloride)s (PVCs) and neutral carriers can produce nearly ideal pH sensors. However, they can show Donnan exclusion failure in low pH bathing solutions. These pH-sensitive PVC membranes illustrate a new dimension, not found for other mobile neutral-carrier-based sensors, i.e., Donnan failure produces fixed positive sites that create a nearly ideal anion sensor. The modification of Donnan theory is derived and illustrated using carrier-based and aminated-PVC-based sensors.

Keywords: Sensors; Potentiometry; Carriers; Donnan failure; Membranes; pH sensors; Poly(vinyl chloride)

The carrier mechanism in sited ion-exchange membranes

Ion-exchange membranes are considered to be homogeneous phases. Within the phase are assumed to be uniformly distributed fixed, covalently-bonded charged sites, e.g. $-SO_3^-$ or $-NR_3^+$ groups synthetically added to polystyrene [1], or $-SO_3^-$ or possibly $-COO^-$ groups unintentionally added to poly(vinyl chloride) (PVC) from manufacturing or impurities [2–5]. The original counterions are those cations in the fixed negative site cases that were used in the synthesis, typically Na^+ or H^+, or Cl^- for the fixed positive site cases. The precise chemical identity of sites in PVC cannot generally be given because of the many different polymerization schemes using different catalysts, initiators, emulsifiers, and suspending agents. In a series of papers the effects of the sites on electrical and chemical properties, including determination of ion-exchange capacities were presented [6–10].

In classical ion-exchange applications, the original counterions, at concentrations nearly equal to the fixed sites, can be substituted by other cations from the bathing solutions. However, selectivities can be altered and often improved using mobile, trapped-site membranes. The sites are added by using very lipophilic salts, e.g. sodium tetraphenylborate (NaTPB) or methyltridodecylammonium chloride. The trapped sites are the anion and the cation, respectively. Fixed sites are permanent in the membrane while trapped mobile sites can slowly be lost to a bathing solution by salt extraction [9–12]. The time for loss can be quite long when the hydrophobicity of the site is great [12,13].

The normal selection of cation or anion counterions is determined by electrostatics and favors small ions of high charge relative to large ions of high charge or small ions of low charge [14]. To

Correspondence to: R.P. Buck, Department of Chemistry, University of North Carolina, Chapel Hill, NC 27599-3290 (USA).
[1] Permanent address: Institute for General and Analytical Chemistry, Technical University of Budapest, Gellért tér 4, H-IIII Budapest (Hungary)

provide an enhanced selection of a specific counterion that is desired for the purpose of making permselective ion sensors, neutral charge selective complexing agents are dissolved in the membrane [15,16]. These are "neutral carriers" and they are added at molar ratios in excess of unity with respect to the fixed or mobile sites [4]. This means that every fixed or mobile site charge is neutralized by the desired ion selected into the membrane by the neutral carrier. When the mole ratio is less that one, the selectivity is progressively lost [9,17,18].

A characteristic property of a neutral carrier membrane is its ability to transport the selected counterion through the membrane from one bathing electrolyte to another under an applied voltage [3,8,10,19–22]. The ion–carrier complex moves through the membrane as a unit, and unloads cations at the exiting interface which builds up a high concentration of free carrier. At the opposite interface, the concentration of free carrier is reduced by uptake of ions from the bathing solution. The current–voltage (I–V) curve is S-shaped, e.g. there are positive and negative limiting currents. This result is interpreted as meaning that the current is indirectly controlled by back-diffusion of free carriers. Various consistencies of measured diffusion coefficients demonstrates the validity of the interpretation [23]. There is no evidence for the cations moving independently of the carriers, i.e. there is no evidence for ion hopping from carrier to carrier [24–26]. Under this applied voltage, the ion–carrier complex moves through the membrane in a constant resistance medium, because the fixed-site case is believed to contain uniformly distributed sites. A nearly constant resistance medium can be constructed for mobile site membranes under the circumstances that the mobile sites are in excess of the carriers. However, for the more usual case that the mobile-site concentration is less than the carrier concentration, the sites themselves become concentration polarized, as well as the free carriers. Then the analysis of the response is more difficult than the fixed-site case [8,10,27,28]. These mobile-site situations have been recently reported in detail by theoretical and experimental analyses [29–31].

THEORY

Modification of Donnan exclusion theory for aminated PVC-based and neutral-carrier-based pH membranes

Normally membranes are designed to contain a high site concentration so that counterions are the only significant ions from the bathing solution passing into and through a membrane. Their concentration in the membrane can be said to be very nearly equal to, but slightly larger than the site concentration itself. This is Donnan exclusion of coions; the general theory for fixed-site membranes was given by Hills et al. [32]. The very small excess of counterions arises from the small, but necessary concentration of extracted coions. Of course, since extraction of whole salt from the bathing solution is allowed (indeed required), it is mass and charge balance, together with an unfavorable salt extraction constant, that keep the concentration of coions in the membrane very low.

One can show that a low ratio between salt partition constant and site density is the figure of merit for Donnan exclusion creation in both fixed- or mobile-site membranes [32–35]. Whenever in a fixed-site membrane the partitioning of external ions into the membrane occurs, the potentiometric response will deviate from Nernstian. If the entering coion and the normally present counterion have identical mobilities, the response will remain constant, independent of the bathing activity since the charge transport by these ions of opposite sign compensate each other. However, it is usual [7,36] that the interfering coion has a higher mobility than the complexed counterions. Then the potentiometric response actually reverses slope and the membrane becomes coion responsive!

Whenever in a mobile-site membrane the site concentration is caused to drop, Donnan exclusion failure can again be the result [37]. The general problem of mobile-site polarization in membranes under d.c. current flow was shown to induce Donnan exclusion failure and permeation of otherwise permselective membranes by coions from the bathing electrolyte. Failure occurs at the side of the membrane with lower site density.

Fixed neutral carrier membranes containing sites

The aminated PVC membranes, responsive to pH, represent a new category of fixed/mobile-site membranes [38–41]. It will be shown that the membranes are susceptible to Donnan exclusion failure as whole acid molecules enter the membrane surface from low pH bathing electrolytes through protonation of the amine groups. However, no anion interference is observed at the same bathing anion concentration level when the pH is higher. Further, the results show that the anions (coions) can be more mobile in the membrane phase than the permeable protons, as indicated by the reverse potentiometric slopes at high bathing acidities.

The assumption is made, and modern theory is based on the condition, that pure pH responses will occur when there are exclusively permeable protons in the membrane accompanied by equal numbers (concentrations) of fixed negative sites and/or mobile, but trapped, negative sites. This is a well-known condition of permselectivity that gives rise to Nernstian responses in other sited membranes. In contrast to the often-studied mobile-neutral-carrier cases, there is no mechanism for the fixed-position amino groups to move very long distances, i.e. it seems that the protons have to hop eventually to new, free amino groups, possibly with the help of water clusters, to maintain their forward progress through a membrane under an applied voltage. Thus protons in aminated PVCs, unlike other carrier-based systems, have to hop or they would not carry current through the membrane. The fact that Nernstian proton responses cannot be observed in bathing electrolytes at low pH values, means that protons are extracted as whole acids or salts into the membranes. But the extraction is not merely promoted and driven by solubility in the membrane. In fact there must be bonding of the protons to amine groups because the extent of extraction is experimentally dependent on the basicity of the amine group [42].

Proposed variation of Donnan failure for fixed-neutral-carrier membranes

The normal mass conditions of a sited membrane are expressed by [7]:

$$[-NR_2] + [-NR_2H^+] = [A] + [AH^+] = [A_T] \quad \text{in the membrane} \tag{1}$$

where A_T = total amine, A = unprotonated amine and [] denotes concentrations. The basicity is measured as

$$K_B = [AH_m^+]/[A_m][H_m^+] = 1/K_A \tag{2}$$

and related to the acid dissociation constant (K_A) of the protonated product in the membrane phase. In fact there must also be some anions from the bathing electrolyte present (X^-), so the real mass balance should consider $[X^-] = [X]$:

$$[-NR_2H_m^+] + [H_m^+] = [AH_m^+] + [H_m^+] = [S] + [X] \tag{3}$$

where $[S] = [S^-]$ = site concentration. Subscripts s and m mean bathing solution species and membrane species, respectively.

There are three interfacial reactions of varying importance. The principal reaction is

$$H_s^+ + A_m \rightleftharpoons AH_m^+ \text{ at the interface} \tag{4}$$

in the presence of sites S^-. However, simultaneously there are the required equilibrium processes going on in parallel:

$$H_s^+ \rightleftharpoons H_m^+ \tag{5}$$

and

$$X_s^- \rightleftharpoons X_m^- \tag{6}$$

The basic salt partitioning equilibrium is thermodynamic and has an equilibrium partition constant K which is composed of single ion partition coefficients. However, the single ion partition coefficients are important because they appear in the interfacial potential difference (pd) expressions above.

$$RT \ln k_i = \mu_{is}^0 - \mu_{im}^0 \tag{7}$$

gives the tendency of a single ion to partition, in terms of the infinite dilute free energy (μ) change from solution to membrane.

The interfacial pds must be given by

$$\phi_m - \phi_s = (RT/F) \ln(k^+ a_s^+ / a_m^+) = -(RT/F) \ln(k^- a_s^- / a_m^-) \tag{8}$$

where a represents activity and ϕ potential. Normally, the first expression is used alone, because the cations are the principal species. However, the second term must also be true and that term allows us to know how small the encroaching anion concentration in the membrane really is.

The partition equilibrium relationship for simple ions is

$$a_m^+ a_m^- / a_s^+ a_s^- = K^2 = k^+ k^- \quad (9)$$

and this equation applies to the elementary process for H^+ and X^-. However, these are not the principal reactions of the dominant species. For Eqn. 4

$$a(AH_m^+)a(X_m^-)/a(A_m)a(H_s^+)a(X_s^-) = K_B K^2 = K_D^2 \quad (10)$$

where the overall constant is called K_D, a distribution coefficient.

With the essential condition that the total amine concentration exceeds the site concentration, conventional Donnan exclusion breakdown should be, and is, observable at high concentrations of lipophilic anions in a sample. As the acidity of the bathing electrolyte on one side is increased, acid extraction can occur with protonation of the membrane amine groups, e.g. formation of $AH_m^+X_m^-$ by coion exclusion failure. With the essential assumption, one can be sure that all extracted acid is combined with A. Then conventional theory [32] can be quickly modified with nothing more than redefinition of the extraction coefficient to account for the principal species rather than the simple salt [33–35]:

$$a(AH_m^+)a(X_m^-)/a(H_s^+)a(X_s^-) = K_D^2[A_T] \quad (11)$$

In the Hills notation [32], the figure of merit (ξ) and mobility function U that appear in the theory would be defined in the present case as:

$$\xi = 2a_{\pm s}K_D\sqrt{[A_T]}/[S]\gamma_{\pm} \quad (12)$$

and

$$U = (D_{AH^+} - D_{X_m^-})/(D_{AH^+} + D_{X_m^-}) \quad (13)$$

where $a_{\pm s}$ is the mean activity of the acid in the bathing solution, $\gamma_{\pm}$ is the mean activity coefficient for $H_s^+X_s^-$, and $\gamma_{(AH^+)}$ is the single ion activity coefficient for AH^+ in the membrane.

The membrane potential difference consists of the interfacial and bulk components in sequence,

$$\phi_r - \phi_l = \frac{RT}{F}\ln\frac{\left\{a_{H^+}/\gamma_{(AH^+)}\left[1+\sqrt{(1+\xi^2)}\right]\right\}_{left}}{\left\{a_{H^+}/\gamma_{(AH^+)}\left[1+\sqrt{(1+\xi^2)}\right]\right\}_{right}} + \frac{URT}{F}\ln\frac{\left\{U+\sqrt{(1+\xi^2)}\right\}_{left}}{\left\{U+\sqrt{(1+\xi^2)}\right\}_{right}} \quad (14)$$

At low bathing activities of acid $a_{\pm s}$ and at high pH values the first term is dominant and the response is Nernstian to $a_{H_s^+}$. However, when the extracted anion concentration exceed the site concentration $[S^-]$, the response peaks and declines with slope URT/F. The latter is generally negative because of the relatively low bound proton mobility. A maximum potentiometric response occurs at a specific value of $a_{\pm s}$ that is directly proportional to site concentration, and inversely dependent on the extraction coefficient.

$$a_{\pm s}(\max) = -[S]\gamma_{\pm}\sqrt{(1-U^2)}/2K_D\sqrt{[A_T]}U \quad (15)$$

When the bound protons are very immobile, the whole membrane can be thought of as an anion exchanger. In fact, the membrane has changed from a cation exchanger with negative sites to an anion exchanger with positive sites.

Consequences of Donnan failure on potentiometric pH responses

Equations 11, 13, 14 and 15 characterize the essential features of Donnan exclusion failure. As the bathing electrolyte activity is increased extraction of H^+X^- into the membrane occurs in ever increasing concentrations. Some of the H^+ remains free, while most is bound to the amine groups of the aminated PVC. The basic salt (HX in this case) extraction is described by Eqn. 11, but the overall partitioning of HX is dominated by binding of H^+ to the neutral carrier or to the aminated PVC in this case. Consequently, the partitioning of HX into the membrane is written in terms of the dominant species in Eqns. 11 and

13. The result of Donnan failure is the presence of significant X^- in the membrane and the operation of a second potential-determining interfacial ion-exchange process that decreases, nullifies or overtakes the pd established by proton exchange. This cancellation occurs because of the opposite sign on the two ion-exchanging species. This conversion of responses from permselective to non-permselective is described by the Nernst–Donnan and Nernst distribution pd expressions and generalizations [43].

As the total species is extracted, the interfacial pd is reduced from Nernstian to about zero. At the same time, the interior diffusion migration pd is modified by the motion of the new anion X^-. When the anion moves faster than the cation, the net pd passes through a maximum. That maximum occurs at the composition given by Eqn. 15. Of course, the result is a maximum only when the function U is negative because of the high interfering anion mobility. If the cation-neutral site complex were more mobile, or had the same mobility as the anion, the response would still show a positive, but sub-Nernstian response of ever diminishing value to the limiting case of zero slope. However, in the present immobilized amine sites only the anion is mobile and so the high concentration response is ideally anion-selective and Nernstian with negative slope.

Expected systematic anion interferences in potentiometric pH responses

The driving force (Gibbs free energy) is contained in the free energy of the extraction process (Eqn. 11). The driving force is a function of the strength of the binding of H^+ to the ligand, as well as the intrinsic oil solubility of the accompanying anion. This is also true for mobile neutral carriers where the driving force is also a function of the binding of the counterion to the neutral carrier as well as the intrinsic oil solublity of the anions. Since the complex formation constants of the best known neutral carriers are of the same order of magnitude (due to the fulfilment of requirements that make them attractive as carriers in liquid membranes), the differences in the anion interference have not been reported as a function of stability constants. In contrast to the other ionophores, pH-sensitive ligands may have widely different acidity constants which determine, basically, the linear response range [42]. Accordingly there are optimal candidates to prove the effects of complex stability on the Donnan failure. This means that the extent of Donnan failure is not solely a function of the anion hydrophobicity that determines the Hofmeister series. By consulting Eqn. 11, it is clear that as the pH is lowered, the driving force is increased as well. At lower pH values more serious anion interference is expected while at a given pH value, the interference should increase with anion hydrophobicity.

EXPERIMENTAL

Materials

For all experiments deionized water (Barnstead Nanopure II) and chemicals puriss or p.a. grade were used. High molecular weight (HMW) poly(vinyl chloride) purchased from Polyscience was used for the synthesis of aminated PVC ($PVC–NH_2$) [40]. All the other materials used for membrane casting (high molecular weight PVC, ionophores, plasticizers, and lipophilic salt additives were products of Fluka: tridodecylamine (TDDA, Fluka 95292); hydrogen ionophore IV (ETH-1758, Fluka 95296); chromoionophore I (ETH-5294, Fluka 27086), 2-nitrophenyl octyl ether (o-NPOE, Fluka 73307); potassium tetrakis(4-chlorophenyl) borate (KTpClPB, Fluka 60591), high molecular weight PVC (HMW-PVC, Fluka 81392).

For the determination of the pH sensitivity of the electrodes at different anion activity levels or to evaluate the anion interferences at different pH values Britton–Robinson buffer (0.0268 M citric acid, 0.0268 M KH_2PO_4 and 0.0268 M boric acid) was used [44]. The pH of the solutions was adjusted by means of a hydrogen-selective glass electrode (Orion Model 91-57) by addition of 0.2 M sodium hydroxide to the stock buffer solution. Following the dissolution of the various salts in the buffer solutions the pH was controlled again and adjusted to the required value if necessary.

By increasing the anion concentration of the

solutions the measured overall cell voltage will be influenced besides the anion interference by changes in (i) primary ion activity, (ii) diffusion potential, and (iii) interfering cation activity. These effects can generally be neglected in the present buffer solutions at low pH values and at low concentration of the interfering anion, i.e. when the ionic strength of the solution is determined by the buffer itself and no cation interference is expected. However, they can also be taken into account at higher anion concentrations using the Debye–Hückel equation, the Henderson formalism and the Nicolsky equation [45].

Ion-selective membranes

The solvent polymeric membranes were prepared as described by Moody et al. [46]. Their most common composition was 1 wt.% ionophore, 64–66 wt.% plasticizer and 33 wt.% PVC and 70 mol% (compared to the ionophore) potassium tetrakis (*p*-chlorophenyl) borate (KTpClPB) as lipophilic salt additive. However, the aminated PVC membranes were cast without additional ionophore but with KTpClPB. The membranes were tested in Philips IS 561 liquid membrane electrode bodies (Glassblaserei Möller, Zürich).

EMF measurements

Cell voltages were measured at room temperature in an air-conditioned laboratory at 22.5 ± 0.5°C with an Orion pH meter (Model 720A) connected to an Orion Model 607 manual electrode switch. As a reference electrode an Orion Model 90-02 Ag/AgCl double junction reference electrode was used throughout. The measured potential values were recorded with an ABB Goertz 420 strip chart recorder.

RESULTS AND DISCUSSIONS

Our earlier papers on hydrogen-sensitive electrodes showed that the response in acidic solutions depends on the polarity of the membrane determined by the polarity of the plasticizer [47], as well as on the kind and concentration of anions in the sample solution [48]. By keeping the membranes in very acidic solutions (pH < 3.0), where the response varies from sub-Nernstian to no pH sensitivity at all, membrane resistances were found to continuously decrease. This resistance decrease was interpreted to be a result of the protonation of the ionophore and a consequent extraction of chloride ions into the membrane to fulfil electroneutrality [48]. A similar decrease in the membrane resistance was reported with potassium-sensitive membranes if oil-soluble anions were present in the sample solution [4]. The protonation of the ionophore is a function of its acidity constant [42], i.e. the deviation from the theoretical Nernstian response is assumed to be seen at different pH values depending on the base character of the carriers or aminated PVCs (Fig. 1). Summing up, the behavior of the pH-sensitive electrodes in the low-pH region, or in other words, the level of anion interference on the hydrogen-sensitive electrodes, is a function of (i) the stability (basicity) constant of the ionophore, (ii) kind and concentration of anions present in the sample solution, and (iii) concentration of the primary ion in the sample.

To show the effect of the known acidity constant of the ionophores, where $pK_a = 14 - pK_b$, the anion concentration was increased at pH = 4.00 and pH = 6.00 (Fig. 2). As expected the

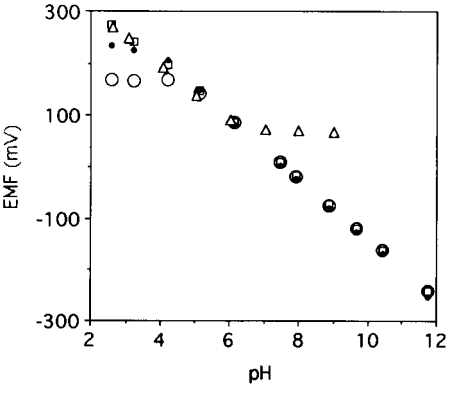

Fig. 1. pH response of different H^+-sensitive, polymeric membrane electrodes after 24 h soaking time in a pH 7.00 buffer. (○) Aminated PVC (PVC–NH_2)-based electrode; (●) ETH-5294 carrier-based electrode; (□) TDDA carrier-based electrode; and (△) ETH-1778 carrier-based electrode. All membranes were cast with o-NPOE as plasticizer and contained KTpClPB as anionic lipophilic site.

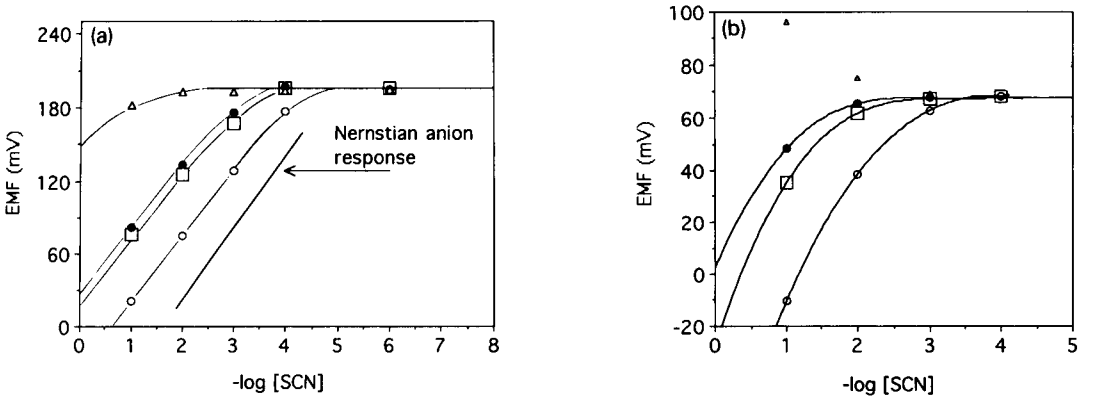

Fig. 2. Thiocyanate interference on pH-sensitive membranes based on fixed or mobile carriers of different acidity constants (□) PVC-NH_2; (●) ETH-5294; (○) TDDA; and (△) ETH-1778. (a) Experiment carried out at pH 4.00; (b) experiment carried out at pH 6.00.

anion interference with membranes fabricated with ETH-1778 ($pK_a = 3.6$) appears at higher concentration than with TDDA ($pK_a = 10.6$) and ETH-5294 ($pK_a = 11.7$)-based membranes. The positive deviation found at pH = 6.00 with the ETH-1778-based membrane (Fig. 2b) is thought to be an effect of cation interference (see the pH response function in Fig. 1). The same trend of anion interference could also be shown in the presence of other anions (e.g. Cl^- or ClO_4^-). However, the required concentration of the interferent (the extrapolated break points on the curves) would be different for each anion, owing to the differences in their lipophilicities (Fig. 3). Accordingly, to show the same trend for chloride interference the experiment should be carried out at much lower pH values, e.g., pH = 2.50. These effects of basicity are predicted by Eqn. 15. For the more basic amine groups, K_D in Eqn. 15 increases so that potentiometric reversal (maximum in the response function) occurs at lower bathing electrolyte activity (higher pH). Similarly, the intrinsic anion hydrophobicity also contributes an increase in the pH of the response maximum. Now it is the increase in K^2, multiplying K_B, in Eqn. 10 that increases K_D in Eqn. 15.

The effect of the primary ion concentration on the anion interferences is shown for Cl^- and SCN^- in Fig. 4a. At low pH values the TDDA electrode shows a nearly pure anion response in the presence of SCN^- and a slight interference at 0.1 M Cl^-. At higher pH values the anion interference disappears (Cl^-) or becomes more and more negligible in the presence of SCN^-. Another representation of the data can be given by plotting the corresponding pH–EMF data at the intersections of perpendicular lines at various interference levels (Fig. 4b). All the data points measured at different interference levels are automatically condensed at pH = 8.0 (no anion interference), while the gap between the points measured at a given pH but different anion concentrations, becomes larger with decreasing pH as the anion interference becomes more serious and approaches the "pure" anion response. Here again, the effect is described by the equilibrium in Eqn. 10.

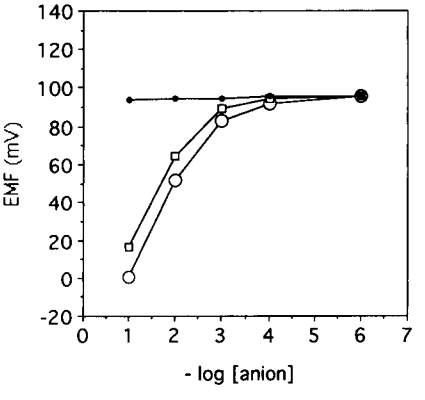

Fig. 3. Anion interference at pH 6 on a TDDA-based pH-sensitive membrane in the presence of anions of different lipophilicities. (○) ClO_4^-; (□) SCN^-; and (●) Cl^-.

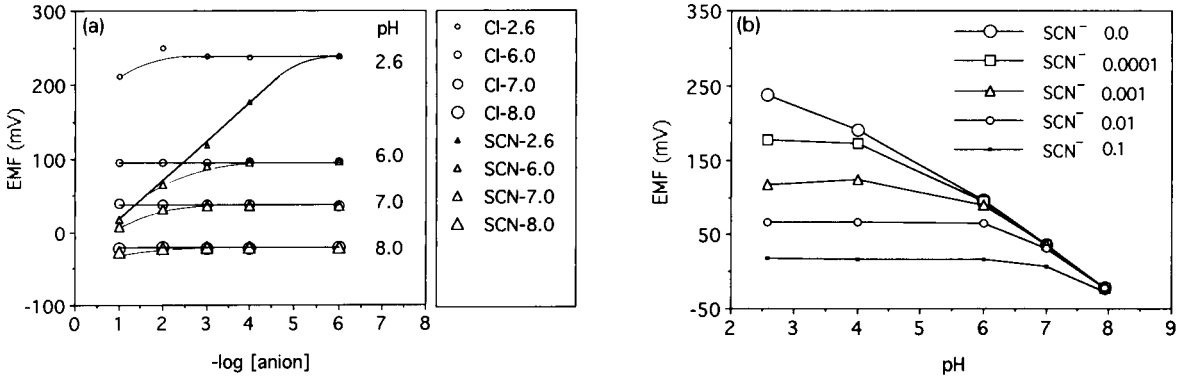

Fig. 4. The effect of primary ion (H^+) and interfering anion (Cl^- and SCN^-) concentrations on the response function of pH-sensitive solvent polymeric membranes. (a) Chloride and thiocyanate interference of a TDDA based pH sensitive electrode at different pH values. (b) Effect of the thiocyanate concentration on the measured EMF at constant pH values as derived from (a).

A conclusion arising from the results is that there should be no anion interference when the pH-sensitive membrane electrodes are used in the physiological pH range (pH ca. 7.4). However, in contrast with the above experiments, a serious interference with the potassium-selective electrode in urine compared to blood serum should be expected. In urine, the normal concentration for potassium is about 10–20 times larger than is blood serum and, as the theory predicts, a larger anion interference is found.

In addition there is an important difference between the long- and short-term behaviour of mobile (ETH-5294 and TDDA) and fixed ionophore-based (PVC–NH_2) electrodes. The pH response function of the former is invariant (long-term behaviour) and their response to sudden activity changes is fast (short-term behaviour). In contrast to these, the pH response of the aminated-PVC-based membranes changes during the first several days in acidic solutions. Their anion interference becomes less pronounced with elapsed time. During this "equilibration" period the PVC-NH_2-based electrodes have a sluggish, transient response. If the pH is changed from high to low values, the electrode apparently intends to respond according to the H^+ activity change of the solution, but, following a potential overshoot, the cell voltage decays to the anion interference level.

Conclusions

Donnan exclusion failure and resulting anion responses of ideally pH-sensitive membrane electrodes are compared for carrier-based and immobile amine "carriers" of aminated PVCs. The Donnan theory can be modified for the fixed, immobile amino PVCs and contrasted with earlier theory for carrier membranes. The principal experimental difference is the well resolved anion interferences for PVCs with immobile amine groups. Donnan failure depends on the basicity of the carriers, the primary ion activity, as well as the hydrophobicity of the anions.

REFERENCES

1 F. Helfferich, Ion Exchange, McGraw-Hill, New York, 1962, Chap. 7, pp. 323–338.
2 M. Perry, E. Lobel and R. Bloch, J. Membr. Sci., 1 (1976) 223.
3 A.P. Thoma, A. Viviani-Nauer, S. Arvanitis, W.E. Morf and W. Simon, Anal. Chem., 49 (1977) 1567.
4 G. Horvai, E. Gráf, K. Tóth, E. Pungor and R.P. Buck, Anal. Chem., 58 (1986) 2735.
5 A. van den Berg, P.D. van der Wal, M. Skowronska-Ptasinska, E.J.R. Sudholter and D.N. Reinhoudt, Anal. Chem., 59 (1987) 2827.
6 K. Tóth, E. Gráf, G. Horvai, E. Pungor and R.P. Buck, Anal. Chem., 58 (1986) 2741.
7 R.P. Buck, K. Tóth, E. Gráf, G. Horvai and E. Pungor, J. Electroanal. Chem., 223 (1987) 51.

8 M.L. Iglehart, R.P. Buck and E. Pungor, Anal. Chem., 60 (1988) 290.
9 E. Lindner, E. Gráf, Zs. Niegreisz, K. Tóth, E. Pungor and R.P. Buck, Anal. Chem, 60 (1988) 295.
10 M.L. Iglehart, R.P. Buck and E. Pungor, Anal. Chem., 60 (1988) 1018.
11 E. Lindner, V.V. Cosofret, T.M. Nahir and R.P. Buck, in A.M. Usmani and N. Armal (Eds.), Polymeric Materials in Biosensors and Diagnostics, American Chemical Society Washington, DC, 1993.
12 O. Dinten, U.E. Spichiger, N. Chaniotakis, P. Gehrig, B. Rusterholz, W.E. Morf, U. Oesch and W. Simon, Anal Chem., 63 (1991) 590.
13 U. Oesch and W. Simon, Anal. Chem., 52 (1980) 692.
14 F. Helfferich, Ion Exchange, McGraw-Hill, New York, 1962, Chap. 5.4.
15 D. Ammann, W.E. Morf, P. Anker, P.C. Meier, E. Pretsch and W. Simon, Ion-Sel. Electrode Rev. 5 (1983) 3.
16 P.C. Meier, D. Ammann, W.E. Morf and W. Simon, in J. Koryta (Ed.), Medical and Biological Applications of Electrochemical Devices, Wiley, Chichester, New York, 1980, pp. 13–91.
17 P.C. Meier, W.E. Morf, M. Labli and W. Simon, Anal. Chim. Acta, 156 (1984) 1.
18 R. Eugster, P.M. Gehrig, W.E. Morf, U.E. Spichiger and W. Simon, Anal. Chem., 63 (1991) 2785.
19 P. Wuhrman, A.P. Thoma and W. Simon, Chimia, 27 (1973) 637.
20 W.E. Morf, P. Wuhrman and W. Simon, Anal. Chem., 48 (1976) 1031.
21 W.E. Morf and W. Simon, Helv. Chim. Acta, 69 (1986) 1120.
22 W.F. Nijenhuis, E.G. Buitenhuis, F.D. Jong, E.J.R. Sudholter and D.N. Reinhoudt, J. Am. Chem. Soc, 113 (1991) 7963.
23 M.L. Iglehart and R.P. Buck, Talanta, 36 (1989) 89.
24 T.M. Nahir and R.P. Buck, Helv. Chim. Acta, 76 (1993) 407.
25 R.D. Armstrong and M. Todd, Electrochim. Acta, 32 (1987) 155.
26 R.P. Armstrong, Electrochim. Acta, 32 (1987) 1549.
27 J.R. Sandifer, M.L. Iglehart and R.P. Buck, Anal. Chem., 61 (1989) 1624.
28 T.M. Nahir and R.P. Buck, J. Electroanal. Chem., 341 (1992) 1.
29 T.M. Nahir and R.P. Buck, Electrochim. Acta, (1993) in press.
30 T.M. Nahir and R.P. Buck, J. Phys. Chem., (1993) in press.
31 T.M. Nahir and R.P. Buck, Talanta, (1993) submitted for publication.
32 G.J. Hills, P.W.M. Jacobs and N. Lakshminarayanaiah, Proc. Roy. Soc. London, Ser. A, 262 (1961) 257.
33 R.P. Buck, F.S. Stover and D.E. Mathis, J. Electroanal. Chem., 82 (1977) 345.
34 F.S. Stover and R.P. Buck, J. Electroanal. Chem., 94 (1978) 59.
35 R.P. Buck, F.S. Stover and D.E. Mathis, J. Electroanal. Chem., 100 (1979) 63.
36 J.H. Boles and R.P. Buck, Anal. Chem., 45 (1973) 2057.
37 F.S. Stover and R.P. Buck, J. Electroanal. Chem., 107 (1980) 165.
38 S.C. Ma and M.E. Meyerhoff, Microchim. Acta I (1990) 197.
39 S.C. Ma, N.A. Chaniotakis and M.E. Meyerhoff, Anal. Chem., 60 (1988) 2293.
40 V.V. Cosofret, E. Lindner, R.P. Buck, R.P. Kusy and J.Q. Whitley, J. Electroanal. Chem., 345 (1993) 169.
41 V.V. Cosofret, E. Lindner, R.P. Buck, R.P. Kusy and J.Q. Whitley, Electroanalysis, (1993) in press.
42 U. Oesch, Z. Brzozka, A. Xu, B. Rusterholt, G. Suter, H.V. Pham, D.H. Welti, D. Ammann, E. Pretsch and W. Simon, Anal. Chem., 58 (1986) 2285.
43 R.P. Buck and P. Vanysek, J. Electroanal. Chem., 292 (1990) 73.
44 D.D. Perrin and B. Dempsey, Buffers for pH and Metal ion Control, Chapman and Hall, London, 1974.
45 P.C. Meier, D. Amman, W.E. Morf and W. Simon, in J. Koryta (Ed.), Medical and Biological Applications of Electrochemical Devices, Wiley, New York, 1980, p. 13.
46 G.J. Moody, R.B. Oke and J.D.R. Thomas, Analyst, 95 (1970) 910.
47 E. Lindner, Th. Rosatzin, J. Jeney, V.V. Cosofret, W. Simon and R.P. Buck, J. Electroanal. Chem., (1993) in press.
48 V.V. Cosofret, T.M. Nahir, E. Lindner and R.P. Buck, J. Electroanal. Chem., 327 (1992) 137.

Analytica Chimica Acta, 282 (1993) 283–287
Elsevier Science Publishers B.V., Amsterdam

Prediction of the equilibrium value of a potentiometric signal. Application of the measuring technique to molecule-sensitive sensors

J. Havas, L. Kecskés and E. Rohonczy-Boksay

Radelkis Electroanalytical Instruments Ltd., R & D Department, Laborc u. 1, Budapest III (Hungary)

(Received 19th May 1993)

Abstract

A measuring technique suitable for the prediction of the electroanalytical equilibrium signal of a potentiometric sensor is described, based on the evaluation of asymptotes of the response of the cell and the confidence interval from the signals measured in the so-called information dominant section of the response. The equilibrium voltage can be evaluated with great precision by comparing the calculated data with a predetermined threshold value. The technique was applied to the determination of the equilibrium signal of a carbon dioxide sensor.

Keywords: Potentiometry; Sensors; Carbon dioxide; Equilibrium potential prediction

Potentiometric indicator electrodes attain their equilibrium potential in a definite time (response time) but not instantaneously when the activity of the solution is suddenly altered in the vicinity of the electrode. The response time depends on the type of indicator electrode, the temperature, the flow-rate of the solution, the direction of the change in concentration, the geometry of the cell, etc. [1–9].

In analytical practice, the response time of the measuring cell, which also contains a reference electrode in addition to the measuring electrode, is significant. The response time of the cell is defined similarly to that of the electrode. The response time of the cell is generally of the order of magnitude of seconds whereas for some types of molecule-selective sensors it increases to minutes.

Correspondence to: J. Havas, Radelkis Electroanalytical Instruments Ltd., R & D Department, Laborc u. 1, Budapest III (Hungary).

The voltage vs. time function of the measuring cell, the response, has an asymptotic character, hence the probability of subjective error in the readings is high especially with serial measurements. Increasing the accuracy of the measurements by the elimination of the subjective errors was first attempted in the design of potentiometric instruments intended for use in clinical laboratory diagnostics. The first approach consisted in setting a predetermined time prior to the reading. Thus the measurement result was displayed only when the predetermined time after the beginning of the measurement had elapsed.

Recently the so-called observation of response has come into general use for the elimination of the subjective error of the determination of the cell voltage, which may be considered as an equilibrium value by a digital or analog computer built into the instrument. The absolute value of the first derivative with respect to time of the electrode response (the absolute value of the rate of change) is calculated (or approached) by that

device and the display of the reading is permitted only when the above derivative is smaller than the preset threshold value.

Another possibility for the elimination of the subjective error of the reading consists in the extrapolation of the time function of the potential setting on the basis of the voltage values observed in the initial period of the measurement. This method can be applied whether the transient function of the voltage change is represented by a relatively simple and reproducible function. The latter technique differs qualitatively from the previous approaches in providing the result of the measurement before the equilibrium (stationary) value of the cell voltage has been attained.

In addition to the elimination of the subjective error of the readings, an advantage of the above three techniques is that they permit the automation of direct potentiometric measurements. It is well known that an automatic instrument needs a signal marking the attainment of the result, which is the precondition for flushing the measuring cell and starting another measurement. A further advantage in this respect, which is also valid in manual operation, is that the instrument constitutes an autonomous source of data. This means that the operator is not required to intervene for the printing of the results if a line printer is attached to the instrument, when a manual or completely automated instrument is connected to organize the data transmission without external operation or command.

The evaluation of the three methods designed for the elimination of the subjective error of readings can be summarized as follows. The application of the preset time before the readings has the drawback that a long time interval must be selected for safety and consequently the time of measurement is considerably lengthened. If the time interval is set by the operator, subjective

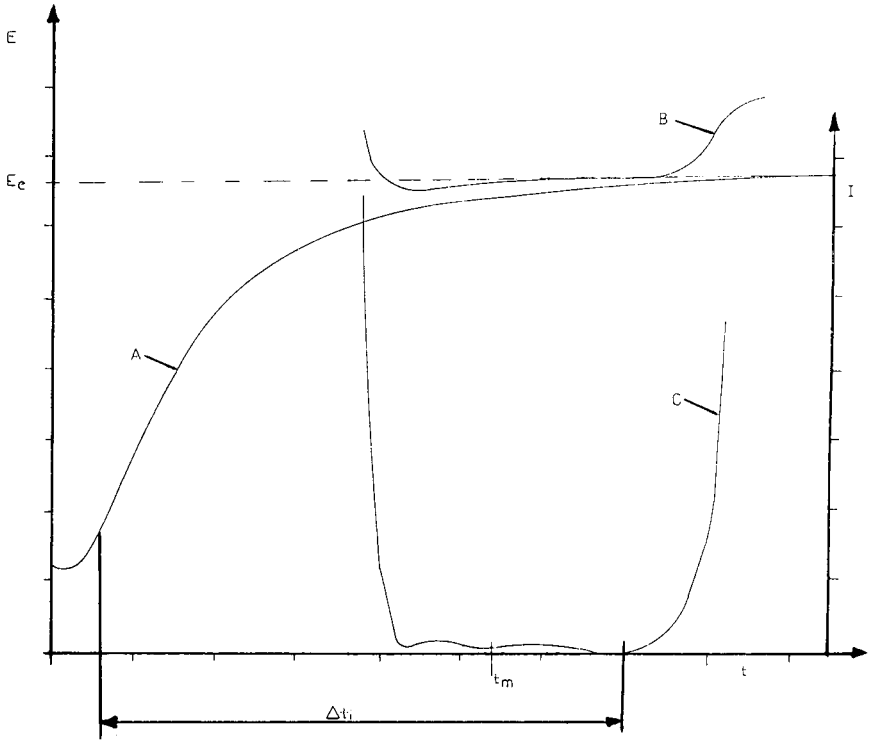

Fig. 1. Typical version of response curves (A) of electroanalytical measuring cells. The measured signal (E) and the calculated asymptote data [measured equilibrium signal (E_e)] as curve B and the actual confidence interval (I) as curve C are plotted against time (t). For t_m, see text; Δt_i = information dominant section.

errors may also arise. The difference is only that the error becomes systematic and constant.

Our experience also supports the fact that the observation of response permits the best reproducibility although it takes a long time to obtain reliable results when cells having a long response time are used.

A reading based on the extrapolation of the initial period of the response has the advantage over the previous techniques that the time of the measurement is considerably shortened. Hence it is expedient to employ it with cells having a long response time. The technique has the drawback that a small measuring error during the initial period where the rate of change is high may cause a large deviation in the estimation of the asymptote representing the measuring result. Hence the reproducibility of the instrument is impaired.

This work was aimed at designing a measuring technique that permits the exclusion of the large deviation in the estimation of the measured signal so that the precision of the measurements can be increased.

THEORETICAL

Curve A in Fig. 1 represents a typical version of the measured signal (E) vs. time (t) of an electroanalytical measuring cell. In the same system of coordinates the asymptotic values are represented as the variation of the estimated equilibrium signals calculated (in a manner to be explained later) from the actual readings referring to Δt_i, the time interval (curve B). In addition, the actual confidence interval (I) characteristic of the relevance of the measurements is shown as curve C. This was calculated on the assumption that the estimated asymptotic values can be considered as individual measured values. It is apparent that the relevance of the measurements has a maximum extending over a considerable time interval as indicated by the minimum of the confidence interval (the latter is a minimum where the average of the asymptotic values corresponds to the best estimate). The measured equilibrium signal (E_e) is obtained with a very close approximation even from the asymptotic values belonging to the initial part of that time interval (t_m).

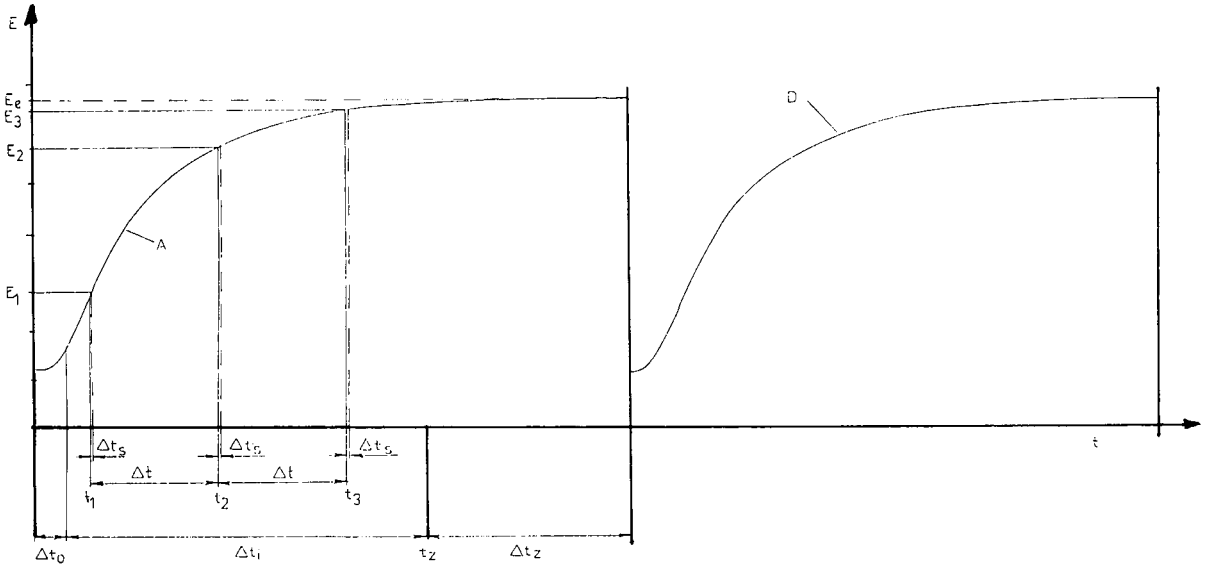

Fig. 2. Response curves of carbon dioxide sensor as measuring cell (A, D). E = measured signal (mV); E_e = equilibrium signal (mV); t = time (s); Δt_o = transient dominant section; Δt_i = information dominant section; Δt_z = disturbed section; for E_1, E_2, E_3, t_1, t_2, t_3, Δt and Δt_s, see text.

It is apparent from Fig. 2 that the function representing the response of electroanalytical measuring cells can be divided into three distinct sections: the first (Δt_o) can be termed as transient dominant section having the influence of various transient interfering effects such as temperature equilibration and diffusion; the second (Δt_i) contains the information sought in the measurement and may be termed the information dominant section; and the third (Δt_z) is strongly influenced by random errors and may be termed as the disturbed section.

In the first and last sections the interfering effects that arise do not permit the calculation of the equilibrium value of the measurement from the readings. The central section of the response, however, is suitable for the calculation of the equilibrium value as the result of the measurement (E_e) from a set of at least three measured voltage data. That value is the asymptote of the voltage function considered an exponential function having a single time constant.

Figure 2 also proves that the information dominant section of the response function can be exactly defined on the basis of the confidence interval characteristic of the given technique, which can be determined by comparison of the data calculated from the sets.

A new measuring technique can be designed on the basis of the above which permits the equilibrium value of the measured signal to be predicted. The technique essentially consists in the measurement of the signal E_1 of the cell at time t_1 (after Δt_o) at the end of the transient section (Fig. 2) followed by the measurement of E_2 and E_3 at times t_2 and t_3, respectively, preceding the disturbed section (t_1, t_2 and t_3 are selected to be $t_2 - t_1 = t_3 - t_2$). The asymptote is calculated from the measured data. Then the actual value of the signal is measured again at $t_1 + \Delta t_s$, $t_2 + \Delta t_s$ and $t_3 + \Delta t_s$ and the calculation of the asymptote is repeated. The absolute value of the difference of the two asymptotes is calculated and compared with the threshold value, which in some instances is determined by the average value of the random error. The calculation of the asymptotes is repeated until the difference in the subsequent values of the asymptotes becomes smaller than the threshold value. The last value of the asymptote obtained in that manner is considered as the equilibrium signal and the concentration or some other related parameter is calculated in the well known manner.

Another possible application of the technique is the following (cf., Figs. 1 and 2). The confidence interval characteristic of the relevance of the measurements is calculated from N predetermined asymptote values which are evaluated from measurements at equal time intervals t_1, t_2, t_3 and $t_1 + k\Delta t_s$, $t_2 + k\Delta t_s$, $t_3 + k\Delta t_s$ (where $k = 1, 2, \ldots, N - 1$). The procedure suitable for the estimation of the asymptote as described earlier is repeated until the confidence interval attains its minimum or it becomes smaller than that selected threshold value. The last estimation of the value of the Nth asymptote obtained in this manner is considered as the equilibrium signal.

MEASURED RESULTS AND THEIR EVALUATION

Determination of the asymptote

The voltage function of a carbon dioxide sensor (Radelkis Type OP-9423) observed in serial measurements is shown in Fig. 2. The response of the first sample of the series is labelled A and the second D. At the end of the transient interval Δt_o ($\Delta t_o = 8$ s) at time t_1 ($t_1 = 8$ s), signal E_1 is measured ($E_1 = -25.8$ mV). Subsequently E_2 and E_3 ($E_2 = -29.3$ mV, $E_3 = -31.1$ mV) are measured at time intervals Δt and $2\Delta t$ ($\Delta t = 10$ s) at times t_2 and t_3 preceding the disturbed section Δt_z ($\Delta t_z = 120$ s). The asymptotes relating to curve A are calculated from the above three measured values. The measurement is repeated at $t_1 + \Delta t_s$, $t_2 + \Delta t_s$, $t_3 + \Delta t_s$, ($\Delta t_s = 0.8$ s) and the asymptote is calculated again. The difference between the two asymptote values is calculated and the absolute value of the latter is compared with the predetermined threshold value K ($K = 0.1$ mV). The above operations are repeated until the difference between two subsequent asymptotes is smaller than the threshold value. The concentration or partial pressure of carbon dioxide was calculated in the well known manner

from the asymptote obtained in the above manner as the equilibrium voltage.

The time required for the determination of the equilibrium signal with the above procedure decreased to 35 s (the other known techniques, even the determination of the quasi-equilibrium signal, require 120–180 s).

The statistical evaluation of the measured data demonstrated that the reproducibility of the measurement is improved by 40–50% compared with those of the known techniques (the average response measured by the proposed method is −33.30 mV, $\sigma = \pm 0.65$ mV, whereas in the observation of the response the average is −33.85 mV, $\sigma = \pm 1.21$ mV).

Determination of the asymptote and the confidence interval

The confidence interval of the measured data is evaluated as follows. A series of measurements of the response for the carbon dioxide sensor are made according to the above procedure. N data sets of three values are used for the calculation ($N = 8$), which are obtained at times $t_1 + k\Delta t_s$, $t_2 + k\Delta t_s$, $t_3 + k\Delta t_s$ (where $k = 0, 1, 2, \ldots, N-1$). The results are given in Table 1. Asymptotes A_i were evaluated from the N-data set (−34.10, −34.15, −34.06, −34.01, −34.84, −33.98, −34.06 and −34.05 mV) followed by calculation of the confidence interval ($I = 0.09$ mV). The latter is compared with the predetermined threshold value ($K = 0.10$ mV). If the confidence interval is smaller than the threshold value the mathematical average of N asymptotes is accepted as the equilibrium signal ($E_e = -34.03$ mV).

If the confidence interval is larger than the predetermined threshold value, the procedure is modified. The first set of three data (E_1, E_2, E_3) is omitted and another set of three data observed at time Δt_s after the reading of the last three data is included in the calculation. This procedure is repeated until the confidence interval becomes smaller than the threshold value K. The average value of the asymptotes is considered as the equilibrium voltage and it is used for the calculation of the concentration or partial pressure of carbon dioxide.

The above measuring technique can be employed in the determination of the equilibrium value of molecular sensors prepared with immobilized enzymes such as urea- [10] and tyrosine-selective sensors [11] in addition to the carbon dioxide electrode.

TABLE 1

Data obtained with use of the carbon dioxide sensor

k	$E_1(t_1 + k\Delta t_s)$ (mV)	$E_2(t_2 + k\Delta t_s)$ (mV)	$E_3(t_3 + k\Delta t_s)$ (mV)
0	−34.90	−34.50	−34.30
1	−34.85	−34.45	−34.28
2	−34.78	−34.43	−34.25
3	−34.70	−34.40	−34.23
4	−34.65	−34.38	−34.20
5	−34.60	−34.35	−34.20
6	−34.58	−34.33	−34.20
7	−34.53	−34.30	−34.18

The authors express their thanks to Mr. Rudolf Hoffmann and Mr. Gyula Tfirst for supplying them with the hardware and software background necessary for these experiments.

REFERENCES

1 E. Lindner, K. Tóth and E. Pungor, Anal. Chem., 48 (1976) 1071.
2 W.E. Morf and W. Simon, in M. Kessler, L.C. Clark, D.W. Lübbers, I.A. Silver, W. Simon (Eds.), Ion and Enzyme Electrodes in Biology and Medicine, Urban and Schwarzenberg, Munich, Berlin, Vienna, 1976, p. 51.
3 A. Shatky, Anal. Chem., 48 (1976) 1039.
4 R. Widick, in M. Kessler, L.C. Clark, D.W. Lübbers, I.A. Silver and W. Simon (Eds.), Ion and Enzyme Electrodes in Biology and Medicine, Urban and Schwarzenberg, Munich, Berlin, Vienna, 1976, p. 54.
5 K. Tóth and E. Pungor, Anal. Chim. Acta, 64 (1973) 417.
6 R.P. Buck, J. Electroanal. Chem., 18 (1968) 363.
7 R.P. Buck, J. Electroanal. Chem., 18 (1968) 381.
8 G. Johansson and K. Norberg, J. Electroanal. Chem., 18 (1965) 239.
9 J. Havas, Ion- and Molecule-Selective Electrodes in Biological Systems, Springer, Berlin, Heidelberg, New York, Tokyo, 1985.
10 J. Havas, E. Rohonczy-Boksay and E. Porjesz, in E. Pungor (Ed.), 1st Bioelectroanalytical Symposium, Mátrafüred, 1986, Akadémiai Kiadó, Budapest, 1987, p. 225.
11 J. Havas and G.G. Guilbault, Anal. Chem., 54 (1982) 1991.

Analytica Chimica Acta, 282 (1993) 289–296
Elsevier Science Publishers B.V., Amsterdam

Electrochemical oxidation of lysergic acid-type ergot alkaloids in acetonitrile. Part 1. Stoichiometry of the anodic oxidation electrode reaction

Tibor Dankházi, Éva Fekete, Krisztina Paál and George Farsang

Institute of Inorganic and Analytical Chemistry, L. Eötvös University of Sciences, P.O.B. 32, H-1518 Budapest 112 (Hungary)

(Received 19th April 1993)

Abstract

The ergot alkaloids are an important group of compounds used extensively in medicine. An intrinsic property of these molecules is that the ergoline compounds decompose spontaneously in an oxidative process. A systematic study was carried out with the aim of describing the stoichiometry of the electrochemical oxidation reaction which simulates the oxidative degradation. Eight ergo- and 9,10-dihydroergopeptides were investigated, including the group of 9,10-dihydroergotoxine alkaloids and simple ergoline derivatives. Cyclic voltammetry, controlled-potential coulometry and isolation and identification of the electrochemically oxidized forms led to the conclusion that the electrochemical oxidation of all lysergic acid-type ergot alkaloids takes place in the same way. The main oxidation product is always a highly conjugated dimer, and the dimerization is located at the indole part of the ergoloid skeleton. The study of the stoichiometry of the oxidative electrode reaction of lysergic acid-type ergot alkaloids is described, which provides a theoretical and experimental basis for the liquid chromatographic or flow-injection determination with amperometric detection of these alkaloids in different pharmaceutical formulations.

Keywords: Coulometry; Voltammetry; Alkaloids; Electrochemical oxidation; Ergot alkaloids; Lysergic acids

The ergot alkaloids are products of *Claviceps purpurea*, a parasitic fungus on rye [1]. Studies of their structures showed that all of the more than twenty compounds isolated and identified [2,3] contain the condensed tetracyclic ring called ergoline by Jacobs and Gould [4]. Two main groups can be distinguished, clavins and lysergic acid derivatives; only the latter group is considered in this paper.

It has been established that the central nervous system is affected by these alkaoids, and muscular system contraction and hormone secretion have also been observed. Since the 1950s, the main research has been aimed at producing semi-synthetic products in order to obtain alkaloids with more specific effects [5–18]. The 9,10-dihydroderivatives belong to this group of compounds and are prepared by the catalytic hydrogenation of the ergot alkaloids [19]. In addition to their different physiological effects, a particular advantage of the hydrogenated compounds is their higher stability in solution [20].

The compounds extracted from ergot contain ergotoxine in the largest amount [21]. It consists of an equimolar mixture of ergochristine, ergocriptine and ergocornine [22]. Later it was found that ergocriptine itself is a mixture of two isomers in a 3 : 1 molar ratio [23].

These compounds are the effective ingredients in a wide range of pharmaceutical preparations,

Correspondence to: G. Farsang, Institute of Inorganic and Analytical Chemistry, L. Eötvös University of Sciences, P.O.B. 32, H-1518 Budapest 112 (Hungary).

which are prepared in the form of tablets, coated tablets and solutions (drops, injections). The solution preparations of the ergotoxines and similar ergopeptide alkaloids are especially sensitive to different degradation processes that take place spontaneously, i.e., isomerization (aci-products) [24] and hydrolysis, the cyclic tripeptide part of ergopeptides disintegrating (depending on the composition of the solvent mixture or the pH of the solution) [25].

An important decomposition process in the case of lysergic acid derivative-type ergot and 9,10-dihydroergot alkaloids is their spontaneous oxidative degradation in solution, which causes the appearance of a yellow colour in solutions prepared for pharmaceutical purposes [26–31].

This spontaneous oxidizability of this type of molecules has led to studies to establish electrochemical methods to determine these compounds based on electrooxidation. Belal and Anderson [32] devised a flow-injection determination of ergonovine maleate with amperometric detection at a Kel-F–graphite composite electrode. A sensitive method was reported by Wang and Ozsoz [33], using enrichment in a lipid-coated glassy carbon electrode followed by differential-pulse anodic stripping of the ergot alkaloids. Extremely good sensitivity and selectivity were achieved by using this lipid-coated electrode, because of the enrichment of hydrophobic alkaloids and selectivity that excluded the effect of polar electroactive species present in large excess, i.e., in urine sam-

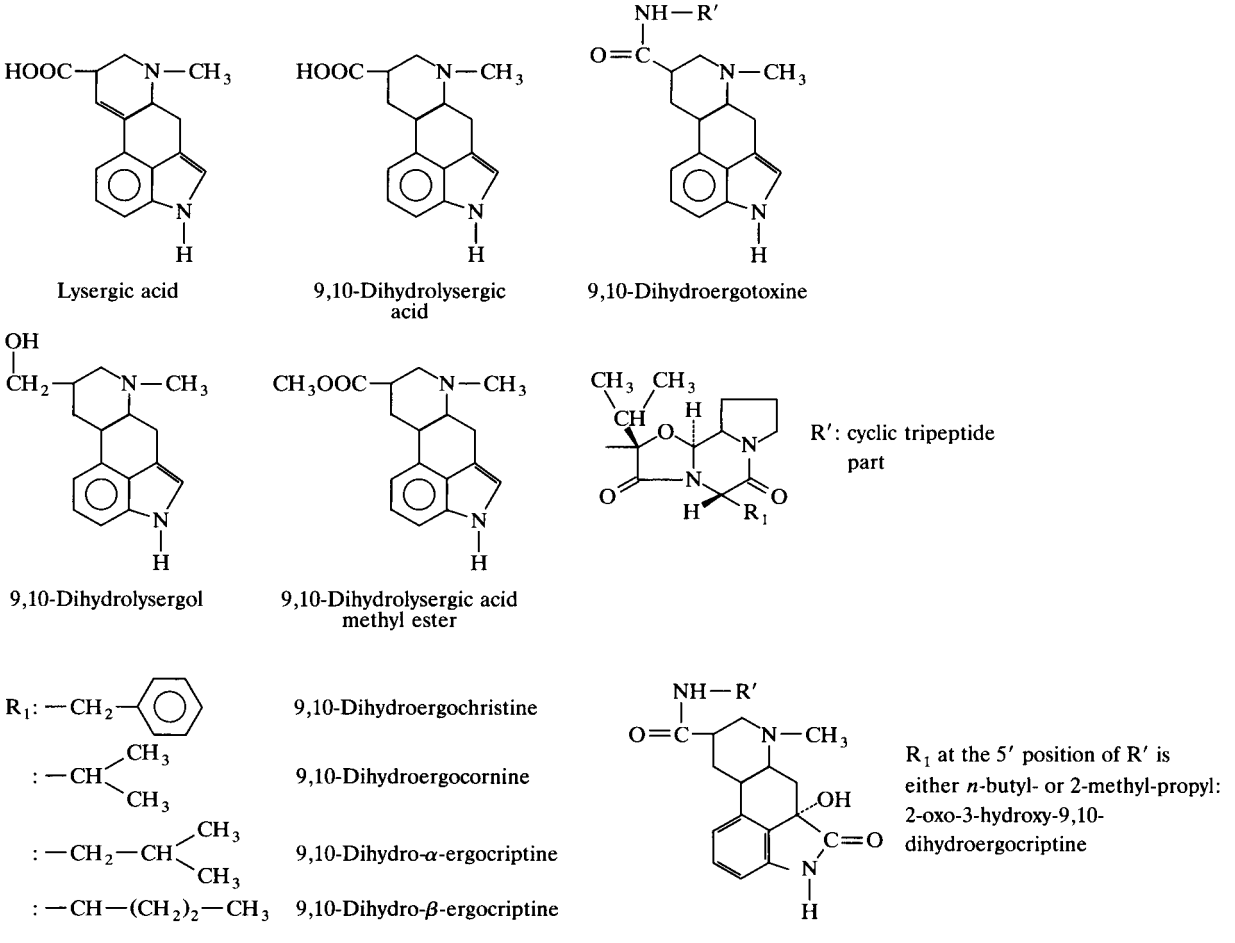

Fig. 1. Compounds studied.

ples. Although one of the most generally applicable methods for the determination of these compounds is liquid chromatography (LC), only UV detection following the separation has been used so far [34,35]. In earlier work, LC with amperometric detection was used in order to control the oxidative degradation of ergopeptide alkaloids [36].

The aim of this work was to determine the stoichiometry of the electrooxidation reaction, which is probably also modelling the spontaneous oxidative degradation reaction. It can be assumed that this reaction takes place when oxidative amperometric detection is used in the determination of these alkaloids by either LC or flow-injection methods [37]. It is probable that the electrooxidation reaction is generally valid for lysergic acid-type ergot alkaloids, as all of the relatively large number of the alkaloids and derivatives investigated showed the same type of electrochemical behaviour as described in this paper.

EXPERIMENTAL

Instrumentation

Cyclic voltammetry (CV) was carried out in a Bruker E-100 universal polarograph connected to a Linseis LY 1700 x–y recorder. The potentiostat input of the polarograph was driven externally by an Elektroflex function generator.

Controlled-potential coulometry (CPC) was performed using a Tacussel ASA4-SHT2 potentiostate connected to an IG 5N current integrator. In both instances laboratory-made glass cells were used with a tight PTFE cover. The electrodes were immersed in the solution through holes drilled in this PTFE lid.

For cyclic voltammetry, Pt disc electrodes of 1, 3 and 5 mm diameter were used as the working electrode, placed in the centre of a cylindrical Pt net that served as the counter electrode. A Tacussel RDJ 10 Ag double-junction reference electrode of the first kind was used. Its potential-determining space was filled with 0.01 M $AgNO_3$ solution dissolved in acetonitrile (MeCN) and its salt bridge was filled with the same base electrolyte solution as used in the electrochemical methods.

In CPC a cylindrical Pt gauze electrode was used as the working electrode and the counter electrode was made from a Pt tube immersed in a glass tube closed at the bottom with a glass frit of G-2 porosity, and filled with the base electrolyte. The solution to be electrolysed was stirred with high-purity nitrogen and with a magnetic stirrer bar.

Spectra in the UV–visible range were measured with a Perkin–Elmer λ15 spectrophotometer. Mass spectra were measured with a Kratos MS 80 spectrometer using chemical ionization.

Chemicals

All the ergot and 9,10-dihydroergotoxine alkaloids (Fig. 1), supplied as methanesulphonate salts and a few other simple ergoloid derivatives were supplied by Gedeon Richter Chemical Works (Hungary) as authentic samples: 9,10-dihydroergotoxine, 9,10-dihydroergochristine, 9,10-dihydroergocornine, 9,10-dihydroergocriptine, 9,10-dihydro-β-ergocriptine, 9,10-dihydrolysergic acid, 9,10-dihydrolysergic acid methyl ester (prepared from 9,10-dihydrolysergic acid according to the procedure developed in the Laboratory of Organic Electrochemistry, Organic Department, Aarhus University, Denmark), 9,10-dihydro-8-hydroxymethyleneergoline (9,10-dihydrolysergol), 2-oxo-3-hydroxyergocriptine, ergotoxine and 8-hydroxymethyleneergoline (lysergol).

All reagents were of analytical-reagent grade unless indicated otherwise. Acetonitrile of spectrophotometric grade (Janssen Chimica, Beerse, Belgium) was kept over 3Å molecular sieve (Merck, Darmstadt) before use. Anhydrous acetic acid, acetic anhydride, concentrated perchloric acid 69.0–72.0% and concentrated ammonia solution 28.0–30.0% (all from Reanal, Budapest) and anhydrous $LiClO_4$ of puriss grade (Fluka, Buchs) were used.

Isolation and identification of the oxidation product

After some failures with extraction, the isolation procedure described under Experimental was successfully followed.

By preparative controlled-potential electrolysis, 1×10^{-3} M 9,10-dihydrolysergol was oxidized in acidic MeCN solvent containing 0.1 M $LiClO_4$ as supporting electrolyte. After completion of electrolytic oxidation, 5–5 ml of the oxidized solution were made slightly alkaline by adding a few drops of concentrated ammonia solution and diluting to 50 ml with water. A 10-ml volume of that solution was treated in a Sep-Pak C_{18} cartridge for rapid sample preparation (Merck). The oxidized compound remained on the column. The column was then washed by water until the conductivity of the eluate decreased to that of water. Subsequently, the oxidized form was eluted from the column with 10 ml of freshly distilled chloroform–methanol (1 + 1). This was repeated and the combined eluate was evaporated in a rotary evaporator at 40°C to remove the eluent.

The oxidation product was dried over P_2O_5 in vacuo. By dissolving it in neutral MeCN it gave a yellow colour and the spectrum showed an absorbance band in the visible range with a maximum at 370 nm. When acidified with water-free perchloric acid it turned deep purple and the wavelength of the absorbance band maximum was 530 nm. This means that the isolated solid product is the main electrooxidation product. The product was tested by thin-layer chromatography on a Whatman K C_{18}/F RP plate. The main product gave a yellow large spot (two other small spots were found). The mass spectrum of the isolated product using chemical ionization was recorded to find the molecular peak of the product. The peak of highest mass number, i.e., the molecular ion peak, was found at m/z 508 ± 1.

RESULTS

Cyclic voltammetry of ergot and 9,10-dihydroergotoxine alkaloids

Cyclic voltammetry (CV) was carried out at Pt disc electrodes in an acetonitrile medium containing the depolarizer (10^{-3}–10^{-4} M) and two "equivalents" of perchloric acid solution. The latter was prepared by dissolving the perchloric acid in anhydrous acetic acid and adding the calculated amount of acetic anhydride, which

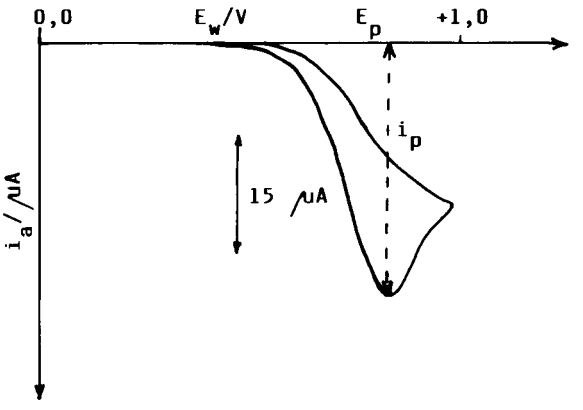

Fig. 2. Cyclic voltammetric curve for 5×10^{-4} M dihydroergotoxine in 0.1 M $LiClO_4$–MeCN base electrolyte containing 1×10^{-3} M perchloric acid. Start potential, 0.0 V; scan rate 0.03 V s^{-1}; working electrode, Pt disc, diameter 5 mm, i_a = anodic current; E_w = working electrode potential vs. 0.01 M Ag^+/Ag double-junction reference electrode of the first kind.

eliminated by hydrolysis all of the water present originally in the perchloric and acetic acid. Acetic acid behaves as an extremely weak acid in MeCN [38]. The CV curves were therefore recorded in acidic water-free MeCN solution, the water content was less than 2×10^{-3}–3×10^{-3} M as checked by the Karl Fischer method using dead-stop end-point detection. The addition of acid was necessary because otherwise the results were irreproducible. In the acidified MeCN–0.1 M $LiClO_4$ base electrolyte neither irreproducibility nor a filming effect at the Pt working electrode was observed.

At the low polarization rates studied (0.01–0.02 to 1–2 V s^{-1}) all of the compounds showed very similar CV behaviour, a single sharp, totally irreversible anodic peak was observed (Fig. 2). The peak current (i_p) values of the different compounds varied slightly at the same concentration, but all of the ergot and 9,10-dihydroergotoxine alkaloids have a single irreversible anodic oxidation peak practically at the same peak potential (E_p). A slight shift was observed towards more positive potentials on increasing the scan rate, and the oxidation peak shifted in a negative direction on increasing the concentration, as is well known for irreversible electrode processes. The

concentration dependences of the peak heights were linear, and i_p also depended linearly on the square root of the scan rate for the compounds studied.

This experimental behaviour did not change when the CV behaviour of 9,10-dihydrolysergol or 9,10-dihydrolsergic acid and its methyl ester was compared. It can be concluded that the electrochemical oxidation takes place in the lysergic acid or 9,10-dihydrolysergic acid skeleton. The fact that the CV curve always showed a single irreversible anodic peak led to the conclusion that, compared with the time scale of CV experiments, a fast, coupled chemical reaction takes place following the electron transfer step in the oxidation.

2-Oxo-3-hydroxyergocriptine is not oxidizable electrochemically.

Controlled-potential coulometry (CPC)

Controlled-potential electrolysis coupled with measurement of the amount of charge needed for complete oxidation of a weighed amount of compound is especially useful for preparing sufficient of the oxidized form for isolation and identification (preparative electrolysis at controlled potential) and for calculating the n_{app} value (the number of electrons exchanged per molecule oxidized). As the controlled-potential method provides a suitable selectivity for the oxidation, Faraday's law can be used to calculate n_{app}.

CPC was carried out for all of the compounds investigated earlier by CV in the same media. All electrolyses were carried out at a 0.2-V more positive potential than the peak potential value E_p found by CV at the given concentration of the compound under study. The electrolyses were carried out in the concentration range 10^{-3}–10^{-4} M. From the measured amount of charge the n_{app} value was calculated in each instance. In each electrolysed solution the number of moles of acid formed was determined by titrating the solution from an Agla micrometer syringe (Burroughs Wellcome) with 1 M piperidine solution dissolved in MeCN. The end-point was indicated by the colour change of the solution followed spec-

TABLE 1

Results obtained by controlled-potential electrolysis of ergoloids

Compound	Amount of compound electrolysed (mol)	n_{app}	Amount of $HClO_4$ formed during electrolysis (mol)
9,10-Dihydroergotoxine	1.0×10^{-3}	1.99	1.98×10^{-3}
	5.0×10^{-4}	1.97	9.92×10^{-4}
	1.0×10^{-4}	1.99	2.01×10^{-4}
9,10-Dihydroergochristine	5.0×10^{-4}	1.96	1.00×10^{-3}
	1.5×10^{-4}	2.02	2.98×10^{-4}
	(six parallel	2.00	3.01×10^{-4}
	measurements)	2.05	2.95×10^{-4}
		1.96	2.89×10^{-4}
		2.03	2.95×10^{-4}
		1.95	3.01×10^{-4}
9,10-Dihydroergocornine	1.0×10^{-3}	1.96	2.01×10^{-3}
	5.0×10^{-4}	2.00	9.98×10^{-4}
	1.5×10^{-4}	2.02	2.97×10^{-4}
	1.0×10^{-4}	2.06	1.98×10^{-4}
9,10-Dihydro-β-ergocriptine	1.5×10^{-4}	1.96	3.01×10^{-4}
9,10-Dihydrolysergic acid	1.0×10^{-4}	1.97	–
9,10-Dihydrolysergic acid methyl ester	1.0×10^{-4}	1.99	2.01×10^{-4}
9,10-Dihydrolysergol	1.0×10^{-3}	1.99	1.95×10^{-3}
	1.0×10^{-4}	1.96	2.01×10^{-4}
2-Oxo-3-hydroxyergocriptine	1.0×10^{-4}	Not oxidizable	

trophotometrically at 530 nm (for the spectrophotometric properties of the oxidized solution, see later). In this way the number of moles of perchloric acid formed per mole of oxidized compound was calculated by taking into account the methanesulphonic acid bound to the reduced form of alkaloids at the start of the oxidation.

In Table 1 the measured n_{app} values and moles of $HClO_4$ per mole of alkaloid are summarized. Both are important quantities from the point of view of the stoichiometry of electrooxidation. These results prove that the electrochemical oxidation of each of the compounds investigated involves two electrons and two protons per mole of starting material. Another important conclusion is that the lysergic acid skeleton is attacked by the oxidation, because no difference was observed in the stoichiometry when either ergopeptide-type alkaloids or the simpler ergoloids were oxidized. 2-Oxo-3-hydroxyergocriptine could not be oxidized using either the CV or CPC technique. This means that the indole part of the lysergic acid skeleton is responsible for the oxidizability of ergot alkaloids.

The oxidized form of the compounds in each instance is deep purple. This was investigated further by spectrophotometry of the oxidized solution.

Spectrophotometric study of the acid–base equilibrium of the oxidized form

After starting the CPC electrolysis, the originally colourless solution turned purple and its intensity increased until the electrolysis was complete. This deep purple solution, when diluted with water (which behaves as a Brønsted base in the aprotic MeCN solvent), changed to greenish yellow. In order to prove that this colour change is an acid–base process, and to measure the acid produced during the electrolysis, an aliquot of totally oxidized solution was titrated with 1 M piperidine solution dissolved in MeCN. The piperidine was added from an Agla micrometer syringe and the colour change was followed by recording the absorption spectra of the titrated solution in the visible range.

Figure 3 shows the spectra of the protonated oxidized form titrated with piperidine. Before

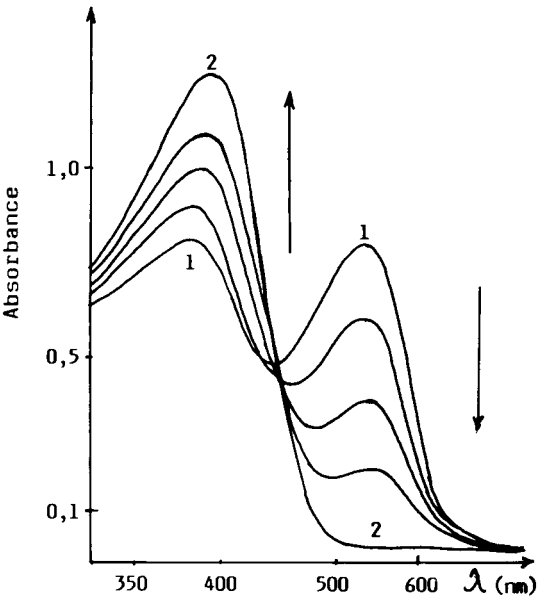

Fig. 3. UV–visible absorption spectra of an aliquot of the oxidized solution of 9,10-dihydroergochristine titrated with 1 M piperidine dissolved in MeCN. The arrows show the effect of addition of piperidine base on the absorption spectra. Curve 1 = spectrum taken before titration; curve 2 = spectrum recorded after addition of two "equivalents piperidine". λ_{max_1} = 530 nm, λ_{max_2} = 370 nm.

starting the titration, the absorption spectrum has two absorption maxima, then on adding increasing amounts of piperidine the peak at 530 nm decreased while that at 370 nm increased. After adding two "equivalents" of piperidine only the absorbance band of the yellow colour remained. The basic form of the oxidized product is yellow. The acid–base process is reversible, because on reacidifying the solution with perchloric acid the red colour of the protonated oxidized form returns.

The intensely coloured oxidation product led to the conclusion that the oxidation product is a highly conjugated compound, which is the result of a relatively fast follow-up reaction of the primary electrooxidation step.

The stoichiometry of the oxidation involves a two-electron, two-proton reaction. It was assumed that the oxidation reaction probably results in a highly conjugated dimeric oxidation product.

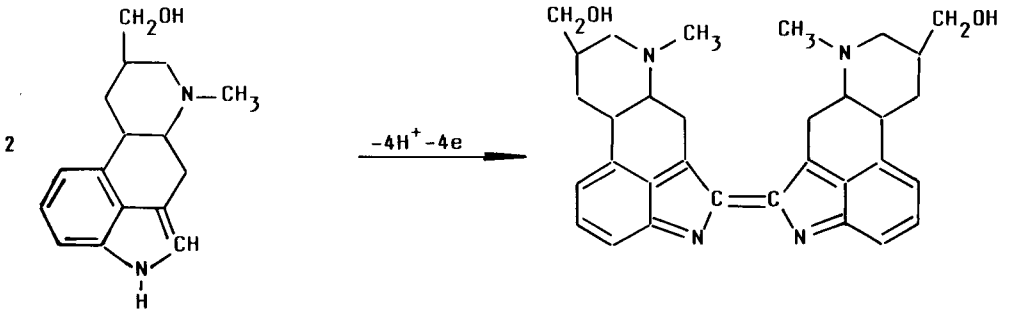

Fig. 4. Stoichiometric equation for the electrooxidation of 9,10-dihydrolysergol in acidic MeCN medium containing 0.1 M $LiClO_4$ base electrolyte.

Isolation and identification of the oxidation product

The CV and CPC measurements led to the conclusion that a simple ergoloid-type compound should be chosen for this purpose, because the interference from the decomposition of the cyclic tripeptide part of ergotoxin alkaloids would aggravate the isolation procedure. It seemed most promising to try the isolation of the oxidation product of 9,10-dihydrolysergol. Unlike lysergic acid it does not contain a basic and an acidic group simultaneously, which could prevent simple isolation; thus either extraction or column chromatography could be used.

Conclusions

From the experimental results, the stoichiometric equation shown in Fig. 4 can be written for the electrooxidation of 9,10-dihydrolysergol. This equation is probably can be taken as generally valid for all lysergic acid derivative-type ergot alkaloids. The intense colour of the product is due to of the highly conjugated dimer. The fact that each mole of oxidized compounds produced 2 mol of perchloric acid, and 2 F of electric charge are consumed per mole is thus explained. The totally irreversible CV behaviour with the formation of the dimer is evident.

The oxidative electrodimerization takes place on the indole part of the lysergic acid skeleton, because the C-2 position of the molecule can be easily attacked (i.e., 2-bromolysergic acid and 2-oxolysergic acid can be prepared [2]). This is evidence for the oxidation of that part of molecule and that all of the ergopeptides and lysergic acid derivatives studied behave very similarly in electrochemical oxidation. When the C-2 position is blocked, i.e., in 2-oxo-3-hydroxy-9,10-dihydroergocriptine, the compound cannot be oxidized electrochemically and shows no CV behaviour. Further proof of the suspected point of attack of the molecules is that none of the oxidized compounds gave the Van Urk reaction, a generally used colour reaction with ergot alkaloids, which also needs an unblocked C-2 position [39].

These experimental results can provide a reasonable explanation for the yellow colour of pharmaceutical solution formulations of different ergot alkaloids (injections and drops) after prolonged storage, because they are solutions either in distilled water or in mixtures of glycerin, propyleneglycol and ethanol. The spontaneous oxidative decomposition of the ergot alkaloids causes the appearance of the yellow colour during storage.

With the knowledge of the electrochemical oxidative behaviour, an LC determination using amperometric detection could be developed. The combination of LC and CPC gave the possibility of distinguishing between the oxidative degradation trend of the alkaloids of the ergotoxine group. These results will be published in further papers.

One of the authors (George Farsang) was introduced to electroanalytical research by Professor Ernõ Pungor, and this paper is dedicated with

great affection to Professor Pungor on the occasion of his 70th birthday. The authors express their gratitude to the Plant Chemistry Department of Gedeon Richter Chemical Works for supplying the samples. Professor Henning Lund (Aarhus University) is thanked for his advice on the preparation of 9,10-dihydrolysergic acid methyl ester. This work was partly supported by the Hungarian National Scientific Research Fund, OTKA I/3, Contract No. 2285, which is gratefully acknowledged.

REFERENCES

1 L.R. Brady, Lloydia, 25 (1965) 1.
2 A. Stoll and A. Hofmann, in R.H.F. Manske (Ed.), The Alkaloids, Vol. 8, Academic Press, New York, 1965, Chap. 21.
3 A. Stoll and A. Hofmann, in R.H.F. Manske (Ed.), The Alkaloids, Vol. 15, Academic Press, New York, 1975, Chap. 1.
4 W.A. Jacobs and R.G. Gould, Jr., J. Biol. Chem., 120 (1937) 144.
5 M.C. Shelesnyak, Am. J. Physiol., 179 (1954) 301.
6 M.C. Shelesnyak, B. Lunenfeld and B. Honig, Life Sci., 1 (1963) 73.
7 E. Flückiger and H.R. Wagner, Experientia, 24 (1968) 1130.
8 E. Billeter and E. Flückiger, Experientia, 27 (1971) 464.
9 E. Flückiger, P.M. Lutterbeck, H.R. Wagner and E. Billeter, Experientia, 28 (1972) 924.
10 P.M. Lutterbeck, J.S. Pryor, L. Varga and R. Wenner, Br. Med. J., (1971) 228.
11 L. Varga, P.M. Lutterbeck, J.S. Pryor, R. Wenner and H. Erb., Br. Med. J., (1972) 743.
12 L. Varga, P.M. Lutterbeck, J.S. Pryor, R. Wenner and H. Erb., Schweiz. Med. Wochenschr., 102 (1972) 1284.
13 K. Rezabek, M. Semonsky and N. Kuharczyk, Nature, 221 (1969) 666.
14 V. Zikan, M. Semonsky, K. Rezabek, M. Auskova and M. Seda, Collect. Czech. Chem. Commun., 37 (1972) 2600.
15 H.G. Floss, J.M. Cassady and J.E. Robbers, J. Pharm. Sci., 62 (1973) 699.
16 G. Stamm, PhD Thesis, Swiss Federal Institute of Technology, Zurich, 1969, No. 4418, p. 53.
17 R.P. Gysi, PhD Thesis, Swiss Federal Institute of Technology, Zurich, 1973, No. 4990, p. 23.
18 H. Tscherter and H. Hauth, Helv. Chim. Acta, 57 (1974) 113.
19 A. Stoll and A. Hofmann, Helv. Chim. Acta, 20 (1943) 2070.
20 A. Végh, Gy. Szász and M. Takács, Gyogyszereszi Kemia, Medicina, Budapest, 1972.
21 K. Rezabek, M. Semonsky and N. Kuharczyk, Nature, 221 (1969) 666.
22 A. Stoll and A. Hofmann, Helv. Chim. Acta, 26 (1943) 1570.
23 P.A. Stadler, S. Guttmann, H. Hauth, R.L. Huguenin, E. Sandrin, G. Wersin, H. Willems and A. Hofmann, Helv. Chim. Acta, 52 (1969) 1549.
24 W. Chlienz, R. Brunner, F. Thuollin and A. Hofmann, Experientia, 17 (1961) 108.
25 W.A. Jacobs and L.C. Craig, J. Am. Chem. Soc., 57 (1935) 960.
26 K. Freter, J. Axelrod and B. Witkop, J. Am. Chem. Soc., 79 (1957) 3191.
27 F. Troxler and A. Hofmann, Helv. Chim. Acta, 42 (1959) 793.
28 H. Köhn, Dtsch. Apoth.-Ztg., 119 (1976) 1884.
29 B. Kreilgard and J. Kisbye, Arch. Pharm., Chem. Sci. Ed., 2 (1974) 1.
30 B. Kreilgard and J. Kisbye, Arch. Pharm., Chem. Sci. Ed., 2 (1974) 38.
31 E. Ermer, Pharm. Ztg., 120 (1975) 149.
32 F. Belal and J.L. Anderson, Talanta, 33 (1986) 448.
33 J. Wang and M. Ozsoz, Electroanalysis, 2 (1990) 595.
34 L. Szepesi, I. Fehér, G. Szepesi and M. Gazdag, J. Chromatogr., 149 (1978) 271.
35 G. Szepesi, M. Gazdag and L. Tardy, J. Chromatogr., 191 (1980) 101.
36 M. Gazdag, G. Szepesi and G. Farsang, in Proceedings of the 3rd Danube Symposium on Chromatography, Siófok (Hungary), 1981, p. 20.
37 J. Inzeffy, Zs. Bertha Somodi, Zs. Papp-Sziklay and G. Farsang, J. Pharm. Biomed. Anal., 11 (1993) 191.
38 I.M. Kolthoff and M.K. Chantooni, J. Am. Chem. Soc., 27 (1965) 4428.
39 H.W. van Urk, Pharm. Weekbl., 66 (1929) 473.

Analytica Chimica Acta, 282 (1993) 297–305
Elsevier Science Publishers B.V., Amsterdam

Liposome immunomigration field assay device for Alachlor determination

Sui Ti A. Siebert, Stuart G. Reeves and Richard A. Durst
Analytical Chemistry Laboratories, Cornell University, Geneva, NY 14456-0462 (USA)

(Received 21st May 1993)

Abstract

The feasibility of a simple, single-use immunomigration system has been demonstrated, using Alachlor as a model environmental contaminant. In the device, capillary action causes Alachlor and Alachlor-tagged, dye-containing liposomes to migrate through an anti-Alachlor antibody zone, on a plastic-backed nitrocellulose strip, where competitive binding occurs. Unbound liposomes continue migration to a liposome capture zone, where they are quantified either visually or by densitometry. The amount of liposome-entrapped dye that is measured in this zone is directly proportional to the Alachlor concentration in the sample.

Keywords: Biosensors; Immunoassay; Alachlor; Liposomes; Herbicides; Field assay

The need for rapid and inexpensive field assays in environmental screening and remediation studies has become more urgent in recent years. The use of conventional analytical methods is generally labor intensive and time consuming, often taking days or weeks from sample acquisition to obtaining the results. Thus when carrying out a preliminary survey of a possibly contaminated site, this delay means that expensive remediation equipment may lie idle for weeks while awaiting results of the initial survey. A simple and quick field assay, especially for initial screening, would prevent this downtime and significantly reduce the cost of remediation.

Immunoassays, which offer high selectivity, sensitivity, speed and simplicity of operation, have recently gained more attention in the area of environmental analysis [1,2]. The immunoassays that have been developed are mainly in the form of ELISAs (enzyme-linked immunosorbent assays), where measurements are made of the color produced from a colorless substrate by the action of an enzyme conjugated to either an antibody or an analyte molecule.

Previous studies [3–6] have demonstrated the advantages of liposome-encapsulated dye rather than enzymatically produced color to enhance the signal obtained in the competitive reaction, and have used this amplification technique in an automated flow-injection immunoassay system for a laboratory environment. Liposomes provide instantaneous, rather than time-dependent enhancement, and have considerable potential for automated assays, the development of generic rather than specific assay reagents, and for multi-analyte assays.

This report describes the use of such liposome enhancement in a field assay, rather than a laboratory format, and expands the area of use into that of environmental toxins, using the herbicide Alachlor as a model analyte. The experimental system is a competitive immunoassay and consists

Correspondence to: R.A. Durst, Analytical Chemistry Laboratories, Cornell University, Geneva, New York 14456-0462 (USA).

of a wicking reagent containing Alachlor-tagged liposomes with entrapped dye and a plastic-backed nitrocellulose strip that has an immobilized antibody competition zone and a liposome capture zone in an ascending sequence. A mixture of the wicking reagent and a sample containing an unknown quantity of Alachlor is allowed to migrate along the strip by capillary action. In the antibody zone, competitive binding with the immobilized anti-Alachlor antibody occurs. The unbound liposomes, proportional to the amount of Alachlor in the sample, are carried into the liposome capture zone where they are concentrated. Measurement of the dye entrapped in the liposomes in either the antibody zone or the liposome capture zone can be used to calculate the amount of Alachlor present in the sample. Immunochromatographic strips, based on similar principles to the device described above, have been reported for clinical use, but they depended on the use of enzymes [7,8] or dye [9] rather than liposomes.

MATERIALS AND METHODS

Materials

Alachlor was purchased from Chem Service (West Chester, PA). Bovine serum albumin (BSA), *N*-succinimidyl-*S*-acetylthioacetate (SATA), dipalmitoyl phosphatidyl ethanolamine (DPPE), cholesterol, poly(vinylpyrrolidone) (PVP, 10 000 mol.wt.), Tween-20, triethylamine, Molybdenum Blue spray reagent, Isosulfan Blue and Sephadex G-50 were purchased from Sigma (St. Louis, MO). Dipalmitoyl phosphatidyl choline (DPPC) and dipalmitoyl phosphatidyl glycerol (DPPG) were obtained from Avanti Polar Lipids (Alabaster, AL). Sulforhodamine B was purchased from Eastman (Rochester, NY), and Fast Green FCF from Allied Chemical (New York, NY). Carnation non-fat dry milk powder (CNDM) was obtained locally. Protein assay dye reagent, goat anti-rabbit IgG alkaline phosphatase conjugate and the substrates for alkaline phosphatase were purchased from Bio-Rad (Hercules, CA). Egg white avidin was obtained from Molecular Probes (Eugene, OR). Whatman (Maidstone) silica gel TLC flexible plates and preparatory silica gel plates, both containing fluorescent indicator, were used. Plastic-backed nitrocellulose membranes with pore size > 3 μm were obtained from Schleicher and Schuell (Keene, NH). A Paasche VL airbrush (Texas Art Supply, Houston, TX) was used for applying the antibody and egg white avidin to the membrane. The rabbit anti-Alachlor IgG used in preliminary investigations was supplied by ImmunoSystems (Scarborough, ME). Subsequent supplies of antiserum were provided by the Cornell University College of Veterinary Medicine, as described below.

Methods

Conjugate and antibody production. Alachlor was conjugated to BSA by modification of a published method, as described elsewhere [10]. Antibodies to the immunogenic conjugate were raised in New Zealand white rabbits by standard procedures (Cornell Veterinary College). The antibodies produced were purified by the caprylic acid–ammonium sulfate precipitation method [11].

Antibody and avidin immobilization. In the strip assay, a protein-binding membrane with a plastic backing to provide rigidity was required, and nitrocellulose membrane supported in this manner was found to be the most suitable. An airbrush was used to dispense the antibody and egg white avidin solutions for immobilization. The membrane was cut to a desired size (7.9 cm high and a suitable width for later subdivision into strips 5 mm wide), thoroughly wetted with 10% methanolic TBS (tris buffered saline, pH 7.0) and dried before application of antibody and avidin solutions. The membrane sheet was mounted on a mobile platform that moved at a constant rate in front of the airbrush used to spray the antibody solution, at a concentration between 0.2 and 1 mg ml^{-1} (depending on preparation), and egg white avidin solution at 1 mg ml^{-1}, onto spatially separate and well-defined zones of the membrane. The protein bands were allowed to air dry for 1 h. The coated nitrocellulose sheet was then immersed in blocking agent (a solution of 2% polyvinylpyrrolidone and 0.002% Tween-20 in TBS) for 1 h on a rotating shaker and dried

under vacuum for 3–4 h. Prepared sheets were stored at 4°C in the presence of silica gel desiccant until ready for use. The sheets were cut into strips using a paper cutter when required. The final strips were 5 × 79 mm with a 5 mm long antibody zone 15 mm above the bottom of the strip and a similar egg white avidin zone 35 mm from the bottom.

Analyte-lipid conjugation. To provide the requisite antigenic sites (epitopes) on the surface of the liposomes for the competitive assay format, it is necessary to form a conjugate between the analyte molecule and a lipid, DPPE, which is then incorporated into the liposome bilayer.

For conjugation of the Alachlor to DPPE, a thiolating reagent, SATA [12], was used as the coupling agent based on a modification of a reported procedure [13]. Twenty mg of DPPE were suspended in 3 ml of 0.7% triethylamine in chloroform and sonicated under nitrogen for 1 min in a 45°C bath. To the DPPE, 2 molar equivalents of SATA in 1 ml of the same solvent were added slowly. The reaction flask was capped and stirred at room temperature for ca. 20 min, the end point of the reaction being indicated by the clearing of the mixture. The solvent was removed on a rotary vacuum evaporator, and 2 ml of 30 mM hydroxylamine hydrochloride in methanol, adjusted to pH 8.2 with NaOH, were added. The reaction mixture was vortexed vigorously and stirred at 45°C for 1 h under nitrogen, maintaining the pH at 8.2 using dilute NaOH in methanol. A 2.8 molar excess (to DPPE) of Alachlor in 1 ml of 30 mM hydroxylamine, pH 8.2 in methanol, was added to the reaction flask. The reaction mixture was stirred at 45°C for 2 h, with the pH being maintained at 8.2, and the reaction was allowed to continue at 45°C overnight (ca. 17 h). The product was purified on a preparatory silica gel plate using the solvent system chloroform–acetone–methanol–glacial acetic acid–water (60:20:20:5:4, v/v). The purified Alachlor–DPPE conjugate was quantified by Bartlett's phosphorous assay [14].

Because radioactive Alachlor was not available for use as a tracer, confirmation of the successful conjugation reaction was achieved by a combined thin-layer chromatographic and an enzyme immunostaining method [15], using an anti-Alachlor antibody supplied by ImmunoSystems. The procedure involved the duplicate chromatographic analysis of the reaction mixture on TLC plates. Whatman Silica Gel/UV plates were prewashed in the solvent described above and dried, and the samples were run in the same solvent. One of the TLC plates was dried, blocked for 1 h in a solution of 1% BSA and 0.5% CNDM in TBS, washed three times for 10 min each in TBST (TBS containing 0.05% Tween-20), and placed overnight in a solution containing the antibody to Alachlor (20 μg/ml in TBST). The plate was washed three times for 10 min each in TBST and placed in a solution containing a goat anti-rabbit alkaline phosphatase conjugate (stock diluted 1:3000 with TBST containing 0.02% BSA) for 2 h. The plate was washed as before and developed with the substrate for alkaline phosphatase (nitroblue tetrazolium in aqueous DMF with magnesium chloride and 5-bromo-4-chloro-3-indolyl phosphate in DMF, prepared according to the manufacturer's instructions). When color development was complete (10 min), the plate was washed in distilled water and dried. A purple spot indicated the presence of Alachlor. The other TLC plate was sprayed with molybdenum blue reagent (1.3% molybdenum oxide in 4.2 M sulfuric acid) which is specific for phospholipids. The Alachlor–DPPE spot appeared purple with the alkaline phosphatase substrate stain and blue with the molybdenum blue spray reagent.

Preparation of dye-encapsulated Alachlor-tagged liposomes

Liposomes were formed by the reversed-phase evaporation method [16,17] from a mixture of DPPC, cholesterol, DPPG, and Alachlor–DPPE conjugate in a molar ratio of 5:5:0.5:0.01. Forty-three μmol of this mixture were dissolved in 4.2 ml of a solvent mixture containing chloroform–isopropyl ether–methanol (6:6:1, v/v). This solution was warmed to 45°C and 0.7 ml of the dye solution was added with swirling. This mixture was sonicated for 5 min under a low flow of nitrogen. The organic phase was removed under vacuum on a rotary evaporator at 40°C until all frothing had stopped. An additional 1.3 ml

aliquot of the dye solution was added, and the liposomes were then sequentially extruded twice through each of two polycarbonate filters of decreasing pore sizes of 1.0 μm and 0.4 μm. The diameters of the liposome preparations were measured by laser scattering in a LA-900 particle size distribution analyzer (Horiba, Irvine, CA), using the manufacturers method, except that the usual sonication step was omitted to avoid lysis (rupture) of the liposomes. Finally, to remove any unencapsulated dye, the liposomes were gel filtered on a 1 × 14 cm Sephadex G-50 column and dialyzed overnight against TBS at 4°C. When stored at 4°C, there was no significant leakage of dye over a period of 9 months.

Sulforhodamine B was chosen as the dye for encapsulation [17,18] because of its fluorescence and high visible extinction coefficient. To prepare the dye, 20 mM Tris was used to buffer the dye solution. The pH was adjusted to 7.0 with NaOH to effect dissolution. The final solution contained 100 mM dye in 20 mM Tris at a pH of 7.0 with an osmolarity approximately equal to TBS, which was the buffer routinely used in all aqueous operations of the experiments. In some experiments 200 mM Sulforhodamine B was used to give a greater color intensity on the strips.

Because Sulforhodamine B is highly fluorescent and this fluorescence undergoes self-quenching when encapsulated, the integrity of the liposomes can be determined by measuring fluorescence intensity before and after lysis. Total and almost instantaneous lysis of the liposomes was effected by addition of a solution (final concentration = 30 mM) of *n*-octyl-β-D-glucopyranoside at room temperature. For these fluorescence experiments, the dye was excited at a wavelength of 543 nm and fluorescence measured at the emission wavelength of 596 nm.

In some experiments the non-fluorescent dyes Isosulfan Blue and Fast Green FCF were encapsulated by the same methods as Sulforhodamine B.

Assay format

The prototype assay device configuration, as shown in Fig. 1, consists of a wicking reagent containing Alachlor-tagged liposomes and a test strip comprised of a wick, an immobilized anti-Alachlor zone and an egg white avidin capture zone in sequence. The assay is performed by dispensing 100 μl (2 drops) of the sample or control solution and 50 μl (1 drop) of a three times concentrated TBS buffer into a 10 × 75 mm glass test tube, mixing the contents, and adding 50 μl (1 drop) of a liposome solution (stock liposome solution diluted 1:50, dilution varying according to preparation). The test tube is shaken mildly to mix the contents and the test strip is inserted into the tube; the strip is left in the tube until the solution front reaches the end of the strip (about 8 min); the strip is removed and air dried. The color intensity of the antibody zone and the avidin zone are estimated either visually or by scanning densitometry [10].

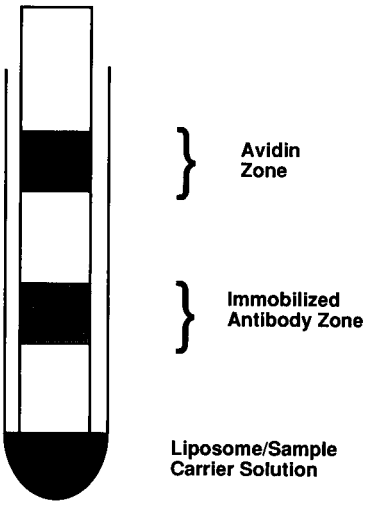

Fig. 1. Immunomigration assay device. The prototype assay device as currently used is shown diagrammatically. The immunomigration strip incorporating the antibody competition and liposome capture zones is inserted into a test tube containing a solution of the sample and liposome reagent.

Detection / quantitation

The measurement of the extent of the competitive binding reactions of the analyte molecules and the tagged liposomes to the immobilized antibodies was optical. Visual estimation of the color intensity can be used, but for more accurate quantitation during development it was found to be preferable to use a computer scanner and

Scan Analysis densitometry software (Biosoft, Ferguson, MO) to convert the red coloration into greyscale readings that can be measured.

RESULTS AND DISCUSSION

Characteristics of liposomes

Initial experiments were carried out using liposomes that had been prepared by the alcohol injection method [19], as had been used successfully in the flow-injection immunoassay system [3–6]. Although these gave every indication of suitability, both the total yield of liposomes per preparation and the amount of dye entrapped per liposome were low. This low yield had been acceptable for the flow-injection studies, where the fluorescence of the dye was being measured, but in the case of the strip assay the method of detection depended on the light absorption of the encapsulated dye rather than the fluorescence of the released dye, and thus was considerably less sensitive. This meant that a much larger quantity of liposomes and amounts of dye per liposome were required for quantitation.

As a result, liposomes were prepared by the reversed-phase evaporation method [16,17], but without extrusion through polycarbonate filters, giving a high yield of liposomes. However, these heterogeneously sized liposomes did not migrate evenly on the test strips used in the assay. This was improved by passing the preparations sequentially twice through each of two polycarbonate filters of 1.0 and 0.4 μm nominal pore diameter. Liposomes passed only through the 1.0 μm filter had a mean diameter of 1.82 μm, with a standard deviation of 0.8, while those passed through both filters had a mean diameter of 0.68 μm with a standard deviation of 0.12 (Fig. 2). This discrepancy between the size of the pores on the polycarbonate filters and the final size of the liposomes is not surprising, as the liposomes are very flexible, and can thus "squeeze" through a pore of smaller diameter. The liposomes of 0.68 μm diameter were a much more homogeneous population than those of 1.82 μm diameter, and both populations migrated more evenly on the nitrocellulose sheets than did the unextruded liposomes. Passing the preparation through an even smaller sized filter (0.2 μm) did not improve the migration behavior, and reduced the yield considerably. Consequently, liposomes that had been passed through the 1.0 and 0.4 μm filters were used in all subsequent experiments.

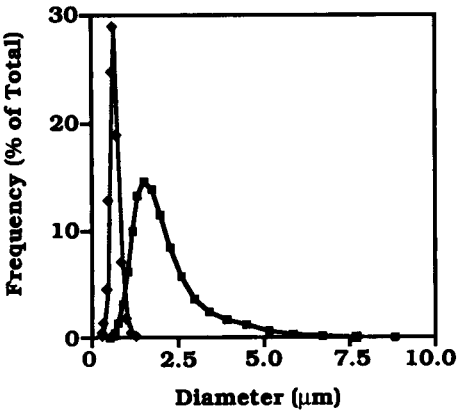

Fig. 2. Size distribution of liposomes. The size distribution of liposomes that have been passed through (a) 1.0 μm filter twice, ■; (b) 1.0 μm filter twice and 0.4 μm filter twice, ♦.

The absorption spectrum of dilute, free Sulforhodamine B gave a peak at 566 nm, with a shoulder at 532 nm. The intact liposomes, containing dye at a concentration sufficiently high to form dimers [18], gave a spectrum with peaks at 532 and 568 nm, with the 568 nm peak at 70% of the height of the 532 nm peak. The addition of surfactant to the liposomes caused lysis of the liposomes and consequent dilution of the dye, and thus converted the spectrum to that of the free dye. This is similar to the results of Chen and Knutson [18].

The presence of Alachlor on the surface of the liposomes was demonstrated by the reversal, by free Alachlor, of antibody-induced aggregation of the liposomes. The aggregated liposomes could be precipitated by centrifugation (data not shown).

The liposomes were stored at 4°C, and the temporal stability was studied over time by measuring the percentage of free dye in the preparation, thereby allowing calculation of the percentage of the liposomes that had lysed. Fig. 3 shows

data for 2 different preparations of liposomes. These were made with the standard lipid mixture with and without the addition of 0.1 mole% DPPE-Alachlor conjugate. As can be seen, the preparation containing no DPPE-Alachlor conjugate showed no loss of free dye from the liposomes over a period of 12 months. The particular preparation containing the conjugate used in the experiments reported here showed some increase in free dye in the suspension, but it was extremely low, with 97% of the liposomes still being intact after 9 months. Other preparations of liposomes containing up to 0.5 mole% Alachlor tagged DPPE have been found to be over 99% intact after 10 months storage.

The characteristics of the liposomes used in these studies are shown in Table I. From the size measurement results, it is possible to calculate that the average volume of a single liposome is 1.7×10^{-10} μl. By assuming the dye encapsulated was equal in concentration to the original dye solution used, and by comparing the fluorescence of lysed liposomes to that of standard Sulforhodamine B solutions, it is possible to calculate that there were ca. 1.2×10^{8} liposomes μl^{-1} and that each liposome contained ca. 9.6×10^{6} molecules of dye. Assuming that the average surface area of the DPPC molecules is 71 Å^2, and that of cholesterol molecules in a mixed bilayer is 19 Å^2 [20], and given that the DPPE-Alachlor is 0.1 mole% of the total lipid, then there are ca. 3500 molecules of Alachlor on the outer surface of a single liposome.

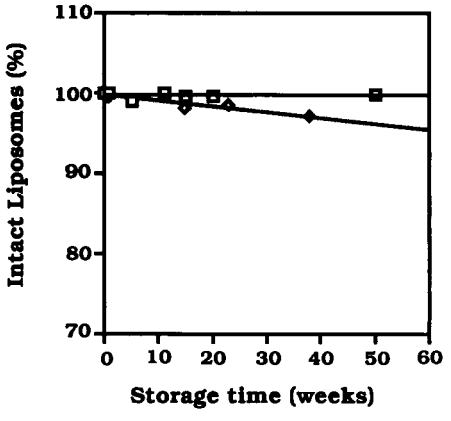

Fig. 3. Stability of liposomes. The decrease in % intactness of liposomes stored at 4°C: (a) liposomes without DPPE–Alachlor, ■; (b) liposomes with DPPE–Alachlor ◆.

TABLE 1

Liposome characteristics

Mean diameter (±S.D.)	0.68 ± 0.12 μm
Volume	1.7×10^{-10} μl
Liposome conc.	1.2×10^{8} lipo μl^{-1}
SRB [a] conc.	100 mM
SRB [a] conc. (molecular) [b]	9.6×10^{6} molec. lipo^{-1}
Alachlor conc. [c]	3.5×10^{3} molec. lipo^{-1}
Stability	> 9 months

[a] Sulforhodamine B. [b] The number of molecules of SRB per liposome. [c] The number of molecules of Alachlor on the outer surface of a single liposome containing 0.1 mole% DPPE–Alachlor.

Assay performance

The prototype device for the assay as currently performed is shown in Fig. 1. The original concept was to have just an antibody zone, where competition would occur for immobilized antibody sites between the analyte-conjugated liposomes and the free analyte in the sample. This would give the usual competitive assay result of more liposomes bound (i.e. more color) when there was less free analyte in the sample. This is however anti-intuitive, and as the strips were designed ultimately to be used in the field by technicians, it was felt that a result where the color was directly proportional to the free analyte would be preferable. For such an assay, a means of collecting and concentrating the liposomes that passed through the antibody zone was required. It was thought that if the liposomes were biotinylated, then a zone of immobilized avidin could be used to collect them. However, it was serendipitously found that egg white avidin, with the carbohydrate moiety still attached, would strongly bind all of the liposomes, without the need of conjugating biotin to them. As the specificity of the assay lies in the immunorecognition reaction in the antibody zone, this collection zone provided a simple solution to give the desired direct readout measurement.

After applying antibody and avidin to the nitrocellulose sheets, it was necessary to block the membrane to reduce non-specific binding and to aid the mobility of the liposomes. Both PVP and BSA were found to be suitable for this purpose, but the former was less expensive and more tractable and was routinely used as the blocking agent. There were still occasional problems of non-uniform migration of liposomes with certain batches of membrane, but these could be alleviated by the use of very low levels of detergent in the blocking solution. Tween-20 at 0.002% was found suitable for this purpose, and at this level of application it did not cause lysis of the liposomes during the 8-min analysis run.

Fig. 4 shows diagrammatically the results obtained with a series of Alachlor standards, with the decrease in color of the antibody zone with increasing concentrations of added Alachlor, and the concomitant increase in the color of the avidin zone.

Dose-response data obtained by scanning densitometry of strips run in the presence of various concentrations of Alachlor are shown in Fig. 5.

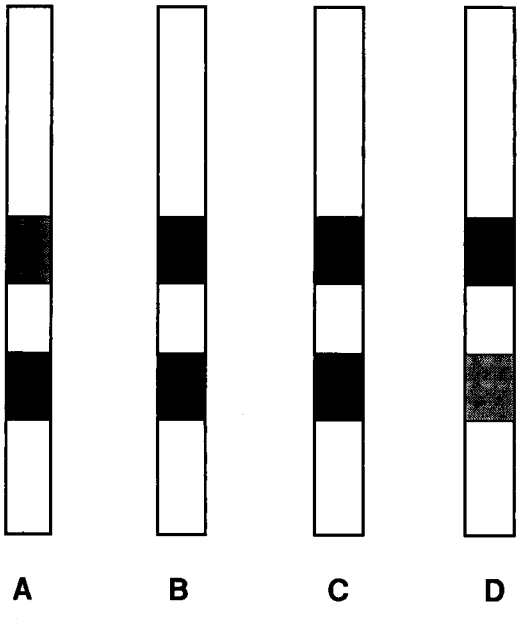

Fig. 4. Alachlor dose-response. This shows the color intensity in the antibody competition and avidin collection zones for standards containing Alachlor in increasing concentrations from A to D.

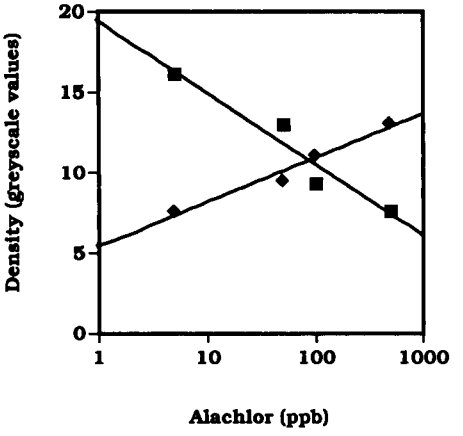

Fig. 5. Alachlor logarithmic dose-response curve. (a) Greyscale density, antibody zone, ■; (b) Greyscale density, avidin zone, ◆.

The response in both the antibody and avidin zones varied logarithmically when measured using scanning densitometry, and both were estimated to be able to detect 5–10 μg/l Alachlor. When these strips were assessed visually, a similar determination could be made, but at low levels of added Alachlor it was somewhat easier to detect increases of red color over a white control (avidin zone) than decreases in color intensity (antibody zone). There are still a few problems with the reproducibility of the strips. These seemed to be due to both heterogeneity in the supplied sheets of plastic-backed nitrocellulose and to uneven application of the protein zones on the strips. These problems are currently being addressed.

Conclusions

These initial experiments were carried out to demonstrate the feasibility of using liposome enhancement of a competitive immunoassay in a format designed for rapid screening of large numbers of samples in the field. It is intended as a single-use device, thus minimizing problems with cross contamination and fouling, which can be serious in extra-laboratory assays.

The assay is currently not as sensitive as an ELISA. For example, the tolerance level of Alachlor in well water is 2 μg/l. This can be

measured using commercially available ELISA kits, but not as yet with the current prototype liposome-strip assay. However, several studies are underway to optimize the performance of the assay to increase the sensitivity.

Future developments

If developed into a commercial kit for field use, various modifications would need to be made to the prototype assay. These might include special holders for the individual strips, in which openings are provided for sample application and optical readout. In such a configuration, the strips could be run in any orientation, e.g., lateral, instead of vertical flow. Such modifications would be in the direction of creating a more "user-friendly" field device.

During the course of this work, preliminary measurements were carried out using hand-held reflectometers to measure the dye intensity in the antibody zone. These meters, which are designed to measure a green/blue color, were components of commercially available blood glucose kits. The dyes Fast Green FCF and Isosulfan Blue were encapsulated in Alachlor-tagged liposomes, and strip assays were carried out as normal. The strips were then cut so that the measurement zone was similar in size and location to the glucose measurement zone on the strips supplied with the meter. It was demonstrated that this type of measurement was feasible, but that a meter specially designed for our particular system would be required.

The development of a dual-strip assay is also being pursued. In this design, after application of the protein zones, the strip would be divided in two by removal of a very thin strip of nitrocellulose from the plastic backing, thereby providing two identical strips with a hydrophobic separation to prevent solution cross-talk. A tolerance level control would be applied to the strip adjacent to the sample, and both would be run simultaneously. This would verify the strip performance and provide a more quantitative interpretation of the strip results.

There is also the possibility of using electrochemical detection. An electroactive species, such as ferrocyanide, could be incorporated into the liposomes, and electrodes printed onto the strip, or the strip placed in contact with the electrodes. After lysis of the liposomes, the quantity of the electroactive species could be determined amperometrically. Preliminary studies on electrochemical detection in a laboratory instrument are already underway, and these will later be applied to the field assays.

Multi-analyte assays are also conceivable, with a series of antibody zones, each against a different analyte, and a series of liposomes tagged with the different analytes. The liposomes attached to each analyte could have a different dye encapsulated, so the results of the assay could be "color coded". In this format it would not be possible to have an avidin collection zone. Alternatively, an avidin collection zone could be incorporated and a multi-wavelength detector used.

This study was partially funded by grants from: the Cooperative State Research Service, U.S. Department of Agriculture, under Subcontract No. USDA-TPSU-CU-7119-757 through The Pennsylvania State University; the CSRS/USDA Water Quality Special Grants Program, Project 93-01360, and the National Institutes of Health, DHSS, under the Superfund Research and Education Grant, G/NIEHS ES-0950. We would like to thank Dr Steve Sundberg (Horiba Inc.) for carrying out measurements of the size distribution of the liposomes, Matt Roberts for preparation of liposomes for those studies and ImmunoSystems Inc. for the gift of antibody used in preliminary experiments and in the immunostaining of the TLC plates. We gratefully acknowledge the assistance of Dr. Terry Spittler and Harry Leichtweis in the synthesis of the Alachlor–DPPE conjugate.

REFERENCES

1 B.M. Kaufman and M. Clower, J. Assoc. Off. Anal. Chem., 74 (1991) 239.
2 J.M. Van Emon and R.O, Mumma (Eds.), Immunochemical Methods for Environmental Analysis, ACS, Washington, DC, 1990.
3 L. Locascio-Brown, A.L. Plant, V. Horvath and R.A. Durst, Anal. Chem., 62 (1990) 2587.

4 R.A. Durst, L. Locascio-Brown and A.L. Plant, in R.D. Schmid (Ed.), Flow Injection Analysis Based on Enzymes or Antibodies, GBF Monograph Series, 14, VCH, Weinheim, 1990, pp. 181–190.
5 W.T. Yap, L. Locascio-Brown, A.L. Plant, S.J. Choquette, V. Horvath and R.A. Durst, Anal. Chem., 63 (1991) 2007.
6 L. Locascio-Brown, A.L. Plant, R. Chesler, M. Kroll, M. Rudell and R.A. Durst, Clin. Chem., 39 (1993) 386.
7 R.F. Zuk, V.K. Ginsberg, T. Houts, J. Rabbie, H. Merrick, E.F. Ullman, M.M. Fischer, C.C. Sizto, S.N. Stiso and D.J. Litman, Clin. Chem., 31 (1985) 1144.
8 M.P. Allen, A. DeLizza, U. Ramel, H. Jeong and P. Singh, Clin. Chem., 36 (1990) 1591.
9 S.C. Lou, C. Patel, S. Ching and J. Gordon, Clin. Chem., 39 (1993) 619.
10 S.G. Reeves, M.A. Roberts, S.T.A. Siebert and R.A. Durst, Anal Lett., 26 (1993) 1461.
11 M.M. McKinney and A. Parkinson, J. Immunol. Methods, 96 (1987) 271.
12 R.J.S. Duncan, P.D. Weston and R.A. Wrigglesworth, Anal. Biochem., 132 (1983) 68.
13 P.C. Feng, S.J. Wratten, S.R. Horton, C.R. Sharp and E.W. Logusch, J. Agric. Food Chem., 38 (1990) 59.
14 G.R. Bartlett, J. Biol. Chem., 234 (1959) 466.
15 I. Mattsby-Baltzer and C.R. Alving, Eur. J. Biochem., 138 (1984) 333.
16 S. Szoka, F. Olsen, T. Heath, W. Vail, E. Mayhew and D. Papahadjopoulos, Biochim. Biophys. Acta, 601 (1980) 559.
17 J.P. O'Connell, R.L. Campbell, B.M. Fleming, T.J. Mercolino, M.D. Johnson and D.A. McLaurin, Anal. Chem., 31 (1985) 142.
18 R.F. Chen and R.J. Knutson, Anal. Biochem., 172 (1988) 61.
19 S. Batzri and E.D. Korn, Biochim. Biophys. Acta, 298 (1973) 1015.
20 J.N. Israelachvili and D.J. Mitchell, Biochim. Biophys. Acta, 389 (1975) 13.

Analytica Chimica Acta, 282 (1993) 307–312
Elsevier Science Publishers B.V., Amsterdam

Flow-injection study of inhibition and reactivation of immobilized acetylcholinesterase: determination of the pesticides paraoxon and carbamoylcholine

I.A. Takruni, Ala'ddin M. Almuaibed and Alan Townshend
School of Chemistry, University of Hull, Hull HU6 7RX (UK)

(Received 25th January 1993)

Abstract

The inhibitory effects of paraxon and carbamoylcholine as examples of organophosphorus and carbamate pesticides, respectively, on the activity of acetylcholinesterase (AChE) immobilized on controlled pore glass have been investigated, using a dual injection flow system and spectrophotometric detection. Reactivation of the inhibited immobilized AChE by pyridine-2-aldoxime methochloride (2-PAM), magnesium or fluoride ions has also been studied. 2×10^{-5} M 2-PAM restores almost 100% of the activity of the immobilized enzyme. Methods for determination of paraoxon and carbamoylcholine are presented, based on the inhibition and reactivation of immobilized AChE as monitored by its catalyzed hydrolysis of acetylthiocholine iodide and the subsequent reaction of the thiocholine produced with 5,5′-dithiobis(2-nitrobenzoic acid). The calibration graphs are linear up to 8×10^{-4} M and 6×10^{-4} M, respectively, with relative standard deviations ($n = 5$) of 5%, and 3σ limits of detection of 5×10^{-5} M and 6×10^{-5} M, respectively.

Keywords: Flow injection; Acetylcholinesterase; Carbamoylcholine; Immobilized enzymes; Paraoxon; Pesticides

Acetylcholinesterase (AChE) is a hydrolase enzyme with rather narrow specificity for acetylcholine and related compounds. It is found in high concentration in nervous tissue. AChE is an active neurotransmitter, and is a target for nerve gases and insecticides. Inhibition of this enzyme produces tetanic shock, with eventual muscle paralysis [1].

The irreversible inhibition of AChE by organophosphorus compounds is well known [2–5]. Several inhibition mechanisms have been suggested, depending on the substrate. These pesticides block the active site serine by nucleophilic attack to produce a serine phosphoester, which is hydrolysed only extremely slowly [1].

Carbamate insecticides, like organophosphorus pesticides, are known to inhibit AChE [5,6]. Their mode of action is similar to that of the organophosphorus compounds except that the AChE is carbamylated. Another noteworthy difference is that carbamate inhibition is more rapidly reversible (i.e., decarbamylation of the inhibited enzyme occurs more readily) [6,7].

Several oximes have been reported to restore AChE activity after the enzyme has been inhibited by organophosphorus compounds [5,8–10]. The property of rapid reactivation appears to be limited to quaternary pyridium compounds containing the aldoximino group. Such compounds

Correspondence to: A. Townshend, School of Chemistry, University of Hull, Hull HU6 7RX (UK).

continue to be reported [9,10] without major improvement over the earliest oximes [5] typified by pyridine-2-aldoxime methochloride (2-hydroxyiminomethyl-1-methylpyridinium chloride, 2-PAM chloride; pralidoxime chloride).

Fluoride and molybdate are also reactivators of phosphorylated cholinesterases [5]. They are both nucleophiles but very different from the compounds discussed above. Sodium fluoride reactivates AChE inhibited by sarin 1/9th as effectively as 2-PAM [5].

Organophosphorus and carbamate pesticides have become increasingly important in recent years because of their wide-ranging biological activity. Among the analytical methods available for their determination are enzymatic methods based on cholinesterase inhibition, which are widely used and can be combined with optical and chromatographic techniques for detection [2,6,8,11].

Recently, Leon-Gonzalez and Townshend [2] reported a flow-injection method for the determination of paroxon based on the inhibition of immobilized AChE held in an on-line reactor in the flow system. The procedure is based on the inhibition of the enzymatic hydrolysis of 1-naphthyl acetate and subsequent reaction of the resulting 1-naphthol with *o*-nitrobenzenediazonium fluoroborate. They established that exposure of the immobilized enzyme to the inhibitor before passing the substrate gave poor reproducibility, and the activity of the enzyme diminished to zero after exposure to only a few samples. However, if the enzyme is exposed to substrate and inhibitor simultaneously, better reproducibility and longer enzyme life are achieved. The procedure developed on this basis allowed analyses at a rate of 60 samples per hour with a limit of detection of 4×10^{-7} M paraoxon. Use of stopped flow allowed analyses at a rate of 30 per hour with a detection limit of 8×10^{-9} M. The technique was successfully adapted for liquid chromatographic detection of carbamate and organophosphorus pesticides [12].

One problem with the procedure was the gradual decrease in enzyme activity over a number of determinations, especially when a stopped flow mode was used. Thus, after 30 injections, with a 35 s stopped flow, nearly all enzyme activity was lost, and was not regenerated by continuous passage of buffer or substrate. The main target of this paper, therefore, is to investigate the possibility of reactivating the immobilized enzyme, thus allowing its useful lifetime to be extended considerably. Regeneration by various oximes of the activity of immobilised AChE inhibited by various pesticides, in flow systems, has been demonstrated by Bhattacharya et al. [13] and by Trammel et al. [14]. On this basis, a flow-injection method could be developed for determination of paraoxon and carbamate pesticides based on inhibition and reactivation of immobilized AChE, in which the column is continually reused.

EXPERIMENTAL

Reagents

Distilled, deionised water was used throughout. Acetylcholinesterase (AChE, E.C. 3.1.1.7 from eel, Type VI-S, 450 U mg^{-1}) and controlled pore glass (CPG-240, 80–120 mesh, mean pore diameter 22.6 nm) were obtained from Sigma. A stock solution of diethyl *p*-nitrophenylphosphate (paraoxon, 0.2 M) was prepared from paraoxon (Sigma, 90%) in acetone. The working standard solutions were obtained by appropriate dilution with water. A stock solution of carbamoylcholine chloride (1×10^{-2} M) was prepared by dissolving 0.2 g (Fluka) in 100 ml of water. A solution of 5,5′-dithiobis(2-nitrobenzoic acid) (DTNB, 1×10^{-3} M) was prepared by dissolving 0.225 g of DTNB (Sigma) in 500 ml of water. A stock solution of 7×10^{-3} M acetylthiocholine iodide (ATCh, Sigma) was prepared by dissolving 0.2 g in 100 ml of water. A 3×10^{-3} M pyridine-2-aldoxime methochloride (2-PAM) solution was prepared by dissolving 0.050 g (Sigma) in 100 ml of water. Potassium phosphate buffers were used throughout. The stock solutions were kept in a refrigerator when not in use.

Enzyme immobilization

The AChE was immobilised on the CPG following the glass activation procedure described earlier [2]. Acetylcholinesterase (5.6 mg, 450 U) was dissolved in 2 ml of cold (4°C) potassium

phosphate buffer (0.1 M, pH 6.0) and added to 0.2 g of the activated glass. The solution was kept at 4°C for 2.5 h. The immobilized enzyme derivative was washed first with the cold phosphate buffer and then with cold water to ensure the removal of any unbound enzyme. The resulting immobilized AChE was packed into a glass minicolumn (20 mm × 2.5 mm i.d). The beads were stored at 4°C in the phosphate buffer (pH 6.0) when not in use.

Apparatus and procedures

The absorbance was measured at 405 nm with an LKB Ultraspec II spectrophotometer equipped with a flow cell (volume 30 μl, light path 10 mm). The peristaltic pump was a Gilson Minipuls 2. The two injection valves were Rheodyne RH-5020 rotary valves (Anachem). The manifold tubes were 0.05 mm i.d. PTFE. The manifold used for paraoxon and carbamoylcholine determination is shown in Fig. 1, in which the two injection valves are connected in series. This two-valve arrangement was used to economise on the use of substrate [15]. The paraoxon or carbamoylcholine solution (60 μl) was injected by injection valve 1 into the carrier stream of 0.05 M phosphate buffer (pH 8.0). ATCh solution (60 μl) was injected manually by valve 2 into the middle of the pesticide zone, exactly 5 s after injection of the pesticide. The flow rate in each channel was 1.0 ml min^{-1}. The concentration of the thiocholine released by the hydrolysis of ATCh, which is a measure of residual enzyme activity and thus of pesticide (inhibitor) concentration, was monitored spectrophotometrically by adding DTNB, which reacts with thiocholine to yield a derivative which absorbs maximally at 405 nm [6].

Reactivation of paraoxon-inhibited AChE was carried out by injection of the reactivator via valve 2 followed by injection of the substrate via the same valve. In the procedure using Mg^{2+}, F^- or MoO_4^{2-}, the reactivator was stopped in the minicolumn for 10 min followed by injection of substrate. 25 s was required for the substrate or reactivator to reach the column from injection valve 2.

RESULTS AND DISCUSSION

The determination of paraoxon or carbamoylcholine is based on the inhibition of immobilized AChE in the presence of substrate; the peaks resulting from the indicator reaction are decreased in proportion to increasing inhibitor concentration. The method used for calibration and analysis involves injection of the inhibitor and the substrate using the double injection flow system shown in Fig. 1. After each sample and substrate injection the reactivator was injected via valve 2 to pass through the inhibited enzyme column followed by the substrate from valve 2 to measure the restored activity. The percent inhibition ($\%I$) was calculated using the relationship $\%I = 100 (A_o - A_i)/A_o$, where A_o and A_i are the peak height absorbances for substrate and substrate plus inhibitor, respectively.

Behaviour of immobilized AChE in the absence of inhibitor

The manifold shown in Fig. 1 but without valve 1 was used for this study. A flow rate of 1.0 ml min^{-1} was used throughout this study to achieve

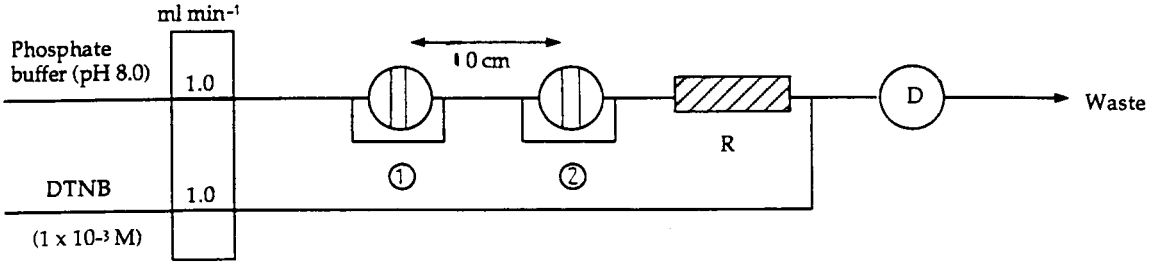

Fig. 1. Manifold used for determination of paraoxon and carbamoylcholine: DTNB = dithiobis(2-nitrobenzoic acid); R = immobilized enzyme reactor; D = spectrophotometer at 405 nm.

a reasonable sampling rate and also sufficient contact time between the substrate and immobilized enzyme (and inhibitor where relevant). The effect of pH on the activity of immobilized AChE was examined by using phosphate buffer (0.05 M) over the pH range 5.0–8.5. The peak height absorbance increased as the pH increased up to pH 8.0, and remained almost constant from pH 8.0 to 8.5. Thus pH 8.0 was chosen for further work.

The effect of DTNB concentration on peak height absorbance was investigated over the range 2×10^{-4} to 1×10^{-3} M. The peak height increased as the concentration of DTNB increased, and was constant at $> 6 \times 10^{-4}$ M DTNB. So 1×10^{-3} M was chosen for further work.

When, under optimized conditions, a solution of ATCh was injected into the manifold the calibration graph was found to be linear up to 8×10^{-5} M. The least squares linear equation and correlation coefficient ($n = 5$) were peak height absorbance = 4757 [ATCH (M)] + 0.017 and 0.998, respectively.

Behaviour of immobilised AChE in the presence of inhibitors

The behaviour of immobilised AChE was studied under the following conditions: 1×10^{-3} M DTNB, pH 8.0 (0.05 M phosphate buffer).

Inhibition by paraxon

The inhibition was studied by observing the effect of different substrate (4.0×10^{-5} to 8.0×10^{-5} M) and paraoxon concentrations (4.0×10^{-5} to 8.0×10^{-5} M) on the activity of the immobilized AChE. The results (Fig. 2) show that the inhibition increases progressively with increase in substrate concentration, and also with increase in inhibitor concentration. Thus the %inhibition is a function of both paraoxon and substrate concentration as was reported earlier [2].

Oxime reactivation

The general mechanism of oxime reactivation of organophosphorus-inhibited AChE involves phosphorylation of the reactivator by the phosphorylated enzyme, thus liberating free enzyme [5]. The ability of 2-PAM to reactivate immobilized AChE inhibited by paraoxon was studied

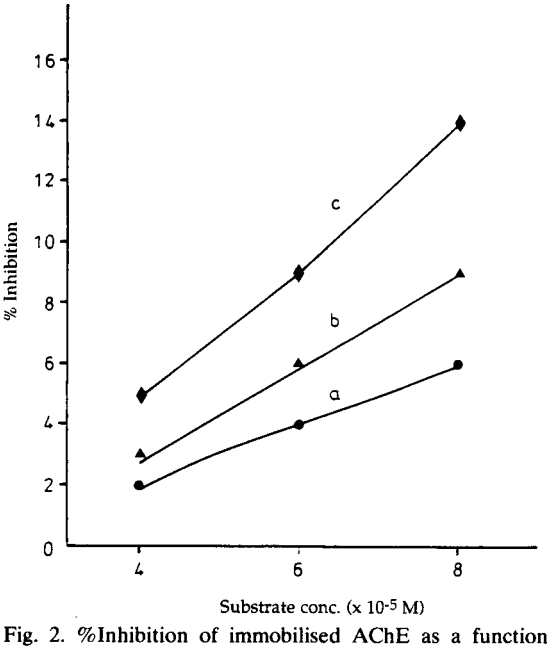

Fig. 2. %Inhibition of immobilised AChE as a function of ATCh and paraoxon concentrations: (●) 4×10^{-5} M; (▲) 6×10^{-5} M; (◆) 8×10^{-5} M; pH 8.0 (0.05 M phosphate), 1×10^{-3} M DTNB.

over the range 6×10^{-6} to 2×10^{-5} M 2-PAM. The results for 4×10^{-4} M paraoxon are shown in Fig. 3. It was found that 2×10^{-5} M 2-PAM restored almost 100% of the activity of the immobilized enzyme. The results showed that the rela-

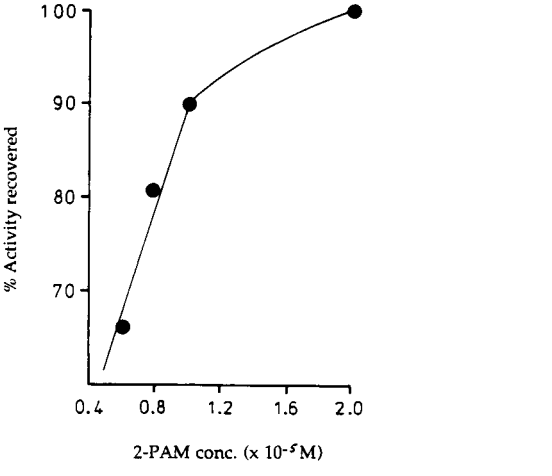

Fig. 3. 2-PAM reactivation of immobilized AChE inhibited by paraoxon, pH 8.0 (0.05 M phosphate), 4×10^{-4} M paraoxon 1×10^{-3} M DTNB, 2×10^{4} M ATCh.

tion between recovered activity and concentration of 2-PAM was linear up to 1×10^{-5} M. No doubt this procedure could be worked up to provide a method for the determination of 2-PAM; initial results showed that a limit of detection (3σ) of 8×10^{-7} M could be achieved. Earlier workers [14] have used such a principle to measure the reactivating capabilities of quaternary pyridinium oximes.

Mg^{2+}, F^- and MoO_4^{2-} reactivation

The mechanism of reactivation by F^- is as follows [5]:

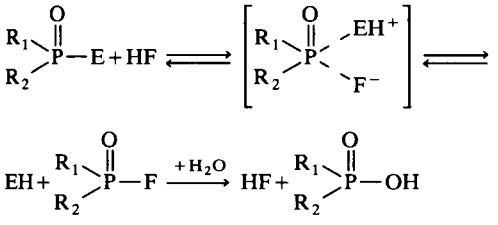

It has been reported that the addition of $MgCl_2$ is essential to reduce the decrease in the activity of soluble [5,8] or immobilized AChE [2], when the enzyme is used repeatedly. Thus the use of $MgCl_2$ to reactivate the inhibited enzyme was investigated. It has also been reported that sodium fluoride or ammonium molybdate reactivated plasma and erythrocyte cholinesterase inhibited by sarin and tetraethylpyrophosphate (TEPP), respectively, although more slowly than 2-PAM [5]. Therefore $MgCl_2$, NaF and $(NH_4)_2MoO_4$ were studied as potential reactivators of immobilized AChE inhibited by paraoxon. Injection of a solution of each compound into the carrier stream over the range 5×10^{-5} to 5×10^{-4} M at pH 8.0, failed to reactivate the enzyme. However, when the stopped flow procedure was used, where the reactivating solution was stopped in the mini-column for 10 min, $MgCl_2$ (5×10^{-5} M) or NaF (5×10^{-4} M) restored 90% and 95% of the enzyme's original activity, respectively. Molybdate failed to reactivate the enzyme; in fact, unexpectedly, it increased the inhibition.

Determination of paraoxon

Paraoxon determination was based on the inhibition and reactivation of immobilized AChE. The inhibitor was injected via valve 1 followed 5 s later by substrate via valve 2. The absorbance is denoted as A_i. Then the reactivator 2-PAM was injected via valve 2 followed by substrate at the same concentration signal as previously to give a signal A_o. There was a linear relation between $\%I$ and inhibitor concentration. A plot of $\%I$ against paraoxon concentration over the range 2×10^{-4} to 1×10^{-3} M in the presence of 2×10^{-4} M ATCh as substrate is shown in Fig. 4. The calibration graph is linear up to 8×10^{-4} M. The least squares linear equation up to this concentration and the relative standard deviation for 5 repeated injections for 6×10^{-4} M were $\%I = 47250$ [paraoxon (M)] + 0.72 and 5%, respectively. The limit of detection (3σ) was 5×10^{-5} M. The correlation coefficient ($n = 5$) and sample throughput were 0.994 and h^{-1}, respectively.

Inhibition by carbamoylcholine

The effect of different substrate (2.0×10^{-5} to 6.0×10^{-5} M) and carbamoylcholine (4.0×10^{-5} to 8.0×10^{-4} M) concentrations on the activity of the immobilized AChE was studied. Table 1 shows that the degree of inhibition is largely independent of substrate concentration, and that it increases with inhibitor concentration.

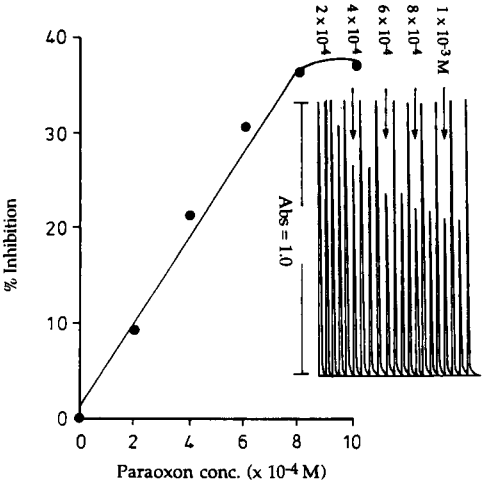

Fig. 4. Calibration graph and peaks for paraoxon, pH 8.0 (0.05 M phosphate), 1×10^{-3} M DTNB, 2×10^{-4} M ATCh.

TABLE 1

%Inhibition of immobilized AChE as a function of ATCh and carbamoylchloride concentrations (mean of 3 measurements)

Inhibitor conc. (M)	Substrate conc. ($\times 10^{-5}$ M)		
	2.0	4.0	6.0
4×10^{-5}	25%	60%	74%
6×10^{-5}	20%	61%	72%
8×10^{-5}	24%	54%	70%

Analytical characteristics

A typical calibration graph for carbamoylcholine over the range 2×10^{-4} to 1×10^{-3} M at 6×10^{-5} M ATCh was obtained under the optimum working conditions specified in the experimental section. The calibration graph was linear up to 6×10^{-4} M with a correlation coefficient of 0.996 ($n = 5$). The least squares linear equation was $\%I = 131600$ [carbamate (M)] − 2.5. The relative standard deviation for 5 repeated injections for 5×10^{-4} M carbamate and sample throughput were 5% and 35 h^{-1}, respectively. The limit of detection (3σ) was 6×10^{-5} M.

Stability of immobilized AChE

AChE immobilized on CPG by linking with glutaraldehyde was quite stable. The minicolumn was used continuously with inhibition and reactivation at room temperature for over 4 months, being stored at 4°C overnight in phosphate buffer (pH 6), without any significant loss of activity.

Conclusions

The determination of paraoxon and carbamoylcholine pesticides by inhibition and reactivation of immobilized acetylcholinesterase was successful and will allow continuous reuse of the minicolumn containing the immobilized enzyme for a period of weeks without any significant loss in enzyme activity. The sensitivity of the method is sufficient for it to be used for preliminary screening in laboratories where a large number of samples of these pesticides has to be processed rapidly. The ability to regenerate inhibited immobilized AChE will also be of value in devices such as sensors for pesticides, which also rely on the inhibition process, and would have otherwise to be discarded after one or two measurements.

REFERENCES

1 C. Walsh, Enzymatic Reaction Mechanisms, Freeman, San Francisco, 1979.
2 M.E. Leon-Gonzalez and A. Townshend, Anal. Chim. Acta, 236 (1990) 267.
3 A. Friboulet, F. Rieger, D. Goudou, G. Amitai and D. Taylor, Biochem. J., 29 (1990) 914.
4 I.L. Garcia, Anal. Biochem., 200 (1992) 176.
5 W.N. Aldridge and E. Reiner, Enzyme Inhibitors as Substrates (interactions of esterases with esters of organophosphorus and carbamic acids), North Holland, Amsterdam, 1972.
6 M.C. Quintero, M. Silva and D. Perez-Bendito, Talanta, 38 (1991) 1273.
7 P.L. Williams and J.L Burson, Industrial Toxicology, Van Nostrand Reinhold, New York, 1985.
8 D.W. Hanke, J. Appl. Toxicol., 10 (1990) 97.
9 G.M. Steinberg, J. Cramer and A.B. Ash, Biochem. Pharmacol., 33 (1977) 439.
10 B. Harver, D.J. Sellers and P. Watts, Biochem. Pharmacol., 33 (1984) 3499.
11 A. Farran, J. de Pablo and S. Hernandez, Anal. Chim. Acta, 212 (1988) 123.
12 M.E. Leon-Gonzalez and A. Townshend, J. Chromatogr., 539 (1991) 47.
13 S. Bhattacharya, C. Alsen, H. Kruse and P. Valentin, Environ. Sci. Technol., 15 (1981) 1352.
14 A.M. Trammel, J.E. Simmons and R.T. Borchardt, Pharm. Res., (1984) 115.
15 A.M. Almuaibed and A. Townshend, Anal. Chim. Acta, 198 (1987) 37.

Analytica Chimica Acta, 282 (1993) 313–316
Elsevier Science Publishers B.V., Amsterdam

Determination of the degree of substitution of hydroxypropylated β-cyclodextrins by differential scanning calorimetry

Cs. Novák, G. Pokol and J. Sztatisz

Institute for General and Analytical Chemistry, Technical University of Budapest, Szt. Gellért tér 4, H-1521 Budapest (Hungary)

L. Szente and J. Szejtli

Cyclolab Research and Development Ltd., Pusztaszeri ut 65, P.O.B. 435, H-1525 Budapest (Hungary)

(Received 6th May 1993)

Abstract

The general specifications of commercially available hydroxypropylated β-cyclodextrins (HPBCDs) usually give information on the solubility, solubilizing potency and average degree of substitution (*DS*) of a given product. The *DS* value is regarded as suitable for quality control purposes. This paper describes a differential scanning calorimetric method to determine the *DS*, based on the fact that the glass temperature interval of the amorphous part of the sample depends on the degree of substitution of the HPBCD.

Keywords: Thermometric methods; Cyclodextrins; Degree of substitution; Differential scanning calorimetry; Hydroxypropylated β-cyclodextrins

One of the most characteristic properties of industrially produced hydroxypropylated β-cyclodextrins (HPBCDs) is their multi-component amorphous nature, which is connected with the low toxicity of the HPBCD inclusion complexes. According to Pitha [1], the amorphous state is a direct consequence of the extremely large number of possible distinct chemical species that can arise from the reaction of a mixture of propylene oxide and β-cyclodextrin. The hydroxypropoxy content of the product measured by gas chromatography (GC) and the results of nuclear magnetic resonance (NMR) and plasma desorption fast atom bombardment mass spectrometry (FAB-MS) are used for quality control. The information obtained from GC and NMR measurements is the average degree of substitution (*DS*) value. By using FAB-MS, the individual *DS* values can be determined; the distribution density curve also gives information about the average *DS* [2]. The main disadvantage of this method is that a chemically degraded molecule is applied for the determination. This paper describes a differential scanning calorimetric (DSC) method for the determination of the DS of HPBCDs.

Correspondence to: Cs. Novák, Institute for General and Analytical Chemistry, Technical University of Budapest, Szt. Gellért tér 4, H-1521 Budapest (Hungary).

EXPERIMENTAL

Seventeen HPBCD samples were prepared by a patented process; the average *DS* values varied between 1 and 16, determined by GC or NMR.

X-ray powder diffraction measurements were carried out with a Philips PW diffractometer and Cu K_α radiation.

Instruments from a DuPont TA system were used in the model thermoanalytical experiments. The sample mass was 5–15 mg. A heating rate of 10°C min^{-1} and an argon atmosphere (10 l h^{-1}) were applied in the thermobalance (Model 951) and the DSC cell (Model 910). In the evolved gas analysis (EGA) device (Model 916 Thermal Evolution Analyser) samples were heated at 8°C min^{-1} in a flow of nitrogen (1.8 l h^{-1}).

RESULTS AND DISCUSSION

The x-ray diffractograms shown in Fig. 1 prove the amorphous state of the sample. The sample with the lowest *DS* value only contained a small, slightly crystallized fraction. This means that the x-ray diffraction technique alone is not suitable for determination of *DS*.

From evaluation of the thermoanalytical curves it was found that the decomposition of the samples became extensive at about 300°C. During the heating period (before the beginning of the decomposition of the HPBCD) a small amount of organic by-product left the sample. It was assumed that it was of technological origin. On the DSC curves this was shown as a broad endothermic effect between 220 and 280°C (see Fig. 2, top curve). The glass transition was represented by the heat capacity shift between 200 and 220°C

Fig. 1. X-ray powder diffractograms of HPBCDs with different *DS* values.

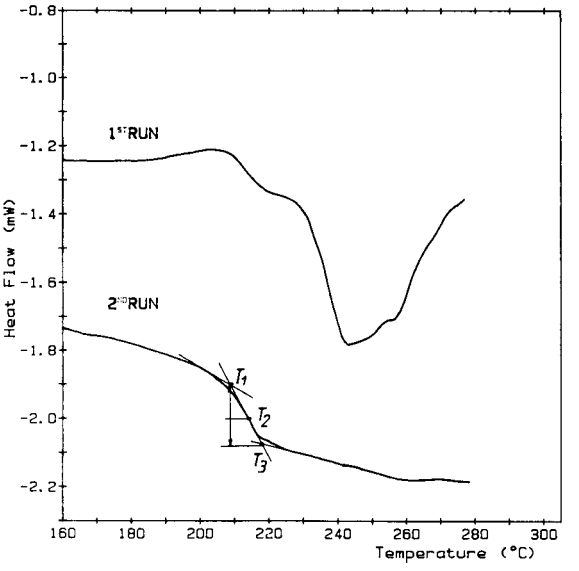

Fig. 2. Results of two DSC runs with a substituted β-cyclodextrin.

(see Fig. 2, bottom curve). T_1 and T_3 represent the intersections of the tangents; T_2 is the temperature where the heat capacity is half way between the initial and final values.

The determination of the glass transition temperature (T_g) intervals was found to be affected by the evolution of the organic by-products, so the runs were repeated with each sample and the T_g values determined from the repeated DSC curves. The DSC curves were first recorded using samples with known DS, then the T_g values were determined and calibration graph were constructed on the basis of the T_1 and T_2 values. These plots are shown in Fig. 3 as functions of average *DS* values determined by NMR. T_3 values could not be used for calibration because their exact determination in some instances was affected by the decomposition of the HPBCD. In Fig. 4 the T_1 calibration graphs as functions of the average *DS* obtained by either GC or NMR measurements are compared. The curves run parallel and close together, so the individual results of these two methods correlate well. The calibration graph enables the *DS* value of any sample to be determined on the basis of its DSC curve.

As mentioned earlier, in the reaction of propylene oxide and BCDs large number of chemically

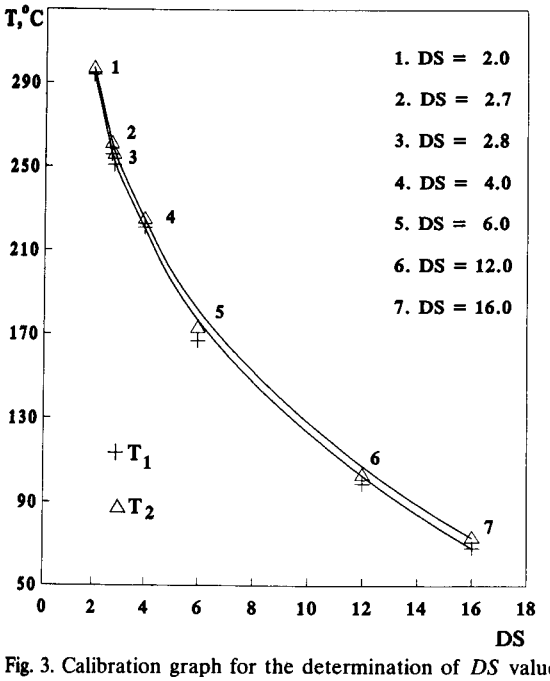

Fig. 3. Calibration graph for the determination of *DS* values on the basis of NMR data. *DS* = (1) 2.0; (2) 2.7; (3) 2.8; (4) 4.0; (5) 6.0; (6) 12.0; (7) 16.0.

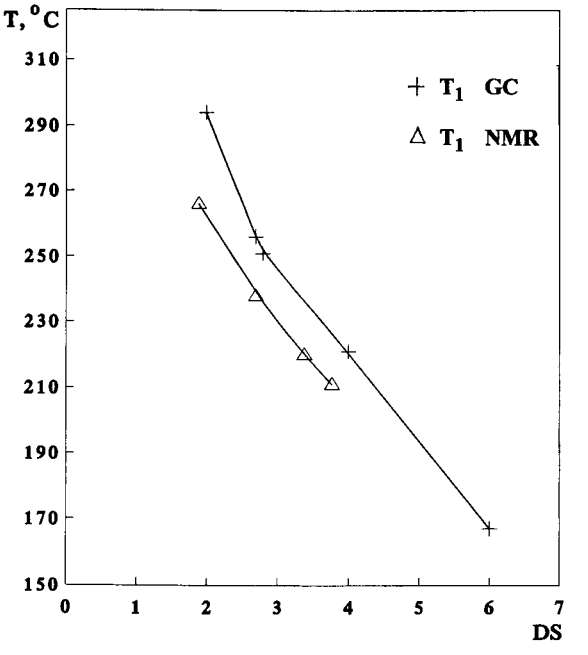

Fig. 4. Comparison of T_1 calibration graphs based on *DS* values from (+) GC and (△) NMR T_1 measurements.

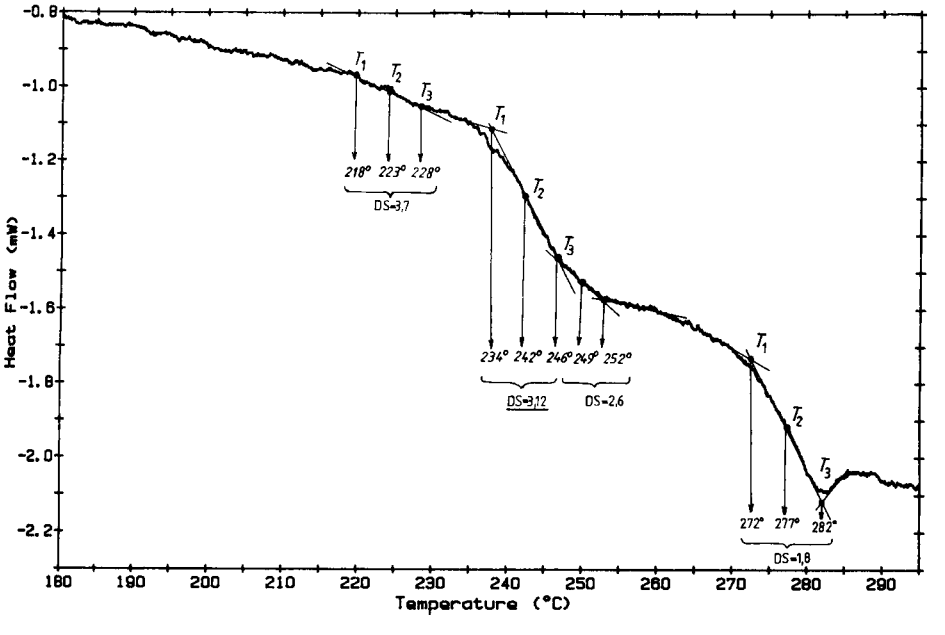

Fig. 5. DSC curve for an HPBCD sample containing several fractions of unknown *DS*.

different fractions are formed. This means that fractions with different degrees of substitution can be found in a sample having different T_g intervals.

The DSC curve in Fig. 5 relates to a sample with an unknown degree of substitution. The curve clearly shows several separate glass transition temperature intervals, proving the presence of several fractions with different *DS* values.

The main advantages of the new method are that it is cheap, simple, reliable and rapid; in addition, individual *DS* values of the various fractions can be determined in one sample.

REFERENCES

1 J. Pitha, J. Cont. Release, 6 (1987) 309.
2 J. Pitha, J. Milecki, H. Fales, L. Pannell and K. Uekama, Int. J. Pharm., 29 (1986) 73.
3 T. Szabó, J. Szejtli, L. Szente, G. Horváth, V. Péterdi, J. Szemán, A. Tóth and P. Komár, Hung. Pat., 202 889 (1988).

END OF PAPERS HONOURING
PROFESSOR ERNÖ PUNGOR

Analytica Chimica Acta, 282 (1993) 319–327
Elsevier Science Publishers B.V., Amsterdam

Bioelectrocatalysis of a water-soluble tetrathiafulvalene–2-hydroxypropyl-β-cyclodextrin complex

Shishan Zhao and John H.T. Luong

Biotechnology Research Institute, National Research Council Canada, Montreal, H4P 2R2 Quebec (Canada)

(Received 10th March 1993; revised manuscript received 6th May 1993)

Abstract

Water-soluble 2-hydroxypropyl-β-cyclodextrin (hp-β-CyD), a cyclic and non-reducing oligosaccharide, was used to enclose tetrathiafulvalene (TTF) to form a water-soluble complex. The molar ratio of hp-β-CyD to TTF in TTF-saturated solutions was about 2.8 and the complex was much more stable than free TTF in aqueous solutions. The cyclic voltammogram of the TTF–hp-β-CyD complex exhibited two oxidation waves with E_p values of 210 mV ($TTF \rightarrow TTF^{+\cdot}$) and 415 mV ($TTF^{+\cdot} \rightarrow TTF^{2+}$) at a glassy carbon electrode vs. Ag/AgCl. The former was relatively reversible and had a pH-independent E_p, while the latter was not reversible due to the decomposition of TTF^{2+} and had a strongly pH-dependent E_p. Application of this novel complex as a homogeneous mediator for the enzyme-catalyzed electrooxidation of glucose, hypoxanthine and lactate, respectively at a glassy carbon electrode was successfully demonstrated. A well-defined catalytic wave was also obtained from NADH, illustrating the feasibility of the TTF–hp-β-CyD complex for bioreactions involving NADH dehydrogenases. The complex for bioelectrocatalysis was then investigated at membrane electrodes of glucose oxidase and xanthine oxidase. Fast response, high sensitivity and a large range of linearity were observed.

Keywords: Biosensors; Cyclic voltammetry; Bioelectrocatalysis; β-Cyclodextrins; Electrooxidation; 2-Hydroxypropyl-β-cyclodextrin; Tetrathiafulvalene

Since the introduction of tetrathiafulvalene–tetracyanoquinodimethane (TTF–TCNQ) into electrochemistry as a specific electrode material [1], intensive research has been focused on the characterization and applications of this organic conducting salt in bioelectrocatalysis [2–6]. Meanwhile the electron donor, TTF, has been successfully applied to bioelectrocatalysis by several researchers [7–14]. TTF is a very efficient mediator with well-defined electron stoichiometry ($n = 1$), low redox potential and relatively reversible heterogeneous and homogeneous electron transfer. Its function in electrocatalysis is based on the anodic creation of the radical cation, $TTF^{+\cdot}$ which can efficiently oxidize various reductants including reduced oxidoreductases.

Correspondence to: J.H.T. Luong, Biotechnology Research Institute, National Research Council Canada, Montreal, H4P 2R2 Quebec (Canada).

An ideal mediator in bioelectrocatalysis must be soluble in aqueous media for homogeneous reactions and/or easily anchored to the surface of an electrode or incorporated into enzymes. In addition to their extremely low solubilities (ca. 1 mg l^{-1}) in aqueous solution, TTF and its salts possess no functional groups for immobilization. Consequently, TTF can only be confined to heterogeneous applications via its physical deposition onto an electrode surface. In view of versatility and electrocatalytic characterization, a water-soluble form of TTF for homogeneous reactions is desired and of great interest.

A simple method for the solubilization of TTF is to incorporate it into a water-soluble complex. The hydrophobic non-charged TTF may form an

inclusion (host–guest) complex with water-soluble cyclodextrins, known as cyclic and non-reducing oligosaccharides consisting of glucose units linked by α-1,4 bonds. The most common cyclodextrins are α-, β-, and γ-cyclodextrins with six, seven and eight glucose units, respectively, that are arranged in a torus shape with an upper and a lower hydrophilic edge and a hydrophobic cavity. Cyclodextrins can form inclusion complexes with various organic compounds by incorporating these guest molecules into their hydrophobic cavities [15]. A derivative of β-cyclodextrin, 2-hydroxypropyl-β-cyclodextrin (hp-β-CyD), appears to be a potential choice since it possesses a very high solubility (50%, w/v in aqueous media) and a reasonable cavity size (approximately 7.8 Å in diameter and 7.8 Å in depth). TTF with a size of 6 Å [16] should fit into the cavity of hp-β-CyD to form a water-soluble complex.

The purpose of this study was to investigate the formation of the water-soluble TTF–hp-β-CyD complex and its electrochemical and bioelectrocatalytic properties. Application of the complex as a mediator for amperometric electrodes of glucose oxidase and xanthine oxidase was also presented and discussed.

EXPERIMENTAL

Chemicals

Hp-β-CyD was obtained from Pharmatec (Alachua, FL) under the trade name Molecusol. The number of substitutions is 6–9 with an average molecular weight of 1570. Glucose oxidase (EC 1.1.3.4, 122,000 U g^{-1}) and NADH (96%) were purchased from Sigma (St. Louis, MO). Xanthine oxidase (EC 1.2.3.2, 170 U g^{-1}) and lactate oxidase (EC 1.13.12.4) were products of Boehringer Mannheim (Mannheim, Germany). All the other chemicals including tetrathiafulvalene (TTF) were products of Aldrich (Milwaukee, WI).

TTFCl was prepared by electrochemically oxidizing TTF in acetonitrile containing 0.1 M tetraethylammonium chloride at pH 7.0 under nitrogen bubbling at a platinum foil electrode poised at 150 mV vs. Ag/AgCl. The dark brown crystals obtained were washed extensively with cold acetonitrile, dried under vacuum and stored at 4°C. Hp-β-CyD was very rapidly dissolved in distilled water or buffer solutions. For the preparation of TTF–hp-β-CyD complexation agents, TTF was added into hp-β-CyD solutions followed by magnetic stirring and a complete dissolution of TTF was achieved within 2 h.

To establish the solubility of TTF in hp-β-CyD, 30 mg of TTF were added to 5 ml of hp-β-CyD solutions at different concentrations. After stirring for 4 h, the resulting solutions were left in the dark overnight for complete sedimentation of undissolved particles and the absorbance was determined at 446 nm. Free TTF-saturated buffer solutions were prepared by following the same procedure except that no hp-β-CyD was present in the buffer solutions and this preparation was done under a nitrogen blanket.

Apparatus

Absorption spectra were acquired on a Beckman DU-7 spectrophotometer. A CV-1B voltammograph equipped with a cell stand and three electrodes (Bioanalytical Systems, West Lafayette, IN) was used to perform electrochemical experiments. The three-electrode system consisted of a glassy carbon electrode (6 mm outer diameter with a conducting area of 3 mm diameter), a platinum wire counter electrode and an Ag/AgCl reference electrode. The glassy carbon electrode was polished using 3-μm alumina and sonicated in distilled water for about 5 min. The resulting electrode was then rinsed thoroughly with distilled water before use.

Preparation of enzyme electrodes

For the preparation of enzyme electrodes, an appropriate enzyme was dissolved in 0.1 M potassium phosphate (pH 7 for glucose oxidase and pH 8 for xanthine oxidase) containing different amounts of the TTF–hp-β-CyD complex. 20 μl of the resulting enzyme solution were then placed onto the surface of a glassy carbon electrode and the enzyme layer was retained by a dialysis membrane (50000 MW cut-off, Spectra/por 7, Spectrum, Houston, TX). The membrane was held tightly in place by an O-ring. Unless otherwise

indicated, electrochemistry was performed at room temperature (22–24°C) in solutions deoxygenated by nitrogen bubbling.

RESULTS AND DISCUSSION

Characterization of TTF–hp-β-CyD complex

Solubilities of TTF in hp-β-CyD solutions were estimated based on the absorption coefficient (215 M^{-1} cm^{-1} at 446 nm) measured a priori using a standard solution containing 6 mM TTF and 20 mM hp-β-CyD. At first, unsubstituted β-cyclodextrin (β-CyD) was examined for the dissolution of TTF. As reported in the literature and observed in this study, β-CyD possessed a very limited solubility in aqueous solutions (1.8%, w/v). It was also found that addition of TTF to a β-CyD solution reduced the solubility of the complexing agent dramatically and caused precipitation. The decrease in solubility may be due to the formation of a more hydrophobic core in the cyclodextrin molecule because of the exclusion of water by a TTF molecule. On the contrary, hp-β-CyD possesses a very high solubility in aqueous solutions (50%, w/v). Such behavior in solubility may be attributed to the steric interactions of the hydroxypropyl groups which prevent hp-β-CyD molecules from stacking together through hydrogen bonding at the upper and lower edges by the hydroxypropyl groups. Unlike β-CyD, hp-β-CyD did not show noticeable changes in solubility in the presence of the guest molecule, TTF. The two other forms of cyclodextrins were not used in this study since α-CyD possesses a considerably lower solubility (12–16%, w/v) and a smaller cavity (4.7–6 Å) while γ-CyD is exorbitantly expensive (US$ 100 per gram). The solubility and cavity size of γ-CyD were reported to be 23% (w/v) and 10 Å, respectively and this compound should be able to enclose the TTF guest (6 Å).

The amount of TTF dissolved in water depended upon the concentration of hp-β-CyD used (Fig. 1). The molar ratio of hp-β-CyD to TTF in TTF-saturated solutions was 2.8 in the lower concentration region of hp-β-CyD below ca. 16 mM. This ratio was independent of concentration of the complexing agent in this lower concentration region, but increased gradually to 5.2 with the concentration of hp-β-CyD increasing to 88 mM. As experimentally demonstrated later, for electrocatalysis a concentration of TTF of 0.2 mM or less was sufficient. Therefore, the concentration of hp-β-CyD required is in the linear region of the dissolution relationship.

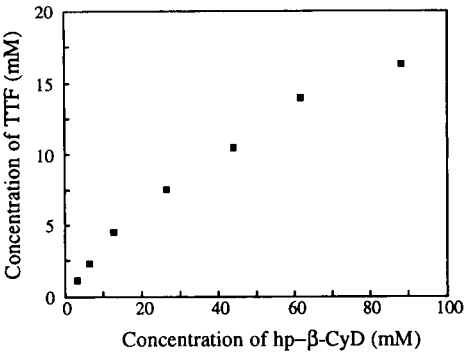

Fig. 1. Dependence of the dissolution of TTF on the concentration of hp-β-CyD in water.

The addition of KCl up to 1 M did not affect the solubility of TTF in hp-β-CyD solutions or the spectrum of the complex. The solubility of TTF in hp-β-CyD solutions was also not affected by pH variation from 3 to 8.5 in 0.1 M potassium phosphate buffer. However, a strong effect of pH on the intensities of the absorption maxima at 446 and 570 nm was observed although the pH did not show considerable effects on the profile of the entire spectrum of the complex. The spectra of the complex at different pH values in phosphate buffer solutions are shown in Fig. 2. The absorption peaks at 446 and 570 nm decreased to a large extent as the pH changed from 3 to 5 and then gradually reached stability with the increase of pH from 5 to 9. The absorption peak at 570 nm and the absorption enhancement at 446 nm in acidic solutions are likely related to the protonation of the electron-dense center of the complex. As shown in Fig. 3, the absorption characteristics of this plausibly protonated species at these two wavelengths were similar to those of $TTF^{+\cdot}$.

As a light-sensitive compound, TTF can easily be oxidized by oxygen in aqueous solutions. A solution prepared by dissolving TTF in deaerated

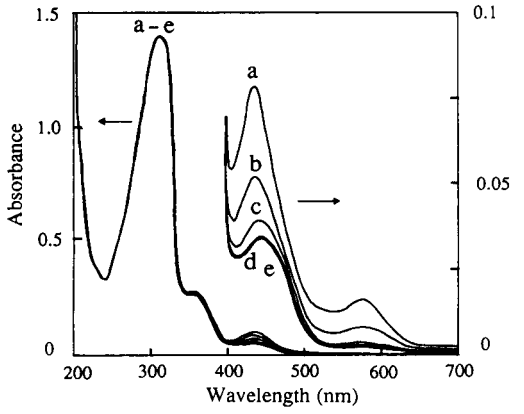

Fig. 2. Spectra of TTF–hp-β-CyD inclusion complex. 1.0 g l^{-1} hp-β-CyD; 0.031 g l^{-1} TTF and 20 mM potassium phosphate at different pH values. (a) 3; (b) 4; (c) 5; (d) 7; (e) 9; (f) 11.

distilled water containing 0.1 M potassium phosphate (pH 7) became cloudy and lost more than 80% of its electrocatalytic activity for glucose oxidase within 8 h in air at room temperature. However, the spectrum of a solution with 6 mM TTF and 20 mM hp-β-CyD in the same buffer (without deaeration) remained unchanged after being stored in air at room temperature for 24 h. When this complex solution was stored in the dark at 4°C, both its spectrum and electrocatalytic activity for the oxidation of glucose catalyzed by glucose oxidase did not exhibit any noticeable changes after four weeks.

The active state of TTF is its radical cation $TTF^{+\cdot}$ which is not stable in aqueous media. Since the stability of the radical cation is very dependent on the matrix of a solution, the effect of hp-β-CyD on the stability of $TTF^{+\cdot}$ in aqueous solutions was investigated. TTFCl was prepared for examination of this effect and the spectrum of a TTF^{+} solution is shown in Fig. 3. Addition of hp-β-CyD to a final concentration of 10 g l^{-1} to a 0.17 g l^{-1} TTFCl solution did not cause any changes of the spectrum (figure not shown). Of course, the spectrum was acquired immediately after the solution had been prepared to avoid decomposition. Kinetic measurements were performed by monitoring the absorption of $TTF^{+\cdot}$ versus time at 578 nm. Experiments in a 0.2 M sodium acetate buffer solution (pH 5.5) with a series of different hp-β-CyD concentrations revealed that the complexing agent destabilized the radical cation. The absorbance at 578 nm diminished very quickly with the increase in the complexing agent (Fig. 4). In pure water or in the acetate buffer solution without the complexing agent the entire spectrum decayed slowly and white precipitate was observed after several hours. In the presence of the complexing agent, a decomposed solution was homogeneous and showed a spectrum similar to that of TTF–hp-β-CyD. However, the absorption intensity of the spectrum was not reproducible. The decomposition of $TTF^{+\cdot}$ in this case is likely related to a disproportionation reaction, i.e., $2TTF^{+\cdot} \rightarrow TTF + TTF^{2+}$. The curves in Fig. 4 are characteristic of a second-order decomposition. As experimentally es-

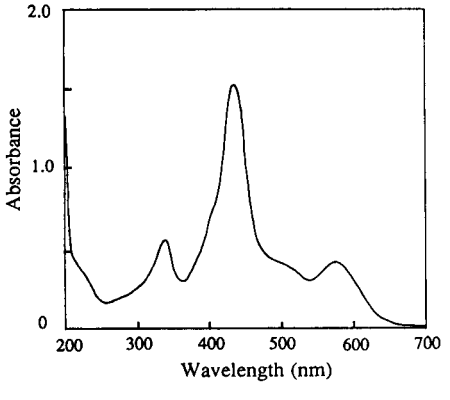

Fig. 3. Spectrum of TTFCl (0.034 g l^{-1}) in water.

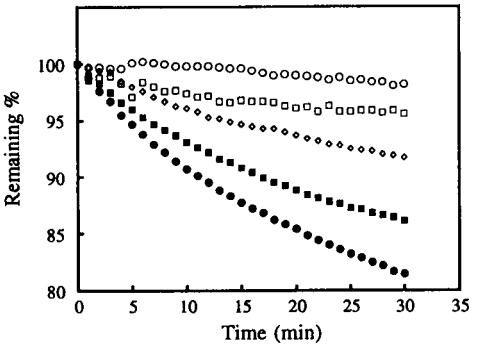

Fig. 4. Effect of hp-β-CyD on the stability of $TTF^{+\cdot}$. Solutions: 0.1 M sodium acetate and 0.1 M KCl at pH 5.5 containing different amounts of hp-β-CyD: (○) 0; (□) 0.5; (◇) 3; (■) 6; (●) 10 mM.

tablished later, a very low concentration of hp-β-CyD (about 0.5 mM) was normally required for the preparation of a TTF solution for electrochemical catalysis. The decomposition of electrogenerated $TTF^{+\cdot}$ caused by the presence of such a low concentration of the complexing agent during an electrocatalytic process should not be problematical.

Electrovoltammetry

The reported oxidation potential of TTF (300 mV vs. SCE [17]) was measured in acetonitrile. No cyclic voltammograms for TTF have been reported in the literature. In this study, a TTF-saturated phosphate buffer at pH 7 exhibited two oxidation waves with E_p values of about 210 and 415 mV, respectively on a glassy carbon electrode (Fig. 5, curve b). The peak currents were very small because of limited solubility of TTF in the buffer solution as mentioned before. As also shown in this figure, the cyclic voltammogram of the TTF–hp-β-CyD complex exhibited similar potentials for the two oxidation waves and the peak currents of the two oxidation waves were proportional to the concentration of TTF–hp-β-CyD. The peak corresponding to the oxidation of TTF to $TTF^{+\cdot}$ at 210 mV was relatively reversible and had a potential split of about 65 mV (Fig. 5, curve f). When the potential was swept to more positive than 350 mV where $TTF^{+\cdot}$ starts to be

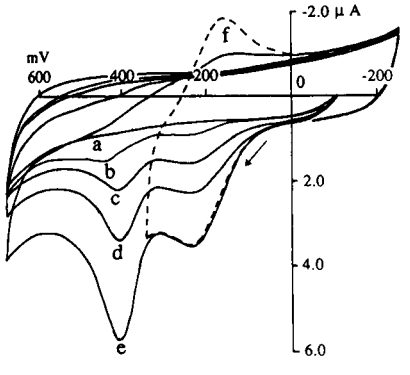

Fig. 5. Cyclic voltammograms of different TTF–hp-β-CyD complex concentrations at a glassy carbon electrode in 0.1 M potassium phosphate and 0.05 M KCl, pH 7. Sweep rate: 20 mV s^{-1}. Hp-β-CyD concentration: (a, b) 0; (c) 0.6; (d) 1.2; (e, f) 2.4 mM. TTF concentration: (a) 0 mM; (b) free TTF-saturated; (c) 0.12; (d) 0.24; (e, f) 0.48 mM.

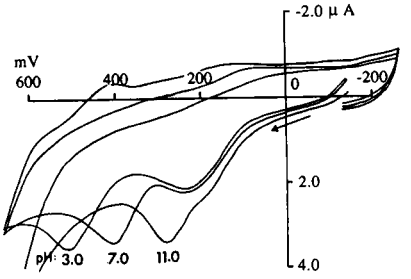

Fig. 6. Effect of pH on the cyclic voltammograms of TTF–hp-β-CyD at a glassy carbon electrode. Solution composition: 0.6 mM hp-β-CyD and 0.12 mM TTF in 0.1 M potassium phosphate buffer containing 0.05 M KCl. Sweep rate: 20 mV s^{-1}.

oxidized to TTF^{2+}, the reversed waves decayed to a certain extent and at last disappeared depending on the completion extent of the oxidation process (Fig. 5, curves c–e). This is indicative of a decomposition reaction following the formation of TTF^{2+}. As experimentally demonstrated later, electrocatalytic activity was hampered in the potential region where $TTF^{+\cdot}$ was converted into TTF^{2+}.

The E_p for the oxidation of TTF to $TTF^{+\cdot}$ was very slightly affected by pH (Fig. 6). However, the E_p for the oxidation of $TTF^{+\cdot}$ to TTF^{2+} was strongly pH dependent. A change from pH 3 to pH 7 and 11 shifted the E_p from 550 mV to 415 and 310 mV, respectively. For electrocatalysis, only the first oxidation step is useful. Obviously, its pH independence is an advantageous property. As a common mediator, it can be easily applied for bioelectrochemical systems optimized at different pH values.

Bioelectrocatalysis

Homogeneous applications of TTF in electrocatalysis are very difficult and limited due to its extremely limited solubility and instability in aqueous media. The inclusion complexation of TTF by hp-β-CyD enables one to manipulate the concentration of TTF in aqueous solutions as desired. A series of experiments was carried out to investigate the electrocatalytic behavior of the TTF–hp-β-CyD complex for the enzymatic oxidation of glucose, hypoxanthine and lactate by using free glucose oxidase, xanthine oxidase and lactate oxidase, respectively. For comparison, attempts

were also made to examine the electrocatalytic behavior of free TTF with a solubility of ca. 1 mg l^{-1}.

Similar catalytic waves were obtained regardless of whether free TTF or TTF–hp-β-CyD complex was used which illustrated that the TTF–hp-β-CyD complex could effectively react with the reduced glucose oxidase like free TTF (Fig. 7A). A comparison of the electrocatalytic efficiency of the complex with free TTF was somewhat difficult because the trace amount of free TTF in solutions could not be measured accurately. However, a TTF-saturated solution was observed to have the electrocatalytic activity of a TTF–hp-β-CyD solution containing 0.015 mM TTF. It was further observed that the catalytic current increased with the concentration of the TTF–hp-β-CyD complex at a constant concentration of the enzyme. In the oxidation of glucose using a fixed amount for both enzyme and substrate, the electrocatalytic peak current increased from 6.7 μA to 8.6, 10.6 and then 12.3 μA with increasing TTF–hp-β-CyD concentrations from 0.024 mM to 0.06, 0.12 and 0.18 mM (Fig. 7A). Enhancement of sensitivity due to increases in the concentration of the complex gradually reached saturation when enzyme activity became rate limiting. Catalytic waves were also obtained for the electrooxidation of hypoxanthine and lactate catalyzed by their enzymes (Fig. 7B and D). It should be noted that the activities of these two enzymes at a reasonable concentration are rate limiting. The specific activity of either xanthine oxidase or lactate oxidase is about 0.15 U mg^{-1} compared to 122 U mg^{-1} of glucose oxidase. Consequently, the catalytic waves could not be enhanced effectively by increasing the concentration of the mediator complex.

Another important observation is the inactivity of TTF^{2+} for electrocatalysis by the three oxidoreductases. When the applied potential was more positive than 350 mV where $TTF^{+\cdot}$ was irreversibly oxidized to TTF^{2+}, the catalytic current dropped rapidly, an indication of the decomposition of TTF^{2+} or its low reactivity toward enzyme.

The electrocatalytic property of the TTF complex for NADH was also investigated since NAD/NADH is the cofactor for about 300 dehydrogenases and, therefore, is of importance in biosensor applications. Conventionally, an overpotential of 500 to 700 mV is needed for the oxidation of NADH on a glassy carbon or platinum electrode [18]. This is a serious drawback because electroactive species such as ascorbic acid, uric acid and acetaminophen are frequently found in food and biological samples and are also oxidized at such potentials.

A well-defined catalytic wave for NADH was obtained with the TTF complex on a glassy carbon electrode (Fig. 7C). Compared with the sensitivity shown in Fig. 7A, B and D, the experi-

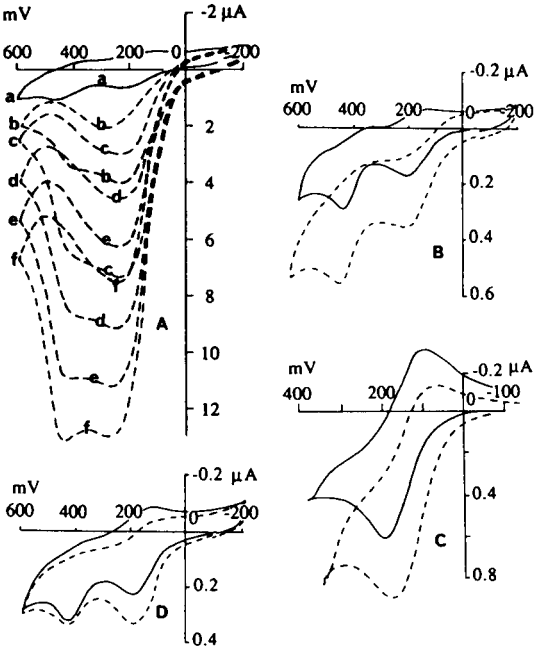

Fig. 7. Bioelectrocatalytic voltammograms of TTF–hp-β-CyD. (———) background, without substrate; (- - - - -) with substrate, catalytic waves. Sweep rate: 20 mV s^{-1}. Buffer solution: 0.1 M potassium phosphate containing 0.05 M KCl and (A) 0.024 mM TTF, 0.12 mM hp-β-CyD and 5 g l^{-1} glucose oxidase at pH 7.0 with or without 6 mM glucose. TTF concentrations: (a) 0 mM; (b) free TTF-saturated; (c) 0.024; (d) 0.06; (e) 0.12; (f) 0.18 mM. hp-β-CyD concentrations: (a, b) 0; (c) 0.12; (d) 0.3; (e) 0.6; (f) 0.9 mM. (B) 0.01 mM TTF, 0.05 mM hp-β-CyD and 4 g l^{-1} xanthine oxidase at pH 8.0 with or without 0.1 mM hypoxanthine. (C) 0.1 mM TTF and 0.6 mM hp-β-CyD at pH 7.4 with or without 50 mM NADH. (D) 0.01 mM TTF, 0.05 mM hp-β-CyD and 2 mg ml^{-1} lactate oxidase at pH 7.0 with or without 1 mM lactate.

mental data obtained revealed a slower reaction between $TTF^{+\cdot}$ and NADH. However, a reasonable sensitivity could be acquired by using a higher concentration of the complex.

Mediated biosensors for glucose and hypoxanthine

Based on the biocatalytic voltammetric results obtained, applications of the TTF–hp-β-CyD complex to amperometric biosensors were investigated. In this series of experiments, glucose oxidase or xanthine oxidase electrodes were prepared as described in the Experimental section. To electrolyte bulk solutions, TTF–hp-β-CyD complex was added as the homogeneous mediator. Although functional, the response was somewhat sluggish, therefore glucose oxidase or xanthine oxidase was dissolved in a buffer containing the same amount of the TTF–hp-β-CyD complex to minimize the initial equilibrium time of the complex between the bulk solution and the enzyme layer. The bioelectrochemical process was initiated by the oxidation of the TTF-hp-β-CyD complex to $TTF^{+\cdot}$ at the electrode which resulted in an increase in the background current. $TTF^{+\cdot}$ was then reduced by the reduced enzyme to regenerate TTF. Since a very low concentration (< 0. 1 mM) of the mediator was required due to its efficiency, the background was low (ca. 20 nA).

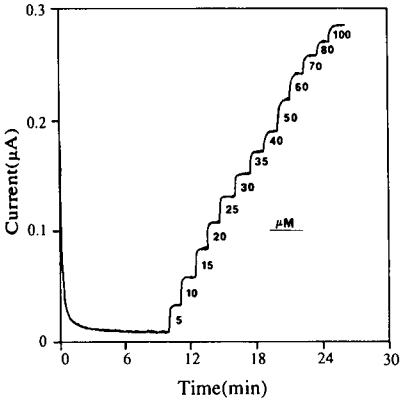

Fig. 8. The response of the hypoxanthine electrode to the stepwise addition of hypoxanthine. Applied potential: 100 mV vs. Ag/AgCl. Enzyme layer: 50 mg ml^{-1} xanthine oxidase. Buffer solution: 0.1 M potassium phosphate (pH 8.0) containing 0.1 mM TTF and 0.6 mM hp-β-CyD.

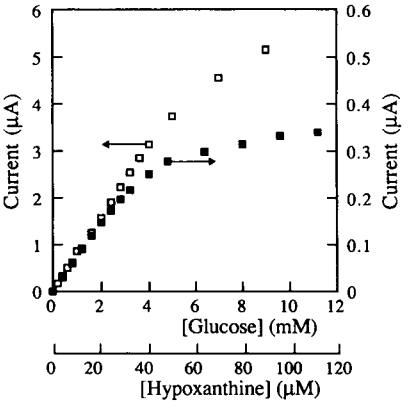

Fig. 9. Responses of the mediated enzyme electrodes. Applied potential: 100 mV vs. Ag/AgCl. Enzyme layer: 50 mg ml^{-1} enzyme. (□) Glucose oxidase electrode in 0.1 M potassium phosphate (pH 7.0) containing 0.05 mM TTF and 0.25 mM hp-β-CyD. (■) Xanthine oxidase electrode in 0.1 M potassium phosphate (pH 8.0) containing 0.1 mM TTF and 0.6 mM hp-β-CyD.

The hypoxanthine electrode attained its steady state in about 10 s in the linear response region and in about 1 min in the plateau region (Fig. 8) and similar behavior was also observed for the glucose electrode (figure not shown). The response current at a given concentration of a substrate did not change over one hour of measurement. As expected, both sensitivity and linear range were dependent on the concentration of mediator. The response current increased proportionally with the increasing TTF concentration up to ca. 3 and 10 mM for the glucose electrode and the hypoxanthine electrode, respectively. Beyond these levels, the current was no longer proportional to the mediator concentration, an indication of the rate-limiting enzyme kinetics. At 0.05 mM TTF, the response to glucose of the glucose electrode was linear up to 4.5 mM with a sensitivity of 0.8 μA mM^{-1}. A significantly higher sensitivity but a lower linear range was observed for the hypoxanthine electrode. At 0.1 mM TTF the linear range and the sensitivity of this electrode were determined to be 0–35 μM and 7 μA mM^{-1}, respectively (Fig. 9). The Lineweaver–Burk plot (1/current vs. 1/concentration) resulted in a correlation coefficient of

0.998 for the glucose electrode and 0.999 for the hypoxanthine electrode. Consequently, the maximum current I_{max} was determined to be 13.8 μA for the former and 0.5 μA for the latter. The corresponding equivalent K_M for these two electrodes was 14.5 and 0.043 mM. These results implied that the behavior of these electrodes was governed by Michaelis–Menten kinetics. The K_M value for soluble glucose oxidase isolated from *Aspergillus niger* with respect to glucose at pH 5.6 was reported to be 33 mM whereas that of xanthine oxidase with respect to hypoxanthine was 0.0013 mM [19].

As mentioned earlier, hp-β-CyD was observed to destabilize the electrocatalytic species $TTF^{+\cdot}$. However, no noticeable variation in response currents was observed by adding up to 3 mM hp-β-CyD in excess over the required amount (less than 0.5 mM) for the dissolution of the mediator. Such a result was not completely unexpected because of the efficient reaction kinetics of $TTF^{+\cdot}$ with the reduced enzymes, i.e. $TTF^{+\cdot}$ species generated on the electrode surface could be rapidly recycled to TTF by reduced enzyme. Consequently, destabilization of $TTF^{+\cdot}$ by hp-β-CyD would be minimal.

Adsorption of cyclodextrin on electrode surfaces was reported in the literature [20,21]. A carbon electrode surface with so-called "acidic carbon oxides" was anticipated to be adsorptive to the TTF complex due to the hydroxyl groups at its two edges. In an effort to develop the mediated biosensors for glucose and hypoxanthine, glassy carbon electrodes with the complex adsorbed on their surfaces were attempted in this study. In this case, external addition of the mediator system is no longer required and such biosensors may be more desirable for many practical applications. After immersion in 8 M NaOH for 24 h and then rinsing with water, the electrodes were immersed in a 0.1 M potassium phosphate solution (pH 7.0) with TTF (1.25 g l^{-1}) and hp-β-CyD (50 g l^{-1}) for about 4 h. The resulting electrodes were thoroughly rinsed with water. An enzyme layer was deposited on the electrodes and retained by a dialysis membrane. In this experiment, the TTF–hp-β-CyD complex was not introduced into the detection chamber.

The enzyme electrodes exhibited reasonable sensitivities, but their linear ranges were somewhat limited. The linear ranges of the glucose electrode and the hypoxanthine electrode were 0–2 mM and 0–20 μM, respectively (Fig. 10). They were stable when stored in the dark at 4°C, but unstable for reuses. Each run of a calibration curve reduced the sensitivity of an electrode by about 15%, an indication of mediator loss from the surface of the electrode. Such behavior was not completely unexpected since $TTF^{+\cdot}$ salt is slightly water-soluble and may dissociate from the hydrophobic cavity of hp-β-CyD to the bulk solution. In addition, the TTF–hp-β-CyD complex is also expected to escape from the surface of the electrode since it can easily diffuse out of the dialysis membrane.

Conclusions

In brief, the formation of water-soluble TTF–hp-β-CyD and its bioelectrocatalytic efficacy opens up homogeneous applications of TTF in amperometric systems. While its complexation with β-CyD reduces the solubility of the complexing agent and results in gradual precipitation, its complexation with hp-β-CyD exhibits a high solubility. The TTF–hp-β-CyD complex has been shown to be a chemically stable and efficient

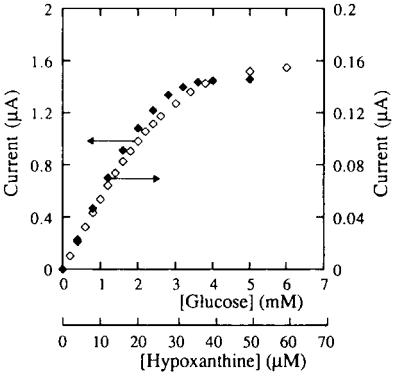

Fig. 10. Responses of the electrodes with preadsorbed TTF–hp-β-CyD complex. Applied potential: 100 mV vs. Ag/AgCl. Enzyme layer: 50 mg ml^{-1} enzyme. (◇) Glucose oxidase electrode (electrode with adsorbed TTF–hp-β-CyD complex) in (pH 7.0) 0.1 M potassium phosphate. (◆) Xanthine oxidase electrode (electrode with adsorbed TTF–hp-β-CyD complex) in (pH 8.0) 0.1 M potassium phosphate.

mediator for electrochemistry of glucose oxidase, lactate oxidase, xanthine oxidase and NADH. The electrochemical and electrocatalytic behavior of the TTF–hp-β-CyD complex is similar to those of free TTF. For amperometric analysis at enzyme electrodes, a very low complex concentration (0.05–0.1 mM) is sufficient to support a large catalytic current.

REFERENCES

1 C.D. Jaeger and A.J. Bard, J. Am. Chem. Soc., 101 (1979) 1690.
2 J. Kulys and G.J.S. Svirmickas, Anal. Chim. Acta, 117 (1980) 115.
3 W.J. Albery and P.N. Bartlett, J. Chem. Soc. Chem. Commun., (1984) 234.
4 W.J. Albery, P.N. Bartlett, N. Bycroff, D.H. Craston and B.J. Driscoll, J. Electroanal. Chem., 218 (1987) 119.
5 K. McKenna, S.E. Boyette and A. Brajther-Toth, Anal. Chim. Acta, 206 (1988) 75.
6 S. Zhao and R.B. Lennox, Anal. Chem., 63 (1991) 1174.
7 A.P.F. Turner, S.P. Hendry and M.F. Cardosi, World Biotechnol. Rep., 1 (1987) 125.
8 B. Gruendig and C. Krabisch, Anal. Chim. Acta, 222 (1989) 75.
9 G. Hari and C.H. Tan, Analyst, 115 (1990) 35.
10 G. Palleshi and A.P.F. Turner, Anal. Chim. Acta, 234 (1990) 459.
11 G. Hari, C.H. Tan and H.M. Ng, J. Electroanal. Chem., 287 (1990) 349.
12 J. Kulys and A. Drungiliene, Anal. Chim. Acta, 243 (1991) 287.
13 J. Kulys and A. Drungiliene, Electroanalysis (New York), 3 (1991) 209.
14 P.D. Hale, L.F. Liu and T.A. Skotheim, Electroanalysis (New York), 3 (1991) 751.
15 F. Cramer, W. Saenger and H.-ch. Spatz, J. Am. Chem. Soc., 89 (1967) 14.
16 D. Philp, A.M.Z. Slawin, N. Spencer, J.F. Stoddart and D.J. Williams, J. Chem. Soc. Chem. Commun., (1991) 1584.
17 D.L. Coffen, J.Q. Chambers, D.R. Williams, D.E. Garraett and N.D. Canfield, J. Am. Chem. Soc., 93 (1991) 2258.
18 A. Torstensson and L.J. Gorton, Electroanal. Chem., 130 (1981) 199.
19 T.E. Barman, Enzyme Handbook, Vol. 1, Springer, New York, 1985, pp. 112–147.
20 T. Matsue, M. Fujihira and T. Osa, J. Electrochem. Soc., 126 (1979) 500.
21 T. Matsue, M. Fujihira and T. Osa, J. Electrochem. Soc., 128 (1981) 1473.

Analytica Chimica Acta, 282 (1993) 329–333
Elsevier Science Publishers B.V., Amsterdam

Adsorptive stripping voltammetry of trace thallium

Joseph Wang and Jianmin Lu

Department of Chemistry and Biochemistry, New Mexico State University, Las Cruces, NM 88003 (USA)

(Received 22nd March 1993)

Abstract

A highly selective and sensitive adsorptive stripping voltammetric procedure for trace measurements of thallium in presence of *o*-cresolphthalein (OCP) is described. The response is not affected by the presence of excess tin, lead or indium, which can interfere severely in analogous anodic stripping measurements. The adsorptive strategy also offers enhanced sensitivity over anodic stripping measurements. The detection limit is 60 ng/l (3×10^{-10} M) with 2-min accumulation, and the relative standard deviation (at the 5 μg/l level) is 3.6%. Optimal conditions were found to be 0.01 M sodium hydroxide containing 5×10^{-7} M OCP, a preconcentration potential of -0.30 V and a differential pulse waveform.

Keywords: Adsorptive stripping voltammetry; Voltammetry; *o*-Cresolphthalein; Thallium

Owing to its remarkable sensitivity and compact instrumentation, stripping analysis has become a powerful tool in trace and field analyses [1–4]. It is highly suitable for trace measurements of thallium ions (which can be readily reduced and form amalgam). Because of the toxic nature of thallium, such procedures are required for its determination in various environmental and biological samples. However, a common problem in conventional stripping measurements of thallium is the difficulty to resolve the thallium response from neighboring peaks associated with the stripping of co-existing metals such as lead, tin, indium or cadmium. Extensive efforts have thus been devoted for improving the selectivity of thallium measurements through the addition of certain complexing agents or surfactants [5–8].

The present article describes an adsorptive stripping voltammetric procedure for highly selective and sensitive measurements of trace levels of thallium. Adsorptive stripping voltammetry has been shown useful for extending the scope of stripping analysis towards numerous elements that cannot be deposited electrolytically [9–11]. It can also serve as an attractive strategy for measuring amalgam-forming metals such as copper [12], lead [13] or tin [14]. For such applications the adsorption strategy can add a new dimension of selectivity through the chemistry involved in the chelate–formation reaction. Likewise, the adsorptive preconcentration of the thallium–*o*-cresolphthalein (OCP) complex is shown below to eliminate major interferences from co-existing metals while retaining (and even enhancing) the remarkable sensitivity of conventional stripping procedures. While (to the best of our knowledge) this is the first reported adsorptive stripping procedure for thallium, OCP has been employed previously for analogous measurements of lanthanides [15] and lead [13].

Correspondence to: J. Wang, Department of Chemistry and Biochemistry, New Mexico State University, Las Cruces, NM 88003 (USA).

EXPERIMENTAL

Apparatus and reagents

An EG&G PAR 264A voltammetric analyzer, a PAR 303A static mercury drop electrode (SMDE), and a PAR 0073 *X–Y* recorder were used to obtain the voltammograms. A medium-size hanging mercury drop electrode (with an area of 0.016 cm^2) was employed. All solutions were prepared from double-distilled water. The stock solution (1000 mg/l) of thallium (atomic absorption standard solution, Aldrich) was diluted daily as required. The ligand (OCP, Aldrich) was dissolved in a few drops of a 1 M NaOH solution and subsequently was diluted to give a 5×10^{-4} M stock solution. A 0.01 M NaOH solution served as the supporting electrolyte.

Procedure

The supporting electrolyte solution (10 ml), containing 5×10^{-7} M OCP, was pipetted into the cell and deaerated by nitrogen for 8 min. The preconcentration potential (usually −0.30 V) was applied to a fresh mercury drop while the solution was stirred. Following the preconcentration step, the stirring was stopped and after 15 s the voltammogram was recorded by applying a negative-going differential pulse scan (with 10 mV/s scan rate and 50 mV amplitude). The scan was terminated at −0.9 V. Aliquots of the thallium standard solution were introduced after recording the background voltammograms. Throughout this operation, nitrogen was passed over the solution. All data were obtained at room temperature.

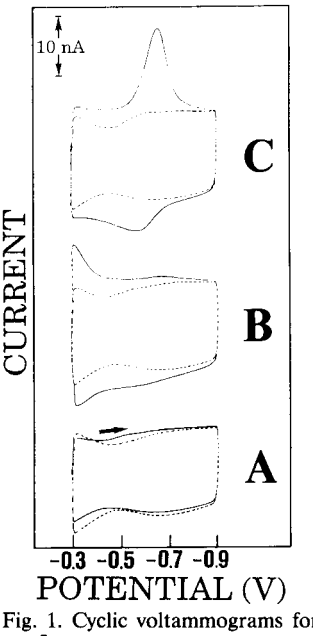

Fig. 1. Cyclic voltammograms for 40 μg/l thallium (A), 5×10^{-7} M OCP (B) and 40 μg/l thallium in the presence of 5×10^{-7} M OCP (C), following 0 and 90 s accumulation at −0.30 V (dotted and solid lines, respectively). Scan rate, 200 mV/s; electrolyte, 0.01 M NaOH.

RESULTS AND DISCUSSION

The suitability of the thallium–OCP complex for adsorptive stripping voltammetry of thallium is indicated from the cyclic voltammograms of Fig. 1. Cyclic voltammetric experiments (performed with and without prior accumulation) resulted in no response in the absence of the ligand (A) or the metal (B). However, when similar experiments were carried out after the complex formation (C), the 90 s accumulation period resulted in a well-defined cathodic peak at −0.66 V, and a smaller and broader peak in the anodic branch ($E_p = -0.57$ V). The second, and subsequent repetitive scans yielded a (50%) smaller and stable cathodic peak, and a highly stable anodic response (not shown). Surface saturation was observed following 100 s preadsorption. The charge (consumed by the surface process at saturation) was found to be 5.7 nC. This charge corresponds to a surface coverage of 3.7×10^{-12} mol/cm^2 and to an area (occupied by an adsorbed complex molecule) of 45 nm^2. A plot of (peak current) vs. (scan rate) for the complex, over the 10–200 mV/s range was linear (with a slope of 0.99). A slope of 1.0 is expected for an ideal reaction of surface reactant. No response is observed for analogous measurements without accumulation (dotted line). The redox process appears to involve the reduction of the metal center [Tl(I)] in the complex, and not the reduction of a ligand functionality involved in the coordination (as in the case of analogous lanthanide–OCP measurements [15]). The fact that a defined

response is observed in cyclic voltammetry for 40 μg/l (ppb) thallium indicates the remarkable sensitivity associated with the coupling of the interfacial and redox behaviors of the thallium-OCP complex. Additional gains can be achieved in a differential pulse stripping operation, as illustrated below.

The strong adsorption of the thallium–OCP complex can be used as an effective preconcentration step, prior to voltammetric measurement. Fig. 2 shows plots of differential pulse peak current vs. preconcentration time at three levels of thallium: 1 (A), 2 (B), and 4 (C) μg/l. The longer the preconcentration time, the more the metal complex is adsorbed and the larger is the peak current. In all three instances, the current increases linearly with time at first [up to 90 (A), 75 (B), and 60 (C) s], and then levels off. An accumulation time of 60 s yields a peak current enhancement of 4, compared to the response following 15 s accumulation. While quantitation at these levels is not feasible without preconcentration, short accumulation periods (15–90 s) offer convenient measurements of these low μg/l concentrations.

Various experimental variables affecting the thallium response were characterized and optimized (Fig. 3). The OCP concentration had a pronounced effect on the stripping current (A). The peak for 10 μg/l thallium increased linearly with increasing OCP concentration up to 1.5×10^{-7} M (i.e. [OCP]/[Tl] of 3) and then started to level off. Different OCP concentration effects are

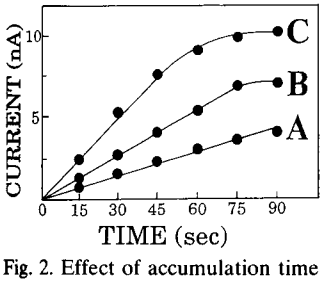

Fig. 2. Effect of accumulation time upon the adsorptive stripping response of 1(A), 2 (B), and 4 (C) μg/l thallium. Preconcentration at −0.25 V, followed by differential pulse measurement with a 50-mV amplitude and 20 mV/s scan rate. Media, 0.01 M NaOH $+5\times10^{-7}$ M OCP.

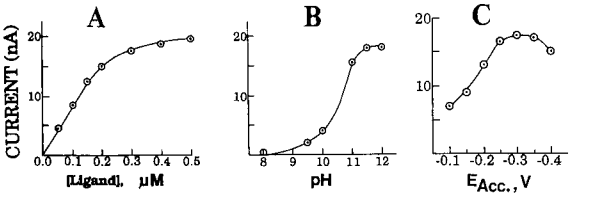

Fig. 3. Effect of OCP concentration (A), pH (B), and accumulation potential (C) on the adsorptive stripping current for 10 μg/l thallium. Preconcentration at −0.25 V for 30 s. Other conditions, as in Fig. 2.

expected at different levels of thallium. The stripping current also depended strongly on the solution pH (B). The peak increased rapidly upon increasing the pH between 8 and 11, and then it started to level off. The dependence of the response on the preconcentration potential was examined over the range −0.10 to −0.40 V (C). The peak increased gradually between −0.10 and −0.25 V, remained stable up to −0.35 V, and then started to decrease. Such a profile is attributed to stronger adsorption around the potential of zero charge. Based on the data of Fig. 3, all subsequent work employed a 0.01 M sodium hydroxide solution, containing 5×10^{-7} M OCP, and an accumulation potential of −0.30 V. In addition, the differential pulse waveform offered improved signal-to-background characteristics (compared to a linear scan) and was used throughout. The presence of oxygen allowed convenient quantitation of concentrations higher than 5 μg/l. However, measurements of lower thallium levels required removal of oxygen, as was employed throughout this study.

The concentration dependence is shown in Fig. 4, which displays voltammograms for successive increases in the thallium concentration in 1 μg/l (4.9×10^{-9} M) steps (peaks a–e). Well-defined peaks are observed ($E_p = -0.59$ V) despite the very short (30 s) preconcentration time. The peaks are proportional to the thallium concentration. These five peaks were part of a series of 11 concentration increments, up to 15 μg/l thallium. The resulting calibration plots, obtained with different preconcentration periods are also shown in Fig. 4 (inset). As expected for processes limited by adsorption, the response is linear for

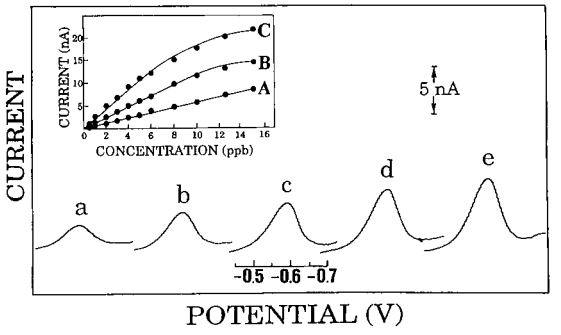

Fig. 4. Stripping voltammograms obtained for solutions of increasing thallium concentration in 1.0 μg/l steps (a–e). Preconcentration at −0.3 V for 30 s; other conditions, as in Fig. 2. Inset are calibration plots for different preconcentration times: 15 (A), 30 (B) and 60 (C) s.

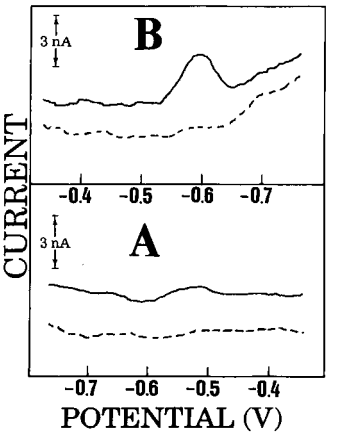

Fig. 5. Measurements of 0.5 μg/l thallium by conventional anodic (A) and adsorptive (B) stripping voltammetry. Preconcentration at −0.3 V for 120 s; other conditions, as in Fig. 2. The corresponding blank voltammograms are shown as dotted lines. The opposite potential scales are attributed to the different scan directions.

dilute solutions (up to 15, 10, and 6 μg/l for preconcentration times of 15, 30 and 60 s, respectively). The slopes of the initial linear portions correspond to 0.57 (A), 1.12 (B) and 1.79 (C) nA · l/μg (correlation coefficients, 0.995, 0.999 and 0.997, respectively). These calibration data indicate that the adsorptive stripping procedure results in low detection limits following short accumulation periods. Unlike analogous adsorptive stripping measurements of lanthanides [15], no free ligand (OCP) peak is observed.

The detectability was calculated from measurements of 0.5 μg/l thallium following a 2-min preconcentration (Fig. 5B). The signal-to-noise characteristics of these data ($S/N = 3$) correspond to a detection limit of 0.06 μg/l (3×10^{-10} M). Analogous measurements of thallium, using conventional stripping voltammetry (in acetate buffer) yield a higher detection limit of 0.3 μg/l (Fig. 5A). The adsorptive accumulation of the thallium–OCP complex results in reproducible stripping peaks. For example, a series of 14 repetitive measurements of 4 μg/l thallium yielded a mean peak current of 6.29 nA, a range of 6.05–6.75 nA, and a relative standard deviation of 3.6%.

A drawback of conventional anodic stripping measurement of thallium is the poor resolution in the presence of lead, tin, indium or cadmium. The selective coordination, associated with the adsorptive approach, can address most of these

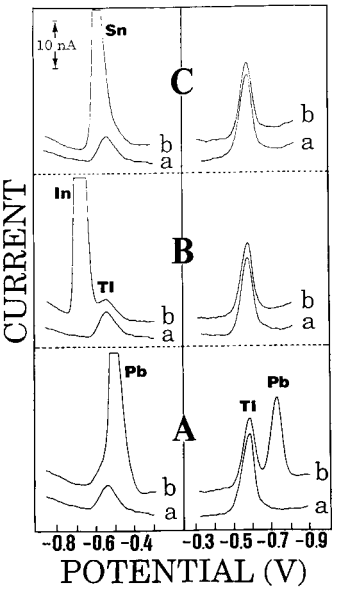

Fig. 6. Measurements of thallium in the presence of lead (A), indium (B) and tin (C) by conventional and adsorptive stripping voltammetry (left and right, respectively). (a) 5 μg/l thallium; (b) same as (a) but after addition of the foreign ion (20 μg/l). Preconcentration for 60 s at −1.0 V (left) and −0.30 V (right). Electrolyte (left), acetate buffer (0.01 M, pH 5). Other conditions, as in Fig. 2.

interferences, and thus offers a highly selective procedure for thallium. For example, Fig. 6 compares voltammograms for 5 μg/l thallium in the absence (a) and presence (b) of 20 μg/l lead (A), indium (B) and tin (C), as obtained by conventional (left) and adsorptive (right) stripping schemes. It is obvious that due to severe peak overlap, thallium cannot be measured selectively by conventional stripping voltammetry. In contrast, no effect of tin or indium on the thallium response is observed in the analogous adsorptive stripping measurements. Even a larger (10-fold) excess of these ions did not affect the thallium peak (not shown). The lead–OCP system exhibits a well-defined adsorptive stripping peak (as was reported in a recent study [13]). Such peak, however, is well resolved from the thallium response ($\Delta E_p = 140$ mV), and the 4-fold excess of lead caused only a 7% decrease of the thallium peak. An 18% diminution of the thallium peak was observed in the presence of a larger (20-fold) excess of lead (not shown). The data of Fig. 6 indicate again that the adsorption strategy offers improved sensitivity and overall detectability compared to conventional stripping measurements [a (left) vs. a (right)]. Other ions tested (at the 25 μg/l level) and found not to affect the response of 2.5 μg/l thallium include Ni(II), Zn(II), Cr(VI), Se(IV), Al(III), Fe(III), Te(IV), Mo(VI), Mg(II), U(VI) and V(V). As common in adsorptive stripping measurements, co-existing surfactants can cause severe depressions of the peak (e.g. 57% decrease in the presence of 2 mg/l gelatin). Such interference can be addressed by UV irradiation or addition of fumed silica.

In conclusion, adsorptive stripping voltammetry has been demonstrated to be an attractive alternative to conventional stripping measurements of trace thallium. The main advantage of the adsorptive approach for thallium is its inherent selectivity accrued from the OCP–thallium chelation reaction. In addition, it offers enhanced sensitivity, and hence lower detection limits. The OCP–thallium procedure should be suitable also for potentiometric stripping measurements, and could be adopted to on-line operations, as desired for continuous monitoring of trace thallium in flowing streams.

This work was supported by a grant from the U.S. Dept. of Energy under contract DE-AC06-76RLO 1830 through subcontract with Pacific Norwest Laboratory.

REFERENCES

1 J. Wang, Stripping Analysis: Principle, Instrumentation and Applications, VCH, Deerfield Beach, FL, 1985.
2 T. Copeland and R. Skogerboe, Anal. Chem., 46 (1974) 1257A.
3 G.E. Bately, Marine Chem., 12 (1983) 107.
4 F. Vydra, K. Stulik and E. Julakova, Electrochemical Stripping Analysis, Wiley, New York, 1976.
5 A. Ciszewski and Z. Lukaszewski, Talanta, 32 (1985) 1101.
6 J. Bonelli, H. Taylor and R. Skogerboe, Anal. Chim. Acta, 118 (1980) 243.
7 Z. Lukaszewski, M. Pawlak and A. Ciszewski, Talanta, 27 (1980) 181.
8 A. Ciszewski, Talanta, 32 (1985) 1051.
9 R. Kalvoda and M. Kopanica, Pure Appl. Chem., 61 (1989) 97.
10 J. Wang, in A.J. Bard (Ed.), Electroanalytical Chemistry, Dekker, New York, 1989, p. 1.
11 C.M.G. van den Berg, Anal. Chim. Acta, 250 (1991) 265.
12 C.M.G. van den Berg, Anal. Chim. Acta, 164 (1984) 195.
13 J. Wang, J. Lu and C. Yarnitzky, Anal. Chim. Acta, 280 (1993) 61.
14 J. Wang and J. Zadeii, Talanta, 34 (1987) 909.
15 J. Wang, P. Farias and J. Mahmoud, Anal. Chim. Acta, 171 (1985) 215.

Analytica Chimica Acta, 282 (1993) 335–343
Elsevier Science Publishers B.V., Amsterdam

Chemically and mechanically resistant carbon dioxide optrode based on a covalently immobilized pH indicator

Bernhard H. Weigl and Andrej Holobar

Joanneum Research, Institutes for Optical Sensors and Sensor Interfaces, Steyrergasse 17, A-8010 Graz; and Karl Franzens University Graz, Institute of Organic Chemistry, Analytical Division, Heinrich-Str. 28, A-8010 Graz (Austria)

Nena V. Rodriguez and Otto S. Wolfbeis

Karl Franzens University Graz, Institute of Organic Chemistry, Analytical Division, Heinrich-Str. 28, A-8010 Graz (Austria)

(Received 5th February 1993; revised manuscript received 12th May 1993)

Abstract

An optical chemical sensor for dissolved carbon dioxide has been developed whose dynamic range was adjusted to CO_2 partial pressures ranging from 0 to 100 hPa. The change in the pH of a buffer layer, caused by diffusion of carbon dioxide through a hydrophobic membrane, is indicated by the colour change of a covalently immobilized dye, and monitored through optical fibers. The sensor also incorporates an optical insulation with a resplendent pigment to increase the reflectivity and to reduce adverse effects of straylight and ambient light. Two methods for layer manufacturing (spreading and spin coating) are described. The sensor membrane is fully LED compatible. The optrode shows a promising performance with respect to chemical and mechanical long term stability, reproducibility, and sterilizability.

Keywords: Sensors; Carbon dioxide optrode

On-line detection of carbon dioxide in industrial process control (i.e., in the beverage industry and in bioreactor monitoring) is still not solved properly. A popular method for measuring CO_2 in the gas phase is infrared absorptiometry at one or more wavelengths [1,2]. However, when used for determining CO_2 partial pressures in liquids [3], many interferents are known to compromise accuracy. Besides, the application of IR monitors in industrial CO_2 monitoring is limited by their price and the lack of mechanical stability.

Correspondence to: O.S. Wolfbeis, Karl Franzens University Graz, Institute of Organic Chemistry, Analytical Division, Heinrich-Str. 28, A-8010 Graz (Austria)

Another often used sensor is the Severinghaus type CO_2 electrode. It is based on the pH change in an aqueous buffer solution induced by the diffusion of CO_2 through a hydrophobic polymer membrane. The pH change is monitored, in principle, by a glass electrode [4]. This sensing scheme has been utilized to design optical chemical sensors [5–7]. In this case, a pH shift causes a change in absorption or fluorescence intensity of a pH indicator dye embedded in a buffer layer. Additionally, the sensitive layer is coated with a hydrophobic membrane in order to prevent proton and ion diffusion. Therefore, only gaseous CO_2 (and other gases) can permeate into the aqueous buffer layer. This simplifies the chemical environ-

ment of the pH indicator and therefore makes possible, in certain cases, to obtain linearizable response functions [8]. The light intensity change can be measured by photodiodes, either directly or through optical fibers.

A recent approach to carbon dioxide sensing involves the use of ion pairs consisting of a pH indicator anion and an organic quaternary ammonium cation [9,10]. These sensors show a very promising behaviour in many respects. Their response times are extremely low in that t_{90} (time to 90% response) can be as low as 200 ms in case of gas phase measurements. They show, in principle, no cross sensitivity to changes in the osmotic pressure of the sample solutions, known to be a problem with all buffer-based CO_2 optrodes and electrodes [11]. However, this type of sensor suffers presently from a limited long-term stability in solutions (a few days) and an irreversible loss in sensitivity when exposed to an environment containing acidic vapours.

The application of optrodes in industrial online monitoring of liquid samples requires sensors to have good chemical and mechanical long-term stability, and high reproducibility. Relatively long response times ($t_{90} \leqslant 5$ min) and limited resolution, in contrast, are tolerable in many cases.

Numerous types of pH indicator dyes have already been used as an optical interface for CO_2 sensing [2]. Vurek et al. designed an absorption based CO_2 sensor utilising phenol red as an indicator [12]. In this paper, we describe the use of a new type of optical pH sensors as a basis for a CO_2 sensor. The pH-sensitive membrane comprises a pH indicator dye which is covalently immobilized on a polymeric support. A thorough characterization of the pH sensor has been given. It lends itself to mass manufacturing [13–15]. This membrane, when treated with appropriate buffer solutions and coated with a hydrophobic polymer provides an excellent CO_2 sensor, as will be shown below.

EXPERIMENTAL

Sensor membranes

A plotter foil (Hewlett Packard 17703T; Hewlett Packard, Vienna) was treated with acetone on one side for a few minutes until a thin layer (a cellulose triacetate membrane) started to peel off. This layer was then removed with triacetate membrane) started to peel off. This layer was then removed with tweezers and the foil was dried at room temperature. The other side of the foil (still coated with the cellulose triacetate) served as a basis for the immobilization of the dye [13].

0.1 g of the dye N9 (Merck, Darmstadt) was finely dispersed in 1.0 g concentrated sulfuric acid and kept in dry atmosphere for 30 min. The mixture was dissolved in 1 l of deionized water and neutralized with 1.8 ml of 32% NaOH (the solution turns from yellow to green). The pretreated plotter foils were placed in this solution for 30 min, during which 25 g of sodium carbonate and another 5.2 ml of 32% NaOH were added. The foils were washed with deionized water until the solution turned to neutral pH. The membranes were dried at room temperature. The resulting pH-sensitive foil is fully transparent and changes its color from yellow to blue as the pH of the sample increases from 5 to 9. It can be stored at room temperature for more than a year without any loss in performance. The average concentration of the dye on the foil is 0.3 mg dye/cm^2. The pK value of the immobilized dye in 0.1 M phosphate buffer is 7.6 at 21°C.

The pH sensitive foils were soaked for 30 min in the respective buffer solutions (see Table 1). All buffer components were of analytical purity

TABLE 1

Sensor material composition for the investigation of the effects of pH and concentration of the internal buffer (hydrogencarbonate/phosphate; pH adjusted with NaOH); coating: a 50-μm layer of GE R43117 without reflective pigment

Sensor	pH	Buffer conc. (mM)
A1	8.0	25
A2	8.5	25
A3	9.0	25
A4	9.5	25
A5	10.0	25
A6	8.5	20
A7	8.5	22
A8	8.5	25
A9	8.5	30

TABLE 2

Sensor material composition for the investigation of the influence of the pigment on the reflectivity of the sensor membrane; buffer and hydrophobic coating as in Table 2

Sensor	pH	Buffer conc. (mM)	Reflective pigment
B1	9.0	25	TiO_2
B2	9.0	25	Perlglanz
B3	9.0	25	Reichbleich-Gold
B4	9.0	25	Aluminium bronze
B5	9.0	25	Altgold
B6	9.0	25	Copper bronze

(Merck). The wet membrane was wiped with a clean-room towel to avoid irregular drying that would cause a spotted surface of the sensor. After drying for 1 h at room temperature in air, the membrane showed the blueish tint of the deprotonated form of the indicator dye due to the slightly basic buffer solutions. It was then ready for the coating procedure using a silicone copolymer (General Electrics, product number GE R4-3117, obtained from TEWEBE, Vienna). Both spin coating and spreading methods were tested.

Spreading

A 40 × 80 mm piece of the soaked membrane was placed on a metal surface with slots on each side which were connected to the vacuum line of a water jet pump so to fix the membrane on the metal plate. About 1 g of the silicone copolymer, optionally mixed with 0.1 g of pigment (see Table 2), was placed on one end of the membrane. A shim was drawn over two guidings on each side of the membrane to spread the polymer constantly over the whole membrane. The height of the guidings was adjustable by using spacer foils of different thickness in order to obtain membranes with thicknesses ranging from 10 to 100 μm (before curing and solvent evaporation) with an accuracy of ± 2 μm.

Spin coating

We used a centrifuge (custom-made by Vianova, Graz) for spin coating of the soaked and dried membranes. It comprised a rotor with a light beam controlled variable rotational speed ranging from 0 to 650 ± 2 rpm. The membranes (50 × 50 mm) were glued on a metal holder with double sided adhesive tape. About 3 g of the silicone copolymer, optionally mixed with 0.3 g pigment (see Table 2), was dispersed on the membrane so that it was totally coated. After 2 min of rotation at 600 rpm, the membranes were removed. Titanium dioxide (p.a.) was obtained from Aldrich (Steinheim). The other pigments were technical products. Perlglanz, a mineralic glimmer pigment, was obtained from Bicolor (Villingen), the other pigments were metallic particles (Table 2) from Blitz (Linz).

After curing the membranes in a drying chamber at 60°C for 6 h, they were placed in the same buffer that was used for soaking before coating. The membranes were stored in this solution until being used, at least for one day. Before use, the membranes were wiped dry with a clean room towel and were then inserted in a flow through cell.

Experimental arrangement

The flow-through cells [12] were made of V4A steel. They consisted of a head with steel tubing connectors, O-rings, the sensor membrane and an optical fiber plug comprising three plastic optical fibers (PMMA fibers, diameter 1 mm, length 1 m, type OKE 110/125, obtained from Hirschmann, Vienna). One of the fibers was connected to a yellow LED (λ_{max} 565 nm). For the test and calibration runs, the second fiber was connected to a Hewlett Packard 8153A light wave multimeter, which monitored the changes in the reflected light due to pH induced color changes in the membrane. The third fiber was not used. In case of sensor membranes which did not contain reflective pigments in the hydrophobic coatings (membranes A1 to A9, Table 1), the back of the flow cell (instead of the reflective coating) reflected most of the light back into the optical fibers. However, since the reflective coating does not optically isolate the sensor completely from the solution, there is always a certain amount of light reflected on the cell back and walls.

Measurements

All sensor membranes were investigated with the PC-controlled gas and liquid flow measurement system Flowlab [15]. It comprised six thermostatic gas equilibration chambers, in which six different, well defined gas mixtures were bubbled through buffer solutions or destilled water. The solutions were connected to a motor valve and pumped over the sensor membranes in the flow through cell by a peristaltic pump. Data acquisition and controlling was provided by a Keithley 575 measurement and control system which itself was controlled by the PC. All measurements were performed at room temperature (25°C) under atmospheric pressure. Calibration graphs were recorded in five tonometered 0.1 M phosphate buffers of pH 7.0. The reflectivity of the hydrophobic coating mixtures was investigated for the "B"-type sensors (Table 2). For this purpose, the response of each membrane was measured in 0.1 M buffer solutions of pH 7.0, tonometered (gas-equilibrated) with nitrogen.

RESULTS AND DISCUSSION

The pH-sensitive material is a yellow, fully transparent plastic foil without any structures or inhomogeneities [13]. The support is composed of two layers: a Mylar support, onto which a cellulose triacetate layer is glued. The dye is covalently immobilized on the cellulose and homogeneously distributed throughout the layer. The acetate functions are hydrolyzed by strong alkali during the immobilization, so that the final foil consists of cellulose on polymer.

The pH indicator N9 is a commercially available azo dye of the general chemical structure given in Fig. 1 [15]. The substituents R′, R″, and R‴ determine pK and color of the dye. The immobilization of dyes via vinylsulfonyl groups has been described [15,17]. In essence, a chromophore (Chr) is functionalized by introducing a hydroxyvinylsulfonyl group to give Chr-SO_2-CH_2-CH_2-OH. This is esterfied by treatment with conc. sulfuric acid to give Chr-SO_2-CH_2-CH_2-O-SO_3H which, on addition of sodium carbonate, is converted into Chr-SO_2-CH=CH_2. In strongly alkaline solution, the vinylsulfonyl group reacts with cellulose (Cell-OH) to give the dye/cellulose conjugate Chr-SO_2-CH_2-CH_2-O-Cell (see Fig. 1).

The pK of an indicator dye is known to depend on the ionic strength of its environment, especially at low ionic strength. Another external effect on the thermodynamic pK is due to osmotic pressure differences between internal buffer layer and sample solution. Since the hydrophobic coating of the CO_2 sensors is impermeable to both liquid water and ions but permeable to water vapours, there is a tendency to establish an osmotic equilibrium between internal buffer and sample solution. For example, if the osmotic pressure of the sample is higher than that of the internal buffer layer, water vapour will diffuse out of the layer into the sample, altering the ionic strength of the internal buffer solution and, consequently, the pK of the dye.

Since diffusion of ions in cellulose (the immobilization matrix for the pH indicator) is relatively slow, it is important to soak the pH sensitive membranes for quite a time (1 h) in the respective buffer solution. For buffers of very low ionic strength, 3 h of soaking time is recommended.

The wiping of the soaked foils is a manufacturing step whose reproducibility is not yet solved

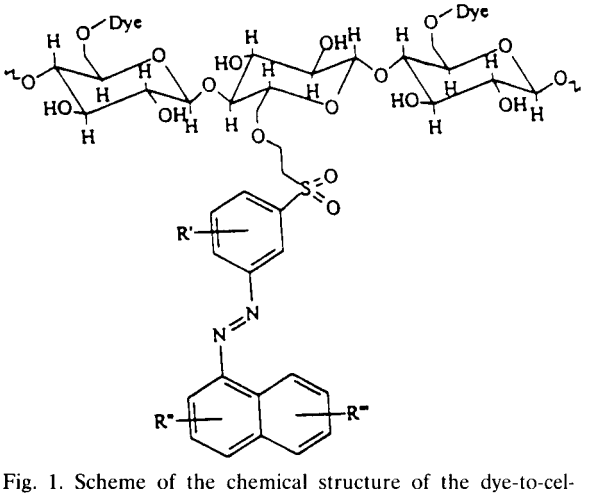

Fig. 1. Scheme of the chemical structure of the dye-to-cellulose conjugate [15]. The azo dye is immobilized covalently on cellulose via a vinyl sulfonyl group. One of the substituents R is a hydroxyl group which, upon dissociation, causes the color change to occur.

properly. It is difficult to remove the total amount of liquid from the surface of the foil at once without scratching the sensor. If droplets of buffer solution remain on the surface, the concentration of buffer and therefore the ionic strength in these droplets increases. Since the pK of the dye depends on the ionic strength of the buffer, this leads to a lower dye^-/H^+dye^- ratio and therefore to darker spots. However, the addition of a few drops of a neutral detergent to 1 l of buffer solution prevented the formation of droplets on the surface and did not seem to influence the performance of the sensor. Drying of the membrane at 60°C for 1 h did not affect dye and polymer.

Reproducible spreading of the hydrophobic coating onto the pH sensor in constant thickness is important with respect to response time, cross-sensitivity to pH and ions, and mechanical stability. The silicone copolymer contains about 50% (w/w) of toluene which evaporates during the drying process. Therefore the layers tend to shrink, depending on the drying temperature. Both moisture (which catalyzes the curing process) and temperature have to be kept constant during layer manufacturing in order to obtain reproducible results.

By both spreading and spin coating, a thickness reproducibility of ± 5 μm was obtained. Figure 2 shows a scanning electron microscope photograph of the surface of a silicone membrane obtained by spreading and containing reflective glimmer crystals (Bicolor Perlglanz) with a thickness of roughly 0.5 μm and a typical diameter of 20 μm. It was found that with spin coating, almost all pigment crystals are covered with polymer, whereas spreading leads to less homogenous surfaces. The particles in the layer often cause scratches on the surface. This, in turn, leads to cross-sensitivity towards pH and ions. Therefore, care has to be taken that the thickness of the layer before curing is larger than the diameter of the largest particle (e.g. > 40 μm). Then, both spreading and spin coating are applicable. However, for the measurements described in the following, all silicone membranes were applied by spreading.

The dynamic range as well as the response time of optical CO_2 sensors of this type is affected by both the pH and the capacity of the

Fig. 2. Electron microscopic photograph of a hydrophobic layer containing pigments and spread onto the pH-sensitive layer. The surface is less homogenous than that obtained by spin coating.

buffer layer. It has been reported that a pH of the buffer solution of typically 1–1.5 above the pK of the indicator dye is most suitable [7,9]. One crucial point is to choose an appropriate buffer so that analytical CO_2 partial pressures vary the pH of the buffer layer such that it remains within the dynamic range of the pH indicator dye. Different pH values and buffer concentrations have been tested.

The second critical point is the hydrophobic coating. The optimal coating is supposed to have a high permeability to CO_2 in order to provide short response and recovery times, not to be permeable for charged species (especially H^+), and not be subject to swelling or turbidification due to moisture. Besides that, such sensor coatings are expected to be chemically and mechanically stable, sterilizable, and to have a good adhesion to the support material. Silicones are known to display high permeability for CO_2. However, most silicones have a shore hardness lower than 30 and therefore are easily scratched, either by hard particles in the sample or when inserted into the cell. Since we focus on sensors for industrial long-term monitoring, a silicone copolymer with a shore hardness of 90, but with a lower permeability was chosen.

Light from an LED is conveyed through optical fibers to the membrane and the reflected light is measured through optical fibers by a photodiode. Thus, a highly reflective coating is preferred. It was found that certain mineral pigments greatly enhance the reflectivity and also reduce the adverse effect of ambient light on the signal. Different types of pigments were investigated.

The "A" sensors were investigated to optimize buffer concentration and pH of the aqueous buffer layer for a given CO_2 partial pressure range. Sensor membranes A1 to A5 have internal buffers of different pH, but at an (almost) constant ionic strength. In Fig. 3, calibration graphs for these sensors are compared. The reflected light intensity decreases with increasing pH of the buffer layer at a fixed CO_2 partial pressure. It can also be seen that the sensors with a higher internal pH show a more constant CO_2 sensitivity over the range from 0 to 80 hPa, whereas the sensors with a lower pH are highly sensitive to low CO_2 levels. The reason for this is that the titration curve of the pH indicator is steep in the pH 6 to 8.5 range and becomes increasingly flat outside this range. Figure 4 shows the normalized

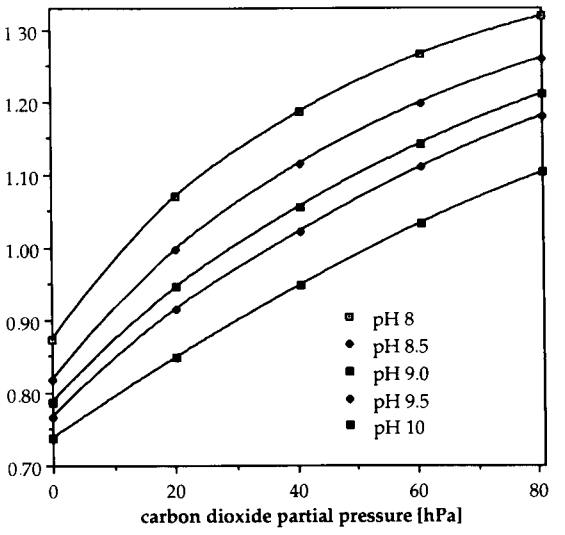

Fig. 3. Comparison of calibration graphs for CO_2 in 0.1 M phosphate buffer solutions of pH 7 obtained from sensors with internal buffers layer with internal buffers of different pHs (buffer concentration 25 mM).

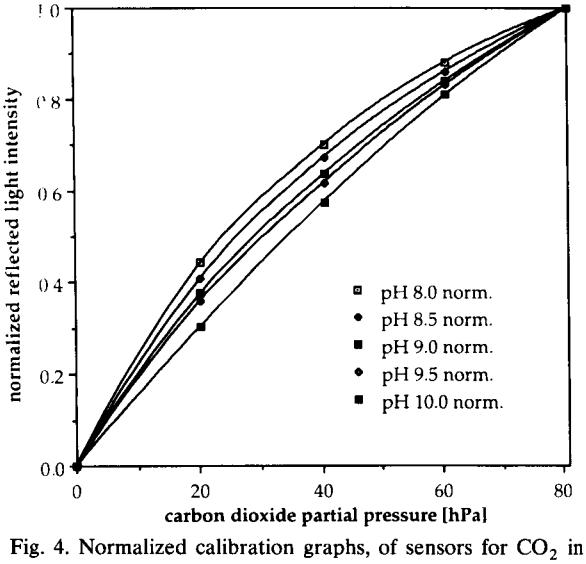

Fig. 4. Normalized calibration graphs, of sensors for CO_2 in 0.1 M phosphate buffer solutions of pH 7 with an 25 mM internal buffer, adjusted to different pHs. The membranes with a lower internal pH show a higher sensitivity to CO_2.

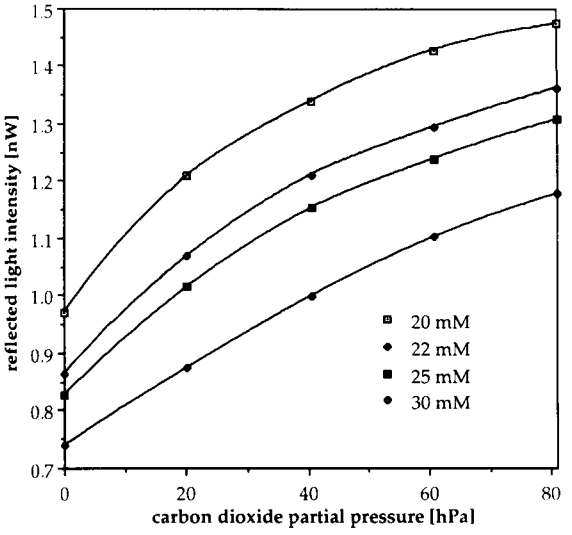

Fig. 5. Comparison of calibration graphs for CO_2 in 0.1 M phosphate buffer solutions of pH 7 obtained from sensors with internal buffers of different buffer capacity (pH 8.5).

calibration graphs of sensors A1 to A5, where the latter effect can be seen more clearly.

Figures 5 and 6 show calibration graphs and normalized calibration graphs of sensors A6 to A9. A similar effect of the pH and capacity of the internal buffer was found. The pH of the buffer layer of these sensors was adjusted to 8.5, and the buffer capacity varied by changing the concentration of the internal buffer components. In this case, the intensity of the reflected light decreases (at a given CO_2 partial pressure) with increasing ionic strength, because the latter lowers the pK of the indicator. Sensors with low buffer concentrations are more sensitive in the lower CO_2 concentration range (Fig. 6). There are several reasons for this effect. High buffer concentrations cause an increase in the buffer capacity of the buffer layer, a fact that reduces the relative signal change due to a certain CO_2 partial pressure. Another reason is due to the lowering of the pK of the dye owing to the increasing buffer concentration. As a result, the sensor now works in the flatter part of the pH calibration.

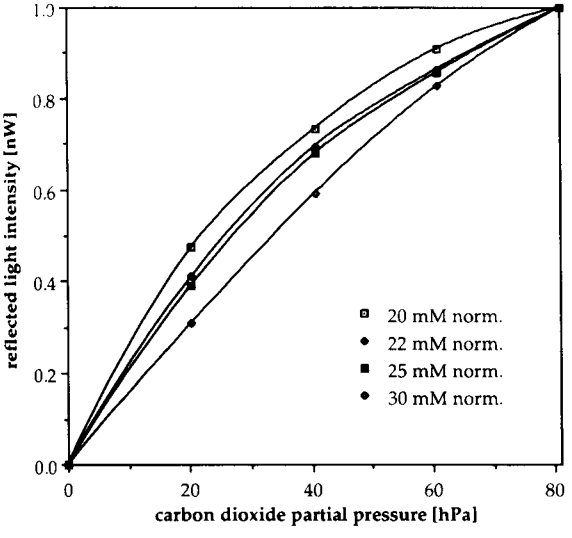

Fig. 6. Normalized calibration graphs for CO_2 in 0.1 M phosphate buffer solutions of pH 7 of membranes with different buffer concentrations at a constant pH.

The "B" sensors were investigated with respect to the reflectivity of their coatings at 0 hPa CO_2. The coatings were mixed with different pigments in order to increase the reflectivity. The intensities of reflected light of these coatings are summarized in Table 3. A glimmer pigment (Bicolor Perlglanz), comprising flat crystals, typically 0.5 μm thick and 20 μm in diameter, is a most suitable material. Figure 7 shows a comparison of calibration graphs obtained with A2 sensors with and without the addition of a reflective pigment to the hydrophobic coating. It can be seen that both absolute signal and relative signal change are enhanced by the addition of reflective pigment. This, fortunately, has no significant effect on the response time, sensitivity, and chemical and mechanical stability.

TABLE 3

Optical damping of sensor membranes with different reflective pigments.

Sensor	Reflective pigment	Optical damping (dB)
B1	Bicolor Perlglanz	3.3
B2	Blitz Reichbleichgold	3.6
B3	Blitz aluminium bronze	3.8
B4	Blitz copper bronze	4.3
B5	Blitz Altgold	5.1
A3	no pigment	6.6
B6	TiO_2 p.a.	7.8

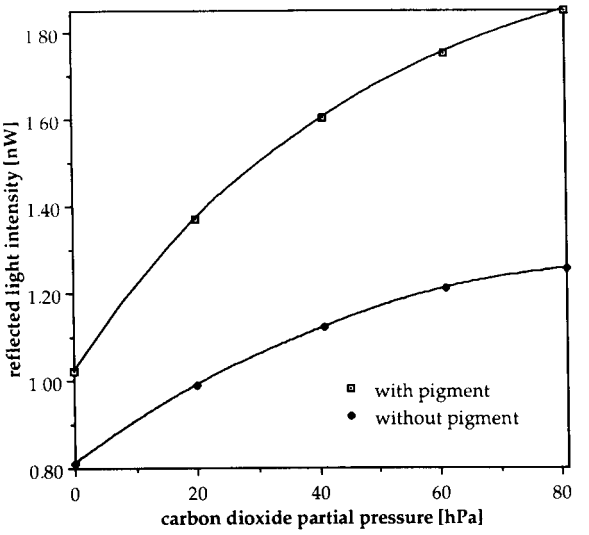

Fig. 7. Comparison of the optical signal obtained with CO_2 optrodes with and without reflective pigments in the silicone coating. Both the absolute and the relative signal change are enhanced by addition of reflective pigments.

The long-term stability of the A2-type sensor was tested in 0.1 M phosphate buffers of pH 7 for more than 6 h of continuous flow. The response curve of this measurement is depicted in Fig. 8. The response times (t_{90}) were in the order of 2–5 min. Reflected light intensity signals and standard deviations are compiled in Table 4. Under these conditions, the accuracy over the 0–1000 Pa range was found to be in the order of ±20 Pa. A

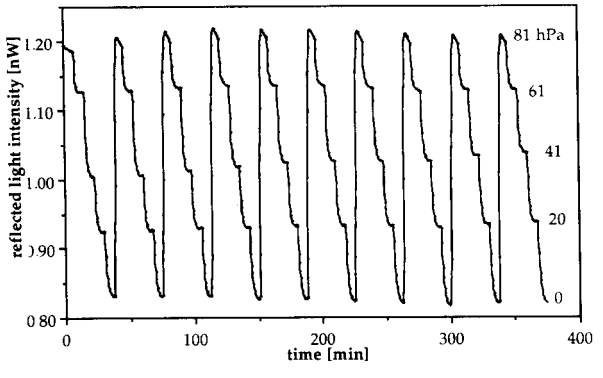

Fig. 8. Response curve of a carbon dioxide sensor in 0.1 M buffers of pH 7.0, tonometered with gas mixtures of varying CO_2 concentrations at atmospheric pressure. The solutions were alternately pumped over the sensor over a period of 6 h.

TABLE 4

Medium reflected light intensities and standard deviations of a long term measurement (see Fig. 9)

CO_2 (Pa)	Medium reflected light intensities (nW)	Standard deviation [a]
0	0.824	0.005
810	0.931	0.004
610	1.021	0.011
410	1.131	0.003
200	1.210	0.007

[a] $n = 10$.

drift to lower signals, caused by equilibration of the internal and external buffer concentration due to the osmotic pressure differences, can be observed. After equilibration (roughly 1 day) in the sample medium, no drift occurs as long as the osmotic pressure of the sample is constant. To minimize the drift, the ion concentration in the internal buffer layer can be adjusted by addition of NaCl so that it matches the ionic strength of the sample solution. It was found that addition of 0.08 mol l^{-1} NaCl to the soaking solution for the "A" type sensors significantly reduces the drift. The addition of NaCl did not change the buffer capacity and therefore the sensitivity of the sensors.

The cross-sensitivity to pH was tested by pumping 0.1 M buffer solutions of pH 5 and pH 11 consecutively over an A2 membrane. The sample buffers were tonometered with nitrogen. As can be seen from Fig. 9, no signal change occurred. Sterilizability was tested by recording a

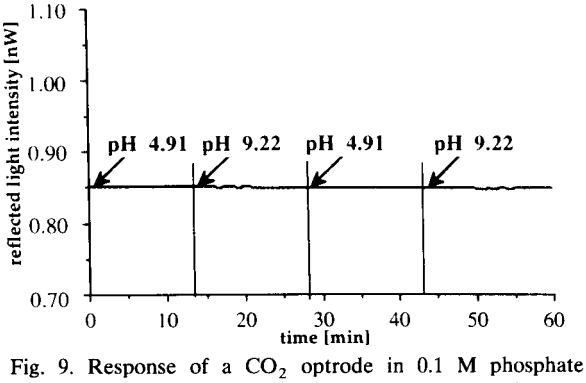

Fig. 9. Response of a CO_2 optrode in 0.1 M phosphate buffers of pH 4.91 and 9.22, both tonometered with nitrogen, showing that the sensor has no cross sensitivity to pH.

calibration graph before and after placing the sensor in a 6% hydrogen peroxide solution at room temperature for 1 h. No sensor degradation was found. The sensor also showed no deterioration within 2 h of storage in 1 M HCl, 0.1 M NaOH or 70% ethanol. Even storage in buffer solutions of pH 7 for half a year had no effect on the slope and the relative signal change of the calibration graph of the sensors.

Conclusions

The carbon dioxide sensor presented here shows an overall performance comparable to available process monitoring electrodes. The chemical and mechanical stability as well as reproducibility and long-term stability are satisfactory. Under certain conditions, the stability of the membrane allows cleaning and sterilization in process, what was not possible with carbon dioxide optrodes before. Given the ease of manufacturing as well as of handling, the sensor offers favourable properties in applications where extremely high resolution and response times are not required.

The use of reflective pigments acting both as an optical isolator and a signal enhancer seems not to be limited to the application in carbon dioxide sensors, but would be useful in many types of optrodes. It can increase the intensity of reflected light by as much as 50%.

We would like to thank Dr. W. Trettnak for helpful discussions and valuable hints. We are also obliged to H. Kraus for performing some of the measurements. The electron microscopic photograph was taken at the Center for Electron Microscopy, Austrian Academy of Sciences, Graz. Spin coating of the sensor membranes was done at the Vianova paint laboratory, Graz. Part of this work was supported by the Austrian National Science Foundation (project 5701-PHY). Other parts of the work were carried out within projects in cooperation with A. Paar KG, Graz and the ESTEC (European Space Research and Technology Center), Noordwijk, Netherlands. B.H.W. gratefully acknowledges a grant from Joanneum Research, Graz.

REFERENCES

1 J. Dakin and B. Culshaw (Eds.), Optical Fibre Sensors, Artech House, Boston, London, 1988.
2 O.S. Wolfbeis (Ed.), Fiber Optical Chemical Sensors and Biosensors, Vols. 1 and 2, CRC Press, Boca Raton, FL 1991.
3 P.A. Wilks, MBAA Technical Quarterly, 25 (1988) 113.
4 J.W. Severinghaus and A.F.J. Bradley, Appl. Physiol., 13 (1958) 515.
5 D.W. Lübbers and N. Opitz, Z. Naturforsch., Part C, 30C (1975) 532.
6 O.S. Wolfbeis, L. Weis, M.J.P. Leiner and W.E. Ziegler, Anal. Chem., 60 (1988) 2028.
7 Z. Zhujun and W.R. Seitz, Anal. Chim. Acta, 160 (1984) 305.
8 M.E. Lopez, Anal. Chem., 56 (1984) 2360.
9 A. Mills, Q. Chang and N. McMurray, Anal. Chem., 64 (1992) 1383.
10 D.B. Raemer, D.R. Walt and C. Munkholm, US Pat. 5,005,572 (1991).
11 M.A. Jensen and G.A. Rechnitz, J. Am. Chem. Soc., 51 (1979) 1972.
12 G.G. Vurek, J.I. Peterson, S.R. Goldstein and J.W. Severinghaus, Fed. Proc., Fed. Am. Soc. Exp. Biol., 41 (1982) 1484.
13 A. Holobar, B.H. Weigl, W. Trettnak, R. Benes, H. Lehmann, N.V. Rodriguez, A. Wollschlager, P. O'Leary, P. Raspor and O.S. Wolfbeis, Sensors Actuators, B11 (1993) 425.
14 B.H. Weigl, A. Holobar, W. Trettnak, I. Klimant, H. Kraus, P. O'Leary and O.S. Wolfbeis, J. Biotechnol., (1993) in press.
15 T. Werner and O.S. Wolfbeis, Fresenius' J. Anal. Chem., 346 (1993) 564.
16 B.H. Weigl, Proc. SPIE, 587 (1991) 288.
17 J. Heyna, Angew. Chem., 24 (1962) 966.

Analytica Chimica Acta, 282 (1993) 345–352
Elsevier Science Publishers B.V., Amsterdam

Potentiometric phosphate selective electrode based on a multidendate–tin(IV) carrier

Nikolas A. Chaniotakis

Department of Chemistry, University of Crete, Irakleon, Crete 71409 (Greece)

Klaus Jurkschat and Andreas Rühlemann

Fachbereich Chemie, Martin Luther Universität, 06099 Halle / S. (Germany)

(Received 5 th March 1993; revised manuscript received 5th May 1993)

Abstract

The incorporation of tris(3-chlorodimethylstannyl-propyl) chlorostannane (carrier 1), a novel tin(IV) based carrier, into a liquid polymeric membrane and its potentiometric properties are examined. Membranes doped with 2 wt% of this carrier are shown to display the highest selectivity for phosphate over many anions reported so far, including that of perchlorate. Its response time is in the order of seconds, while its detection limit is 1×10^{-5} M. The ability for a multidentate coordination between the carrier and the phosphate anion is postulated to be the reason for the response, while the observed high selectivity is proposed to be due to the higher tendency for bond formation between the phosphate oxygens and the tin(IV) metal centers. On the other hand the lifetime of the electrode is short, due probably to the hydrolysis of the carrier in the membrane phase.

Keywords: Potentiometry; Multidentate–tin(IV) carrier; Phosphate selective electrode; Tin

Phosphate containing products are used extensively in many areas of human activities such as in detergents and fertilizers. The use of these phosphate based materials has taken its toll on the environment as large quantities continuously find their way into lakes and rivers, contributing to a large extent in the eutrofication of these water reservoirs [1]. At the same time phosphate containing species leach into underground water reservoirs making it unsafe for human consumption. The need for an analytical procedure for the monitoring and routine analysis of phosphate in all aqueous environments is thus necessary. The lack of a technique for the continuous on-line monitoring of phosphate mandates that its measurement being carried out using different wet chemistry procedures, in a discrete sample mode. There are currently a few wet chemistry methods for the determination of phosphate, all of which are based on the colored complex formed between phosphate and molybdenum(IV) [2,3].

This spectrophotometric analysis of phosphate requires the use of sodium molybdate as well as a strong reducing agent. These procedures are not only time consuming, but they also suffer from interferences, generate heavy metal waste products, and operate with discrete samples. An analytical method without the drawbacks of the currently used wet chemical procedures for the detection and monitoring of phosphate is thus urgently needed. Ion selective electrodes (ISEs) not only avoid the problems of the wet chemical

Correspondence to: N.A. Chaniotakis, Department of Chemistry, University of Crete, Irakleon, Crete 71409 (Greece); or to K. Jurkschat, Fachbereich Chemie, Martin Luther Universität, 06099 Halle/S. (Germany).

procedures but they also offer the advantages of low cost of production, ease of fabrication and use, fast response time and the possibility for on-line monitoring. Even though there are a few reports on phosphate ISEs based on carriers such as cerium hydrogen phosphate, [4,5], tin(IV) complexes [6–8], silver phosphate complexes [9–11] as well as enzymatic reactions [12–14], not one of them has been successful in actual phosphate monitoring. The problems of interferences, stability and peculiar pre-treatment procedures has not allowed for their application. For these reasons ISE applications for phosphate sensing have not been as successful as they have been for other anions and cations.

The difficulty in the selective sensing and monitoring of phosphate, a very hydrophilic anionic ligand, has proven to be very difficult mainly due to two reasons: (a) it is difficult to accommodate the large structure of this anion into a cavity of a host molecule, and (b) the four oxygen atoms surrounding the phosphorous atom generate a very hydrophilic sphere which is reflected in the large energy of hydration of the phosphate anion. Those two characteristics of the phosphates bring it to bottom of the Hofmeister selectivity series [15]:

$$ClO_4^- > IO_4^- > SCN^- > I^- > Sal^- > NO_3^- > Br^-$$

$$> Cl^- > NO_2^- > HCO_3^- > SO_4^{2-} > H_2PO_4^-$$

A successful phosphate selective membrane should thus be able not only to reject the lipophilic interfering anions such as perchlorate, iodide etc., but also to have the ability to selectively and reversibly extract the anion into the membrane phase. Only under these conditions the desired selectivity for phosphate will be obtained. There are two characteristics of the phosphate anions that can be utilized for the development of a selective phosphate carrier both for ISE application as well as in membrane transport. Those are: (a) the formation of multiple hydrogen bonding between the four oxygen atoms of the phosphate and any surrounding hydrogens [16–18] and (b) the ability of the phosphate oxygen atoms to form stronger metal complexes than those with similar structures such as perchlorate and sulfate [19].

Efforts for the development of a phosphate ISE should thus be based either on extraction via

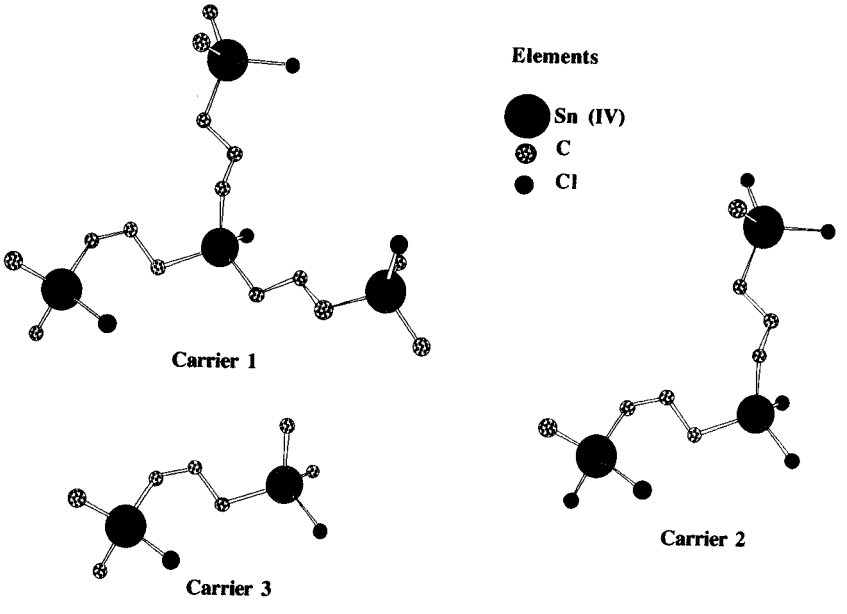

Fig. 1. Cylindrical bond. 3-Dimensional representation of the three carriers used.

hydrogen bonding or on the selective ligand formation of phosphate oxygens with organometallic carriers. It has been shown that tin(IV) containing organometallic compounds can bind to phosphate [6–8], and also to other oxoanions [20]. Our efforts are directed toward the development of a synthetic liquid polymeric membrane based on a selective phosphate carrier that will allow for the potentiometric determination of phosphate in aqueous and other biologically important solutions. We were interested in utilizing the high affinity for coordination of the phosphate oxygens towards Sn(IV). Here we report the results obtained with an ion-selective electrode using a plasticized liquid poly(vinyl chloride) (PVC) based membrane doped with a large Sn(IV)-based carrier. The present article shows that the obtained selectivity of the electrode which is based on the tris(3-chlorodimethylstannyl-propyl)chlorostannane [1] (Fig. 1), has the best selectivity towards phosphate over perchlorate, iodide, thiocyanate, and other lipophilic anions reported so far. The obtained selectivity, $H_xPO_4 > Sal^- > ClO_4^- > NO_3^- > SO_4^{2-} > Cl^- > Br^- > SCN^- > NO_2^-$ is clearly of the anti-Hofmeister type and could lead to the development of a potentiometric system for the selective determination of phosphate in complex aqueous solutions. The high selectivity of this carrier is probably due, and can be explained only via a selective coordination of the tin centers to the oxygen atoms of the phosphate anion.

EXPERIMENTAL

Apparatus

Potentiometric data were recorded in two fashions: multichannel experiments were performed using a Macintosh computer equipped with a analog/digital input/output board. Electrodes were connected to the computer via a custom built electrode interface module as previously described [21]. Data acquisition was controlled by Lab. Tech. Notebook software (Laboratory Technologies Co., Wilmington, MA). For single channel measurements, the signal from a Cole Palmer Chemcadet pH/mV meter (Cole-Palmer, Chicago, IL) was recorded on a Gow-Mac 70–150 strip-chart recorder. For most studies, potential measurements were obtained relative to a double-junction Ag/AgCl reference electrode (Orion Research No. 900200). The outer filling solution was 10 mM in KCl. Membranes were mounted in Philips electrode bodies (IS-561, Glasblaserei Müller, Zürich). Measurements were made in thermostated double-walled beakers at 25°C. The calibration curves and the comparison studies were performed using the standard addition method with a single addition for the selectivity studies and multiple additions for the calibration curves. The pH measurements were obtained with an Orion Research combination glass electrode (Model 81–02).

Reagents

The carriers 1, 2 and 3 (Fig. 1) were synthesized according to the procedures described herein. MES (4-morpholinoethane sulfonic acid), and HEPPS (4-(2-hydroxyethyl)piperizine-1-propanesulfonic acid) were obtained from Aldrich (Milwaukee, WI). Tetrahyrofuran (THF) was freshly distilled before use. Dioctyl sebacate (DOS) and PVC were purchased from Fluka (Ronkonkoma, NY). All other reagents used were analytical-reagent grade. Deionized, 16 MΩ water was used to prepare all aqueous solutions. Buffer concentrations of 50 mM total ionic strength were used.

Membrane preparations

Potentiometric liquid membranes were prepared using PVC (32 wt%), DOS (66 wt%), and the carrier (2 wt%) with a total weight of 150 mg. The membrane components were dissolved in 3 ml THF, placed in an ultrasonic bath for 5 min, and poured into a glass ring with 1.5 cm id. on a glass plate. The solution was allowed to evaporate overnight in the hood covered with two Kim wipes for controlled evaporation of the THF. After evaporation the membranes were cut with a No. 2 cork cutter, and placed into the electrode bodies for testing. The internal solution was made up of 1.0 mM KH_2PO_4 and 10 mM KCl, while the electrochemical circuit was completed with a double junction Ag/AgCl reference electrode.

After each measurement, the electrode was kept in air or in a 50 mmol/l MES buffer, pH 5.5, solution. Calibration curves were generated by the standard addition of 0.001 and 0.100 M of the appropriate salt prepared in MES buffer of 50 mM.

Membrane treatment and storage

Most of the membranes prepared with the carriers were tested immediately after their placement into the electrode bodies. In order to determine the life time of the membranes, the electrodes were stored in MES buffer solutions with the same ionic strength as that of the test solution, or in buffer solutions containing 1 mM of the salt. The unused portions of the membrane were kept in sealed vials at room temperature for future testing.

Synthesis of tris(3-chlorodimethylstannyl-propyl)chlorostannane (carrier 1)

To a magnetically stirred solution of $Me_3SnCH_2CH_2CH_2MgCl$, prepared from 25 g (0.104 mol) $Me_3SnCH_2CH_2CH_2Cl$ and 2.4 g magnesium in 200 ml diethyl ether, was added a solution of 8.2 g (0.034 mol) $MeSnCl_3$ in 50 ml benzene and 100 ml diethyl ether over a period of 1 h. The reaction mixture was refluxed for 6 h and then hydrolyzed under ice cooling. The organic layer was separated, dried over Na_2SO_4 and filtered. The solvent was removed in vacuo and the residue fractionated under reduced pressure to give 8.9 g (35%) $MeSn(CH_2CH_2CH_2SnMe_3)_3$ (b.p. 150–155°C, 10^{-4} mmHg). $MeSn(CH_2CH_2CH_2SnMe_3)_3$ (3.8 g, 5 mmol) and Me_2SnCl_2 (4.4 g, 20 mmol) were kept for 12 h at 60–70°C. The Me_3SnCl formed was distilled under reduced pressure (0.01 mmHg, bath temperature 70°C) into an ice-cooled trap. The residue was recrystallized from THF–diethylether to yield 3.9 g (93%) carrier 1 as colorless crystals, m.p. 94–95°C.

Analysis found: C, 21.54; H, 4.38; Cl, 17.10%. Calculated $C_{15}H_{36}Cl_4Sn_4$ (833.05): C, 21.63; H, 4.36; Cl, 17.02%. ^1H NMR ($CDCl_3$): $\rho SnCH_3$, 0.66 ppm, $^2J(^{119}Sn-^1H)$ 55 Hz; $\delta SnCH_2$, 1.40 ppm; δCH_2, 2.08 ppm. ^{119}Sn NMR ($CDCl_3$): ρ(a) 137.6 ppm, (b) 162.3 ppm; ^{13}C NMR ($CDCl_3$): ρ(1) 22.2 ppm, $^1J(^{119}Sn-^{13}C)$ 23 Hz; ρ(2) 22.2 ppm, $^2J(^{119}Sn-^{13}C)$ 23 Hz; ρ(3) 23.0 ppm, $^1J(^{119}Sn-^{13}C)$ 386 Hz, $^3J(^{119}Sn-^{13}C)$ 69 Hz; ρ(4) −1.4 ppm, $^1J(^{119}Sn-^{13}C)$ 350 Hz, where the letters (a) and (b) as well as the numbers correspond to atoms as follows:

(a) 1 2 3 (b) 4

$Cl-Sn[CH_2CH_2CH_2Sn(CH_3)_2Cl]_3$

Synthesis of 1,3-bis(chlorodimethylstannyl)propane (carrier 3)

11.3 g (0.1 mol) 1,3-dichloropropane, dissolved in 100 ml diethylether was added dropwise under mechanical stirring to a solution of 0.2 mol Me_3SnNa in 250 ml liquid ammonia at −70°C. The reaction mixture was stirred for 1 h followed by slow evaporation of the ammonia. The residue was filtered off to remove the NaCl followed by evaporation of the solvent. The remaining oil was fractionated twice to give 30.3 g (82%) $Me_3SnCH_2CH_2CH_2SnMe_3$ (b.p. 110–112°C, 10 mmHg). 19.5 g (0.05 mol) $Me_3SnCH_2CH_2CH_2SnMe_3$ and 22 g (0.1 mol) Me_2SnCl_2 were kept for 12 h at 60–70°C. The Me_3SnCl formed was removed under reduced pressure (0.01 mmHg, bath temperature 70°C) into an ice-cooled trap. The residue was recrystallized from diethylether to give 18.1 g (88%) colorless crystals of **2**, m.p. 80–81°C.

Analysis found: C, 20.57; H, 4.40; Cl, 17.20%. Calculated $C_7H_{18}Cl_2Sn_2$ (410.54): C, 20.48; H, 4.42; Cl, 17.27%. ^1H NMR ($CDCl_3$): $\delta SnCH_3$, 0.66 ppm, $^2J(^{119}Sn-^1H)$ 55 Hz; $\delta SnCH_2$, 1.37 ppm $^2J(^{119}Sn-^1H)$ 51 Hz; δCH_2, 2.06 ppm $^3J(^{119}Sn-^1H)$ 69 Hz. ^{119}Sn NMR ($CDCl_3$): δ 161.2 ppm.

Synthesis of bis(dichloromethylstannylpropyl)dichlorostannane (carrier 2)

To a magnetically stirred solution of $Me_3SnCH_2CH_2CH_2MgCl$, prepared from 30 g (0.125 mol) $Me_3SnCH_2CH_2CH_2Cl$ and 5 g (0.125 mol) Mg in 200 ml ether, was added a solution of 12 g (0.055 mol) Me_2SnCl_2 in 50 ml benzene and 50 ml ether over a period of 1 h. The reaction mixture was refluxed for 6 h and then hydrolyzed under ice cooling with aqueous NH_4Cl. The or-

ganic layer was separated, dried over Na_2SO_4 and filtered. The solvent was removed in vacuo and the residue fractionated in vacuo to give 18.3 g (55%) $Me_2Sn(CH_2CH_2CH_2SnMe_3)_2$ (b.p. 124–127°C, 0.05 mmHg). 4.5 g (0.008 mol) $Me_2Sn(CH_2CH_2CH_2SnMe_3)_2$ were dissolved in 50 ml dry acetone. 13 g (0.045 mol) $HgCl_2$ were added in small portions to the magnetically stirred solution. The reaction mixture was then refluxed for 48 h followed by evaporation of the solvent. The MeHgCl formed was removed by sublimation under reduced pressure (0.001 mmHg) into a dry ice cooled trap.

The residue was recrystallized from CH_2Cl_2 in a soxhlet to yield 5g (91%) $Cl_2Sn(CH_2CH_2CH_2SnCl_2Me)_2$ as colorless solid, m.p. 144–145°C.

Analysis found: C, 14.26; H, 2.57%. Calculated $C_8H_{18}Cl_6Sn_3$ (683.08): C, 14.07; H, 2.66%. ^1H NMR ($CDCl_3$): $\delta SnCH_3$, 1.23 ppm, $^2J(^{119}Sn-^1H)$ 66 Hz; $\delta SnCH_2$, 1.92 ppm; δCH_2, 2.37 ppm. ^{119}Sn NMR ($CDCl_3$): δ107.3 ppm (1 Sn); δ 125.8 ppm (2 Sn).

RESULTS AND DISCUSSION

Phosphate sensor based on carrier 1

After the initial tests indicating a response and high selectivity toward phosphate, we were interested in determining the basic characteristics of the electrode such as the membrane composition, the pH effect, the slope and detection limits at different pHs, and the response time.

The concentration of the carrier in the membrane phase did not affect the response of the membrane, as long as this concentration was kept above 1%. Membranes with lower concentration usually showed very little or no response at all to any anions. For the pH response the electrode was compared with a glass pH electrode in NaOH–HCl solutions. Figure 2 illustrates the absolute cell potentials of the carrier 1 based electrode versus the pH of the solution. The effect of the OH^- is minimal in the range between pH 5 and 8. In order to minimize the pH effect on the phosphate response, solutions with pH of 5.5 (MES buffer) were then employed.

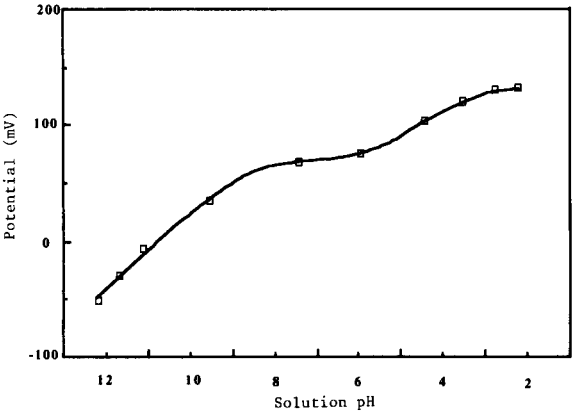

Fig. 2. Typical pH effect on the emf of the carrier 1 based electrode.

Figure 3 shows that at this pH the slope of the electrode is near 40 mV/decade, while the detection limit approaches 10^{-5} M. At a pH of 5.5, the phosphate is in the monobasic form (H_2PO^-) and the electrode slope should be 59.2 mV/decade (Eqn. 1).

$$H_2PO^-_{4(sol)} + carrier_{(mem)} \rightleftarrows (carrier\text{–}H_2PO_4)^-_{(mem)}$$

$$slope_{theor.} = -59.2 \text{ mV, } 25°C \quad (1)$$

Subsequently, and in order to determine the reason for the observed subnernstian slope of the electrode, the dibasic form of the phosphate was examined. This was achieved by using a buffer at pH of 8.5 (HEPPS buffer). Data obtained under

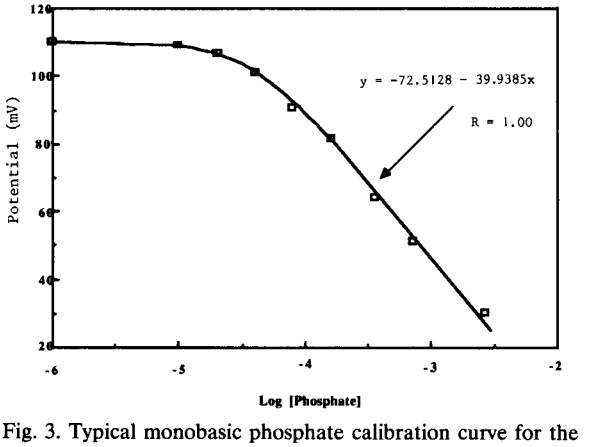

Fig. 3. Typical monobasic phosphate calibration curve for the carrier 1 based liquid membrane electrode in 50 mM MES, pH 5.5.

these conditions agreed with the expected (Eqn. 2), that is a decrease in slope of 30 mV/decade, with a simultaneous increase in the detection limit (data not shown).

$$HPO^{2-}_{4(sol)} + \text{carrier } 1_{(mem)} \rightleftarrows (\text{carrier } 1\text{–}HPO_4)^{2-}_{(mem)}$$

$$\text{slope}_{theor.} = -29.6 \text{ mV}, 25°C \quad (2)$$

While the potentiometric behavior of the electrode at pH 8.5 can be explained theoretically, its low slope at pH 5.5 can not. On the other hand, the tendency of the phosphate anion to form bidentate ligands is also known [22,23]. In the case a bidentate complex between the phosphate ion (in the dibasic or monobasic form) and the carrier can be formed, the lower slope could be justified taking into account that the only ionic species crossing the interface are the $H_2PO_4^-$ and H^+, as follows (Eqn. 3):

$$H_2PO^-_{4(sol)} + \text{carrier } 1_{(mem)} \rightleftarrows$$

$$(\text{carrier } 1\text{–}HPO_4)^{2-}_{(mem)} + H^+_{(sol)}$$

$$\text{slope}_{theor.} = -29.6 \text{ mV} \quad (3)$$

Under these conditions it can be postulated that protons are exchanged between the membrane phase and the aqueous solution when monobasic phosphate ions enter the membrane, leaving a net charge of more than -1 in the membrane phase. In this case the observed lower potentiometric slope can be justified. The ability for the bidentate ligand formation is also supported by the molecular model of the complex.

An other explanation for the observed subnernstian behavior of the above electrodes might be the generated internal diffusion potential. This will indeed be the situation in the case that there is a countertransport of protons during the phosphate extraction [24]. Additionally, the direct exchange between the protons in solution and the membrane which results in the described limited pH sensitivity of the electrode might also complicate the mechanism of response toward the phosphate anion, and thus contribute to the observed potentiometric slopes.

The coordination between carrier 1 and the phosphate is very fast, Fig. 4. The $t_{90\%}$ values (time required to reach 90% of emf change) when

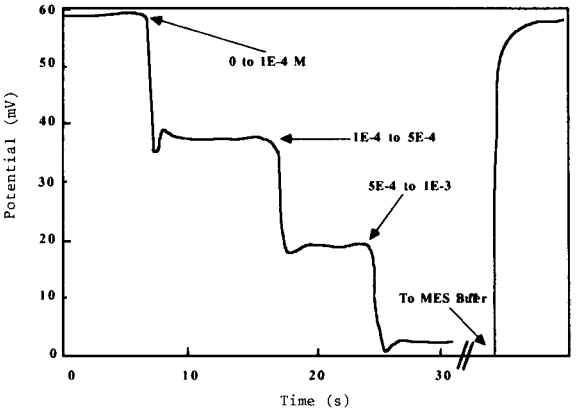

Fig. 4. Typical dynamic response for the carrier 1 based liquid membrane electrode toward standard additions of monobasic phosphate in 50 mM MES.

additions of phosphate were made into the test solution are very short, and in the order of a few seconds. The base line return is also very fast, and it is completed by the time the electrode is washed with water or buffer solution for a few seconds.

The responses in mV of the potentiometric electrode system based on the carrier 1 for a series of common anions was then measured in solutions buffered with MES at pH 5.5. The potentiometric response for a concentration change between 0 and 9.1×10^{-3} M to monobasic phosphate was examined and compared with the same changes in concentration of the potassium salts of iodide, bromide, chloride, nitrite, perchlorate, salicylate, thiocyanate, and acetate, in the same buffer, Table 1. The observed potentiometric response of the carrier 1 towards phosphate is probably based on the oxophilic character of the tin(IV), while the enhanced selectivity towards this anion over perchlorate can be explained based on the difference in the tendency of the two oxoanions to form metal ion complexes [19]. It is well known that the tendency of the perchlorate ion to form complexes with metal ions is much less that of the other oxoions, and decreases in the order of: $PO_4 > SO_4 > ClO_4$. The observed potentiometric selectivity $HPO_4^{2-} > SO_4^{2-} > I^- > Br^- > Cl^- > NO_2^- > ClO_4^- > F^-$ of carrier 1 based membranes correlates very well

TABLE 1

Overall potentiometric response for a carrier 1, 2 and 3 based liquid membrane electrode in 50 mM MES pH 5.5 at 9.1×10^{-3} M anion concentration

Anion	Change in potential (mV)		
	Carrier 1	Carrier 2	Carrier 3
$H_2PO_4^-$	−91	−44	−50
SO_4^-	−25	−38	−30
I^-	−21	−36	−22
Br	−14	−14	−17
Cl^-	−13	−25	−15
NO_3^-	−11	−10	−12
ClO_4^-	−9	−35	−15
Sal	−6	−59	−37
SCN^-	0.0	−45	−20
Acetate	0.0	−5	−7

with the theory of complex formation for the different metal complexes. For a more quantitative treatment of the data the selectivity coefficients for each electrode system should be calculated. From the potentiometric response towards phosphate and to the other anions this is not possible, not only due to the difference in the charge between the ions, but also due to the very small response to some of the anions tested. Instead, the overall potentiometric response of the electrode toward the different anions tested for a change in concentration between 0 and 9.1×10^{-3} M in MES buffer pH 5.5 is given for comparison (Table 1).

In order to examine the possibility of multidentate complex formation between the carrier and the phosphate anion, two other (Fig. 1, carriers 2 and 3) structurally related tin(IV) based compounds were also examined potentiometrically. It is interesting to note that even though the selectivity towards phosphate over other lipophilic anions remained high, the overall response of these sensors was lower than that obtained when carrier 1 was employed (Table 1). These results support the hypothesis of multidentate complex formation between the phosphate anion and the tin based carrier 1.

The most serious problem of the present electrode system is its very short lifetime. Electrodes that were examined after a 24-h immersion in the test electrolyte solution with or without phosphate showed a potentiometric selectivity for anions similar to the unfavourable Hofmeister pattern. The reasons for this short lifetime are currently under investigation.

The high potentiometric selectivity of carrier 1 for phosphate suggests that this molecule could indeed be an efficient carrier for phosphate across other synthetic organic as well as biological membranes. The possibility to apply the carrier 1 as a transport compound for nucleoside phosphates such as ATP and cyclic GMP across different organic membranes is currently under investigation in our laboratories.

Conclusion

The incorporation of the organometallic carrier 1 in a liquid polymeric membrane has shown a profound anti-Hofmeister potentiometric selectivity, with phosphate being the preferred anion. This potentiometric response is believed to be due to the oxophilicity of the tin(IV) centers, while the high selectivity over perchlorate due to higher reactivity of the phosphate oxygens over those of perchlorate. The linear range of response for phosphate is between 10^{-2} and 10^{-5} M, with response times in the order of a few seconds; however the life time of the electrode is very short.

We would like to thank professor Mark Meyerhoff of the Department of Chemistry at the University of Michigan for his assistance in examining some of the electrodes. We would also like to thank Orion Research for the kind donation of the reference and pH electrodes.

REFERENCES

1 H.S. Stoker, S.L. Seager, in J. Bockris (Ed.), Environmental Chemistry, Plenum Press, New York, 1978, Chap. 13.
2 Receuil des Methodes Internationales d'Analyse des Vins, 5th edn., Office International de Vinge et du Vin, Paris, 1978.
3 P. Sundraud and E. Flores. Connaiss. Vigne Vin, 1 (1969) 57.
4 M. Seitz, Dissertation, Frankfurt/Main, 1986.
5 W. Godiker and K. Camman, Anal. Lett., 22 (1989) 1237.

6 S.A. Glazier and M.A. Arnold, Anal. Chem., 63 (1991) 754.
7 V.M. Shkinev, B.Y. Spinakov, G.A. Varobeva and Y.A. Zolotov, Anal. Chim. Acta, 167 (1985) 145.
8 S.A. Glazier and M.A. Arnold, Anal. Chem., 60 (1988) 2540.
9 I. Novozamsky and W.H. Van Riemsdijk, Anal. Chim. Acta, 85 (1976) 41.
10 J. Ruzicka, C.G. Lamm and J. Tjell, Anal. Chim. Acta, 62 (1972) 15.
11 J. Tacussel and J.J. Fombon, in E. Pungor and I. Buzás (Eds.), Ion Selective Electrodes, Conference, Budapest, 1977, Akademiai Kiadó, Budapest, 1978, p. 567.
12 G.C. Guilbault and P.J. Brignac, Anal. Chim. Acta, 56 (1971) 139.
13 M. Nanjo, T.J. Rohm and G.C. Guilbault, Anal. Chim. Acta, 77 (1975) 19.
14 T. Katsu and T. Kayamoto, Anal. Chim. Acta, 265 (1992) 1.
15 F. Hofmeister, Arch. Exp. Pathol. Pharmakol., 24 (1888) 247.
16 H. Futura, M.J. Cyr and J.L. Sessler, J. Am. Chem. Soc., 113 (1991) 6677.
17 H. Luecke and F.A. Quiocho, Nature, 347 (1990) 402.
18 I. Tabushi, Y Kobuke and J. Imuta, J. Am. Chem. Soc., 102 (1980) 1744.
19 B. Douglas, D.H. MacDaniel and J.J. Alexander, Concepts and Models of Inorganic Chemistry, Wiley, New York, 2nd edn., 1983, p. 597.
20 N.A. Chaniotakis, A.M. Chasser, M.E. Meyerhoff and J.T. Groves, Anal. Chem., 60 (1988) 185.
21 M.E. Collison, G.V. Aebli, J. Petty and M.E. Meyerhoff, Anal. Chem. 61 (1989) 2365.
22 B. Anderson, R.M. Milburn, J. MacB. Harrowfield, G.B. Robertson and A. M. Sargeson, J. Am. Chem. Soc., 99 (1977) 2652.
23 F.A. Cotton and G. Wilkinson, Advanced Inorganic Chemistry, Interscience, New York, 1988.
24 W.E. Morf, The Principles of Ion-Selective Electrodes and of Membrane Transport, Studies in Analytical Chemistry, Vol. 2, Akademiai Kiado, Budapest, 1981.

Analytica Chimica Acta, 282 (1993) 353–361
Elsevier Science Publishers B.V., Amsterdam

A mediated amperometric enzyme electrode using tetrathiafulvalene and L-glutamate oxidase for the determination of L-glutamic acid

Nicholas F. Almeida and Ashok K. Mulchandani

Chemical Engineering Department, University of California, Riverside, CA 92521 (USA)

(Received 25th February 1993; revised manuscript received 10th May 1993)

Abstract

A mediated amperometric sensor for measuring L-glutamate is described. The sensor is based on a carbon paste electrode containing the electron transfer mediator tetrathiafulvalene (TTF), and the enzyme L-glutamate oxidase immobilized on the electrode surface. The enzyme is crosslinked with glutaraldehyde and the matrix held on the electrode surface using an electrochemically deposited polymer. TTF is shown to efficiently reoxidize the reduced flavin adenine dinucleotide centers of glutamate oxidase, permitting operation of the sensor at low applied potentials. The electrode, when operated at +0.15 V (vs. Ag/AgCl), responded linearly to L-glutamate concentrations up to 0.8 mM, the lower detection limit being 2.6 μM, with a response time of 2 min. The sensor was used for the determination of L-glutamate in food samples, with excellent correlations achieved when compared to results obtained by enzymatic analysis using glutamate dehydrogenase. The enzyme electrode exhibits excellent reproducibility and stability, retaining more than 90% of its original activity over a period of 3 weeks.

Keywords: Amperometry; Biosensors; Carbon paste; Electropolymerization; Enzyme electrodes; Glutamic acid; Glutamate oxidase; Tetrathiafulvalene

Glutamic acid is contained in many foodstuffs, often serving to enhance the flavor of those foods. The amount of glutamic acid present can therefore be used to evaluate food quality. Glutamic acid production by fermentation has grown rapidly to meet the increased demand, prompting the need for an accurate measurement for on-line monitoring and process control. A quantification of glutamic acid is also useful in the clinical diagnosis of some myocardial and hepatic diseases [1]. There is therefore an increasing necessity for a convenient analytical method for accurate and reliable measurement of glutamic acid.

Correspondence to: A.K. Mulchandani, Chemical Engineering Department, University of California, Riverside, CA 92521 (USA).

Several bioelectrode configurations using immobilized enzymes like glutamate decarboxylase [2], glutamate dehydrogenase [3,4], and glutamine synthetase [5], plant tissue [6], and whole microorganisms [7,8] have been proposed for the detection of glutamic acid, but the methods suffer from a number of drawbacks [9]. The isolation and purification [10] of L-glutamate oxidase (GO), a flavoprotein enzyme with excellent substrate specificity, offered alternative approaches for the measurement of glutamic acid. This enzyme catalyzes the oxidative deamination of L-glutamate to produce ammonia and hydrogen peroxide as follows:

$$\text{L-glutamate} + O_2 + H_2O \xrightarrow{\text{GO}} \alpha\text{-ketoglutarate} + NH_3 + H_2O_2 \quad (1)$$

Enzyme electrodes using this enzyme have been constructed by Yamauchi et al. [11], Wollenberger et al. [9], Yao et al. [12] and Chen et al. [13]. These electrodes are based on monitoring either the amount of oxygen consumed or the amount of hydrogen peroxide formed according to the above reaction. The former is strongly influenced by fluctuations in the dissolved oxygen concentration, whereas the latter approach requires the application of a potential (typically 0.7 V vs. Ag/AgCl), at which interferences from other electroactive species, such as ascorbic and uric acid, in the sample being analyzed may be significant [14].

These problems may be overcome by using a mediated enzyme electrode configuration. The mediator, usually a low molecular weight species, shuttles electrons between the redox center of the enzyme and the working electrode, thereby eliminating the need for dioxygen as the electron acceptor. The reaction scheme can now be represented as follows:

$$\text{L-glutamic acid} + GO_{ox} \rightarrow \alpha\text{-ketoglutarate} + NH_3 + GO_{red} \quad (2)$$

$$GO_{red} + M_{ox} \rightarrow GO_{ox} + M_{red} \quad (3)$$

$$M_{red} \rightleftarrows M_{ox} + e^- \quad (4)$$

where M represents the mediator. By choosing a suitable mediator, which possesses a low overpotential for regeneration at the electrode, the operating potential for the enzyme electrode can be lowered significantly, thereby reducing possible interference from other electroactive species that may be present in the samples being analyzed. A variety of mediators have been employed [15–21] in developing biospecific electrodes for monitoring glucose and some other chemicals, but to date, there has been only a single report [21] of a mediated enzyme electrode, using dimethylferrocene as the mediator, for measuring L-glutamic acid. For the present work, we have used tetrathiafulvalene (TTF) as the mediator, because of its extremely low solubility in aqueous solutions, and the low potential required for regenerating the mediator at the electrode, compared to most of the other mediators that have been used. The low solubility of the mediator permits its immobilization on the electrode surface and serves to enhance the stability of the electrode since the possible decrease in response caused by any depletion of the mediator is reduced. This is of critical importance for the potential use of these devices as implantable probes in clinical applications, or for long-term use for in situ measurements (like fermentation monitoring).

This paper describes the construction and application of an enzyme electrode for the determination of L-glutamic acid in food samples, using the highly specific L-glutamate oxidase, immobilized via crosslinking and electropolymerization on the surface of the electrode, and TTF, immobilized via mixing in the carbon-paste used to form the electrode.

EXPERIMENTAL

Materials

L-Glutamate oxidase (EC. 1.4.3.11, rated activity 24.9 U/mg protein), from *Streptomyces* Sp. X119-6, was purchased from Yamasa Shoyu (Chiba, Japan). Bovine serum albumin, horseradish peroxidase, L-glutamate dehydrogenase (EC 1.4.1.4), β-NADP, NADH peroxidase (EC 1.11.1.1), β-NADH and 4-aminoantipyrine were purchased from Sigma (St. Louis, MO). Graphite powder (Grade #38), L-glutamic acid, phenol, and glutaraldehyde were from Fisher Scientific, and the tetrathiafulvalene, mineral oil (white, light), resorcinol and 1,3-phenylenediamine were purchased from Aldrich (Milwaukee, WI). All other chemicals were of analytical-reagent grade or better. The soya sauce (Kikkoman Foods, Walworth, WI), chicken soup (Borden, Columbus, OH), seasoning (American Home Foods, New York) and party dip (HVR, Oakland, CA) were purchased from a local supermarket.

Electrode construction

The carbon paste was prepared by mixing the appropriate amount of TTF (1 μmol/mg graphite powder) in acetone with graphite powder. After all the acetone had evaporated, mineral oil (20% w/w) was added to the graphite–TTF mixture, which was mixed with a stainless-steel spatula

until a paste with an even consistency was obtained. The paste was packed into the well of a Kel-F electrode holder (Bioanalytical Systems (BAS), W. Lafayette, IN, Part MF2010, inside diameter: 3 mm). The electrodes were polished by rubbing gently on a piece of weighing paper, which produced a flat shiny surface, with an area of approximately 0.07 cm^2. A 0.5 mm deep dent was made in the polished surface, using a machined tool for good reproducibility. This was done to prevent the crosslinking solution dropped on the electrode surface from spreading onto the electrode holder and to reduce the shearing effect of the stirred solution on the film.

Determination of enzymatic activity of glutamate oxidase

The activity of glutamate oxidase was assayed by two different procedures. The first method involved monitoring the rate of oxidation of NADH (at 340 nm) by the H_2O_2 produced in the presence of NADH peroxidase, using a dual beam spectrophotometer (Cary 1E, Varian, Australia). The sample cuvette contained 0.15 mM NADH, 0.54 U NADH peroxidase and 20 mM L-glutamic acid in 50 mM phosphate buffer, pH 7.0 and the enzyme (0.02–0.05 U) in a total volume of 1 ml. For the blank, 50 mM phosphate buffer, pH 7.0 was used instead of glutamic acid. The initial rate of change in absorbance was used to calculate the enzymatic activity. The second method involved monitoring the initial rate of production of the quinoneimine dye produced by the oxidation of phenol in the presence of 4-aminoantipyrine, using horseradish peroxidase as the catalyst. The reaction mixture contained 3 mM phenol, 3 mM 4-aminoantipyrine, 2.5 U horseradish peroxidase and 21 mM L-glutamic acid, in 50 mM phosphate buffer, pH 7, the total volume being 1 ml. For the blank, buffer was used instead of the glutamic acid. The red dye produced has an absorption maximum at 500 nm, with an absorption coefficient of 13000 M^{-1} cm^{-1} [22].

Enzyme immobilization and electropolymerization

L-Glutamate oxidase was immobilized on the surface of the modified carbon paste electrode via crosslinking with glutaraldehyde. Since varying amounts of glutamate oxidase were used, appropriate amounts of bovine serum albumin (BSA) were added to adjust the total protein content to 3% (w/w) as it was observed that higher concentrations of protein resulted in films which exhibited poor adherence to the carbon paste surface. 5 μl of the crosslinking solution (typically containing 2 U (0.0975 mg) of glutamate oxidase and 0.0525 mg BSA in 0.05 M phosphate buffer, pH 7) was dropped on the electrode surface, using a Hamilton syringe, and the crosslinking reaction was allowed to proceed at 20°C for 2 h.

The enzyme-bearing electrode was then used as the working electrode in an electrochemical cell containing a deaerated solution of 1.5 mM each of resorcinol and 1,3-phenylenediamine. The choice of monomers and the conditions of polymerization chosen were based on the results reported by Yacynych and co-workers [23–25], who showed that the electropolymerized film obtained using the above-mentioned monomers offers good protection and stability to the immobilized enzyme and exhibits good permselectivity, helping to reduce possible interferences and electrode fouling. The working electrode potential was cycled between 0.0 V and +0.6 V, at 20 mV/s. A total of 8 successive cycles was used, by which time a polymer film was formed that served to anchor the crosslinked enzyme to the carbon paste electrode. The cyclic voltammogram was recorded on an X–Y recorder. An inert atmosphere was maintained at all times during the electropolymerization, by blanketing the surface of the cell solution using nitrogen.

After the electropolymerization, the enzyme electrode was rinsed using deionized water and soaked in 0.1 M phosphate buffer (NaPB), pH 7, containing 0.1 M glycine for 2 h, to remove any loose enzyme and unreacted glutaraldehyde, and neutralize any residual aldehyde groups that may be present in the crosslinked film.

Enzyme-electrode stabilization

Prior to using the enzyme electrodes for any experiments, the electrodes were stabilized by holding the potential at +0.10 V in an electro-

chemical cell containing 5 mM L-glutamic acid in 0.1 M NaCl–0.1 M NaPB for 10 h. Following this preconditioning, the electrodes were found to give a more stable and reproducible response for long periods of time, with the background current also stabilizing relatively quickly on every use. A similar behavior has been observed for ferrocene-mediated enzyme electrodes used for measuring glucose [15,16].

Electrochemical methods

The cyclic voltammetry and constant potential measurements were performed using a Bioanalytical Systems (BAS) Voltammograph (Model CV 27) along with a low current module (BAS – Model PA1), and an *X–Y–t* chart recorder (BAS – MF8050). All the experiments were carried out in a conventional 3-electrode electrochemical cell (BAS, Model C2 cell stand with a Faraday cage), with a Ag/AgCl reference electrode (BAS – MF2063), and a platinum wire auxiliary electrode (BAS – MF1032). To prevent any competitive oxidation of the reduced glutamate oxidase by dissolved oxygen, all the solutions used for the constant potential measurements were thoroughly deoxygenated by purging with nitrogen for at least 30 min prior to use. An oxygen-free environment was maintained at all times during the measurements by blanketing the surface of the electrochemical cell with nitrogen.

Glutamate determination by spectrophotometric assay using glutamate dehydrogenase

Glutamic acid present in samples of soya sauce, chicken soup, seasoning and a party dip was measured by an enzymatic assay using glutamate dehydrogenase (GlDH) and $NADP^+$, according to the following reaction:

$$\text{L-glutamic acid} + NADP^+ + H \xrightleftharpoons{\text{GlDH}} \alpha\text{-ketoglutarate} + NADPH + NH_4^+ \quad (5)$$

The increase in NADPH, as measured by the change in absorbance at 340 nm, is proportional to the amount of glutamic acid in the cuvette. The chicken soup and the seasoning samples were prepared by dissolving known weights of cubes/powders in 100 ml of 50 mM Tris–HCl buffer of pH 8.5. The mixtures were heated to just boiling, cooled and then filtered through Whatman No. 1 filter paper to remove the fat and other insolubles. The party dip powder was mixed well with 100 ml of 50 mM Tris–HCl buffer and then filtered through Whatman No. 1 filter paper. The soya sauce was used as obtained from the supermarket. The prepared solutions were diluted appropriately using 50 mM Tris–HCl buffer of pH 8.5 and 0.1 ml aliquots added to a cuvette containing 3 mM NADP and 7 U GlDH in a total volume of 1.0 ml.

Glutamate determination by the biosensor

A glutamate oxidase electrode that was stabilized was first calibrated using L-glutamic acid, at a potential of +0.15 V (vs. Ag/AgCl), the electrochemical cell solution containing a deoxygenated solution of 0.1 M NaCl–0.1 M NaPB of pH 7.0. The calibrated electrode was then stabilized (until a constant background current was reached) in a fresh deoxygenated solution of 0.1 M NaCl–0.1 M NaPB of pH 7.0. Known volumes of the sample to be analyzed for glutamic acid content were added to the solution in the cell, and the catalytic current was recorded as a function of time. This procedure was repeated for the different samples tested. The glutamic acid content of the samples was determined from the standard calibration curve. The samples were diluted, if necessary, using 0.1 M NaPB, pH 7.0.

RESULTS AND DISCUSSION

Cyclic voltammetry

Figure 1 shows typical cyclic voltammograms obtained for a carbon paste electrode containing TTF and glutamate oxidase, in the absence and presence of the substrate, glutamate. The presence of glutamate results in a distinct increase in the catalytic (oxidation) current along with a decrease in the reduction current. This is an indication of the efficiency of TTF in serving as an electron transfer mediator between the flavin redox centers of the glutamate oxidase and the carbon paste electrode. Increasing the glutamate

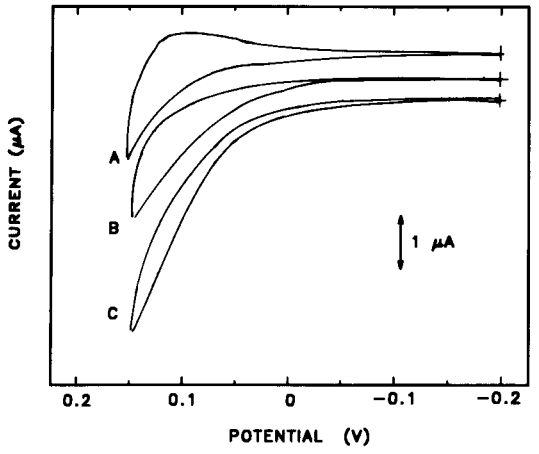

Fig. 1. Cyclic voltammograms at the carbon paste–TTF–glutamate oxidase electrode in 0.1 M phosphate buffer, pH 7. (A) without L-glutamic acid; (B) with 1 mM L-glutamic acid; (C) with 4 mM L-glutamic acid. Scan rate: 1 mV/s; enzyme loading: 2 U.

concentration proportionately increases the catalytic current. The TTF system permits the use of a lower operating potential for the enzyme electrode.

Optimization of parameters

Electrode composition and enzyme immobilization. The composition of the carbon paste, which contained graphite, mineral oil and TTF, was chosen based on some preliminary experiments with a glucose oxidase electrode and on results published by Gunasingham and Tan [17], and Hale et al. [18], who used carbon paste and TTF to prepare enzyme electrodes for measuring glucose and acetylcholine, respectively. They observed that increasing the TTF loading beyond a certain point (10–20% by weight) causes a decrease in the currents because of a decrease in the electrical conductivity of the paste [17]. We used carbon paste modified with approximately 13% (w/w) TTF.

The concentration of protein and glutaraldehyde in the crosslinking mixture for enzyme immobilization was chosen so as to obtain a uniform film that adhered strongly to the carbon paste, permitting the electrodeposition of a copolymer of 1,3-phenylenediamine and resorcinol, which served to anchor and retain the immobilized enzyme on the electrode surface. A total protein concentration of 3% (w/w) and a glutaraldehyde concentration of 2.5% (w/w) resulted in a reproducible and adherent film.

Effect of pH. The soluble glutamate oxidase exhibits a fairly broad optimum, between pH 6.5 and pH 8.5 [10]. The effect of the pH of the solution on the sensitivity of the electrode to glutamate was studied by varying the pH of the phosphate or citrate–phosphate buffer (0.1 M) between 5 and 8. Three different electrodes were used for the measurements to avoid possible "memory effects" caused by successive changes in pH. All the electrodes were first tested at pH 7.0 to check for reproducibility, which was found to be excellent. As seen in Fig. 2 (the data points represent the mean of three measurements, with the error bars indicating the standard deviation), the response of the electrode was found to be the highest at a pH of 7.0. This pH optimum compares well with results reported by others [9,13] using glutamate oxidase. At pH 5, while the electrode is allowed to stabilize, there is apparently a significant loss of TTF from the electrode surface, probably because of an increased solubility

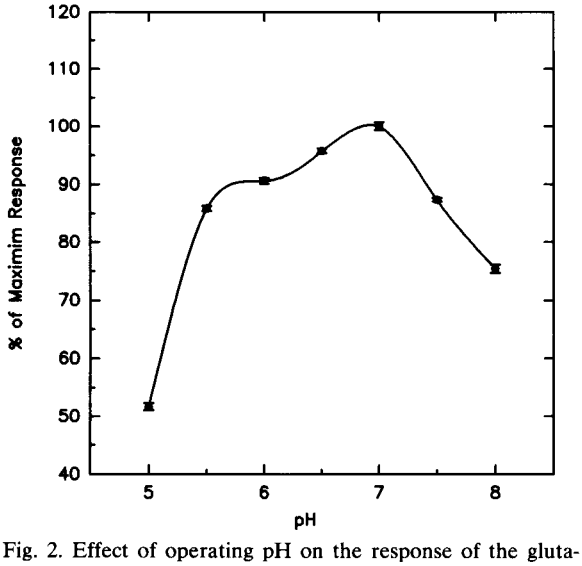

Fig. 2. Effect of operating pH on the response of the glutamate sensor. Steady state current measured at an operating potential of +0.15 V (vs. Ag/AgCl).

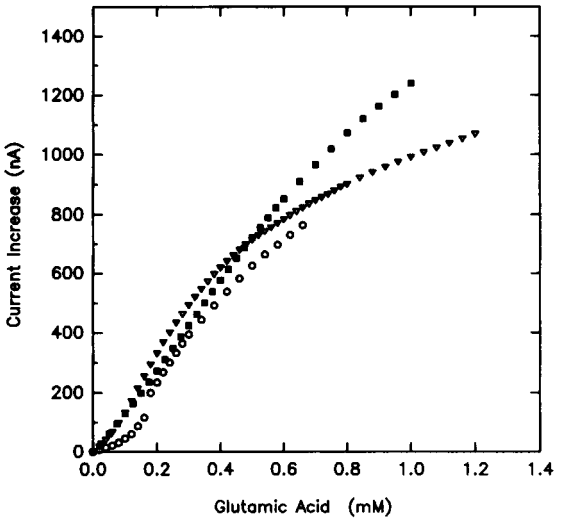

Fig. 3. Effect of operating potential on the response to glutamic acid. Steady state currents were measured at operating potentials of (○) 0.07 V, (▽) 0.10 V and (■) 0.15 V, vs. Ag/AgCl, at pH 7.0 and 25°C.

of the oxidized form of TTF. The electrode used at pH 5, when used again at pH 7, does indeed exhibit a significant decrease in response to glutamic acid. All measurements with the glutamate electrodes used in the following studies were performed at pH 7.

Effect of operating potential. The results obtained in the cyclic voltammetry studies (Fig. 1) demonstrate that a catalytic (oxidative) current is obtained at electrode potentials positive of +0.05 V (vs. Ag/AgCl). Therefore, current vs. concentration curves were obtained with the enzyme electrode at operating potentials of +0.07, +0.1 and +0.15 V (Fig. 3). These results show that the sensitivity and the linear range of detection are direct functions of the operating potential, with the highest sensitivity and linear range obtained at +0.15 V. This enhanced linear range and the increased sensitivity with applied potential can be attributed to an increased driving force for the electrochemical reaction, which results in a more rapid reoxidation of the reduced FAD centers of the glutamate oxidase.

Attempts were also made to measure the response at +0.2 V. However, at this potential, while the electrode was being stabilized in 0.1 M NaCl–0.1 M NaPB, pH 7 (to obtain a constant background current), the solution in the cell gradually turned yellow. This was apparently the result of a continuous depletion of TTF from the electrode surface, because there was a significant decrease in the response of the electrode to glutamate when used again at +0.15 V. The sensor can however operate at significantly low potentials compared to the sensors based on monitoring the formation of hydrogen peroxide. At these potentials, possible interference from other substances present in the samples would also be significantly lower.

Effect of enzyme loading. While maintaining a constant total protein concentration, using bovine serum albumin, so as to eliminate variations in the properties of the resulting crosslinked enzyme film, the glutamate oxidase loading on the electrode surface was varied and the response of the electrode to glutamic acid measured at +0.15 V. As can be seen in Fig. 4, increasing the enzyme loading beyond 2 U does not result in any further increase in the catalytic current. The glutamate oxidase loading was therefore kept at 2 U for all other experiments. Similar enzyme loadings have been used by Cattaneo et al. [26] and Vahjen et

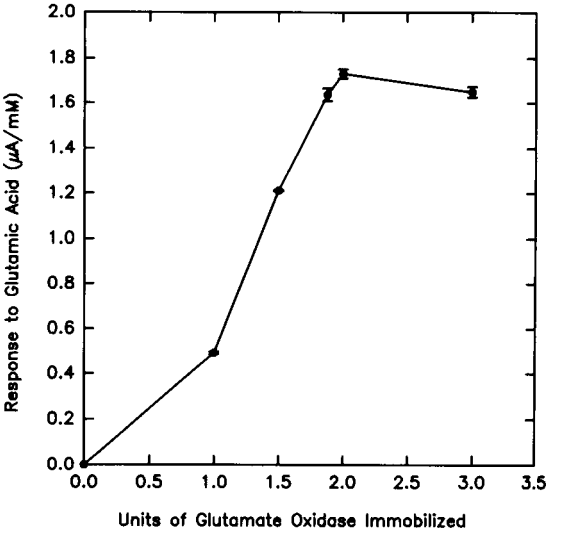

Fig. 4. Effect of glutamate oxidase loading on the response of the electrode to glutamic acid (response obtained at pH 7.0 with an operating potential of +0.15 V, vs. Ag/AgCl).

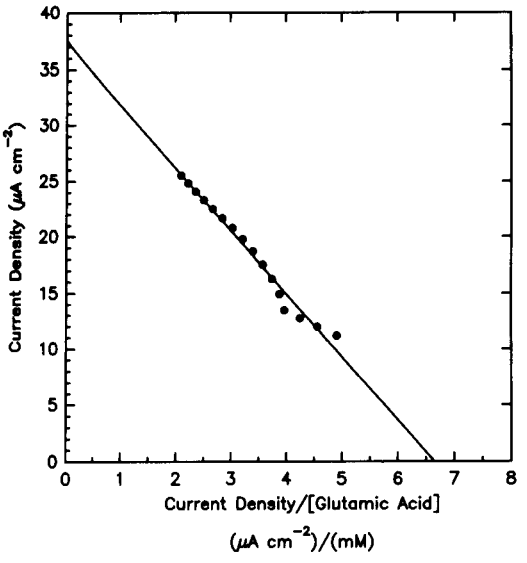

Fig. 5. Electrochemical Eadie–Hofstee plot for the glutamate electrode operated at +0.15 V, vs. Ag/AgCl, and pH 7.

al. [21], although lower enzyme loadings (0.5 U/cm^2) were found to be optimum by Wollenberger et al. [9] who immobilized the enzyme on a polyethylene support and used a non-mediated enzyme electrode configuration, measuring the H_2O_2 produced (reaction 1).

Determination of the apparent Michaelis–Menten constant

The linear response range of the glutamate sensor can be estimated from a Michaelis–Menten analysis of the glutamic acid calibration curves shown in Fig. 3. The apparent Michaelis–Menten constant, K_m^{app} can be determined from the electrochemical Eadie–Hofstee form of the Michaelis–Menten equation [19,27,28]

$$j = j_{max} - K_m^{app}(j/C)$$

where j is the steady-state current density, j_{max} is the maximum current density measured under conditions of enzyme saturation and C is the glutamate concentration. From the slope of the plot of j vs. j/C (Fig. 5), the K_m^{app} is determined to be 5.73 mM. The response to glutamic acid can therefore be expected to be strictly linear for concentrations ≤ 0.57 mM (0.1 K_m^{app}) [19,29]. This is in accord with our observation that the response is linear up to a glutamate concentration of approximately 0.6 mM. Glutamate oxidase electrodes have been reported to respond linearly to L-glutamate concentrations ranging from a minimum of 1 μM to a maximum of 2 mM, with significant variations between the ranges reported by the different groups [9,11–13].

Effect of oxygen on the enzyme electrode

Figure 6 shows glutamate calibration curves for the enzyme electrode in nitrogen-saturated and air-saturated phosphate-buffered chloride solution, obtained at +0.15 V. A significant decrease in the catalytic current (greater than 70%) is observed for the air-saturated buffer over the entire range of glutamate concentrations studied. This is contrary to other studies [15,19,28] reported in the literature for mediated glucose electrodes using glucose oxidase. The decrease in the catalytic current in the air-saturated buffer, compared to the nitrogen-saturated buffer, can be a result of either a lower second order rate constant for the reoxidation of the reduced enzyme with TTF (compared to the rate constant for reoxidation of glutamate oxidase by oxygen, which is the natural electron acceptor), and/or

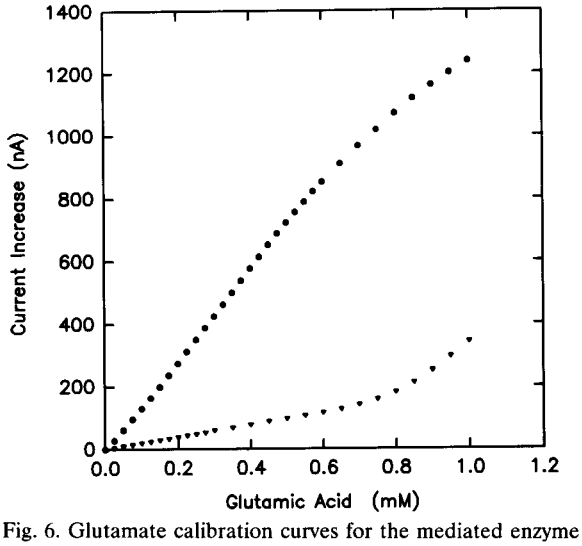

Fig. 6. Glutamate calibration curves for the mediated enzyme electrode poised at +0.15 V (vs. Ag/AgCl), in (●) nitrogen-saturated, and (▼) air-saturated phosphate buffer (0.1 M, pH 7) containing 0.1 M NaCl.

an increased solubility of oxygen in the enzyme–polymer matrix. Similar experiments using a TTF-mediated glucose oxidase electrode (results not shown) indicate that the properties of the polymer matrix are not responsible for the increased sensitivity to oxygen because the decrease in catalytic current for the glucose oxidase electrode in the air-saturated buffer is only about 13% over a wide range of glucose concentrations, this decrease being lower than that reported by Greg and Heller [28] and Hale et al. [19], but higher than that reported by Cass et al. [15]. We therefore believe that the second order homogenous rate constant for the reoxidation of the reduced glutamate oxidase by TTF is significantly lower than the rate constant for reoxidation of some other redox enzymes, like glucose oxidase [17] and choline oxidase [18], by TTF.

Application of the glutamate electrode

The glutamate electrode, when operated at +0.15 V (vs. Ag/AgCl), responded linearly to L-glutamate concentrations up to 0.8 mM, with the lower detection limit being 2.6 μM (3 times the standard deviation obtained for a blank). The response time, measured as the time required for the catalytic current to reach a stable value after addition of the sample to the electrochemical cell containing only buffer and electrolyte, was typically 2 min.

The glutamate oxidase electrode was used to determine the glutamate content of some food samples. The results are shown in Table 1, which also provides a comparison of the amperometric determination to that obtained using the spectrophotometric assay for L-glutamate. The good correlation obtained between the two methods indicate that the sensor is very reliable for the measurement of glutamate in food samples. Similar results might be expected for the determination of glutamate in serum and cell cultures.

TABLE 1

Determination of L-glutamic acid in food samples using the amperometric sensor and by an enzymatic method using glutamate dehydrogenase

Sample	L-Glutamic acid concentration [a] (%, w/w)		Relative error (%)
	Enzymatic method	Amperometric method	
Soy sauce	74.69 ± 0.08 [b]	77.85 ± 2.25 [b]	4.23
Chicken soup mix	4.19 ± 0.06	4.11 ± 0.17	1.91
Seasoning	14.43 ± 0.46	14.42 ± 0.51	0.07
Party dip	11.48 ± 0.19	11.50 ± 0.17	0.17

[a] Results are average of 4 measurements. [b] Results for soy sauce presented as mM.

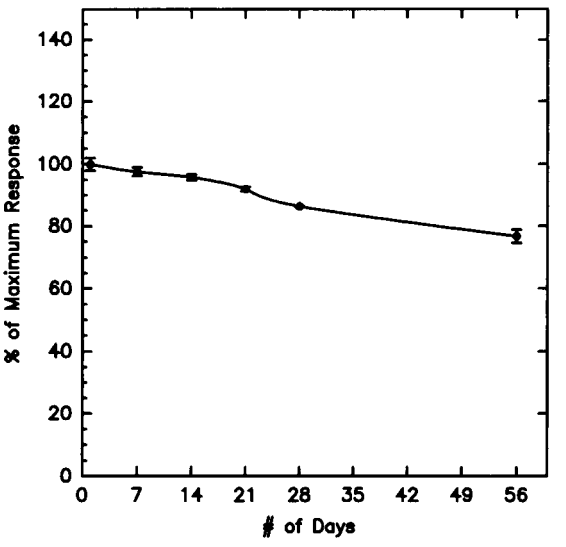

Fig. 7. Stability of the glutamate sensor. The enzyme electrode was stored at 4°C in 0.1 M phosphate buffer, pH 7.

Stability of the glutamate electrode

The response of the electrode is highly stable and reproducible, as indicated by the standard deviation observed for the different measurements. The long term stability of the electrode is also very good, as can be seen from Fig. 7, which shows the percentage decrease in the response of the electrode over an eight week period, during which time the electrode was stored in 0.1 M phosphate buffer of pH 7.0, at 4°C. The electrode retains more than 90% of its original activity over a period of three weeks, and 80% of it's original activity after 8 weeks.

Conclusion

The TTF-mediated glutamate electrode described is suitable for the determination of L-

glutamate in food samples. Use of the mediator permits operation at low applied potentials, reducing possible interference from other electroactive species that may be present in the samples. The amperometric electrode offers advantages of reduced analysis times compared to the enzymatic assay used for determination of glutamate and does not require any complicated sample preparation. The electrode exhibits good stability and reproducibility, and the configuration lends itself to adaptation in flow-injection systems for the determination of glutamic acid and glutamine in cell cultures.

This work was supported by National Science Foundation Grant BCS 9309741.

REFERENCES

1 B. Rietz and G.G. Guilbault, Anal. Chim. Acta, 77 (1975) 191.
2 B.K. Ahn, S.K. Wolfson, Jr, and S.J. Yao, Bioelectrochem. Bioenerg., 2 (1975) 142.
3 A. Malinauskas and J.J. Kulys, Anal. Chim. Acta, 98 (1978) 31.
4 D.P. Nikolelis, Analyst, 112 (1987) 763.
5 T. Iida, T. Kawabe and T. Hisatomi, in J.-L. Aucouturier et al. (Eds.), Proceedings of the 2nd International Meeting on Chemical Sensors, Bordeaux, 1986, pp. 592–595.
6 S. Kuriyama and G.A. Rechnitz, Anal. Chim. Acta, 131 (1981) 91.
7 M. Hikuma, H. Obana, T. Yasuda, I. Karube and S. Suzuki, Anal. Chim. Acta, 116 (1980) 61.
8 K. Riedel and F. Scheller, Analyst, 112 (1987) 341.
9 U. Wollenberger, F.W. Scheller, A. Böhmer, M. Passarge and H.G. Müller, Biosensors, 4 (1989) 381.
10 H. Kusakabe, Y. Midorikawa, T. Fujishima, A. Kuninaka and H. Yoshino, Agric. Biol. Chem., 47 (1983) 1323.
11 H. Yamauchi, H. Kusakabe, Y. Midorikawa, T. Fujishima and A. Kuninaka, in Proceedings of the 3rd Eur. Cong. Biotechnol., DECHEMA, Verlag Chemie, Weinheim, 1984, pp. 705–710.
12 T. Yao, N. Kobayashi and T. Wasa, Anal. Chim. Acta, 231 (1990) 121.
13 C.Y. Chen and Y.C. Su, Anal. Chim. Acta, 243 (1991) 9.
14 M.F. Cardosi and A.P.F. Turner, in A.P.F Turner, I. Karube and G.S. Wilson (Eds.), Biosensors: Fundamentals and Applications, Oxford Science Publications, 1990, pp. 257–275.
15 A.E.G. Cass, G. Davis, G.D. Francis, H.A.O. Hill, W.J. Aston, I.J. Higgins, E.V. Plotkin, L.D.L. Scott and A.P.F. Turner, Anal. Chem., 56 (1984) 667.
16 J. Wang, L.H. Wu, Z. Lu, R. Li and J. Sanchez, Anal. Chim. Acta, 228 (1990) 251.
17 H. Gunasingham and C.H. Tan, Analyst, 115 (1990) 35.
18 P.D. Hale, L.F. Liu and T.A. Skotheim, Electroanalysis, 3 (1991) 751.
19 P.D. Hale. L.I. Boguslavsky, T. Inagaki, H.I. Karan, H.S. Lee, T.A. Skotheim and Y. Okamoto, Anal. Chem., 63 (1991) 677.
20 N.C. Foulds and C.R. Lowe, Anal. Chem., 60 (1988) 2473.
21 W. Vahjen, J. Bradley, U. Bilitewski and R.D. Schmid, Anal. Lett., 24 (1991) 1445.
22 K. Tamaoku, Y. Murao, K. Akiura and Y. Ohkura, Anal. Chim. Acta, 136 (1982) 121.
23 S.V. Sasso, R.J. Pierce, R. Walla and A.M. Yacynych, Anal. Chem., 62 (1990) 1111.
24 R.J. Geise, J.M. Adams. N.J. Barone and A.M. Yacynych, Biosensors Bioelectronics, 6 (1991) 151.
25 A.N. Nguyen, J.H.T. Luong and A.M. Yacynych, Biotech. Bioeng., 37 (1991) 729.
26 M.V. Cattaneo, J.H.T. Luong and S. Mercille, Biosensors Bioelectronics, 7 (1992) 329.
27 R.A. Kamin and G.S. Wilson, Anal. Chem., 52 (1980) 1198.
28 B.A. Greg and A. Heller, Anal. Chem., 62 (1990) 258.
29 L. Gorton, H.I. Karan, P.D. Hale, T. Inagaki, Y. Okamoto and T.A. Skotheim, Anal. Chim. Acta, 228 (1990) 23.

Analytica Chimica Acta, 282 (1993) 363–367
Elsevier Science Publishers B.V., Amsterdam

Enzyme-based chemically amplified flow-injection determination of catechol and catecholamines using an immobilized tyrosinase reactor and L-ascorbic acid

Yasushi Hasebe, Kenichiro Takamori and Shunichi Uchiyama

Department of Environmental Engineering, Saitama Institute of Technology, 1690, Fusaiji, Okabe, Saitama 369-02 (Japan)

(Received 13th January 1993; revised manuscript received 4th May 1993)

Abstract

Substrate recycling of polyphenols takes place when the substrate is added to a solution containing tyrosinase and L-ascorbic acid. The current of the oxygen electrode detector in a flow-injection system with an immobilized tyrosinase reactor was significantly amplified when the carrier solution contained L-ascorbic acid, because the *o*-quinone compounds produced from substrates by the tyrosinase reaction are chemically reconverted to the original polyphenols by L-ascorbic acid. The establishment of a cyclic reaction of substrates in the enzyme reactor leads to amplification of oxygen consumption. The amplification factor increased with decreasing substrate concentration and was found to be larger than 100 when the substrate concentration was below 1×10^{-7} M. The detection limits of polyphenols (catechol, L-dopa, dopamine, noradrenaline and adrenalin) were 10^{-7}–10^{-9} M in the presence of 1×10^{-3} M L-ascorbic acid in the carrier (pH 6.5, flow-rate 2.5 ml min^{-1}).

Keywords: Amperometry; Enzymatic methods; Flow injection; Amplification; Catechol; Catecholamines; Enzyme reactor; Polyphenols

The enhancement of the output signal of a biosensor system is an important subject for the determination of trace amounts of analyte, and substrate recycling using two or more kinds of enzymes has been utilized to develop highly sensitive enzyme electrodes [1–3], flow-injection analysis (FIA) systems [4–6] and an optical sensor [7]. In these methods, the sensor response based on the consumption or accumulation of electrochemically or optically detectable substances and/or calorimetric changes is amplified by a repeated enzymatic reaction during the substrate recycling. On the other hand, it has been demonstrated recently that the substrate recycling of L-ascorbic acid takes place by combining the ascorbate oxidase reaction and chemical reduction of dehydroascorbic acid to ascorbic acid by dithiothreitol [8], and a chemically amplified vitamin C sensor has been proposed, using an immobilized enzyme oxygen electrode in dithiothreitol solution [9]. Further, more recently, it has been found that the cyclic reaction between catechol and *o*-benzoquinone also takes place when a reducing agent such as L-ascorbic acid is added to the sample solution containing tyrosinase and catechol, and the determination of catechol at the 10^{-8} M level has been achieved by using an oxygen electrode modified with a potato-tissue membrane which has tyrosinase activity (the amplification factor is more than 400) [10]. It is well known that tyrosinase has a broad enzyme activity for polyphenol compounds and catalyses not

Correspondence to: Y. Hasebe, Department of Environmental Engineering, Saitama Institute of Technology, 1690, Fusaiji, Okabe, Saitama 369-02 (Japan).

only catechol but also catecholamines such as L-dopa, dopamine, noradrenaline and adrenaline. Therefore, if L-ascorbic acid can regenerate catecholamines from enzymatically produced catecholaminequinones without inhibition of tyrosinase activity, the following cyclic reaction of polyphenols might be possible:

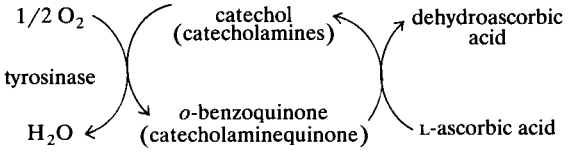

During the above cyclic reaction scheme, the dissolved oxygen continues to decrease owing to the repeated enzymatic reaction. Consequently, a small amount of polyphenols should be determinable by monitoring the amplified change in oxygen consumption. In this study, this amplification principle was introduced with a flow-injection system consisting of a tyrosinase reactor and an oxygen electrode detector, and the amplification characteristics of catechol and catecholamines obtained by using carrier containing L-ascorbic acid were investigated.

EXPERIMENTAL

In order to perform a typical flow-injection method, an analytical pump (Sanuki Industries, SNK DMX-2000) with a sample injector (injection volume 100 μl) was connected to an oxygen electrode (Denki Kagaku Keiki) with a PTFE tube (0.5 mm diameter) and an immobilized tyrosinase reactor (50 mm length, 3 mm diameter, volume ca. 0.35 cm^3) was connected between them. Dissolved oxygen-saturated phosphate buffer solutions (0.01 M) containing L-ascorbic acid were used as carriers. Immobilized tyrosinase glass beads were prepared by diazo coupling methods using 20 mg of tyrosinase (EC 1.14.18.1, from mushroom; Sigma) and 0.8 g of controlled-pore glass (Electro-Nucleonics; aminoaryl-CPG, pore size 500 Å, particle size 80–120 mesh, amino group content 76 μmol mg^{-1}) in a similar manner to previous studies [11,12]. The coupling yields were ca. 10% and the catechol oxidase activity of tyrosinase in the reactor was ca. 60000 U mg^{-1}. The enzyme reactor was stored in a refrigerator at 4°C after measurement [0.01 M phosphate buffer (pH 6.5) was used as a stored eluent]. The standard sample solution was injected with the sample injector and the reduction current of dissolved oxygen in the carrier was monitored by a downstream oxygen electrode detector and recorded by a one-pen recorder (Nippon Denshi Kagaku, Unicorder U-228). The electrode potential was maintained at −0.7 V vs. Ag/AgCl by a potentiostat (Nikko Keisoku, NPOT-2501). The base current of dissolved oxygen maintains a constant value throughout the continuous measurement of more than twenty samples (at least for 3 h). Standard sample solutions of catechol and catecholamines were prepared by dissolving the analytical-reagent grade catechol or catecholamines in phosphate buffer solution.

RESULTS AND DISCUSSION

Typical current responses of catechol (1×10^{-5} and 5×10^{-6} M) obtained by using carriers with and without L-ascorbic acid are shown in Fig. 1. The results indicate that the current responses are significantly amplified when 1×10^{-3} M L-

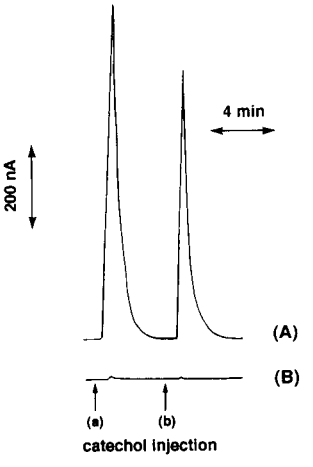

Fig. 1. Typical (A) amplified and (B) non-amplified current responses of catechol using 10 mM phosphate buffer (pH 6.5) with and without 1×10^{-3} M L-ascorbic acid. Flow-rate: 2.5 ml min^{-1}. Sample: (a) 1×10^{-5} and (b) 5×10^{-6} M catechol.

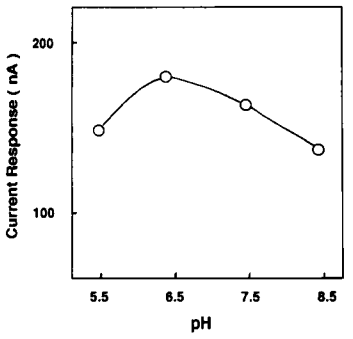

Fig. 2. Effect of pH of the carrier without L-ascorbic acid on the current response of 1×10^{-4} M L-dopa. Flow-rate: 2.5 ml min^{-1}.

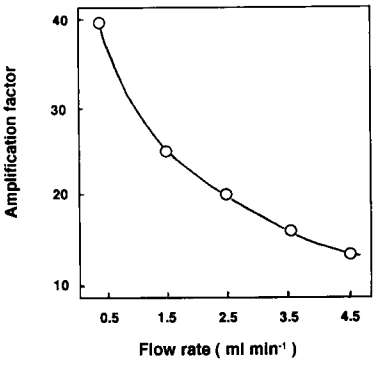

Fig. 3. Effect of flow-rate of 10 mM phosphate buffer (pH 6.5) containing 1×10^{-3} M L-ascorbic acid on the amplification factor for measurement of 1×10^{-5} M L-dopa.

ascorbic acid is present in the carrier, supporting the establishment of a cyclic reaction of catechol in the enzyme reactor in which *o*-benzoquinone produced in the tyrosinase-catalysed reaction is chemically reconverted to the original catechol by L-ascorbic acid and reoxidized by tyrosinase. Thus, a large amount of oxygen was consumed in the repeated enzymatic reaction.

In order to establish the optimum conditions for amplification, first the effect of the pH of the carrier on the current responses for 1×10^{-4} M L-dopa was examined (Fig. 2). The largest response was obtained when the pH of the carrier was 6.5. Therefore, the remaining experiments were carried out by using carrier solutions adjusted to pH 6.5.

In general, the retention time of the sample in the enzyme reactor is inversely proportional to the flow-rate of the carrier, and the amplification factor should increase with decrease in the flow-rate. Therefore, the effect of the flow-rate on the amplification factor (i.e., the ratio of the amplified to the non-amplified current value) for 1×10^{-5} M L-dopa was investigated (Fig. 3). The amplification factor increased markedly with decrease in flow-rate. This observation indicates that a decrease in flow-rate results in an increase in the number of cycles of the substrate (i.e., the turnover number of the tyrosinase reaction), which contributes directly to the amplification factor.

The effects of the L-ascorbic acid concentration in the carrier on the current responses of L-dopa are shown in Fig. 4. The current responses are highly dependent on the concentration of L-ascorbic acid, and a largest response was obtained when the L-ascorbic acid concentration was 5×10^{-3} M. However, when the concentration of L-ascorbic acid was more than 5×10^{-3} M, the current baseline of dissolved oxygen decreased because of oxidation of L-ascorbic acid by dissolved oxygen, and the current response was suppressed. On the other hand, it is well known that catecholaminequinones are less stable and are spontaneously converted into catecholchrome, which has an indole skeleton (maximum absorption peak at 475 nm) [13]. No colored

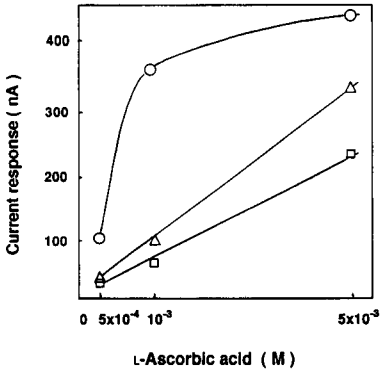

Fig. 4. Effect of L-ascorbic acid concentration in the carrier on the amplified current responses of each concentration of L-dopa: (○) 5×10^{-4}; (△) 1×10^{-4}; (□) 5×10^{-5} M. Phosphate buffer (10 mM, pH 6.5) containing 1×10^{-3} M L-ascorbic acid was used as a carrier. Flow-rate: 2.5 ml min^{-1}.

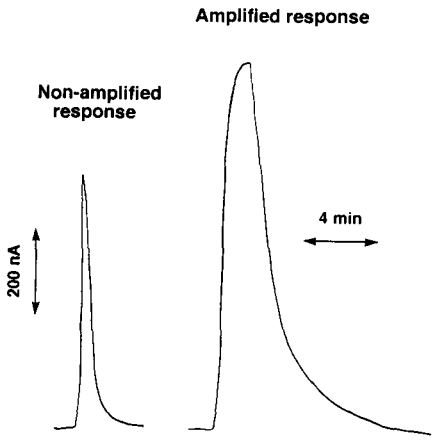

Fig. 5. Comparison of the current peak shapes of amplified and non-amplified responses obtained for the determination of 5×10^{-4} M catechol. Phosphate buffer (10 mM, pH 6.5) containing 1×10^{-3} M L-ascorbic acid was used as a carrier. Flow-rate: 2.5 ml min^{-1}.

species (475 nm) could be detected within 20 min after addition of 5×10^{-5} M L-dopa to tyrosinase solution containing more than 1×10^{-3} M L-ascorbic acid, suggesting that L-ascorbic acid rapidly reduce the quinone compound to the original substrate and suppresses the generation of catecholchome dye. In the present FIA method, sufficiently large amounts of L-ascorbic acid can be continuously supplied from the carrier stream, which is an important advantage for signal amplification over batch methods in which the reducing agent consumed by cyclic reaction is not compensated for [8–10].

Figure 5 compares the peak shapes of amplified and non-amplified responses for a sample of high concentration (5×10^{-4} M L-dopa). The amplified peak was four times broader than the non-amplified peak, which suggests that repetition of the enzyme–substrate complex formation prolongs the retention time of the sample in the reactor. This also supports the assumption that signal amplification occurs as a result of the cyclic reaction between catecholamine and catecholaminequinone in the enzyme reactor.

The results for several concentrations of samples (catechol, dopamine and L-dopa) are summarized in Table 1. The amplification factor increased substantially on decreasing the substrate concentration. When the substrate concentration

TABLE 1

Results for catechol, dopamine and L-dopa obtained with the FIA system using 1×10^{-3} M L-ascorbic acid solution as a carrier at a flow-rate of 2.5 ml min^{-1}

Concentration (M)	Catechol		Dopamine		L-Dopa	
	i (nA) [a]	A.F. [b]	i (nA)	A.F.	i (nA)	A.F.
5×10^{-5}	810	12	890	25	720	11.3
1×10^{-5}	790	56	440	61	190	11.8
5×10^{-6}	650	100	240	67	100	12.5
1×10^{-6}	140	110	70	97	20	12.5
5×10^{-7}	70	140	50	139	10	15.6
1×10^{-7}	40	285	30	416	6	37.5
5×10^{-8}	30	469	20	555	–	–

[a] i = Response current value. [b] A.F. = amplification factor.

is very low, e.g., 10^{-8}–10^{-9} M, the amount of the immobilized tyrosinase and the concentration of L-ascorbic acid relative to one substrate molecule become extremely high, and therefore the number of cycles per unit time at low concentrations of substrate is large compared with that at high concentrations. Therefore, a large amplification factor was obtained in the lower concentration range of the substrate. In contrast, when a high concentration of sample was injected, dissolved oxygen and L-ascorbic acid decreased rapidly, resulting in a small number of cycles of the substrate. Consequently, this system is superior for the measurement of low-concentration samples. The relative standard deviation of the current responses was below 5% for eight measurements.

Figure 6 shows the amplified and non-amplified calibration graphs for dopamine using carriers with and without L-ascorbic acid. When the

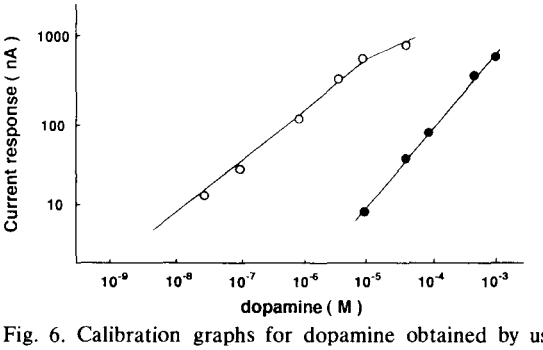

Fig. 6. Calibration graphs for dopamine obtained by using phosphate buffer (10 mM, pH 6.5), (○) with and (●) without L-ascorbic acid. Flow-rate: 2.5 ml min^{-1}.

TABLE 2

Results for polyphenol compounds obtained with the FIA system at a flow-rate of 2.5 ml min^{-1}

Substrate	Reducing agent (1×10^{-3} M)	Detection limit (M)	Amplification factor (substrate concentration)	Dynamic range (M)
Catechol	L-Ascorbate	2×10^{-9}	469 (5×10^{-8} M)	5×10^{-5}–5×10^{-9}
	None	2×10^{-6}	1	1×10^{-3}–5×10^{-6}
L-Dopa	L-Ascorbate	1×10^{-8}	37.5 (1×10^{-7} M)	5×10^{-4}–5×10^{-8}
	None	5×10^{-6}	1	1×10^{-3}–1×10^{-5}
Dopamine	L-Ascorbate	1×10^{-9}	555 (5×10^{-8} M)	5×10^{-5}–5×10^{-9}
	None	2×10^{-6}	1	5×10^{-3}–5×10^{-6}
Noradrenaline	L-Ascorbate	5×10^{-7}	12.5 (5×10^{-6} M)	5×10^{-4} -1×10^{-6}
	None	1×10^{-5}	1	1×10^{-3}–1×10^{-5}
Adrenaline	L-Ascorbate	5×10^{-7}	11 (5×10^{-6} M)	1×10^{-3}–1×10^{-6}
	None	1×10^{-5}	1	1×10^{-3}–1×10^{-5}

carrier contained 1×10^{-3} M L-ascorbic acid, the dynamic range of the calibration graph was shifted toward a more than two decade lower concentration range compared with the non-amplified response. The current response was linear over the range 1×10^{-5}–5×10^{-8} M dopamine and the detection limit was 1×10^{-9} M.

The characteristics obtained with this FIA system are summarized in Table 2. These results can presumably be explained in terms of the order of polyphenol oxidase activities for catechol compounds and the reduction rates of individual quinones by L-ascorbic acid. When another reducing agent such as the hexacyanoferrate(II) ion, which has been used for the regeneration of catechol from *o*-benzoquinone in a potentiometric phenol sensor using an immobilized tyrosinase electrode [14], was used in place of L-ascorbic acid, the current response was suppressed, probably because the enzyme activity of the tyrosinase reactor was inhibited.

The present FIA system has the following features compared with other amplification systems using two enzymes: it is relatively easy to establish the optimum measurement conditions; the inhibition of signal by other oxidizing agents can be easily avoided by the pre-addition of L-ascorbic acid to the sample solution; trace amounts of polyphenols (1×10^{-6}–1×10^{-9} M) can be determined using simple equipment and procedure; and the present tyrosinase reactor retains its enzymatic activity for 20 days (more than 90% signal response compared with that on the first day), but the signal response suddenly decreased to less than 60% after 20 days. Consequently, the present system is expected to be very useful for the measurement of total catecholamines in the biological samples. However, in order to detect each polyphenol compound independently, it is necessary to introduce a separation column in this FIA system, and this feature is now under study.

REFERENCES

1 F. Schubert, D. Kirstein, K.L. Schröder and F.W. Scheller, Anal. Chim. Acta, 169 (1985) 391.
2 F. Mizutani, T. Yamaoka and Y. Tanabe, Anal. Chim. Acta, 177 (1985) 153.
3 T. Yao, H. Yamamoto and T. Wasa, Anal. Chim. Acta, 236 (1990) 437.
4 F. Sheller, N. Siegbahn, B. Danielsson and K. Mosbach, Anal. Chem., 57 (1985) 1740.
5 M.U. Asouzu, W.K. Nonidez and M.H. Ho, Anal. Chem., 62 (1990) 708.
6 T. Yao, N. Kobayashi and T. Wasa, Electroanalysis, 3 (1991) 493.
7 A.W. Wang and M.A. Arnold, Anal. Chem., 64 (1992) 1051.
8 S. Uchiyama, Talanta, 39 (1992) 1289.
9 S. Uchiyama, Y. Hasebe and S. Suzuki, Electroanalysis, in press.
10 S. Uchiyama, Y. Hasebe, H. Shimizu and H. Ishihara, Anal. Chim. Acta, 276 (1993) 341.
11 S. Uchiyama, F. Umesato, S. Suzuki and T. Sato, Anal. Chim. Acta, 230 (1990) 195.
12 J.K. Inman, and H.M. Dintzs, Biochemistry, 8 (1969) 4074.
13 J.L. Sidwell and G.A. Rechnitz, Biotechnol. Lett., 7 (1985) 419.
14 J.G. Schiller, A.K. Chen and C.C. Liu, Anal. Biochem., 85 (1987) 25.

Analytica Chimica Acta, 282 (1993) 369–378
Elsevier Science Publishers B.V., Amsterdam

Enhanced selectivity in flow-injection analysis for L-amino acids using electrodialysis with amino acid oxidation

J.C. Cooper, J. Danzer and H.-L. Schmidt

Lehrstuhl für Allgemeine Chemie und Biochemie, Technische Universität München, 85354 Freising-Weihenstephan (Germany)

(Received 18th March 1993; revised manuscript received 14th May, 1993)

Abstract

A method has been developed for continuous determination of the concentration of one amino acid in a mixture, using electrodialysis combined with a flow-injection system. Using a non-specific L-amino acid oxidase column and electrochemical detection of enzymatically produced hydrogen peroxide, the concentration of a particular amino acid in a mixture could be determined by first performing a separation step using an electrodialysis unit. Using the separation of arginine as a model system, it was possible to determine the concentration of this amino acid in the presence of two or three of a group of nine amino acids.

Keywords: Flow injection; Amino acids; Electrodialysis

Amino acid analysis is usually performed using methods based on liquid or gas chromatography. Whilst these techniques have very low detection limits, they are not suitable for continuous monitoring of amino acid concentrations as might be required in a fermentation process, for example.

Continuous measurement of amino acids can be performed by flow-injection analysis (FIA) together with an enzyme-based detector or biosensor. Dehydrogenases have been used for enzyme-based amino acid biosensors [1,2] or in an FIA system for amino acids [3], an advantage of the dehydrogenases being their high selectivity. However, dehydrogenases have not been found for every amino acid, and dehydrogenase reactions are reversible which means that the position of equilibrium does not necessarily favour the products of the reaction. The dehydrogenase reaction can be measured photometrically via the reduced cofactor NADH, but electrochemical detection is complicated by the need for a high overpotential, and accompanying side-reactions which result in electrode fouling [4].

Alternatively, oxidases can be employed as the sensing element for amino acid detection. Oxidases specific for a particular amino acid have been used to develop amino acid biosensors [5], but again, a specific oxidase has not been found for every amino acid. Non-specific amino acid oxidases also exist, which react with a range of amino acids. These have been employed in an FIA system for L-amino acids, based on a coupled photometric reaction using peroxidase [6], and for amino acid biosensors based on electrochemical detection of oxygen or hydrogen peroxide [7–9]. These non-specific amino acid sensors can only give a measure of the total amino acid concentration.

Correspondence to: J.C. Cooper, present address: Bayer AG, ZF-TPF5, 51368 Leverkusen (FRG).

It may, however, be possible to determine a particular amino acid concentration in the presence of others (perhaps an amino acid for which a specific oxidase has not been discovered) by using a non-specific amino acid oxidase in combination with a separation process for amino acids. By incorporating a separation step and the amino acid detector into an FIA system, continuous monitoring of a particular amino acid in a mixture could be achieved. A separation step combined with a non-specific amino acid detector in an FIA system could potentially be used as a multi-analyte sensor, able to continuously measure individual concentrations of a range of amino acids, by manipulating the conditions of the separation process.

There is a large variation of isoelectric point amongst the amino acids, and this might be used as the basis of the separation process, by electrodialysis. Separation by electrodialysis depends on the selection of a pH such that the amino acid(s) of interest has a different net charge and migrates away from the remaining amino acids in the sample phase into an acceptor phase, under the influence of the electric field in the electrodialysis cell. Electrodialysis has been reported for separation of alanine and aspartic acid [10], and for extraction of ephedrine from spiked plasma [11]. Either one or both of the sample and acceptor phases remained stationary, and there was a delay whilst electrodialysis takes place, before analysis of the samples. However, it is also possible to use electrodialysis in a flow-through mode and with this technique, analysis of the electrodialysed samples can be performed continuously. An application has been reported by our group for separation of leucine from ketoleucine during flow-injection analysis with leucine dehydrogenase [3]. Here we report on the feasibility of using a non-specific FIA system for L-amino acids, combined with continuous electrodialysis, for determination of one amino acid in a mixture. Separation of arginine in the presence of other amino acids was used as a model for the investigation, and the amino acid detection was performed using a non-specific oxidase together with electrochemical detection of enzymatically produced hydrogen peroxide.

EXPERIMENTAL

Materials

L-Amino acid oxidase (L-AAOD, EC 1.4.3.2.) from *Crotalus adamanteus* (0.54 U/mg solid), and from *Crotalus atrox* (0.7 U/mg solid), were obtained from Sigma (St. Louis., CA). L-Amino acid oxidase from *Colletotricum* sp. (274.3 U/ml, Toyo Jozo, Japan), was a kind gift from Prof. R.D. Schmid, Braunschweig. Catalase (EC 1.11.1.6., 2100 U/mg) from *Aspergillus niger* was purchased from Serva, Heidelberg. All reagents were of analytical grade.

Working electrodes were made by sealing a 1-mm diameter piece of platinum, soldered to a copper wire, into a piece of glass tubing. The electrochemical flow-through cell and the electrodialysis cell were built in-house. Anion-exchange membranes were purchased from Reichelt Chemietechnik, Heidelberg, and cation-exchange membranes were from Serva, Heidelberg.

Construction of enzyme electrodes and columns

L-AAOD electrodes using the enzyme from *C. atrox* were made by crosslinking onto a platinum electrode (diameter 1 mm). 50 μl of a solution containing 100 mg/ml L-AAOD, 100 mg/ml BSA and 2.5% glutaraldehyde was pipetted onto the electrode surface. This was allowed to dry, and then covered with a piece of dialysis membrane (cut-off 10 000), secured with an O-ring.

L-AAOD-CPG columns were made by first immobilising the enzyme on controlled pore glass (pore size 350–1400 Å, 120–200 mesh, Fluka, Ulm), which had been modified with 3-aminopropyltriethoxysilane and activated with glutaraldehyde. For L-AAOD from *C. adamanteus*, 5, 10 or 20 mg enzyme was incubated with 120 mg activated CPG in 0.5 ml 0.1 M phosphate buffer pH 7 at 4°C overnight; the column using 5 mg enzyme was found to have the highest enzyme activity. All further columns were made using this enzyme to CPG ratio (8.3 mg enzyme and 200 mg CPG). For L-AAOD from *Colletotrichum sp.*, either 10 or 20 U were incubated with 200 mg activated CPG. For both types of enzyme column, the washed enzyme-CPG was loaded into a glass column (2.3 cm × 0.5 cm i.d.) and held in place by two plastic flow-through plugs. Adsorbed enzyme

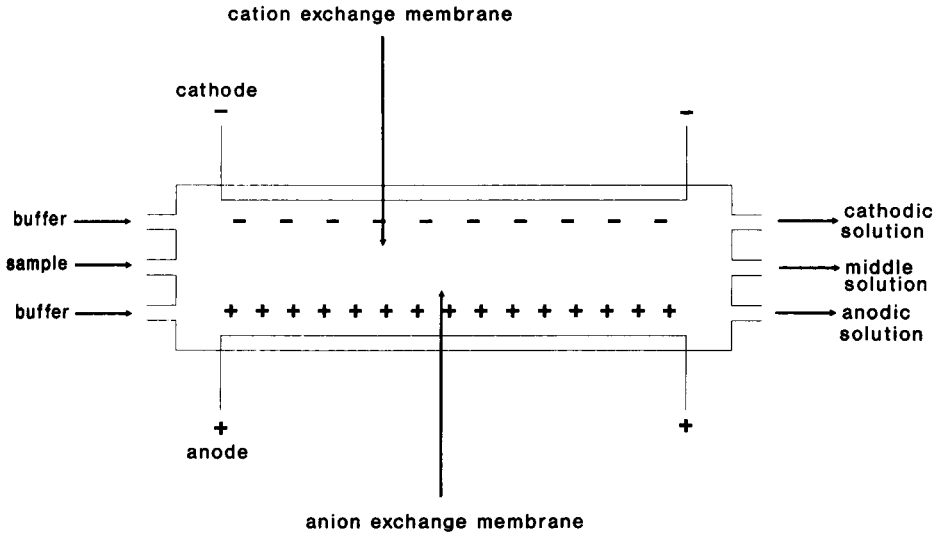

Fig. 1. Diagram of the electrodialysis unit.

was removed by pumping 1 M NaCl, then 0.1 M potassium phosphate pH 7, through the column. Catalase columns were made by the same method, using 10 mg enzyme and 200 mg CPG.

Electrodialysis

The electrodialysis cell for the separation of amino acids consisted of a flow-through cell (length 30 cm) divided into three compartments

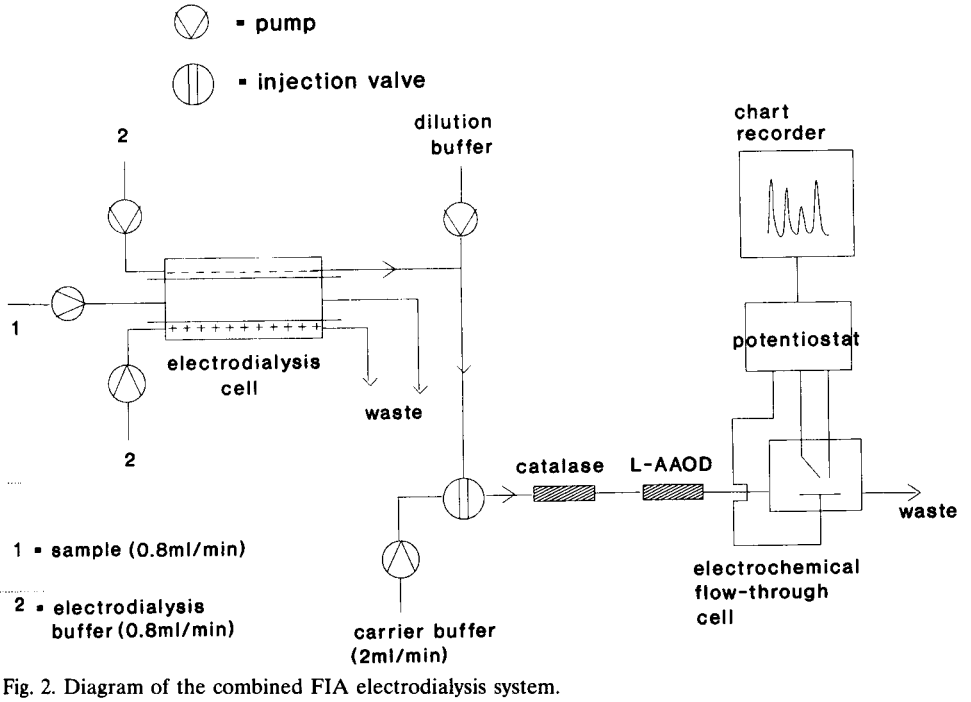

Fig. 2. Diagram of the combined FIA electrodialysis system.

by two ion-exchange membranes (Fig. 1). The sample to be electrodialysed (made up in the electrodialysis buffer) was continuously pumped into the middle compartment, and electrodialysis buffer was pumped through the anodic and cathodic compartments, all at 0.8 ml/min. A potential of 20 V was applied across the electrodialysis cell. At this potential, hydrogen and oxygen evolution occur at the cathode and anode respectively, which results in a large change in the pH of the anodic and cathodic solutions during electrodialysis, and so it was necessary to adjust the sample pH before injection to the L-AAOD electrode or column. For the solutions from the anodic and middle compartments, this was achieved with 0.2 M phosphate buffer pH 7.6, by diluting the sample with buffer in the ratio 1:4 and 1:2, respectively. The cathodic solution was diluted with 0.2 M sodium citrate pH 3, either by pipetting or by mixing with a peristaltic pump, in the sample to buffer ratio of 2:3, to achieve a final pH of approximately 7.5.

Flow-injection system

A Tecator FIAstar 5020 Analyser was used for flow-injection analysis of amino acids, together with either an L-AAOD column or electrode and an electrochemical cell. The electrochemical cell employed a three-electrode arrangement, with a saturated calomel reference electrode (SCE), and a platinum counter electrode. For measurements using an L-AAOD electrode, the latter was mounted directly in the electrochemical cell as the working electrode and poised at +0.7 V vs. SCE. For measurements using L-AAOD columns, the column(s) was installed directly before the electrochemical cell in the flow system, and an unmodified platinum electrode was used as the working electrode, at +0.7 V vs. SCE. Current peaks were measured using a Bank Elektronik

TABLE 1

Migration of individual amino acids during continuous electrodialysis of 10 mM solutions in 0.2 M pyrophosphate pH 8.0. [The eluents of the three compartments of the electrodialysis cell were added to special dilution buffers (as described in the Experimental section) to give a final pH of approximately 7.5, and then analysed in a FIA system by three columns of L-AAOD from *C. adamanteus* (carrier buffer 0.2 M phosphate pH 7.6), measuring electrochemically the hydrogen peroxide formed above the background for electrodialysis of pure buffer]

Amino acid	Isoelectric point	Response (nA) above background for:				Relative [d] activity of L-AAOD (%)	
		Cathode chamber	Middle chamber	Anode chamber	Total (%)	L-AAOD-CPG [a]	Solutions assay [b]
Aspartic acid (asp)	2.77	0	0.10	0	0.1	6	0.25
Cysteine (cys)	5.05	0.19	3.30	22.51	32.9	389	–
Asparagine (asp)	5.41	0	0.05	0.19	0.3	9	7.3
Phenylalanine (phe)	5.48	0	37.61	41.36	100	100	100
Glutamine (gln)	5.65	0	0.14	0.44	0.7	13	19
Tyrosine (tyr)	5.66	0.43	40.46	68.61	138.7	147	–
Methionine (met)	5.74	0.24	11.16	2.57	17.7	32	214
Trytophan (trp)	5.89	0.33	1.99	118.71	153.3	467	–
Valine (val)	5.96	0	0.68	0.24	1.2	11	14
Isoleucine (ile)	5.98	0	9.32	5.09	18.2	49	85
Alanine (ala)	6.0	0	1.41	0.05	1.8	6	5.8
Leucine (leu)	6.02	0	2.62	3.59	7.9	54	162
Histidine (his)	7.59	3.97	5.46	7.08	20.9	48	35
Lysine (lys)	9.74	0	0	0	0	3	–
Arginine (arg)	10.76	1.1	0.97	0	2.6	11	39
Ascorbic acid [c]	–	0.58	5.67	83.41	–	–	–

[a] Measured with three L-AAOD columns (*C. adamanteus*) pH 7.6 via electrochemical oxidation of hydrogen peroxide formed. [b] Coupled fluorescent assay at pH 7.5 using L-AAOD (*C. adamanteus*) and peroxidase [12]. [c] For comparison. [d] Response given relative to that for phenylalanine (taken as 100%).

potentiostat (Standard Wenking ST 72) together with a Keithley Instruments 440 digital picoammeter and plotted on a Kipp and Zonen BD 8 multi range recorder. A complete arrangement is displayed in Fig. 2.

RESULTS AND DISCUSSION

Preliminary investigation of feasibility of electrodialysis

Separation by electrodialysis requires selection of conditions such that the species of interest i.e. the amino acid to be measured, has a different net charge, and therefore migrates in a different direction to the other components of the mixture into an acceptor phase. In our continuous electrodialysis unit, the sample to be electrodialysed is pumped into the middle compartment of the electrodialysis cell, and electrodialysis buffer is pumped through the outer compartments. One of the buffer-filled compartments functions as the acceptor phase, depending on the direction of migration of the amino acid of interest. The compartments are separated by ion-exchange membranes (Fig. 1). A potential is applied across the electrodes and electrodialysed samples are collected from the appropriate outlet for introduction, after dilution, into the enzyme-based part of the FIA system.

Preliminary experiments showed that continuous separation of amino acids by electrodialysis in the flow system is incomplete. For example, the migration of leucine under different continuous electrodialysis conditions was tested using electrochemical (L-AAOD–CPG column with enzyme *C. adamanteus* and unmodified platinum working electrode) or spectrophotometric (leucine dehydrogenase column with photometric detection of NADH, see [3] for details) detection methods. The results using both methods were in agreement. It was found that during electrodialysis at pH 6.0 where leucine is neutral, there was no migration to either pole, as expected. At pH 10.15, leucine is anionic, but only 35% of the amino acid migrated to the anode. Migration was never complete, especially with more concentrated samples, and this is probably associated with the dimensions of the electrodialysis cell and the permeability of the ion exchange membranes.

Table 1 shows the results of a corresponding investigation of the individual migration of 10 mM concentrations of all the amino acids, using 0.2 M pyrophosphate pH 8 for electrodialysis and measured in the FIA system (as in Fig. 2) with 3 L-AAOD columns (*C. adamanteus*) without a catalase column, at pH 7.6. At this pH for electrodialysis, only arginine and lysine should be cationic and migrate to the cathode. The remainder should be anionic and migrate to the anode, but it can be seen that for most of the amino acids, a significant activity could be measured in the middle compartment, indicating that only partial migration has taken place. Tryptophan and ascorbic acid did migrate well, however. The separation of the latter is of particular interest for measurement in real blood samples since the co-oxidation of ascorbic acid can interfere with analyte determination based on hydrogen peroxide oxidation. Significant activity could be detected in the cathodic compartment for arginine, as expected, and also for histidine. L-AAOD from *C. adamanteus*, however, has a low relative specificity for lysine (see Table 1), and so any lysine migrating to the cathode will not produce an enzymic response. The sum of the responses for each individual amino acid was compared to the relative activity of L-AAOD from *C. adamanteus*, as measured with L-AAOD columns at pH 7.6, and also to relative activity data from the literature [12] (see 1st–3rd columns from right in Table 1). The sum of the responses from all 3 chambers was rather lower (relative to the phenylalanine response) than would be expected from the relative activity of L-AAOD from *C. adamanteus*, but otherwise the trend of the relative responses after electrodialysis was in agreement with that for the enzyme from this source. Histidine is probably only slightly anionic at pH 8, but its migration to the cathode is still difficult to explain. Later experiments using electrodialysis at pH 10 did not reduce migration of histidine to the cathode, even though it should be completely anionic at this pH. Testing with ninhydrin showed that the responses measured for arginine and histidine are

really due to amino acids, and not a break-down product of electrodialysis.

Thus it seemed sensible to choose an amino acid for use in a model system whose isoelectric point is at one end of the range. Arginine was selected to demonstrate the principle of determination by combined electrodialysis and FIA. This has the advantage that there is a reasonable separation between its isoelectric point and that of the other basic amino acids (unlike in the middle of the range where the amino acid isoelectric points are close together).

Optimisation of the combined FIA electrodialysis system

Selection of L-*AAOD and optimisation of enzyme-based amino acid detection.* The L-AAOD from *C. adamanteus* is not optimal as the detector for arginine because the selectivity of the enzyme for arginine is low compared to the response to other amino acids. The response to arginine, measured in a simple FIA system (consisting of the FIA system as described in the Experimental section but without the preceding electrodialysis unit) at pH 7.6 was only 11% of that to an equivalent concentration of phenylalanine. In addition, the L-AAOD from *C. adamanteus* has a low specific activity and hence it was necessary to use 3 sequential columns to obtain enough immobilised enzyme activity.

Therefore the selectivity of L-AAOD from other sources was compared, to try to find an enzyme with a larger relative response to arginine, and the L-AAOD detection procedure was optimised. L-AAOD from *C. atrox*, immobilised by glutaraldehyde crosslinking with bovine serum albumin (BSA) on a platinum electrode, was also investigated but did not provide any improvement in selectivity for arginine. The response to arginine at pH 8 was 4.5% of that to an equivalent concentration of phenylalanine. [In addition, the stability of the L-AAOD (*C. atrox*) electrodes was poor; these lost 85% of their response to 10 mM phenylalanine at pH-7 within 5 days.]

L-AAOD was also obtained from *Colletotrichum* sp. Using the enzyme immobilised on a CPG column, a large response to arginine was observed, which was 97% of that for an equivalent concentration of phenylalanine. This enzyme has a higher selectivity for arginine, and the specific activity is also higher, so it was possible to immobilise more units of enzyme activity per column than with L-AAOD from *C. adamanteus*. L-AAOD from *Colletotrichum* sp. immobilised on a CPG column was chosen as the most suitable for arginine detection. The pH dependence of the response to arginine is shown in Fig. 3 for one column using the enzyme from *Colletotrichum* sp., compared to 3 columns using the enzyme from *C. adamanteus*. L-AAOD from *Colletotrichum* sp. has a maximum response for 10 mM arginine at pH 7.6, whereas the maximum response of the enzyme from *C. adamanteus* is at a pH > 8. At pH 8, the peak height for *C. adamanteus* decreased with time, so pH 7.6 was generally used for arginine measurements with the enzyme from either source. The storage stability of the enzyme columns is shown in Fig. 4. The activity of the *C. adamanteus* L-AAOD

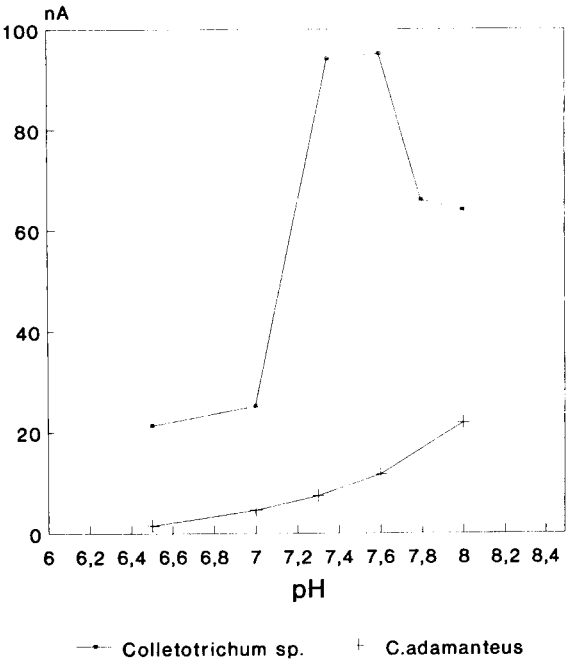

Fig. 3. Variation with pH of response to 10 mM arginine for L-AAOD immobilised on CPG columns. One column (10 U immobilised) was used for the enzyme from *Colletotrichum* sp., and three columns (4.5 U per column) were used for the enzyme from *C. adamanteus*.

columns stabilised on the 3rd day after immobilisation on CPG, and remained so for a further 14 days (activity measured 9 times in this period). Thereafter activity started to decrease. The activity of L-AAOD from *Colletotrichum* sp. also stabilised on the 3rd day after immobilisation on CPG and remained stable for a further 47 days (activity measured 10 times in this period). Therefore the L-AAOD–CPG column with the enzyme from *Colletotrichum* sp. has the advantage of longer stability of response, as well as higher relative selectivity for arginine.

Optimisation of electrodialysis conditions. It was observed that a peak occurred in the FIA system for the cathodic solution obtained for electrodialysis of buffer alone, which became larger with the age of the columns. The undesirable background peak could be reduced to a significant extent by incorporation of a catalase column before the L-AAOD columns(s), and this suggests that at least part of the background peak arises from hydrogen peroxide produced by electrodialysis of water in the electrodialysis cell.

Initially phosphate was used for electrodialysis, but the results were not good. Better separation was obtained with pyrophosphate pH 8.0. Migration of arginine to the cathode was also found to improve on increasing the pyrophosphate concentration from 0.1 to 0.2 M. The pump speed had little effect on migration of amino acids during electrodialysis, probably because of the large amount of gas produced in the electrode compartments. The potential across the electrodes in the electrodialysis cell was chosen as 20 V: 10 V was insufficient to produce good migration, and 30 V was too high, resulting in melting of the ion exchange membranes.

Although L-AAOD from *Colletotrichum* sp. was selected in the previous section as optimal for detection of arginine in the model electrodialysis FIA system, the enzyme also has a high relative selectivity for lysine. Under the electrodialysis conditions selected (0.2 M pyrophosphate pH 8), lysine will co-migrate with arginine to the cathode. No electrodialysis conditions could be found where arginine and lysine could be completely separated. It was therefore necessary to compromise by accepting interference from lysine in order to obtain a large enzymic response to arginine.

Influence of other amino acids on the separation of arginine. Before attempting complex mixtures, the influence of the presence of one other amino acid on arginine migration to the cathode was investigated. A solution containing 5 mM arginine and 5 mM of one other amino acid was electrodialysed and the response for the cathodic solution was compared with that for electrodialy-

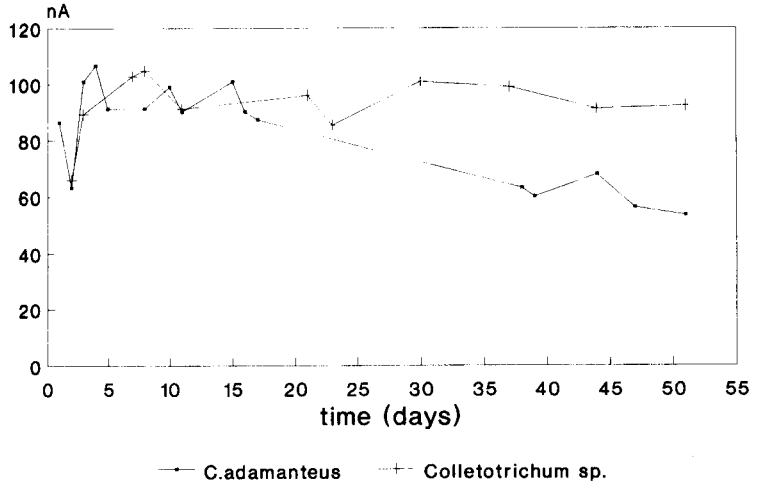

Fig. 4. Stability of L-AAOD–CPG columns for the enzyme from *C. adamanteus* and from *Colletotrichum* sp. The columns were as for Fig. 3, and the response was measured to 10 mM phenylalanine in 0.2 M potassium phosphate, pH 7.6.

sis of arginine alone (10 mM of each for lysine), shown in Fig. 5.

In the presence of nine of the amino acids, the response for electrodialysis of arginine plus a second amino acid differed by less than 10% from that for arginine alone (see next section). A larger response than arginine alone would occur if the second amino acid co-migrates to the cathode, and this is observed for electrodialysis of the arginine–lysine pair, as expected. However, a larger response is also seen in the presence of amino acids that were not expected from the results in Table 1 to migrate to the cathode. In addition, a smaller response is observed in the presence of some amino acids than for arginine alone, so it appears that amino acids may have a positive or negative influence on arginine migration, regardless of how they migrate themselves under these conditions. It is interesting that threonine (isoelectric point 6.53) does not influence arginine migration whereas both leucine and proline (6.02 and 6.3) do. Probably the influence of the second amino acid depends not only on the separation of its isoelectric point from that of arginine, but also on the individual amino acid characteristics.

Combined FIA system and its application

The combined FIA system used for determination of arginine concentrations in a mixture of amino acids is shown in Fig. 2. The sample was introduced into the electrodialysis cell and the cathodic solution was collected, which should contain the separated arginine. This was diluted with buffer to reach a pH of approximately 7.5, and the sample was measured in the FIA system with a *Colletotrichum* sp. column at pH 7.6.

Based on the results in Fig. 5, the following amino acids were chosen for inclusion in more complicated mixtures: asparagine, aspartic acid, glutamine, serine, valine, glycine, isoleucine, alanine, threonine. In each case the response for the amino acid plus arginine deviated by less than 10% from that for arginine alone. A calibration graph for arginine concentrations from 0 to 8 mM was obtained using the combined FIA electrodialysis system and this was used to estimate the arginine concentration in several mixtures. The

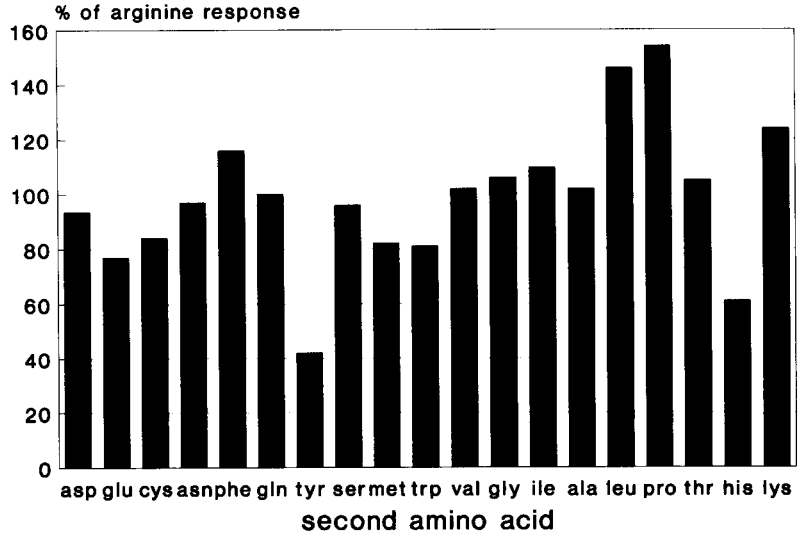

Fig. 5. Influence of the presence of one other amino acid on migration of arginine. The response obtained for electrodialysis of 5 mM arginine is taken as 100% and the responses measured for electrodialysis of 5 mM arginine in the presence of 5 mM of one other amino acid are given relative to this (10 mM of each for lysine as the second amino acid). 20 U of enzyme (*Colletotrichum* sp.) were immobilised on the enzyme column.

TABLE 2

Determination of arginine concentrations in mixtures, using the combined FIA electrodialysis system [10 U were immobilised on the L-AAOD-CPG column (*Colletotrichum* sp.)]

Other amino acids (concentration, mM)	Arginine (mM)	
	Added	Determined
thr 5; ile 5	5.0	5.1
ile 2; ala 1; asp 6	5.0	5.3
asn 3; ser 3	5.0	5.3
ser 1; val 1; gly 3	3.0	2.9
ser 3; val 4	3.0	2.6
asn 3; gln 3	6.0	6.1
ala 5; gln 5	5.0	4.8
ala 10; gln 10	5.0	4.8
thr 5; ala 5; gln 5	5.0	4.6
asn 5; gln 5	5.0	4.9
asn 3; gln 1; ser 3	7.0	7.7

results are given in Table 2 and in most cases, the estimated arginine concentration is in good agreement with that known to be in the mixture. Thus in the presence of some of the 9 amino acids listed above, good separation of arginine was achieved in these concentration ranges.

Conclusions

A method has been developed for continuous determination of one amino acid in a mixture, using separation by electrodialysis combined with a FIA system. The separation of arginine was used as a model to demonstrate the possibility of continuous amino acid measurement, and a group of nine amino acids were found in whose presence arginine concentrations could be determined with good accuracy using the combined FIA system. However, the presence of amino acids other than these nine interferes in the separation. The sensitivity of the system is limited because samples must be diluted into electrodialysis buffer before the separation step, and further dilution takes place in the FIA system. Sensitivity might be improved, and resolution of more complex mixtures achieved, by using a higher capacity electrodialysis cell e.g. the type used for desalinisation of water, which consists of several pairs of concentric ion-exchange membranes. Separation of arginine is just one application and it should also be possible to use the system for separation of other amino acids from a mixture e.g. by changing the electrodialysis conditions so that the desired amino acid migrates to the anode, or, in the absence of arginine and lysine, by migration of other amino acids to the cathode. The combined FIA system described here could be applied to determination of one amino acid in the presence of a few others, such as in the fermentation of bacteria which over-produce amino acids.

Another possibility is to use the combined FIA electrodialysis as a type of sensor "array" for simultaneous determination of concentrations of a pair of amino acids (in the absence of any others). Recent work in our group has shown that if two amino acids are measured by two independent sensors, the concentration of each amino acid can simultaneously be calculated by using an algorithm on the responses of the two sensors [13]. The FIA electrodialysis system described here might also be used as a sensor array to measure two amino acids whose partition ratios in the electrodialysis cell compartments are very different. For example, if the amino acid pair was leucine and isoleucine, it can be seen in Table 1 that more leucine partitions into the anodic compartment than remains in the middle, whereas the opposite is true for isoleucine. As long as the migration of leucine and isoleucine is independent of the other amino acid (which as shown for arginine in Fig. 5 is not always the case), it should be possible to work out an algorithm to calculate the individual concentrations of the two amino acids, based on the response obtained for the anodic and middle solutions after electrodialysis of a leucine–isoleucine mixture. Such a possibility would be particularly interesting because separation of leucine and isoleucine by normal electrodialysis would be difficult since their isoelectric points are so close together.

This work was supported by the Fraunhofer Gesellschaft, Institut für Lebensmitteltechnologie und Verpackung, München.

REFERENCES

1 S. Yabuki, F. Mizutani and M. Asai, Biosensors Bioelectronics, 6 (1991) 311.

2 E. Dempsey, J. Wang, U. Wollenberger and M. Oszoz, Biosensors Bioelectronics, 7 (1992) 323.
3 R. Kittsteiner-Eberle, I. Ogbomo and H.-L. Schmidt, Biosensors, 4 (1989) 75.
4 J. Moiroux and P. Elving, Anal. Chem., 50 (1978) 1056.
5 J.L. Romette, D. Thomas, J.S. Yang and H. Kusakabe, Biotechnol. Bioeng., 25 (1983) 2557.
6 G. Marko-Varga, E. Dominguez and M. Carlsson, GBF Monographs, 14 (1991) 165.
7 M. Nanjo and G. Guilbault, Anal. Chim. Acta, 73 (1974) 367.
8 C. Tran-Minh and G. Broun, Anal. Chem., 47 (1975) 1359.
9 T. Yao and T. Wasa, Anal. Chem., 209 (1989) 259.
10 H. Strathmann and H. Chmiel, Chem.-Ing.-Tech., 56 (1984) 214.
11 A.J.J. Debets, W. Th.Kok, K.-P. Hupe and U.A.Th. Brinkman, Chromatographia, 30 (1990) 361.
12 L.A. Lichtenberg and D. Wellner, Anal. Biochem., 26 (1968) 313.
13 U. Engelbrecht and H.-L. Schmidt, unpublished work.

Analytica Chimica Acta, 282 (1993) 379–388
Elsevier Science Publishers B.V., Amsterdam

Dual flow-injection analysis system for determining bromide and reactive phosphorus in natural waters

Paul R. Freeman, Barry T. Hart and Ian D. McKelvie

Water Studies Centre and Department of Chemistry, Monash University, P.O. Box 197, Caulfield East, Victoria 3145 (Australia)

(Received 3rd March 1993; revised manuscript received 18th May 1993)

Abstract

An inexpensive, dual flow-injection instrument for simultaneously determining low concentrations of both bromide and dissolved reactive phosphorus in natural waters is reported. An in-line C_{18} resin column was needed to remove interference in the bromide determination from dissolved organic matter present in most natural waters. The bromide method had a detection limit of 4 μg Br l^{-1} and was linear over the range 0–2 mg Br l^{-1} with good precision [C.V. 5.3% at 0.1 mg Br l^{-1} ($n = 10$) and 0.5% at 2.0 mg Br l^{-1} ($n = 10$)]. The dissolved reactive phosphorus method had a detection limit of 0.6 μg P l^{-1} and was linear over the range 0–50 μg P l^{-1} with good precision [C.V. 2.9% at 2.0 μg P l^{-1} ($n = 3$) and 0.5% at 50 μg P l^{-1} ($n = 3$)]. The dual method can analyse 30 samples per hour when analysing P and Br sequentially (35 samples per hour in simultaneous analysis mode) and has been used in field experiments to determine the spiralling of phosphorus in Myrtle Creek, Australia.

Keywords: Flow injection; Bromide; Nutrient spiralling; Organic matter, dissolved; Phosphorus

Despite phosphorus being one of the main nutrients controlling excessive algal growth in rivers and streams, its behaviour in these systems is still poorly understood. Although the dynamics of phosphorus in rivers and streams is considerably more complicated than in lakes, the development of the concept of phosphorus "spiralling" has been an important conceptual advance in understanding the behaviour of phosphorus [1–5]. In a particular system, the spiralling of phosphorus, which couples downstream displacement with conventional nutrient cycling, will be a time-varying function of physical (e.g., flow), chemical (e.g., adsorption) and biological (e.g. microbial uptake and decomposition) processes.

A number of methods have been used to study nutrient dynamics in streams [6]. Whole-stream solute injection experiments, where the reactive solute (e.g., phosphate) is injected with a conservative solute (e.g., bromide, chloride or rhodamine), have the advantage that both the ecological and the hydrological features of the stream are incorporated. This technique has been particularly useful in studying the biogeochemistry of nutrients [1–5,7,8] and heavy metals [9–11].

A particular difficulty with whole-stream experiments is the very large number of analyses required to provide the spiralling information. Much of our effort in recent years has been devoted to the development of rapid and inexpensive (and ultimately field-based) analytical methods based on flow-injection analysis (FIA) technology, for the determination of nutrients and conservative tracers. Previously, we reported low cost FIA instruments that can be used on-site (in a caravan) to determine dissolved organic phosphorus [12] and very low concentrations (ca. 0.1 μg l^{-1}) of dissolved reactive phosphorus

Correspondence to: I.D. McKelvie, Water Studies Centre and Department of Chemistry, Monash University, P.O. Box 197, Caulfield East, Victoria 3145 (Australia)

(DRP) [13]. We have also recently reported an FIA method for determining dissolved organic carbon in natural waters [14].

Bromide has been found to be the best conservative tracer for use in the Australian streams studied [5]. A number of flow injection methods have been reported for the determination of bromide. Both Anagnostopoulou and Koupparis [15] and Anfalt and Twengstrom [16] reported FIA methods for bromide determination based on the phenol red method; in this determination, chloramine-T oxidises any bromide in the sample to bromine, which in turn reacts with phenol red under acidic conditions (pH approximately 5–6) to produce an amount of a coloured compound (bromophenol blue) proportional to the original bromide concentration. Other spectrophotometric flow-injection methods for bromide include that reported by Yonehara et al. [17], where the catalytic effect of bromide on the hydrogen peroxide oxidation of pyrocatechol violet was used, and by Almuaibed and Townshend [18] using a silver thiocyanate minicolumn with the liberated thiocyanate determined spectrophotometrically with iron(III). Van Staden [19] used a coated tubular solid state bromide selective electrode for the determination of bromide in soils by flow-injection potentiometry.

In this paper we report the development of a dual channel FIA instrument that can be used on-site to obtain the concentrations of bromide and phosphorus simultaneously. The phosphate determination followed closely the method previously reported by Freeman et al. [13]. Bromide was determined colorimetrically using the phenol red procedure [20] and a manifold configuration similar to that reported by Anagnostopoulou and Koupparis [15]. This development should considerably reduce the time taken for whole-stream nutrient addition experiments and will allow more

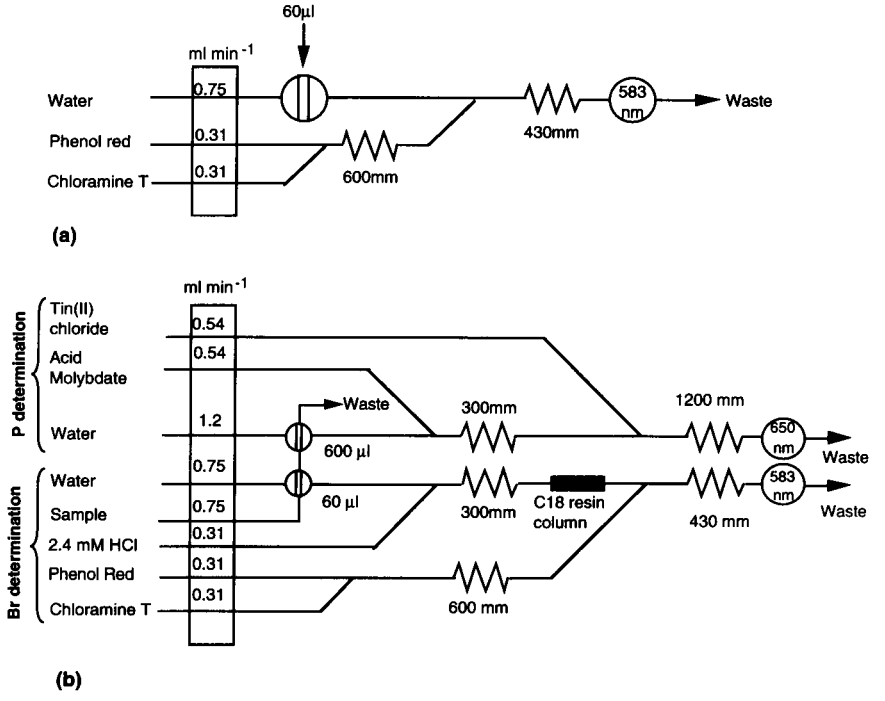

Fig. 1. (a) Development manifold for the determination of bromide using the phenol red procedure. (b) Dual manifold for the determination of bromide and dissolved reactive phosphorus.

immediate information on the progress of the experiment to be obtained

EXPERIMENTAL

Reagents

All reagents were analytical reagent grade. Deionized water (Waters Milli-Q) was used to prepare all reagents. Acidic molybdate and tin(II) chloride reagents for determination of dissolved reactive phosphorus were prepared as described by Freeman et al. [13]. Phenol red and chloramine-T trihydrate were prepared as a 20 mg l^{-1} solution in 0.05 M acetate buffer and 200 mg l^{-1} in Milli-Q water respectively (20 mg l^{-1} solution in 0.5 M acetate buffer and 800 mg l^{-1} in Milli-Q water respectively for the reagents of Anagnostopoulou and Koupparis [14]).

Manifolds

The manifold configuration for determination of bromide is shown in Fig. 1a, while Fig. 1b shows the dual bromide/phosphate manifold, which includes an in-line clean-up column to eliminate naturally occurring dissolved organic compounds which interfere with the bromide determination. PTFE tubing (0.5 mm i.d.) was used exclusively in the manifolds, and two Ismatec CA-4-E panel mount peristaltic pumps (pump speed 20 rpm) were used for sample and reagent delivery. The injection system was controlled by a laptop IBM PC/XT compatible computer (Bondwell PRO-8T) interfaced to the instrument. This interface also enabled the computer to digitise the detector output, display it on screen and save data to disc.

Injection system

Sample injection for bromide analysis was achieved using a solenoid valve system, and a pneumatically-actuated Rheodyne 5020 valve was used for phosphate determinations. The Rheodyne system was used because it had been utilized in a DRP analyser developed previously [13]. The solenoid injection system used for bromide utilized a pair of Lee LFAA miniature 3-way solenoid valves. These were connected such that it was possible to substitute the sample for the carrier, with the carrier going to waste (Fig. 2). By suitable selection of sample flow-rate and solenoid switching time, the volume of sample metered into the carrier stream could be accurately controlled. At the end of the injection sequence, the carrier was restored and the sample diverted to waste. In this system, the sample and carrier flow-rates were the same. This eliminated any change in the final reagent composition and minimized flow disturbances and concomitant detector responses. The valves were

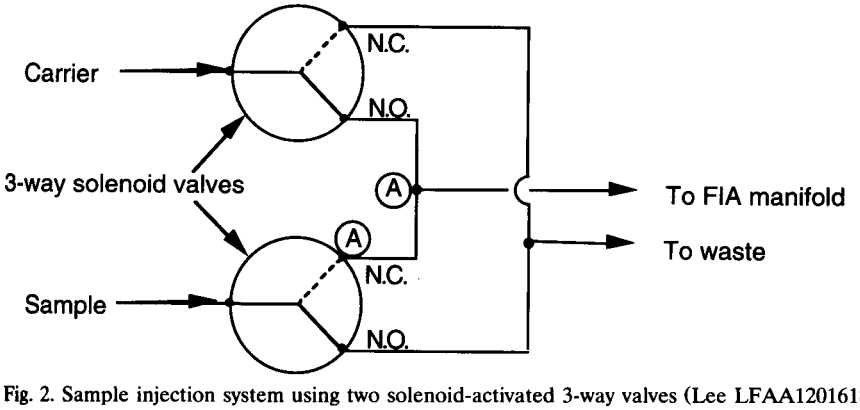

Fig. 2. Sample injection system using two solenoid-activated 3-way valves (Lee LFAA1201618H).

wired in parallel and activated from the computer through a solid state relay. Plumbing connections were made using 1.59 mm stainless steel tee-pieces (SGE SSLHT/16) and 0.3 mm i.d. PTFE tubing.

Computer interface

The computer interface was designed and built in-house such that it could be connected to any computer having a RS232C serial interface. It consisted of an 8-bit microprocessor controller (Motorola 68HC705) which had three 8-bit input/output ports, 176 bytes of RAM, 7744 bytes of EPROM and a TTL level serial interface, and a 12-bit dual-slope analogue-to-digital converter (Intersil ICL7109). The interface could individually switch two solid state relays and digitise two analogue voltage signals, essentially simultaneously, at up to 8 samples per second per input. Control software on the computer was written in QuickBasic (Microsoft).

Determination of bromide and dissolved reactive phosphorus (DRP)

Bromide was determined colorimetrically using the chloramine-T–phenol red procedure of Anagnostopoulou and Koupparis [15]. The amount of bromophenol blue produced was measured photometrically using a simple photometer previously reported by Freeman et al. [13], but with a ultra-bright yellow light emitting diode (LED) source (RadioSpares 588-279) and a photodiode detector (RadioSpares 303-719). These components were mounted in a black perspex flow cell (20 mm optical path length). The λ_{max} for the bromophenol blue species at the pH of the test was 590 nm which was close to the wavelength of maximum emission for the yellow LED (583 nm).

The determination of dissolved reactive phosphorus has been reported previously and involves the phosphomolybdate method with stannous chloride reduction [13]. Tartaric acid was added to the molybdate reagent to eliminate interference from silicate.

A dual flow-injection manifold (Fig. 1b) was constructed to measure bromide and dissolved reactive phosphorus simultaneously in water samples collected from whole-stream release experiments. The two flow-injection systems were connected in series so that the waste line from the bromide injector was connected to sample inlet line of the Rheodyne valve. Since the carrier was directed to waste during the sample injection to the bromide line, it passed through the phosphate injector and because it was distilled water, did not cause any interference with the phosphate analysis. Thus, so long as the timing of the two injection sequences was consistent and reproducible, the amount of distilled water and sample injected into the phosphate manifold was also constant.

Recording of the phosphate and bromide detector outputs was accomplished using the two channel analogue to digital interface described above.

Resin cleanup procedure

Preliminary experiments showed that less than 100% recovery of added bromide was achieved with some natural water samples, presumably because of reaction between bromide and certain brominable organic compounds present. Experiments using anionic (AG1-X8, AG3-X4), cationic (AG50-X8) and non-ionic (XAD-2, XAD-8, C_{18} Sep-Pak) resins indicated that only the non-ionic resins showed any potential to reduce the concentration of natural organic matter in natural waters. For this reason, only the three non-ionic resins XAD-2 (Amberlite, 20–50 mesh), XAD-8 (Amberlite, 20–50 mesh), and resin from a C_{18} Sep-Pak (Millipore–Waters) were evaluated. Small columns containing each resin were prepared from 2.8 mm internal diameter PVC peristaltic pump tubing. The influence of the amount of resin was investigated using different length columns (20 mm, 50 mm and 90 mm) of the XAD-8 resin only.

Two matrices were used to assess the recovery of bromide; Milli-Q water and a solution made by adding dissolved organic matter (DOM, 4.8 mg C l^{-1}) to Milli-Q water (DOM was obtained by leaching leaves collected from beside Myrtle Creek). Experiments were undertaken at pH 2 and pH 3, adjusted using hydrochloric acid. Each experiment used the standard bromide manifold

shown in Fig. 1a, but with the resin column placed in the carrier line after the sample injection valve.

RESULTS AND DISCUSSION

Injection system

The solenoid injection system was investigated for its suitability in semi-automated field FIA systems as an alternative to the conventional rotary injection valve. It was considered to have a number of advantages over its counterpart, namely; in Australia, it is relatively inexpensive when compared with a rotary injection valve and associated pneumatic or electrical actuator assembly, uses little power (490 mW) and operates from a low voltage DC supply (e.g., 12 V) making it suitable for battery operation, is compact (approximately $40 \times 30 \times 15$ mm), has a fast response (12 ms) and is very reliable (manufacturer's quoted lifetime of approximately 200 million cycles).

The system has one disadvantage which results from the internal dead volume of the solenoid valves and the connecting tubing, namely that the first few injections in a sequence of replicate injections may not fully represent the actual sample being analysed. This occurs because the first injection volume includes a portion of the previous sample contained in the valve and tubing between the valve outlet and the tee-piece connecting to the carrier line of the manifold (between points marked A in Fig. 2). The magnitude of this effect depends on the volume of the next sample injected. In the system described, when injection volumes of approximately 60 μl are used, only the first injection is affected. This problem was overcome by making one sacrificial injection.

Optimization of bromide method

The initial FIA conditions used were based on those reported by Anagnostopoulou and Koupparis [15]. Four pump tubes were used (two 1.6 ml min^{-1} and two 0.61 ml min^{-1}), however mixing coils of different lengths were employed and the XAD-2 resin column used by Anagnostopoulou and Koupparis [15] was omitted, because it was thought to be unnecessary with the pristine stream waters being analysed. The flow-injection manifold arrangement for this initial system is shown in Fig. 1a, but with the two mixing coils swapped around. The injection volume was 60 μl. This system was found to have an unacceptably noisy baseline, with the quality typical of that found previously in the development of the FIA DRP method and thought to be due to differences in mixing efficiency.

Manifold / reagent experiments. A series of experiments were conducted in which the concentrations and flow-rates of phenol red and chloramine-T lines were decreased in an attempt to reduce the baseline noise and optimise the reagent concentrations. The initial flow-rates were reduced proportionally, keeping the same relative flow-rates of carrier and reagents, namely: carrier, 0.75 ml min^{-1}; phenol red, 0.31 ml min^{-1}; chloramine-T, 0.31 ml min^{-1}. At these lower flow-rates, the sensitivity decreased by 72% at 2 mg Br l^{-1} but the baseline noise remained essentially unchanged. Despite the loss in sensitivity, these flow-rates were adopted because of the lower reagent consumption (a major consideration for field use) and the slight improvement in linearity.

The order of the reagent addition was also tested. Adding the chloramine-T before the phenol red (with a 430 mm mixing coil in between) resulted in a slight loss in sensitivity (17% at 1 mg Br l^{-1}) compared to adding the phenol red first. Interestingly, both these sequential additions of reagents were more sensitive than when the reagents were used in the premixed configuration; e.g., the phenol red then chloramine-T sequence had twice the sensitivity compared with the premixed configuration. Unfortunately, the sequential addition of reagents resulted in an approximate doubling of the baseline noise, so that little overall advantage was gained with this configuration. The pre-mix configuration was selected for the final setup.

A series of experiments to investigate the effect of modifying the concentrations of the two reagents (phenol red–acetate buffer and chloramine-T) were undertaken. Chloromine-T was varied four-fold (from 0.8 g l^{-1} to 0.2 g l^{-1}) and

the acetate buffer in the phenol red reagent was varied ten-fold (from 0.50 M to 0.05 M). The influence of these changes on the signal peak height are shown in Table 1.

Reduction of the chloramine-T concentration four-fold and the acetate buffer concentration ten-fold produced almost a three-fold increase in sensitivity over that obtained using the previously reported reagent concentrations [15]. Additionally, these reduced reagent concentrations resulted in improved linearity for the range 0–5 mg l^{-1} ($r^2 = 0.968$ for original reagents; $r^2 = 0.986$ for final reagents), and less baseline drift. The baseline noise also decreased slightly from 5 mV to 3 mV, probably because of reduced fluctuations in refractive index and absorbance during the mixing processes when the diluted phenol red reagent was used. This decreased baseline noise coupled with the sensitivity increase meant that the signal-to-noise ratio actually increased (e.g., at 2 mg Br l^{-1}, the signal to noise ratio was 38 with the original reagents and 88 with the final reagent composition.

Removal of interference from dissolved organic matter

Preliminary experiments with natural waters from Myrtle Creek, a small stream with quite low concentrations of dissolved organic matter (ca. 2 mg C l^{-1} [4]), showed that the recovery of bromide was reduced by approximately 25%. This was somewhat unexpected as we did not expect any significant interference at these low DOM concentrations.

TABLE 1

Variation in peak height response to changes in phenol red, chloramine-T and acetate buffer concentrations

Chloramine-T (g l^{-1})	Phenol red (g l^{-1})	Acetate buffer (M)	Peak height [a] (mV)
0.8	0.02	0.50	133 (3.0)
0.4	0.02	0.50	297 (5.8)
0.4	0.01	0.25	355 (1.2)
0.4	0.02	0.05	338 (2.0)
0.2	0.02	0.05	351 (1.2)

[a] Average of triplicates, standard deviation in brackets.

TABLE 2

Recovery of bromide (%) added to Milli-Q and Myrtle Creek water containing different concentrations of added ammonium ions

Ammonia conc. (mg l^{-1})	Bromide conc.			
	0.25 mg l^{-1}		1.0 mg l^{-1}	
	Milli-Q	Myrtle Ck	Milli-Q	Myrtle Ck
Nil	100	77	100	82
0.1	94	73	100	81
1.0	91	67	101	80

Of the many compounds that are known to interfere with the phenol red bromide determination [15,21,22], two, ammonia and brominable organic compounds, were assessed as the most likely interferences in the Myrtle Creek samples analysed. To test this, a series of experiments in which samples of either distilled water and Myrtle Creek stream water were spiked with known quantities of either ammonia or dissolved organic carbon together with bromide and the bromide concentration determined.

The experimental results show that the interference from ammonia is small (Table 2). For example, in Milli-Q water an added concentration of 1 mg l^{-1} of ammonia resulted in a 9% reduction in the recovery at 0.25 mg l^{-1} of bromide, but no reduction in recovery at a higher bromide concentration of 1.0 mg l^{-1} In Myrtle Creek water, the recovery of bromide was reduced by 23% at 0.25 mg Br l^{-1} and by 18% at 1.0 mg Br l^{-1} even when no ammonia was added. Subsequently, the addition of ammonia caused a further reduction in recovery at the lower bromide concentration, but little change at the higher bromide concentration (Table 2).

Anagnostopoulou and Koupparis [15] overcame the problem of brominable organic compounds in pharmaceutical preparations by removing them using an XAD-2 resin column placed in the flow-injection manifold immediately after the injection valve.

As well as investigating the XAD-2 resin, two other resins (C_{18} and XAD-8) were tested for their efficiency at removing dissolved organic matter in natural waters. Samples of Milli-Q wa-

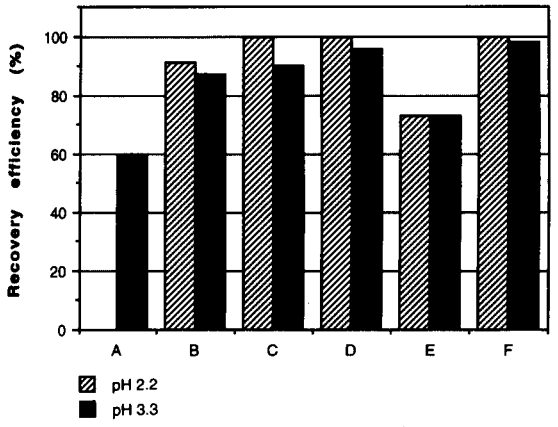

Fig. 3. Recovery efficiency for 1.0 mg Br l^{-1} added to Milli-Q water containing 4.8 mg C l^{-1} using different resin columns. A, no column; B, 20 mm XAD-8 column; C, 47 mm XAD-8 column; D, 90 mm XAD-8 column; E, 50 mm XAD-2 column; F, 20 mm C_{18} column.

ter containing 1.0 mg Br l^{-1} and 4.8 mg C l^{-1} (as leaf leachate) were adjusted to either pH 2.2 or pH 3.3 using hydrochloric acid and analysed for bromide using the FIA manifold shown in Fig. 1a, except that the test resin column was inserted in the carrier line immediately after the injection valve but before the reagent confluence point. No changes were made to the composition of the carrier or reagents.

Acidification of the samples was performed to increase the degree of protonation of the acidic functional groups of the dissolved organic carbon compounds. This enhances their affinity for the non-ionic resin material, and hence their removal from solution.

The experimental results showed that the recovery efficiency depended on the resin type, the column length and the pH of the sample (Fig. 3). The 20 mm C_{18} column gave the best recovery followed by the three XAD-8 columns (90 mm, 47 mm and 20 mm) and then the 50 mm XAD-2 column. It is not possible from these experiments to determine whether the better performance of the C_{18} resin was a function of the resin material or the smaller particle size (and hence larger surface area), or both.

There was little difference in the recovery of 1.0 mg Br l^{-1} at pH 2.2 (101%) and at pH 3.3 (98%) for this C_{18} column. For both the C_{18} and XAD-8 columns, the recovery appeared to be greatest at pH 2.2, although the difference between pH 2.2 and pH 3.3 was not significant. The slightly better recovery of bromide at the lower pH is probably related to the greater uptake of the dissolved organic matter at this lower pH, and the consequent smaller amount left in solution to interfere with the bromide determination.

Although the 47 mm XAD-8 column produced good recovery of 1.0 mg Br l^{-1} at both pH 2.2 (101%) and pH 3.3 (90%), the peak appearance time and peak dispersion increased as a consequence of the length of the column.

There was little difference in sensitivity at the two pH values with either the XAD-2 or XAD-8 columns. For example, for a 1.0 mg Br l^{-1} standard the peak height at pH 2.2 was 89% of that at pH 3.3 for both the XAD-2 (50 mm) and XAD-8 (47 mm) columns. With a 0.25 mg Br l^{-1} standard the peak height at pH 2.2 was 92% of that at pH 3.3 for the XAD-2 column, and 94% for the XAD-8 column.

During these experiments, it was noted that when a sample consisting only of Milli-Q water and added dissolved organic matter was injected into the manifold without a resin column, a small negative peak was produced at the time corresponding to the bromide peak. This is probably due to the dissolved organic matter binding a fraction of the phenol red, leading to a small reduction in the colour of the reagent. A negative response was also produced by the blank solutions (with and without added dissolved organic matter) at pH 2 (but not at pH 3) for all the resin columns tested.

It was decided that the best combination of conditions required to reduce the DOM interference was a C_{18} resin column run at pH 3. The choice of pH 3 was a trade-off between a slightly lower recovery, and the absence of negative peaks. Another advantage in using pH 3 was the considerably lower chloride concentration (345 mg l^{-1} at pH 2 compared with 35 mg l^{-1} at pH 3) resulting from the use of less hydrochloric acid. The lower chloride concentration should also allow the C_{18} column to be used in conjunction with the ion-exchange preconcentration method

(using AG1-X8 resin) for the determination of very low concentrations of dissolved reactive phosphorus described by Freeman et al. [13]. It was previously shown that the ion-exchange preconcentration efficiency was sensitive to the chloride concentration, which needed to be kept below 100 mg Cl l^{-1}.

Fig. 1b shows the modified bromide manifold, with in-line acidification of the samples and a resin column to remove dissolved organic matter. The hydrochloric acid line merges with the sample from the injection valve prior to the resin column. A 300 mm mixing coil was inserted after the confluence point to ensure adequate mixing of the sample and acid. The concentration of hydrochloric acid was calculated to produce a nominally pH 3 carrier stream prior to the resin column and the point at which the reagents are added. The actual pH of the acidified carrier was measured as 3.3. Acidification of the carrier had only a slight affect on the pH of the final reaction mixture (measured on the eluent after the flow cell), decreasing it from 4.67 to 4.63. This is similar to the final mixture pH in the manifold configuration without the acid line (pH 4.68). Obviously the buffer capacity is sufficient to overcome the additional acid.

Precision and linearity

The precision of bromide and phosphate determinations using the dual manifold configuration, recorded as the relative standard deviation for 10 determinations at concentrations of 0.1–2.0 mg l^{-1} for bromide and 2.0–50.0 μg l^{-1} for phosphorus are shown in Table 3. The phosphate data are taken from Freeman et al. [13]. Precision for the bromide determination ranged between 0.3 and 5.3% and for phosphorus between 0.5 and 2.9%.

Linearity of the bromide FIA method was determined using eight standards in the range 0–2 mg Br l^{-1} and gave the following linear regression:

$$\text{peak height (mV)} = -0.78 + 170[\text{Br(mg } l^{-1})]$$

$$r^2 = 0.998$$

The relationship between peak height and bromide concentration was slightly sigmoidal, but is well approximated by a linear regression. The linear regression equation obtained for the dissolved reactive phosphorus determination using standards in the range 0–50 μg P l^{-1} was:

$$\text{peak height (mV)} = 1.53 + 6.25[\text{P}(\mu\text{g } l^{-1})]$$

$$r^2 = 1.000$$

The detection limit for the bromide determination was 4 μg Br l^{-1} and for phosphorus was 0.6 μP l^{-1} In both cases the detection limit was taken as 3 times the standard deviation of the determinand in Milli-Q water for 10 determinations.

TABLE 3

Precision [as coefficient of variation (C.V.)] for the bromide and soluble reactive phosphorus determinations in the dual FIA system measured in Milli-Q water standards

Bromide			Phosphorus		
Conc. (mg Br l^{-1})	Peak ht. (mV)	C.V. ($n = 10$) (%)	Conc. (μg P l^{-1})	Peak ht. (mV)	C.V. ($n = 3$) (%)
0.0	0.7	28	2.0	14.0	2.9
0.10	12.8	5.3	5.0	28.8	2.8
0.25	29.6	0.8	10	65.9	1.3
0.50	68.1	2.3	20	130	1.8
0.75	109	0.7	50	313	0.5
1.0	154	0.4			
1.5	248	0.3			
2.0	336	0.5			

Application of the dual system

The stimulus for developing the dual FIA system reported here was to simplify the analysis of the large number samples collected during whole-stream experiments undertaken to provide information on the spiralling (cycling) of phosphorus in small streams. Whole-stream experiments involve adding a solution of orthophosphate and bromide (as the conservative tracer) to a stream at a constant rate over a known time period, with samples collected over time at one or more downstream sites; ideally, the release time should be sufficient for the phosphorus and bromide concentrations to reach a plateau at the downstream locations.

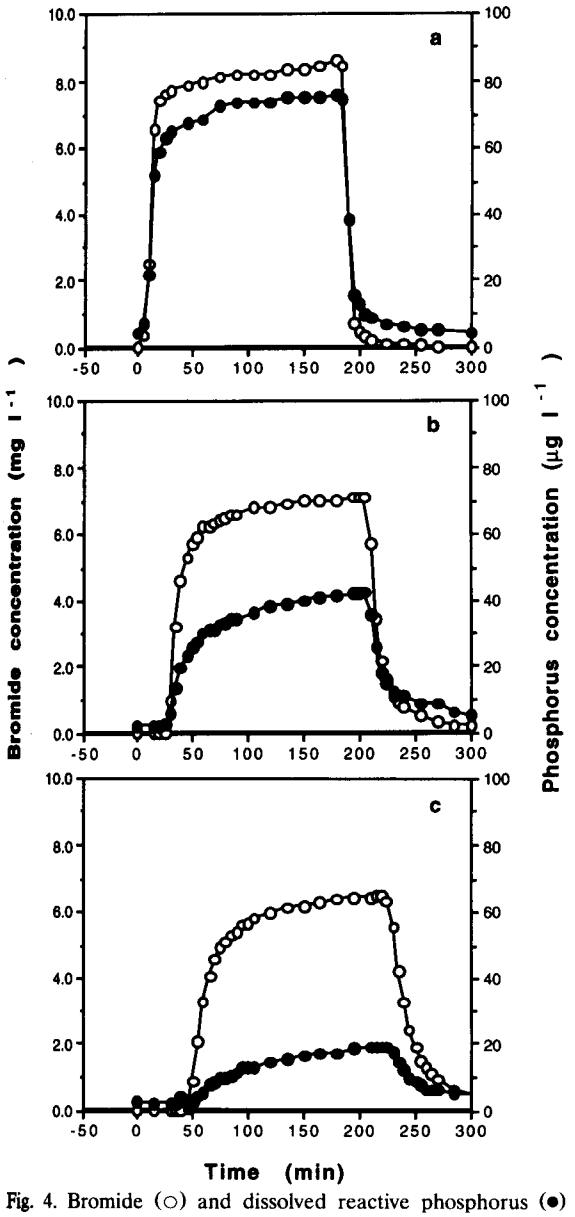

Fig. 4. Bromide (○) and dissolved reactive phosphorus (●) concentration vs. time at three distances (a, 23 m; b, 101 m; c, 157 m) downstream of a release of bromide and orthophosphate made over 3 h to Myrtle Creek, Australia.

Figure 4 shows the results of the changes in the concentrations of both DRP and bromide with time at three downstream locations for a three hour release experiment undertaken in Myrtle Creek, Australia. Samples were taken by hand at approximately 5 min intervals during the passage of the pulse and at 15 min intervals for a further 3 h after the pulse had passed. The samples were filtered (0.4 μm Nuclepore) and then analysed (in triplicate) using the dual FIA instrument located in a caravan at the side of the stream. The change in the bromide concentration with distance downstream is mainly due to dispersion, but also to short-term losses of bromide in off-channel pools (transient storage). The behaviour of conservative solutes such as bromide can be well simulated using a one-dimensional transient storage computer model [4–8]. In addition to dispersion and transient storage, the phosphorus concentration was reduced during the downstream passage of the pulse due to uptake by the sediments [4,5].

In simultaneous mode (i.e., phosphorus and bromide analysed at the same time) approximately 35 samples h^{-1} can be analysed. In sequential mode, where the bromide analysis is followed by the analysis of phosphorus, a slightly reduced sample throughput of ca. 30 sample h^{-1} was achieved.

The authors express their gratitude to the Australian Water Research Advisory Council (now the Land and Water Research and Development Corporation) for funding this study. We are also grateful to the Melbourne Water Corporation for permitting us the use of Myrtle Creek, and to Pat O'Shaughnessy for facilitating our studies.

REFERENCES

1 J.W. Elwood, J.D. Newbold, R.V. O'Neill R.V. and W. Van Winkle, in T.D. Fontine and S.M. Bartell (Eds.), Dynamics of Lotic Ecosystems, Ann Arbor Sci. Publ., Ann Arbor, MI, 1983, pp. 3–27.
2 P.J. Mulholland, A.D. Steinman and J.W. Elwood, Can. J. Fish. Aquatic Sci., 47 (1990) 2351.
3 J.L. Meyer, W.H. McDowell, T.L. Bott, J.W. Elwood, C. Ishizaki, J.M. Melack, B. L. Peckarsky, B.J. Peterson and P.A. Rublee, J.N. Am. Benthol. Soc., 7 (1988) 410.
4 B.T. Hart, P. Freeman, I.D. McKelvie, S. Pearse and G.R. Ross, Verh. Internat. Verein. Limnol., 24 (1990) 2065.
5 B.T. Hart, P. Freeman and I.D. McKelvie, Hydrobiol., 235/236 (1992) 573.
6 Stream Solute Workshop, J.N. Am. Benthol. Soc., 9 (1990) 95.

7 F.J. Triska, V.C. Kennedy, R.J. Avanzino, G.W. Zellweger and K.E. Bencala, Ecology, 70 (1989) 1877.
8 F.J. Triska, V.C. Kennedy, R.J. Avanzino, G.W. Zellweger and K.E. Bencala, Ecology, 70 (1989) 1893.
9 B.M. Chapman, D.R. Jones and R.F. Jung, Geochim. Cosmochim. Acta, 47 (1983) 1957.
10 J.S. Kuwabara, H.V. Leland and K.E. Bencala, J. Environ. Eng., 110 (1984) 646.
11 D.M. McKnight, B.A. Kimball and K.E. Bencala, Science, 240 (1988) 637.
12 I.D. McKelvie, B.T. Hart, T.J. Cardwell and R.W. Cattrall, Analyst, 114 (1989) 1459.
13 P.R. Freeman, I.D. McKelvie, B.T. Hart and T.J. Cardwell, Anal. Chim. Acta, 234 (1990) 409.
14 R.E. Edwards, I.D. McKelvie, P. Ferrett, B.T. Hart, J.B. Bapat and K. Koshi, Anal. Chim. Acta, 261(1992) 287.
15 P.I. Anagnostopoulou and M.A. Koupparis, Anal. Chem., 58 (1986) 322.
16 T. Anfalt and S. Twengstrom, Anal. Chim. Acta, 179 (1986) 453.
17 N. Yonehara, S. Akaike, H. Sakamoto and M. Kamada, Anal. Sci., 4 (1988) 273.
18 A.M. Almuaibed and A. Townshend, Anal. Chim. Acta, 245 (1991) 115.
19 J.F. Van Staden, Analyst, 112 (1987) 595.
20 APHA, Standard Method for Analysis of Waters and Wastewaters, 19th edn., American Public Health Association, Washington, DC, 1990.
21 L.B. Basel, J.D. Defreese and D.O. Whittemore, Anal. Chem., 54 (1982) 2040.
22 D. Jones, CSIRO Div. of Coal Research, personal communication.

Analytica Chimica Acta, 282 (1993) 389–395
Elsevier Science Publishers B.V., Amsterdam

Flow system based on sequential delivery of air-sandwiched solutions into a micro cell for spectrophotometric catalytic analysis

Susumu Kawakubo, Masaaki Iwatsuki and Tsutomu Fukasawa

Department of Applied Chemistry and Biotechnology, Faculty of Engineering, Yamanashi University, Takeda-4, Kofu-shi 400 (Japan)

(Received 16th March 1993; revised manuscript received 17th May 1993)

Abstract

An air-sandwiched sample, reagent solutions and water with a total volume of 317 μl are sequentially delivered by air carrier through PTFE tubing of 1 mm i.d. into a micro cell, where the solutions are mixed to start reaction, and the absorbance is measured against reaction time. This flow system was compared with the stopped-flow/flow-injection and manual batch techniques with regard to the determination of 20–500 ng of sulphide by measuring the decolorization rate of Methyl Orange with bromate. In the proposed flow system, a micro sample is diluted only with limited small volumes of reagent solutions and free from the additional dilution due to dispersion of the reacting solution. Therefore, the absolute sensitivity was ten times that of the manual batch technique using a millilitre-level sample and three times that of the stopped-flow/flow-injection technique.

Keywords: Catalytic methods; Flow system; UV–Visible spectrophotometry; Sulphide

Any catalytic analysis based on the measurement of a parameter related to reaction rate is intrinsically susceptible to the influence of reaction conditions such as reagent concentrations, reaction time and temperature of reacting solution, in addition to the other reaction conditions in static methods such as conventional spectrophotometry. In the manual batch technique, however, rigid control of such reaction conditions is not easy, especially for small volumes of solutions.

Flow-injection analysis (FIA) [1,2] allows easy control of the reaction conditions even with the use of microsamples of 10–100 μl. However, the sensitivity of determination is decreased owing to significant dilution of the sample due to dispersion of the reacting solution in addition to dilution with reagent solutions. The small pulse-like variations of reagent concentrations in an FIA system caused by pumping also lead to an amplified and synchronized variation of the reaction rate, which also affects the precision and sensitivity of catalytic analysis [3]. The stopped-flow (SF)/FIA technique [1] using a short reaction tube allows the dispersion of the sample zone to be decreased, but does not make the dispersion negligible. In a "monosegmented continuous-flow analysis" (MCFA) method [4,5], which was proposed to decrease the dispersion, the reagents and sample solutions were first mixed at a mixing point, sandwiched between two air bubbles and then introduced into a reaction tube by a water carrier stream. After a fixed time, the central part of the reacting solution was taken into the another water carrier stream to be delivered into a flow cell. However, the MCFA system still seems

Correspondence to: S. Kawakubo, Department of Applied Chemistry and Biotechnology, Faculty of Engineering, Yamanashi University, Takeda-4, Kofu-shi 400 (Japan).

to be accompanied by dilution and dispersion comparable to those in SF/FIA. The dispersion was effectively eliminated in an air-segmented continuous-flow analysis (ASCFA) method [2], using a Technicon AutoAnalyzer, in which solution streams were segmented by many air bubbles. However, this requires electronically discrete measurement [6] or physical removal of air bubbles [2] from the reacting sample zone for absorbance measurements. In addition, a well controlled system is required to supply stable and continuous streams of air and reagent solutions, because the volume of air bubbles is altered by variations of the pressure in the flow system. Hence the ASCFA instrument is complicated and expensive.

Gas (or air) carrier flow systems [7–12] are potentially usable in microscale kinetic analysis. In automated micro batch analysers [7–11], a nitrogen gas pressure was applied for defined periods to deliver limited volumes of reagent solutions without any dispersion through parallel tubings from the reservoirs to a reaction chamber, where the absorbance measurement was carried out. However, this delivery technique required a microcomputer for rapid and accurate control of the delivery time. In another air carrier flow system [12], limited volumes of solutions were sequentially or simultaneously loaded through a split-loop injector [13] or other types of injection system into a flow line, and then delivered into a flow cell through a mixing coil by the aspiration of the carrier.

This paper describes a flow system based on the sequential delivery of air-sandwiched solutions (SDAS) through a short tube by air carrier into a micro cell, where the reaction is started and the absorbance is measured for microscale catalytic analysis. The SDAS technique is free from both dispersion and the effect of flow-rate variations of the air carrier, and the sample solution is not accompanied by any dilution except for limited dilution with reagent solutions. Thereby the SDAS technique allows more sensitive and precise analysis than FIA and the other techniques described above. The analytical performance of the SDAS technique was investigated in detail by mixing of Methyl Orange (MO) solution and water, and compared with that of the manual batch and the SF/FIA techniques for the catalytic determination of sulphide using a colour-fading reaction of MO with bromate [14].

EXPERIMENTAL

Reagents

All chemicals were of analytical-reagent grade and distilled deionized water was used throughout. MO solutions were prepared by dissolving the reagent in dilute HCl. The concentration of HCl in the MO solution was determined by acid–base titration with standard Na_2CO_3 solution. Bromate solution was prepared by dissolving the potassium salt in water. A stock standard of solution sulphide (2.00 g S^{2-} l^{-1}) was prepared by dissolving $Na_2S \cdot 9H_2O$ in 0.052 M $NaHCO_3$–0.048 M Na_2CO_3 buffer solution (pH 10), followed by the iodimetric titration. Working standard sulphide solutions were prepared by diluting the stock standard solution with water.

SDAS technique

SDAS flow system. Figure 1 shows the flow system of the proposed SDAS technique. The air carrier was supplied into the flow line by an Atto Model SJ-1220 peristaltic pump (P_1) through a Millipore filter (F) with pore size of 0.2 μm. Three septum-type injectors (I_1–I_3), a valve-type injector (I_4) consisting of two three-way valves with a sample loop (117 μl; the fractional volume is due to the rough design of the loop) and a laboratory-made 10-mm micro cell (C) were connected in series by PTFE tubing and Daiflon connectors of 1 mm i.d. A flow line as short as possible was constructed to minimize the flow resistance of solution. A strongly acidic reagent solution was fed into I_4 by an Atto Model SJ-1211 peristaltic pump (P_2). The flow rate of the air carrier in the system was adjusted at 13 ml min^{-1} without any solution. The injectors and flow line were immersed in a thermostated water bath (30 ± 0.5°C) to keep the injected solutions at a constant temperature. The micro cell was kept at the same temperature by circulating the water

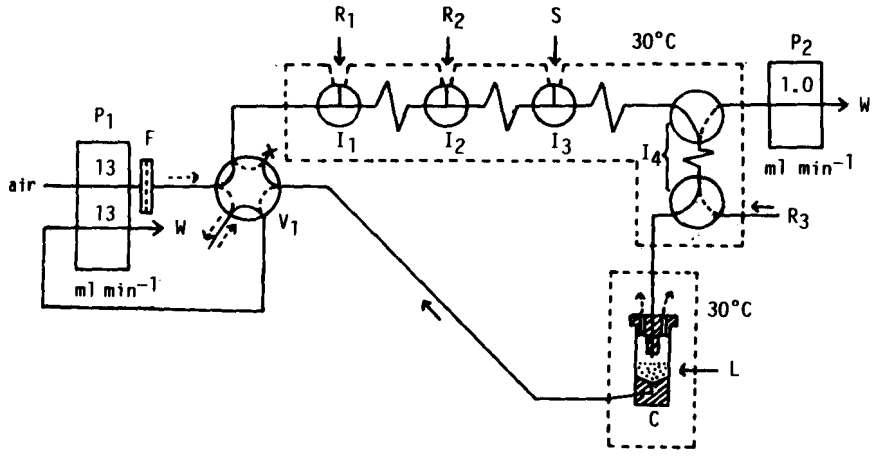

Fig. 1. SDAS flow system. P_1, P_2 = peristaltic pumps; F = filter; R_1 = water; V_1 = six-way valve; R_2 = $KBrO_3$ solution; R_3 = MO–HCl solution; S = sample; I_1–I_3 = syringe-type injectors; I_4 = valve-type injector; C = micro cell (see Fig. 2); L = irradiation light beam; W = waste.

from the same water-bath to a cell holder of a spectrophotometer as shown later.

Figure 2 shows the details of the micro cell, which was made of hydrophobic acrylic resin plates of 3 mm and 1 mm thickness and PTFE tubing of 1 mm i.d. The dimensions of cell were designed to exclude air bubbles in the reacting solution and to minimize the residual solution on its wall and funnel-like bottom after a measurement. After absorbance measurement, the solution in the cell was drained out and discarded by the operation of P_1. The irradiation beam was masked to give a beam cross-section of 1.5 mm × 5 mm.

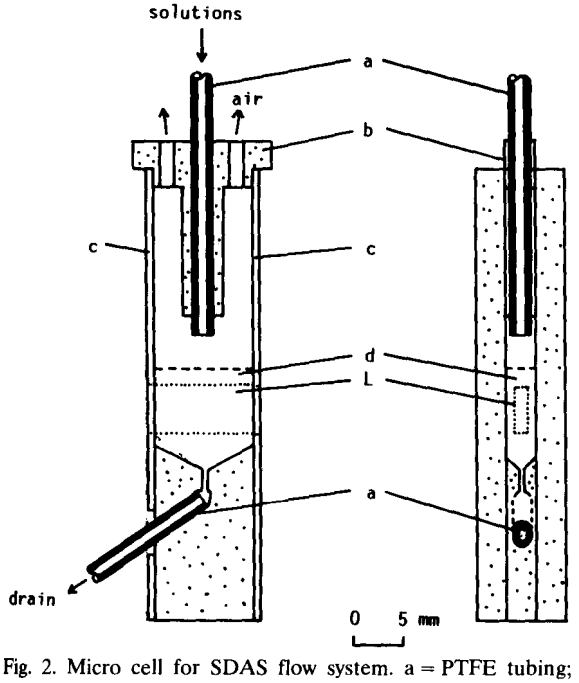

Fig. 2. Micro cell for SDAS flow system. a = PTFE tubing; b = removable tube guide; c = transparent acrylic resin plate; d = mixed solution (ca. 300 μl); L = irradiation light beam.

The absorbance change of MO at 490 nm was measured using a Shimadzu Model UV-160 spectrophotometer with a built-in data processor, by which the reaction rate [$v = \Delta$(absorbance)/Δ(time)], corresponding to the rate constant of a pseudo-zero-order reaction, was automatically printed out.

Catalytic determination of sulphide. Water (R_1, 50 μl), 0.013 M potassium bromate solution (R_2, 50 μl), the sample or standard sulphide solution (S, 100 μl) and 4.9×10^{-5} or 15×10^{-5} M MO–0.54 M HCl solution (R_3, 117 μl) were sequentially introduced into the flow line through the injectors (I_1–I_4) by microsyringes and the operation of P_2. After standing for 2 min, air carrier was introduced for about 15 s by the operation of P_1 to deliver the air-sandwiched solutions into the micro cell. In the cell, the air carrier was separated and removed from the solution. The reac-

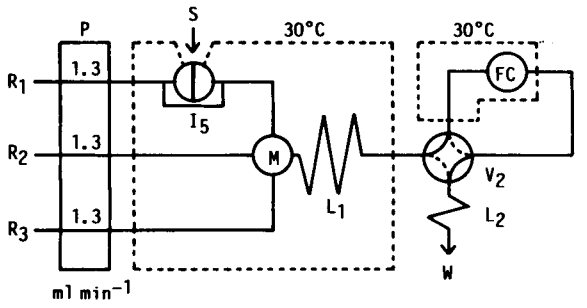

Fig. 3. SF/FIA system. P = peristaltic pump; R_1 = water; R_2 = $KBrO_3$ solution; R_3 = MO–HCl solution; S = sample; I_5 = valve-type injector; M = mixing joint; FC = flow cell (10 mm path length and 1.5 mm i.d.); L_1 = mixing coil (4 m × 0.5 mm i.d.); L_2 = back-pressure coil (0.6 m × 0.5 mm i.d.); V_2 = four-way valve; W = waste.

tion was started at the initial concentrations of 1.8×10^{-5} or 5.4×10^{-5} M MO, 2.0×10^{-3} M $KBrO_3$ and 0.20 M HCl. The reaction rate was calculated from the absorbance change for reaction times of 30 and 40 s, corresponding to 38 and 48 s after the start of pumping, respectively. The calibration graph was constructed by plotting the reaction rate against amount of sulphide. The cell was washed with 300 μl of water injected in I_1 before and after each measurement.

SF / FIA technique

The SF/FIA determination of sulphide was carried out for comparison with the SDAS technique as follows. Figure 3 shows the flow system constructed for this purpose. Water carrier (R_1) and solutions of 6×10^{-3} M $KBrO_3$ (R_2) and 5.4×10^{-5} (or 16×10^{-5}) M MO–0.60 M HCl (R_3) were pumped so as to be at the same concentrations as those in the SDAS technique at the mixing joint (M). A sample (S) of 100 μl was injected by a microsyringe into the water carrier stream through a valve-type injector (I_5) with a septum-type injection port. The flow paths in the four-way valve (V_2) were changed at 45 s after the injection to stop the flow of the sample zone at the flow cell (FC). The reaction rate between reaction times of 30 and 40 s, corresponding to 5 and 15 s after the change of flow paths, was printed out using the same spectrophotometer as described for the SDAS technique.

Manual batch technique

Sulphide was also determined by a manual batch technique for comparison with the techniques described above. Sample and reagent solutions and water kept at 30°C in a water-bath before analysis. A sample solution of less than 2 ml was taken in a 20-ml glass test-tube and diluted to 2 ml with water. After adding 2 ml of 4.5×10^{-5} or 14×10^{-5} M MO–0.50 M HCl solution, the reaction was started by adding 1 ml of 0.010 M bromate solution. An aliquot was immediately taken into the usual 10-mm glass cell. The reaction rate between reaction times of 30 and 40 s was printed out using the same spectrophotometer as described for the SDAS technique.

RESULTS AND DISCUSSION

Mixing of solutions in the SDAS flow system

At lower flow-rates, the compressed air carrier gave significant variations in the flow-rate of sandwiched solution zones in the flow line. Moreover, some parts of the solutions injected were mixed with each other and reacted in the line, because the solution zones moved slowly in the flow line. On the other hand, at too high flow-rates the solution zone broke into several smaller zones, gave rise to air bubbles in the mixed solution in the cell and splashed the solution on the wall of the cell. These effects did not allow exact and reproducible control of the reaction time. Therefore, an air flow-rate of 13 ml min^{-1} was selected in the present flow system.

The time required for complete mixing and the reproducibility of absorbance measurements were investigated as follows. Water volumes of 50 μl (R_1), 50 μl (R_2) and 100 μl (S) and a solution of 4.9×10^{-5} M MO–0.54 M HCl (absorbance 1.770) of volume 117 μl (R_3) were introduced through injectors I_1, I_2, I_3 and I_4, respectively, into the SDAS flow system (Fig. 1), and the absorbance was measured as described under Experimental. Figure 4 shows the absorbance change after the start of pumping by operation of P_1. Peak 1 in Fig. 4A was temporally caused by the introduction of the MO solution (R_3) momentarily across the light path. The shoulder 2 was

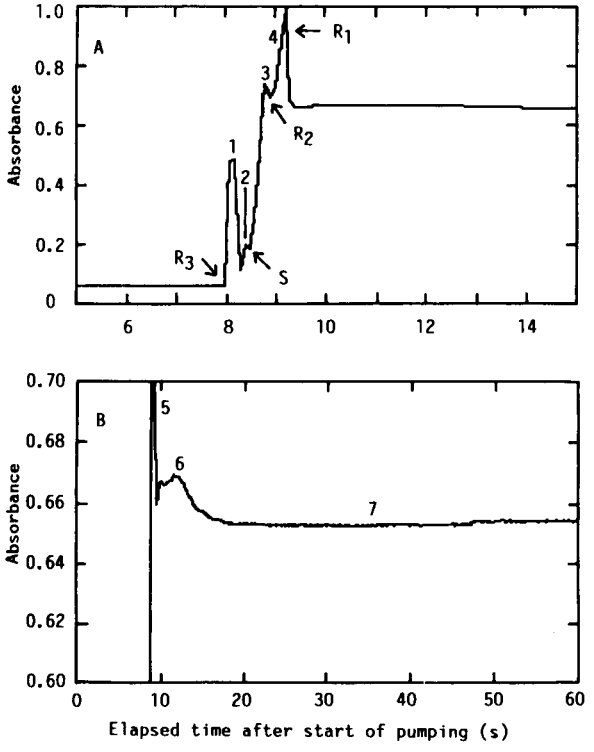

Fig. 4. Absorbance change on mixing of MO and water by the SDAS technique. (B) The absorbance scale of 0.6–0.7 in (A) is enlarged and the time scale is reduced for observation of the mixing state. Arrows indicate inflow points of 50 μl of water each as R_1 and R_2, 100 μl of water as S and 117 μl of 4.9×10^{-5} M MO–0.54 M HCl solution as R_3. See text for numbers 1–7.

caused by partially masking the light path with the upper part of the MO solution introduced into the cell. Peaks 3 and 4 were temporal absorbances of heterogeneous MO solution including some bubbles, just after S and R_2 of water were introduced and mixed with the MO solution. The light path was covered completely by the dilute MO solution after the introduction of R_2. Therefore, the inflow point of R_1 was unclear in Fig. 4A, and distinguished by the introduction of the MO solution in place of water through I_1 in another experiment. The sharp peak 5 in Fig. 4B, shown with an enlarged absorbance scale and a reduced time scale, is the unresolved peaks 3 and 4 in Fig. 4A. The diffuse peak 6 shows a small absorbance change in the process of complete mixing after the introduction of R_1. The absorbance 7 shows that at mixing equilibrium.

On the basis of the above description, Fig. 4A shows that the final solution R_1 was introduced into the cell within 2 s after inflow of the first solution R_3 and within 0.5 s after inflow of R_2. The absorbance of the homogeneous solution within a deviation of 0.2% was obtained in 8 s after inflow of the final solution as shown in Fig. 4B. The relative standard deviation for five measurements of the absorbance at the mixing equilibrium was 1% with an average absorbance of 0.647, which agreed with the calculated value (0.653) within the deviation.

On the other hand, the absorbance became lower and its reproducibility became poor when the MO solution was introduced through I_1. This indicates that the final solution (R_1) washed out the other three solutions but partially remained in the flow line. The variable volume of residual solution may give a significant variation in the results in the catalytic analysis using micro volumes of solutions. Therefore, the volume of the residual solution and its variation should be evaluated.

Residual solution in the flow line and cell of SDAS flow system

The volume of residual solution in the flow line was measured as follows. MO solution of 3.1×10^{-4} M MO–0.1 M HCl was introduced into the flow line through injectors I_1–I_4 (Fig. 1) and then drained out from the cell. After removal of the air filter (F) and the cell (C), the residual MO solution in the flow line was washed out into a 5-ml volumetric flask by introducing a few millilitres of water through the tubing of pump P_1. Then the absorbance of the diluted residual MO solution in the flask was measured after the volume had been made up to 5 ml with 0.1 M HCl. The volume α (μl) of the residual MO solution was calculated by use of the equation $\alpha A_0 = 5000 A_m$, where A_0 and A_m are absorbances of the MO solutions introduced and measured, respectively.

The volume of residual solution in the cell was measured as follows. MO solution of 4.9×10^{-4}

M MO–0.1 M HCl was introduced into the flow line and drained out from the cell as described above. Then 300 μl of 0.1 M HCl were placed in the cell with a micropipette and the absorbance was measured. The volume β (μl) of the residual solution was calculated from $\beta A_0 = (\beta + 300)A_m$.

Five repeated measurements of α and β gave $\alpha = 7 \pm 2$ μl and $\beta = 4 \pm 0.4$ μl. The standard deviations of the residual volumes suggest that a total volume of more than 200 μl of sample and reagent solutions is required to decrease the variation of the reagent concentrations in the cell to within 1%. Because of the non-negligible α value, washing water as R_1 should be injected to deliver the sample and reagent solutions completely into the cell.

The volume of the mixed solution in the cell is calculated based on the α and β values. The solutions (total volume 317 μl) introduced through the injectors are mixed with 7 μl of the remaining water in the flow line and leave 7 μl of water (R_1). Then the delivered solutions are mixed with a 4 μl of remaining water in the cell, and the final solution volume in the cell becomes 321 μl, i.e., only of 1% excess with respect to the total volume introduced. Therefore, the reaction will proceed under the same reaction conditions as in the manual batch technique. Hence the reaction conditions studied in the conventional manual batch technique can be used for the present SDAS technique, but cannot be used in the FIA technique because of the undefined dilution of the sample by the dispersion.

Catalytic determination of sulphide using different solution delivery techniques

The amount of sulphide was determined by the measurement of the decolorization rate of MO after the induction period [14]. To accelerate the reaction, the concentration of HCl used in this study was about twice that specified in the literature [14]. The reaction rate was considerably influenced by the concentrations of hydrochloric acid and bromate and the reaction temperature, whereas it was independent of the concentration of MO in the range 1.8×10^{-5}–5×10^{-5} M. Figure 5 shows the absorbance change in the MO–bromate reaction using the SDAS technique.

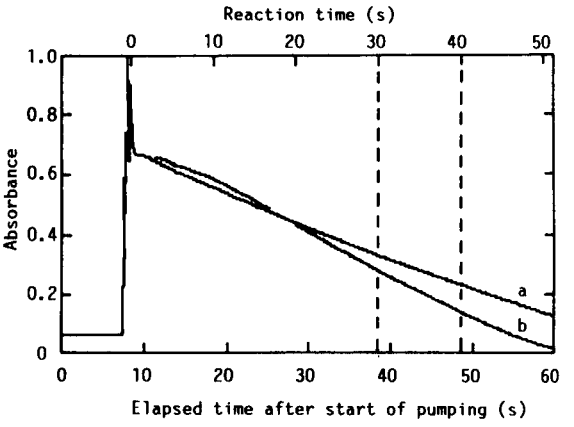

Fig. 5. Absorbance change in MO–bromate reaction by the SDAS technique. (a) Blank; (b) 100 ng S^{2-}; Reaction conditions: 1.8×10^{-5} M MO, 2.0×10^{-3} M $KBrO_3$, 0.20 M HCl, 30°C.

The analytical performances of the SDAS, manual batch and SF/FIA techniques are summarized and compared in Table 1. The absolute

TABLE 1

Comparison of analytical performance in the catalytic determination of sulphide using different solution delivery techniques

Parameter	SDAS	SF/FIA	Manual batch method
Injection or added sample (ml)	0.1	0.1	2
Reacting solution (ml)	0.321	–	5
Absolute sensitivity [a] $[\times 10^{-4}\ v\ (\text{ng}\ S^{2-})^{-1}]$	19	5.7	1.2
Relative sensitivity [a] $[\times 10^{-4}\ v\ (\text{ng}\ S^{2-}\ \text{ml}^{-1})^{-1}]$:			
For sample solution	1.9	0.6	2.4
For reacting solution	6.1	–	6.0
Detection limit (ng S^{2-})	18	51	220
Reproducibility of determination:			
Added (ng S^{2-})	100	300	1500
Found (ng S^{2-})	105 ± 5	286 ± 18	1510 ± 150 [b]
Determination range (ng S^{2-})	0–500	0–2000	0–8000

[a] $v = \Delta(\text{absorbance})/\Delta(\text{time})$ = reaction rate (min^{-1}). [b] 1550 $\pm$ 280 ng ($n = 5$) by an unskilled analyst.

sensitivity [v(ng S^{2-})$^{-1}$] for a sample solution or reacting solution is defined as the slope of calibration graph for the sulphide amount. The relative sensitivity [v(ng S^{2-} ml^{-1})$^{-1}$] for a sample or reacting solution is defined as the product of the absolute sensitivity and the volume of sample or reacting solution, respectively. The detection limit is defined as the amount of sulphide corresponding to three times the standard deviation ($n = 5$) of the reaction rate for a blank test. The reproducibility of determination was calculated from five determinations of ca. 300 ng sulphide ml^{-1} in the reacting solution. For the study of the upper limit of the linear range of calibration, a higher concentration of MO (5.4×10^{-5} M) was used, because at lower concentrations MO disappears within the reaction time.

The absolute sensitivity of the SDAS technique was three and sixteen times those of the SF/FIA and manual batch techniques, respectively. The relative sensitivity for sample solution by the SDAS technique was three times that of the SF/FIA technique and comparable to that of the manual batch technique. The relative sensitivity by the SDAS technique agreed with that by the manual batch technique. The exact relative sensitivity cannot be evaluated in SF/FIA, because the sulphide is dispersed and its concentration is not uniform in the flow cell. The detection limit with the SDAS technique was three and ten times lower than those with the SF/FIA and manual batch techniques, respectively. The calibration graphs for sulphide were linear up to 8000 and 500 ng in the manual batch and SDAS techniques, respectively.

This work was supported by a Grant-in-Aid (No. 62550543 and No. 02650538) for Scientific Research from the Ministry of Education, Science and Culture, Japan. The authors thank Mr. T. Ikeda and Mr. M. Suzuki for experimental assistance.

REFERENCES

1 J. Ruzicka and E.H. Hansen, Flow Injection Analysis, Wiley-Interscience, New York, 1981.
2 M. Valcárcel and M.D. Luque de Castro, Flow-Injection Analysis: Principles and Applications, Ellis Horwood, Chichester, 1987.
3 S. Kawakubo, T. Katsumata, M. Iwatsuki, T. Fukasawa and T. Fukasawa, Analyst, 113 (1988) 1827.
4 C. Pasquini and W.A. de Oliveira, Anal. Chem., 57 (1985) 2575.
5 C. Pasquini, Anal. Chem., 58 (1986) 2346.
6 C.J. Patton, M. Rabb and S.R. Crouch, Anal. Chem., 54 (1982) 1113.
7 J.A. Sweileh and P.K. Dasgupta, Anal. Chim. Acta, 214 (1988) 107.
8 J.A. Sweileh, J.L. Lopez and P.K. Dasgupta, Rev. Sci. Instrum., 59 (1988) 2609.
9 L. Ping and P.K. Dasgupta, Anal. Chem., 62 (1990) 85.
10 P.K. Dasgupta and K. Petersen, Anal. Chem., 62 (1990) 395.
11 S. Dong and P.K. Dasgupta, Talanta, 38 (1991) 133.
12 K. Petersen and P.K. Dasgupta, Talanta, 36 (1989) 49.
13 J. Ruzicka and E.H. Hansen, Anal. Chim. Acta, 173 (1985) 3.
14 L.M. Tamarchenko, Zh. Anal. Khim., 33 (1978) 824.

Analytica Chimica Acta, 282 (1993) 397–406
Elsevier Science Publishers B.V., Amsterdam

Volumetric triangle-programmed flow titrations based on precisely generated concentration gradients

B. Fuhrmann and U. Spohn

Institut für Biotechnologie, Martin-Luther Universität Halle-Wittenberg, Weinbergweg 16a, 06120 Halle (Germany)

(Received 27th February 1993; revised manuscript received 20th May 1993)

Abstract

Linear concentration gradients were generated by means of computer-controlled micropumps to implement triangle-programmed flow titrations. Precise determinations could be performed under defined conditions without calibration. The use of inverse flow-rate gradients enables volumetric titrations to be performed in constantly flowing streams. The mixing of flow-rate gradients of the titration reagent and the sample solution, which are inverse to each other, opens up a way to titrate samples with concentrations varying over several orders of magnitude. The zone sampling out of precisely defined triangle concentration profiles and the injection into a continuously streaming sample or standard solution opens up a way to methods of flow-injection analysis (FIA) with improved reliability and on-line calibration. The titrations and the FIA procedures are controlled and analysed automatically by a personal computer. A compact and fully automated flow titrator was developed.

Keywords: Flow injection; Titrimetry; Computer-controlled titrations; Concentration gradients; Flow-rate gradients; Flow titrations; Tailing; Zone sampling

Despite of the obvious advantages, flow titrations with concentration gradients are not widely applied. Blaedel and Laessig [1,2] made the first attempts to employ flow-rate changes of the titration reagent to titrate continuously flowing sample solutions. Two peristaltic pumps were used. The sample solution was pumped with a constant flow-rate. The second pump rate was controlled electromechanically by the difference between the signal of a potentiometric flow detector and the equivalence point resulting in a concentration gradient of the reagent depending on the sample concentration.

Fleet and Ho [3] and Nagy et al. [4] introduced the generation of linear concentration gradients to perform flow titrations. Nagy and coworkers [4–9] used the triangle-programmed coulometric generation of the titration reagent. The miniaturization of the flow channel system allows nearly absolutely working flow gradient titrations with coulometric reagent generation [10–12]. Up to now no volumetric triangle-programmed flow titration was described in the literature. Rios et al. [13] used computer-controlled flow-rate gradients in unsegmented flow through systems to enhance the applications of flow-injection analysis. Later, Valcarcel's group [14–17] applied such flow-rate gradients to generate concentration gradients after continuously mixing with a constantly flowing solution. One programmable pump with variable flow-rate and one pump working at a fixed flow-rate were used. Recently volumetric flow titrations were implemented on this basis [18, 19]. All volumetric and most of the coulometric flow gradient titrations have to be calibrated. The determination range of such flow titrations is

Correspondence to: U. Spohn, Institut für Biotechnologie, Martin-Luther Universität Halle-Wittenberg, Weinbergweg 16a, 06120 Halle (Germany)

restricted by the maximum concentration of the titration reagent.

The objectives of our work were rapidly working volumetric flow titrations based on precisely generated concentration gradients with a simplified calibration. Further, the determination range should be extended, and the third aim was the development of a rapidly working on-line calibration procedure for the flow-injection analysis on the basis of triangle-programmed concentration profiles.

EXPERIMENTAL

Reagents

Glucose dehydrogenase (GDH; EC 1.1.1.47) from *Bacillum megaterium* (Merck, Darmstadt) and NADH (grade I, content around 100%; Boehringer, Mannheim) were used. All other chemicals were of analytical grade and from Merck. The buffer and standard solutions were made with deionized and bidistilled water.

GDH was immobilized on aminosilylated controlled-pore glass (BIORAN, sieve faction 180–200 μm, Schott, Mainz, Germany) as described earlier [20]. The immobilizate was packed into a Plexiglas cartridge (inner diameter 3 mm, packing bed length 10 mm). The cofactor solution contained 4 mM NAD^+ in 0.2 M potassium phosphate buffer (pH 7.4).

1 ml Bromothymol Blue solution (1 g l^{-1}) was added to 1 l of a 2.2 mM NaOH solution. Thereafter this titration reagent was standardized with a 10 mM HCl solution (Merck) and potentiometric titration with a pH glass electrode. To verify the HCl standard solution it was coulometrically titrated with electrogenerated hydroxide ions in a batch titration procedure according to [21].

All buffer and carrier solutions were made from bidistilled and de-ionized water.

Apparatus

Figure 1 shows the measuring set-up for the automated flow titrations. The titration reagents, the sample and the standard solutions are propelled by miniaturized pumps with a rotating plunger (TEC-S, from 2 to 3 μl per rotation;

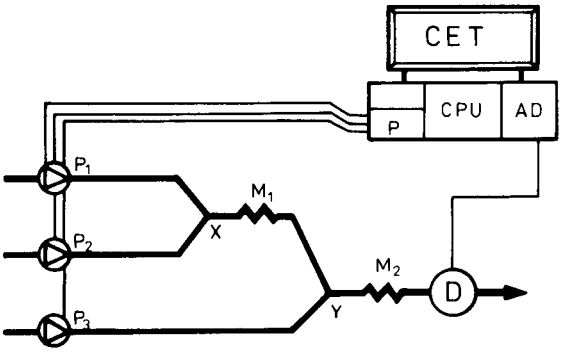

Fig. 1. Flow titration set-up; P = pump card; AD = analog/digital converter; CPU = central processor unit; CET = software control and evaluation in the PC; P_{1-3} = pumps; $M_{1,2}$ = mixing coils, D = detector.

Tecuria, Switzerland) or piston pumps (Dosimat 665, 5 ml pistons, 0.5 μl pump steps, Metrohm, Switzerland). A home-made PC interface board (Fig. 2) allows the simultaneous and automatic control of up to six pumps of both types.

To follow the titration courses a photometric detector with a flow cell volume of 9 μl (UVIS 200, Linear Instruments Cooperation, USA) or a fluorescence detector (F-1050, Merck-Hitachi, Germany) with a 12 μl flow cell were used. The determination reactions take place in reaction coils with a length of 10 cm and an inner diameter of 0.5 mm for acid base titrations or in a packed-bed enzyme reactor. To degass the reaction mixture a microporous polypropylene tube (0.2 μm pore size, 60% porosity, 0.6 mm inner diameter and 100 mm lenght; ENKA, Wuppertal,

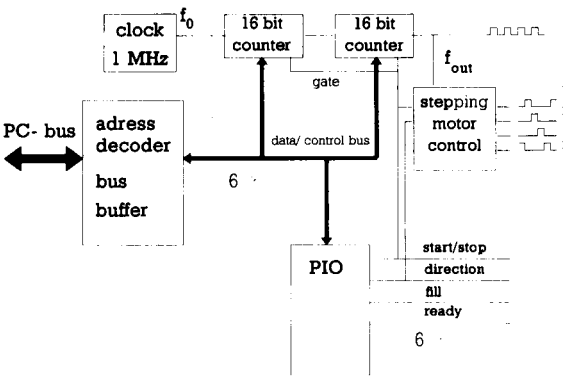

Fig. 2. Pump control card; see text for detailed explanation.

Germany) was placed between the flow reactor and the detector.

The pump control card (Fig. 2) and a detector control card are mounted into a personal computer (IBM-AT). The detector control card contains a current follower circuit, an analog/digital converter, a voltage adjustable potentiostat and an interface for the control of up to 8 magnetic valves.

Pneumatically actuated injection valves (Rheodyne 9010, Cotati, FL) and six-way valves (Rheodyne 9060) can be controlled by the corresponding solenoid valve kits (Rheodyne 7163). This allows the implementation of automated FIA procedures.

The pump control card contains an address decoder delivering the chip selected signals for 16-bit counters and for a parallel input/output circuit. The data and control bus are buffered. Two 16-bit timers in series deliver a variable frequency f_{OUT} from a 1 MHz quarz oscillator providing a high resolution of the pump rates. f_{OUT} is the ratio of the desired flow-rate $\dot{V}$ ml min^{-1}) to the pumped volume per step S (μl). The rotating plunger pumps work with stepper motors. The stepper motors are controlled by the corresponding control circuit. The pulse inputs of the piston pumps are connected to the output of the second 16-bit counter.

Six such channels are placed on the pump control card. Both piston and stepper motor driven pumps can be connected to each channel. An additional 24-bit parallel input/output circuit (PIO) generates start/stop signals, signals for switching over the pump directions. The pump control is simple and robust. The two timers per pump channel are programmed with the counting numbers n_1 and n_2. The flow-rate $\dot{V}$ (ml min^{-1}) correlates with the product $n_1 n_2$ according to eq.:

$$\dot{V} = 0.06 f_0 S n_1 n_2 \quad (1)$$

where f_0 (s^{-1}) is the oscillator frequency, n_1 and n_2 are integer numbers between 1 and 65535, and S and $\dot{V}$ can be preadjusted.

By using two 16-bit timers in series a high digital resolution of the pump rate control is obtained. The maximum relative error made by digitalization depends on S and f_0 and can be calculated for a desired flow rate $\dot{V}$ from the corresponding product $n_1 n_2$ according to:

$$\Delta\dot{V}/\dot{V} = \frac{1}{n_1 n_2 + 1} \quad (2)$$

The desired flow gradients are approximated by discrete change of the flow rate $\dot{V}_d$ after a corresponding time difference t_d. t_d can be adjusted between 0.1 and 1 s allowing an almost continuously flow-rate change for gradient lengths τ between 60 and 600 s. The time difference t_d corresponding to the volume rate step $\Delta\dot{V}$ is generated via an interrupt-controlled counter loop by the computer. After each t_d the two pump channel timers will be loaded with new n_1 and n_2 values.

If desired the linear flow gradient

$$\dot{V}(t) = \dot{V}_{max} t/\tau \quad (3)$$

could be replaced by other time-dependent functions $\dot{V}(t)$.

RESULTS AND DISCUSSION

Preliminary investigation

The relative standard deviations of the pump rates are 0.5% ($n = 5$, $\alpha = 0.05$) for the stepper motor driven pumps and 0.03% ($n = 5$, $\alpha = 0.05$) for the piston pumps. The pump rates were determined by weighing bidistilled and thermostated water pumped during an exactly defined time measured with a quarz clock. The pumps were switched automatically by the computer. The pulsation of the TEC-S pumps has a relatively low amplitude, because one rotation of the plunger corresponds to 3 μl. These pumps have the advantage of a very small total volume of around 20 μl of the inflow, the pump chamber and the outflow.

Flow titrations with single triangle concentration profiles

The reagent solution pump P_1 and the diluent pump P_2 (Fig. 1) are controlled to generate flow gradient profiles with the shape of isosceles triangles inverse to each other. After mixing at point

X the resulting flow-rate $\dot{V} = \dot{V}_T(t) + \dot{V}_D(t)$ consisting of the diluent flow $\dot{V}_D(t)$ and the reagent flow $\dot{V}_T(t)$ is constant. But the molar flow-rate of the titrant can be calculated according to:

$$\dot{n}_T(t) = \begin{cases} \dot{n}_{T,max} t/\tau & 0 < t < \tau \\ \dot{n}_{T,max}(2 - t/\tau) & \tau < t < 2\tau \end{cases} \quad (4)$$

The concentration gradient profile is calculated from

$$c_T(t) = \dot{n}_T(t)/\dot{V} \quad (5)$$

At the mixing point Y the reagent T is mixed continuously with the sample solution pumped with the constant flow-rate $\dot{V}_S$. For the determination reaction

$$aS + bT \rightarrow \text{reaction products} \quad (6)$$

the equivalence condition

$$b\dot{n}_S = a\dot{n}_T \quad (7)$$

is valid. The sample concentration c_S can be calculated from the time difference Δt between the two equivalence points $t_{eq,1}$ and $t_{eq,2}$, the stoichiometric factors a and b, the total and the sample flow-rate according to:

$$c_S = (1 - \Delta t/2\tau)\frac{a\dot{V}c_T}{b\dot{V}_S} \quad (8)$$

The system was tested for the titration of hydrochloric acid solutions in the range from 0.25 to 1.5 mM with a 1.87 mM hydroxide standard solution. The diluent solution contained 5 μM Bromothymol Blue. Figure 3 shows the comparison between the precalculated working lines and the measured calibration lines for different titration times 2τ. The mean absolute deviation of the measured Δt_m from the Δt values precalculated from Eqn. 8 was smaller than 1 s. The standard deviations are smaller than 0.5 s ($n = 4$, $\alpha = 0.05$). The concentration gradient profiles were generated by means of the piston pumps. Similiar results could be obtained with the rotating plunger pumps TEC-S.

To experimentally approximate the titration model described theoretically by Eqns. 4 and 5 the influence of the axial dispersion deforming the generated concentration profiles has to be

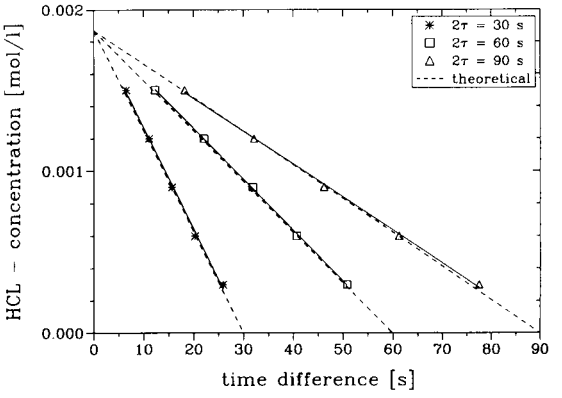

Fig. 3. Precalculated working and calibration lines for the alkalimetric flow titration of hydrochloric acid with 1.87 mM NaOH; $\dot{V}_D + \dot{V}_T = 0.7$ ml min^{-1} and $\dot{V}_S = 0.7$ ml min^{-1}.

investigated. As described earlier [10] the so-called tailing g of the triangle concentration profile in flowing streams is caused by the axial dispersion σ^2. g is defined as

$$g = \frac{\Delta t_{m,o} - 2\tau}{2\tau} \quad (9)$$

for the sample concentration $c_S = 0$ and

$$g_i = \frac{\Delta t_{m,i} - \Delta t_i}{\Delta t_i} \quad (10)$$

for the sample concentration $c_{S,i}$. $\Delta t_{m,o}$ and $t_{m,i}$ are the measured time differences between the intersection points of the measured linear concentration gradients with the detector basis line for the sample concentration c_S. Δt_i is the precalculated time difference for the corresponding sample concentration. Correction factors $f_{m,o}$ and $f_{m,i}$ can be defined as

$$f_{m,o} = \Delta t_{m,o}/2\tau \quad (11)$$

and

$$f_{m,i} = \Delta t_{m,i}/\Delta t_i \quad (12)$$

The average correction factor f_m is defined as the slope of the regression line calculated from all measured $\Delta t_{m,i}$ values and the corresponding Δt_i values calculated by using the model Eqns. 8, 15, 17 or 18, respectively. Figure 4 shows the comparison between a precalculated and a measured concentration time profile. The smaller g_i

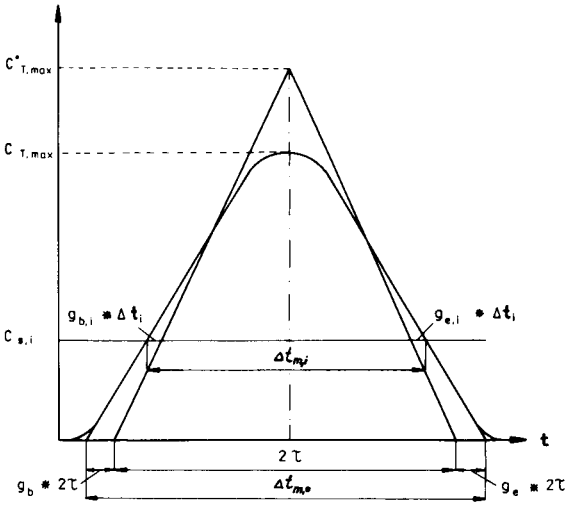

Fig. 4. Comparison between the precalculated and the measured concentration profile of the titration reagent; $c_{o,max}$ = precalculated maximum concentration of the titration reagent; c_{max} = measured maximum concentration; $c_{s,i}$ = sample concentration level; other symbols as explained in the text.

and g the tighter the precalculated triangle profiles can be approximated. Figure 8 shows two blank titration curves. A g value of 0.000 ± 0.001 ($n = 10$, $\alpha = 0.05$) was found. Figure 5 shows the dependence of the tailing g on the titration times 2τ. If the detector has been placed behind the mixing coil M_1 (Fig. 1) decreased tailing values are achieved. The replacement of the piston pumps for the TEC-S rotating plunger pumps had no significant influence on the tailing values.

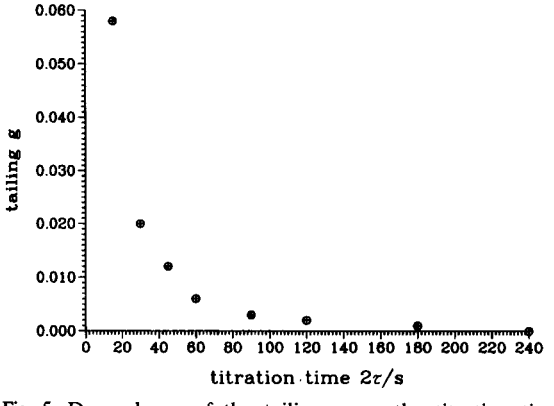

Fig. 5. Dependence of the tailing g on the titration time; experimental conditions as in Fig. 3.

No pulse damping is necessary. As can easily be seen from Fig. 3 the tailing g_i values should be very small because there are small differences between precalculated and measured time differences also for sample concentrations greater than zero. As shown in Fig. 4 there is a connection between the tailing values g and g_i, the correction factors $f_{m,o}$ and $f_{m,i}$, the titration time 2τ and the time differences Δt_i. The axial dispersion model [22–25] could be used to describe the contributions of the flow channel components to the axial dispersion between the profile generation and the detection. A more practical approach is possible by the equations

$$\Delta t_{m,i} = \Delta t_i(1 + g_{i,M_1} + g_{i,M_2} + g_{i,Z_1} + g_{i,Z_2} + g_{i,D} + g_{i,R}) \quad (13)$$

and

$$g_i = g_{i,M_1} + g_{i,M_2} + g_{i,Z_1} + g_{i,Z_2} + g_{i,D} + g_{i,R} \quad (14)$$

with the tailing $g_{i,M_{1,2}}$ in the mixing coil M_1 and M_2, $g_{i,Z_{1,2}}$ in the connecting tubes 1 and 2, $g_{i,D}$ caused by the detector and $g_{i,R}$ caused by the chemical reaction.

As described earlier [10] the tailing can be reduced by shorter tubings, smaller tube diameters, the avoidance of changing the cross-sectional areas in the flow channel system and the application of rapidly responding detectors with small measuring volumes. Coiled tubes, knotted-type reactors and single bead-string reactors are useful to prolong the residence time and enhance the mixing of the sample with the reagent because the radial dispersion is favoured in comparison to the axial dispersion.

g and g_i consist of the two components $g_b(g_{b,i})$ and $g_e(g_{e,i})$ at the beginning and at the end of the triangle profile, respectively. If g_i and g are small enough the correction factors approach the value 1. This would imply that absolute flow through titrations could be approximately achieved by presupposing the use of exactly defined standard solutions for these titrations. The tailing g, caused by the axial dispersion σ^2, is an essential but in most cases not precalculable titration parameter. The influence of the axial dispersion σ^2 on the concentration gradients cannot be

excluded or precalculated for most of the known volumetric and coulometric flow gradient titrations. Therefore these titrations have to be calibrated. Because of the attainable small relative axial dispersion and the resulting short tailing the use of the TEC-S pumps allows very short sample exchange times around 30 s without any carry-over effect. Depending on the titration time 2τ up to 60 titrations can be performed per hour with $1.00 < f_m < 1.02$.

Flow titrations with two concentration gradients

Based on the fact that a simplified flow channel set-up has a reduced tailing g caused by a smaller axial dispersion σ^2 the direct mixing of a triangle profile of the titration reagent with an inverse triangle profile of the sample solution should also enable precise flow titrations. For the corresponding experiments pump the P_3, the connecting tube and the mixing point Y were eliminated from the set-up shown in Fig. 1.

By means of pump P_1 and pump P_2 two flow-rate gradient profiles are generated inversely to each other. P_1 and P_2 propel the reagent and the sample solution, respectively. Obviously two equivalence points result. The resulting flow-rate in the mixing coil M_1 was constant. It was proved that the sample concentration c_S can be calculated approximately from the time difference $\Delta t_{m,i}$ measured between the two equivalence points

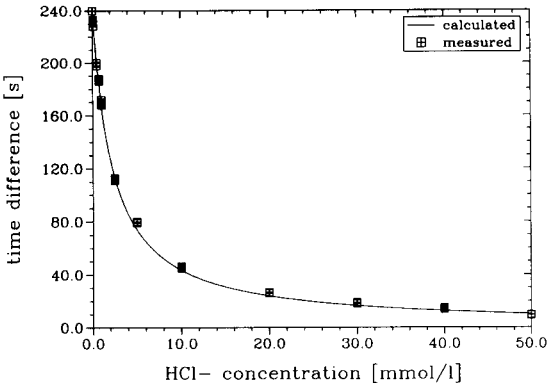

Fig. 6. Flow titrations with two concentration gradients, precalculated and measured calibration lines for the alkalimetric titration of HCl with 2.12 mM NaOH. $\dot{V}_T = 0.542$ ml min^{-1}, $\dot{V}_S = 0.519$ ml min^{-1}, $2\tau = 240$ s.

and the molar flow balance according to

$$c_{S,i} = \frac{ac_T}{b} \frac{2\tau - \Delta t_{m,i}/f_m}{\Delta t_{m,i}/f_m} \quad (15)$$

with $f_m = 1$.

Figure 6 shows the comparison between the precalculated and the measured time differences for the titration of hydrochloric acid with 2.12 mM NaOH for the titration time $2\tau = 240$ s. The NaOH standard solution contained 6.5 μM Bromothymol Blue.

TABLE 1

Alkalimetric titrations with two concentration gradients, ($\alpha = 0.05$, $n = 5$)

	$2\tau = 240$ s		$2\tau = 120$ s	
HCl concentration taken (mM)	Measured time difference (s)	HCL concentration found (mM)	Measured time difference (s)	HCl concentration found (mM)
0	240.1 ± 1.1	−0.001	119.8 ± 0.6	0.0
0.1	230.1 ± 1.1	0.096	115.0 ± 0.6	0.097
0.5	197.4 ± 1.0	0.479	98.5 ± 0.5	0.485
0.75	179.9 ± 0.8	0.742	90.1 ± 0.5	0.737
1.0	166.6 ± 0.7	0.978	83.3 ± 0.5	0.978
2.5	112.5 ± 0.6	2.516	57.4 ± 0.4	2.421
5.0	74.3 ± 0.5	4.951	41.4 ± 0.3	4.215
10.0	45.1 ± 0.4	9.594	23.9 ± 0.3	8.926
20.0	25.5 ± 0.3	18.67		
30.0	18.2 ± 0.3	27.05		
40.0	14.0 ± 0.3	35.84		
50.0	11.6 ± 0.3	43.71		

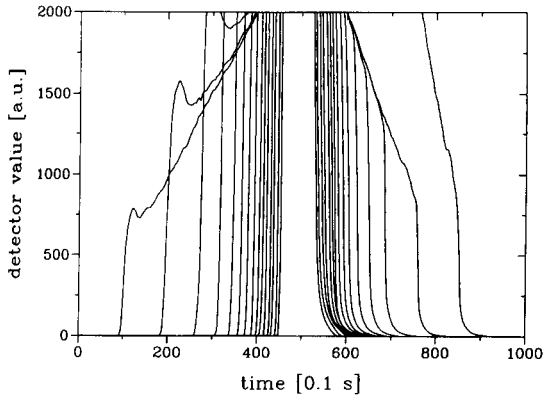

Fig. 7. Photometric flow titration curves, titration with two concentration gradients; c_{HCl} = 0.5, 1, 2, 3, 4, 5, 6, 7, 8, 9, 10, 12, 14, 17 and 20 mM, with 1.87 mM NaOH; $\dot{V}_T = \dot{V}_S$ = 0.5 ml min^{-1}, 2τ = 90 s.

The precalculated and the measured time differences agree relatively good in the concentration range from 0.1 to 20 mM. The standard deviation lies between 0.4 and 1.2% in the concentration range from 0.1 to 10 mM ($n = 5$, α = 0.05). Also greater concentrations could be titrated with good precision. But in this case the accuracy will be deteriorated by the decreasing time differences between the equivalence points. These results were obtained with the rotating plunger pumps TEC-S. An additional calibration gives the correction factor f_m in the correlation

$$\Delta t_i = \Delta t_{m,i}/f_m \quad (16)$$

where the factor was $f_m = 1.0074 \pm 0.0001$.

Table 1 shows the comparison between the titration results for $2\tau = 240$ s and $2\tau = 120$ s without calibration.

Figure 7 shows a series of the corresponding photometric titration curves for $2\tau = 90$ s. All titration curves have almost the same signal height independent of the sample concentration. Apparently the working range of this titration method is only limited by the resolution of the time difference measurements. In practice up to 3 orders of the concentration magnitude can be titrated with the same reagent solution. The corresponding photometric signal courses (Fig. 8) for the blank titration prove the assumption that precisely defined triangle concentration profiles are generated also by the double gradient technique.

FIA zone sampling out of triangle programmed concentration profiles

In many cases flow detectors have an unsufficient long-term stability for on-line process analysis. Frequent recalibration would be necessary. In the reversed FIA mode precisely defined volumes of different standard solutions can be injected into continuously flowing sample solutions as proposed by Tyson [26] to calibrate a FIA set-up.

It would be worthwhile to use also linear concentration gradients to calibrate FIA determination procedures. As demonstrated by the precisely implementable flow titrations, precisely defined triangle concentration profiles can be handled. According to Fig. 9 the two computer-con-

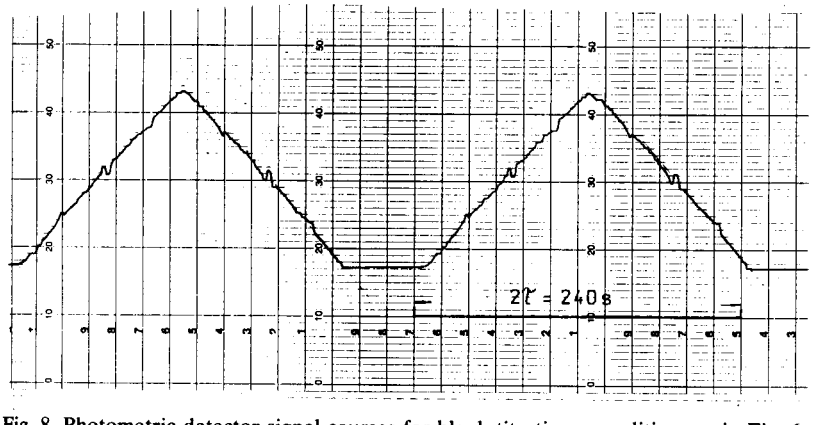

Fig. 8. Photometric detector signal courses for blank titrations, conditions as in Fig. 6.

trolled pumps (TEC-S) generating precisely defined concentration gradients are connected to the injection valve of the FIA set-up.

In a first experiment a standard stock solution of glucose is continuously mixed with distilled water in the coil M to generate triangle concentration profiles. Precisely defined concentration zones are cutted out of the concentration profiles and injected with constant sampling frequency $f_s = 1/32\ s^{-1}$ into the glucose sample solution propelled by pump P_3. The injection volume was 10 μl. In this standard addition method the sample stream is continuously mixed with the NAD^+ solution. The glucose is oxidized enzymatically to gluconic acid producing NADH in the enzyme reactor ER. Figure 10 shows the fluorimetrically detected peak signal sequence. Two interpolation lines were calculated by linear regression analysis for the peak heights on both sides of the interrupted triangle profile. The time difference Δt between the points of intersection with the zero line depends on the sample concentration c_S. The sample concentration can be calculated according to

$$c_S = \left(1 - \frac{\Delta t_{m,i}}{f_m 2\tau}\right) c_{max} \qquad (17)$$

from the measured time difference $\Delta t_{m,i}$ for $f_m = 1$. c_{max} is the concentration of standard stock solution of glucose. Table 2 gives a summary of the obtained results.

The absolute deviation of the measured from the added glucose concentration was smaller than 0.015 mM using a 1 mM standard stock solution. The measured Δt_m values agreed very well with the precalculated Δt values so that no additional

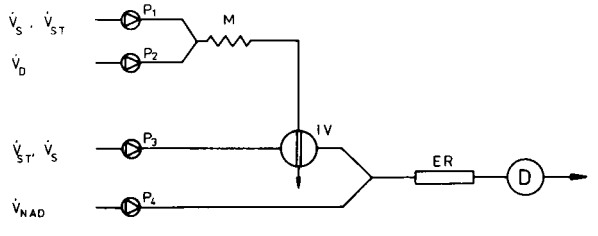

Fig. 9. FIA set-up. P_{1-4} = pumps; 1 = standard stock solution; 2 = diluent; 3 = sample solution; 4 = NAD^+ solution; M = mixing coil; IV = injection valve; D = fluorescence detector.

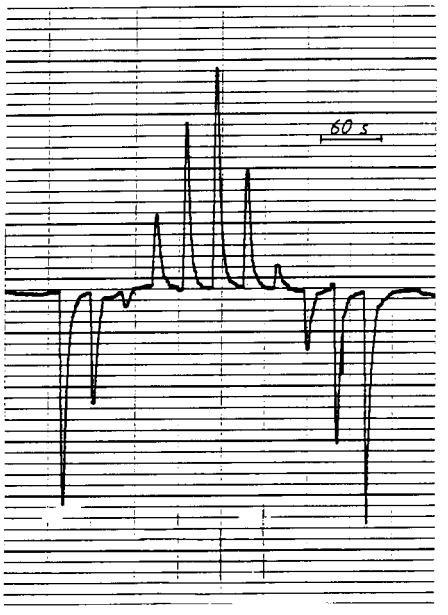

Fig. 10. Fluorimetric peak signal sequence for the FIA zone sampling out of a isoceles triangle concentration profile; c_{max} = 1 mM glucose; c_S = 0.5 mM glucose; c_{NAD} = 4 mM in 0.2 M; KP_i = buffer, pH 7.4; 2τ = 300 s; $f_s = 1/30\ s^{-1}$; $\dot{V}_{ST,max}$ = 0.7 ml min^{-1}; $\dot{V}_S$ = 0.7 ml min^{-1}; $\dot{V}_{D,max}$ = 0.7 ml min^{-1}; $\dot{V}_{NAD}$ = 0.7 ml min^{-1}.

calibration is necessary in this case ($\Delta t_{m,i} = f_m \Delta t_i + b$ with the average correction factor $f_m = 1.009 \pm 0.0206$ and $b = -(7.157 \pm 0.055)$ s; $\alpha = 0.05$, $n = 3$, $r^2 = 0.9999$). It should be noted that the deviation of f_m from 1.000 is very small and obviously determined by the deformation of the triangle concentration profil used for the calibration. Precisely defined glucose standard solutions, the absence of a blank value and small tailing values of the triangle concentration profil $g_i < 0.01$ are the essential precautions to approximate an absolute FIA determination.

The detection range is determined by c_{max} and can therefore be easily adapted. The pump P_1 may be connected to stock solutions with very different concentrations by means of the six-way valve controlled by the PC.

It should be noted that Eqn. 17 is analogous to Eqn. 8. Additionally, a time difference is measured making the method more independent of the detector stability than directly detecting flow methods. Because very small amounts of in situ

produced standard solutions are injected and mixed into a relatively great volume of sample solution, a benificial adaptation to the sample matrix is possible. The accuracy is essentially predetermined by the tailing of the triangle concentration profile.

Also, the reverse case of the described FIA calibration method was investigated. Different sample solutions were mixed with the diluent to generate triangle sample concentration profiles. In this sample addition method 10 μl of the on-line diluted sample solution were injected into a continuous stream of a glucose standard solution propelled by P_3. After replacing the concentration c_S for c_{max} and vice versa the analytical results can be calculated according to Eq. 18 in its rearranged version

$$c_S = c_{max} \frac{2\tau}{2\tau - \Delta t_{m,i}/f_m} \quad (18)$$

resulting in hyperbolic calibration lines. Table 2 contains some of the corresponding results. In the concentration range from 0.1 to 0.25 mM a good agreement between the taken and found glucose concentrations is achieved. Also in this case the measured Δt_m values agreed well with the precalculated Δt values ($\Delta t_m = f_m \Delta t + b$, $f_m = [0.9853 \pm 0.0142]$, $b = -[0.1811 \pm 0.0450]$ s, $\alpha = 0.05$, $n = 3$, $r^2 = 0.9999$), so that an additional calibration is only necessary if higher accuracies are needed. Figure 11 shows the comparison between the precalculated and the measured dependence of the time differences on the given glucose concentrations for the reversed and the normal FIA method. The advantage of this modified normal FIA procedure is the smaller ratio of the sample to the standard solution amount interacting with the immobilized enzyme and the detector. The determination range can be apparently extended to even higher sample concentrations. But not precisely measurable small $\Delta t_{m,i}$ values would be the consequence.

TABLE 2

Enzymatic FIA determination of glucose ($n = 3$, $\alpha = 0.05$, $2\tau = 600$ s, $\dot{V}_{NAD} = 0.5$ ml min^{-1})

	Standard addition method $c_{max} = 1$ mM $\dot{V}_S = 0.5$ ml min^{-1} $\dot{V}_{ST} = 0.6$ ml min^{-1} $\dot{V}_{NAD} = 0.5$ ml min^{-1}		Sample addition method $c_{max} = 0.1$ mM $\dot{V}_S = 0.6$ ml min^{-1} $\dot{V}_{ST} = 0.5$ ml min^{-1} $\dot{V}_{NAD} = 0.5$ ml min^{-1}	
Glucose concentration taken (mM)	Glucose concentration found (mM)		Glucose concentration found (mM)	
	Without calibration	After calibration	Without calibration	After calibration
0	0.001 ± 0.001	−0.002 ± 0.001		
0.1	0.101 ± 0.005	0.097 ± 0.005		
0.12			0.1193 ± 0.0004	0.1197 ± 0.0004
0.14			0.139 ± 0.001	0.140 ± 0.001
0.17			0.167 ± 0.001	0.169 ± 0.001
0.2	0.204 ± 0.002	0.199 ± 0.002	0.195 ± 0.004	0.198 ± 0.004
0.25			0.245 ± 0.002	0.251 ± 0.002
0.3	0.309 ± 0.001	0.303 ± 0.001	0.290 ± 0.003	0.299 ± 0.003
0.4	0.413 ± 0.003	0.406 ± 0.002	0.377 ± 0.002	0.394 ± 0.002
0.5	0.511 ± 0.001	0.497 ± 0.001	0.467 ± 0.005	0.495 ± 0.005
0.6	0.608 ± 0.005	0.599 ± 0.002	0.564 ± 0.012	0.607 ± 0.012
0.7	0.706 ± 0.002	0.697 ± 0.002	0.636 ± 0.008	0.693 ± 0.008
0.8	0.815 ± 0.003	0.805 ± 0.003	0.726 ± 0.005	0.803 ± 0.005
0.9	0.905 ± 0.007	0.894 ± 0.007	0.838 ± 0.006	0.944 ± 0.006

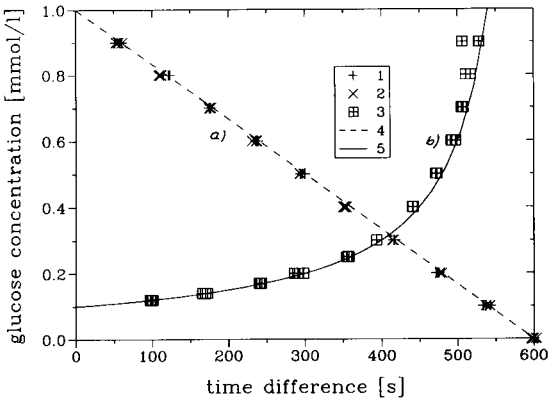

Fig. 11. Comparison between measured and precalculated working lines for the enzymatic FIA determination of glucose; a = standard injection; b = sample injection FIA; 1, 2 and 3 = measured values (1 with Dosimat 665 piston pumps, 2 and 3 with TEC-S micropumps); 4 and 5 = precalculated working lines; conditions as shown in Table 2.

Conclusions

Precisely generated triangle concentration profiles open up a way to more reliable procedures in flow analysis. Volumetric triangle-programmed flow titrations can be implemented in short capillary tubes. The volumetric version widens the application field of the flow-through triangle-programmed titration introduced by Nagy and coworkers [4–7] as a coulometric titration technique.

The continuous mixing of triangle concentration profiles with inverse triangle profiles of the titration reagent and the sample solution, respectively, allows the extension of the determination range over three orders of magnitude. The application of linear concentration gradients has the advantage of non-distorted photometric and fluorimetric titration curves also under flow-through conditions. This simplifies the automatic evaluation of the titration curves.

Reversed FIA procedures can be rapidly calibrated by means of triangle-programmed concentration gradients generated on-line from a standard stock solution and a diluent. The corresponding generation of triangle-shaped gradient profiles of the sample substance and the zone sampling into a constantly flowing standard solution allows the reliable and precise analysis of the sample solution with a simplified calibration procedure based on one standard stock solution.

REFERENCES

1 W.J. Blaedel and R.H. Laessig, Anal. Chem., 36 (1964) 1617.
2 W.J. Blaedel and R.H. Laessig, Anal. Chem., 37 (1965) 332.
3 B. Fleet and A.Y. Ho, Anal. Chem., 46 (1974) 9.
4 G. Nagy, K. Toth and E. Pungor, Anal. Chem., 47 (1975) 1460.
5 G. Nagy, Z. Fehér, K. Toth und E. Pungor, Anal. Chim. Acta, 91 (1977) 87.
6 G. Nagy, Z. Fehér, K. Toth und E. Pungor, Anal. Chim. Acta, 91 (1977) 97.
7 G. Nagy, Z. Fehér, K. Toth und E. Pungor, Anal. Chim. Acta, 100 (1977) 181.
8 Z. Fehér, G. Nagy, K. Toth and E. Pungor, Analyst, 104 (1979) 560.
9 Z. Fehér, I. Kolbe and E. Pungor, Fresenius' Z. Anal. Chem., 332 (1988) 345.
10 U. Spohn, G. Nagy and E. Pungor, Anal. Sci., 2 (1986) 423.
11 U. Spohn, B. Fuhrmann and K.-H. Mohr, in F.W. Scheller and R.D. Schmid (Eds.), Biosensors: Fundamentals, Technologies and Applications, GBF Monograph, Vol. 17, VCH, Weinheim, 1992, p. 291.
12 B. Fuhrmann, U. Spohn and K.-H. Mohr, Biosensors Bioelectron. 9 (1992) 653.
13 A. Rios, M.D. Luque de Castro and M. Valcárcel, Talanta, 32 (1985) 845.
14 M. Agudo, J. Marcos, A. Rios and M. Valcárcel, Anal. Chim. Acta, 239 (1990) 211.
15 A. Rios and M. Valcárcel, Talanta, 38 (1991) 1359.
16 J. Marcos, G.del Campo, A. Rios and M. Valcárcel, Fresenius' J. Anal. Chem., 342 (1992) 76.
17 J. Marcos. A. Rios and M. Valcárcel, Anal. Chem., 62 (1990) 2237.
18 J. Marcos, A. Rios and M. Valcárcel, Anal. Chim. Acta, 261 (1992) 489–494.
19 J. Marcos, A. Rios and M. Valcárcel, Anal. Chim. Acta, 261 (1992) 495.
20 U. Spohn, R. Eberhardt, B. Joksch, R. Wichmann, Ch. Wandrey and H. Voß, in R.D. Schmid (Ed.), Flow Injection Analysis (FIA) Based on Enzymes or Antibodies GBF Monograph, Vol.14, VCH, Weinheim, 1991, p. 51.
21 J.K. Taylor and S.W. Smith, J. Res. Natl. Bur. Std., 63A (1959) 153.
22 J.M. Reijn, H. Poppe and W.E. van der Linden, Anal. Chim. Acta, 145 (1983) 59.
23 J.M. Reijn, W.E. van der Linden and H. Poppe, Anal. Chim. Acta, 114 (1980) 105.
24 J.M. Reijn, W.E. van der Linden and H. Poppe, Anal. Chim. Acta, 123 (1981) 229.
25 J.M. Reijn, W.E. van der Linden and H. Poppe, Anal. Chim. Acta, 126 (1981) 1.
26 J. Tyson, Fresenius' Z. Anal. Chem.329 (1988) 663.

Analytica Chimica Acta, 282 (1993) 407–415
Elsevier Science Publishers B.V., Amsterdam

Neural networks for interpretation of infrared spectra using extremely reduced spectral data

M. Meyer, K. Meyer and H. Hobert

Institut für Physikalische Chemie, Friedrich-Schiller-Universität Jena, Lessingstrasse 10, O-6900 Jena (Germany)

(Received 21st December 1992)

Abstract

In order to classify infrared (IR) spectra into structural groups the application of artificial neural networks is a powerful tool. The network architecture used for this work was a back propagation model with one hidden layer. For the minimization of the network the number of input elements has been reduced extremely. Instead of the whole infrared spectrum (512 measuring points) the score values calculated by principal component analysis (PCA) involving the spectra of the training set (700) and the prediction set (348) were used as input elements for the network. The number of principal components or scores per spectrum as network input, respectively, has been varied (4, 6, 8 and 10) to find out the minimal spectral information needed for a sufficient prediction ability of the network. 13 IR sensitive structural patterns have been defined as output elements of the network. Results obtained for the training and prediction step are discussed. The prediction performance of the neural network operating with such extremely reduced spectral data is surprisingly good.

Keywords: Infrared spectrometry; Principal component analysis; Neural networks

The application of artificial neural networks for interpretation of spectral data increased in the last few years and is an established alternative approach to other methods like library search, pattern recognition and knowledge based expert systems. Different types of spectra have been used for spectral interpretation by neural networks (infrared, mass, NMR, UV spectra). The Review article of Zupan and Gasteiger [1] gives a good summary concerning these investigations, which can be completed with some more recent papers [2–4]. In most of the cases the spectral information used as network input was directly the digitized spectrum so that the number of input elements can vary in the range between 100 and 4000, approximately. We have also used 128 or 512, respectively, measuring points of infrared spectra in our recent studies [5]. This kind of representation of spectral data implies some disadvantages with regard to neural network application. With a high number of elements in the input layer and because of better recognizability of the network desirable high number of hidden layer elements the total number of network nodes increases rapidly. The result is a significant enhancement of computing time required for the training sessions. Furthermore, in most of infrared spectra (but not only in these) the spectral information is distributed not evenly over the whole spectral region, but it is concentrated in distinct ranges of the spectrum corresponding with the structural pattern. Therefore it is favorable to reduce the spectral data by PCA in order to extract the useful information from the origi-

Correspondence to: M. Meyer, Institut für Physikalische Chemie, Friedrich-Schiller-Universität Jena, Lessingstrasse 10, O-6900 Jena (Germany).

nal spectrum. The spectral interpretation will be performed in two steps, the reduction of data by PCA and the classification into structural classes by the neural network. The performance of the network in prediction of functional groups has been investigated using different numbers of principal components.

EXPERIMENTAL

For the spectral interpretation two self-made computer programs written in TurboPascal 6.0 for PCA and for simulation of the neural network were used. Spectra with 512 measuring points from the IR database of our library search system SUSY [6] were used for the training and the prediction set. The training set consists of 700 spectra, whereas 348 spectra have been chosen for the prediction set. All spectra were normalized to a vector length of one.

PCA

The dimension of the data matrix **D** used for the PCA calculations is defined by the number of spectral measuring points (512) and the size of the training set (700). PCA was performed using the NIPALS algorithm, which gives with some modifications the same results like an eigenanalysis of the 512 by 512 covariance matrix **Z** computed from the 512 points by 700-data matrix **D**.

$$\mathbf{Z} = \mathbf{D} \cdot \mathbf{D}^T$$

The eigenanalysis of the covariance matrix **Z** results in n eigenvalues in an n by n diagonal matrix Λ, n eigenspectra in the n by 512 matrix **R**, and 700 score vectors in an n by 700 score matrix **Q**.

$$\mathbf{R} \cdot \mathbf{Z} \cdot \mathbf{R}^T = \Lambda$$

$$\mathbf{R} \cdot \mathbf{D} = \mathbf{Q}$$

But it is favorable to compute the eigenvalues, eigenspectra, and scores directly from the spectra of the training set using the NIPALS procedure, because the manipulation of such a large 512 by 512 data matrix with a PC with 640-kB memory is very difficult and requires much computing time. The NIPALS procedure allows to calculate the scores and eigenspectra more quickly and to abort the computations if the desired number n of principal components is reached. The details of the NIPALS algorithm are described, e.g., by Martens and Naes [7]. After PCA the information at the 512 measuring points of the training set spectra in the data matrix **D** is reduced to a maximum of 10 score values per spectrum in matrix **Q**. These 10 principal components maximum should reflect the most significant features of the whole training set. The data matrix **D** can be considered as the sum of the linear combination of the eigenspectra for the n principal components weighted by the score values and the residual matrix $\mathbf{D}_S$, which contains beside noise and errors also the special features of the spectra.

$$\mathbf{D} = \mathbf{Q} \cdot \mathbf{R}^T + \mathbf{D}_S$$

With an increasing number of principal components the score vectors describe more special features of the individual spectra and the elements of the residual matrix $\mathbf{D}_S$ are decreased. All spectra of the training set can be visualized as points in an n-dimensional hyper space, but although the spectra have been normalized to unity vector length before PCA the spectra points lie not near the surface of an unit hyper sphere, as long as the residual matrix $\mathbf{D}_S$ contains not only noise. Nevertheless, the position of the spectral points in the n-dimensional hyper space or the score vectors, respectively, can be used for a separation of the spectra into groups. For the classification of a set of 348 unknown spectra $\mathbf{D}_U$ at first the pseudo-score matrix $\mathbf{Q}_U$ must be computed using the eigenspectra of the training set and the 348 unknown spectra of the prediction set.

$$\mathbf{R} \cdot \mathbf{D}_U = \mathbf{Q}_U$$

If the positions of the unknown spectra in the n-dimensional hyper space of the training set are determined, it is possible to classify them into the defined groups.

Classification

Common procedures for separation and classification [8] need large differences between the features of the objects of different classes, as

small as possible deviations within the classes, and a well-defined training set. In the general case of spectral interpretation of organic compounds the different C–H content and the various functional groups of the compounds prevent the separation into distinct classes. Even if the training set consists only of spectra of monofunctional compounds and allows a separation of the spectra into classes with regard to their functional groups, it is impossible to determine all functionalities of compounds with more than one functional group in one step using the common classification procedures. In contrast to these approaches the neural network enables to detect simultaneously all functionalities of a compound. The investigations should demonstrate that the advantages of data reduction by PCA can be also useful for the spectral interpretation by a neural network.

The network has a three-layered architecture with an input layer, one hidden layer and an output layer. The input layer consists of a varying number of NIPALS scores (4–10) for each spectrum of the training set and the prediction set. The size of the hidden layer was defined by 30 network elements. The 13 output units of the network correspond with 13 predefined IR sensitive structural patterns (Table 1).

TABLE 1

IR sensitive structural pattern as output elements of the network

No.	Structural pattern	Frequency in training set	Frequency in prediction set
1	Alcohol	153	75
2	Amine	85	32
3	Ketone	60	44
4	Ester	61	50
5	Aldehyde	25	14
6	Carboxylic acid	96	18
7	Amide	39	39
8	C–Halogen group	132	83
9	Nitro group	69	13
10	Sulfo group	25	9
11	Ether	74	58
12	Aromatic C–H group	410	161
13	Aliphatic C–H group	482	305
Total		1711	901

RESULTS AND DISCUSSION

For the present work the NIPALS calculations were restricted to a number of 10 eigenspectra and 10 corresponding scores. The set of obtained eigenspectra are shown in Fig. 1. The first eigenspectrum is a positive linear combination of the training set spectra and can be interpreted as a mean spectrum of all these spectra. In all of the further eigenspectra both positive and negative combinations are possible as it is seen in the feature of the eigenspectra. The function of each of the consecutive eigenspectra is to separate as much as possible spectral patterns present in the data set from each other. Spectral features of functional groups with great intensity values which are not strongly overlapped with other characteristic features, will separate much better than patterns of functionalities with weak absorption bands or spectral pattern overlap with some others. For instance it is obvious that alcohols and compounds containing a carboxylic group can be discriminated very well (mainly by the second eigenspectrum) whereas the separation of amines or compounds with a sulfo group from all others is relatively poor.

Training step

The training of the neural network has been performed using 4, 6, 8 or 10 scores as representation of each spectrum of the training set. When the convergence of minimization of the output error became slow the training session was stopped. The output error has been defined as the deviation of the current network output to the given target values of the output layer. The values achieved after the training step are given in Table 2. To judge the success of network learning it is useful to have a look at the recognizing level for the defined structural groups. In Table 3 the results of network training for all numbers of scores used as input are summarized. All functionalities found correctly are called "true", functional groups which are present in a substance but not found by the network are called "false – ". Finally, substructures found by the network which are not present in a substance are named "false + ". It can be seen that for some

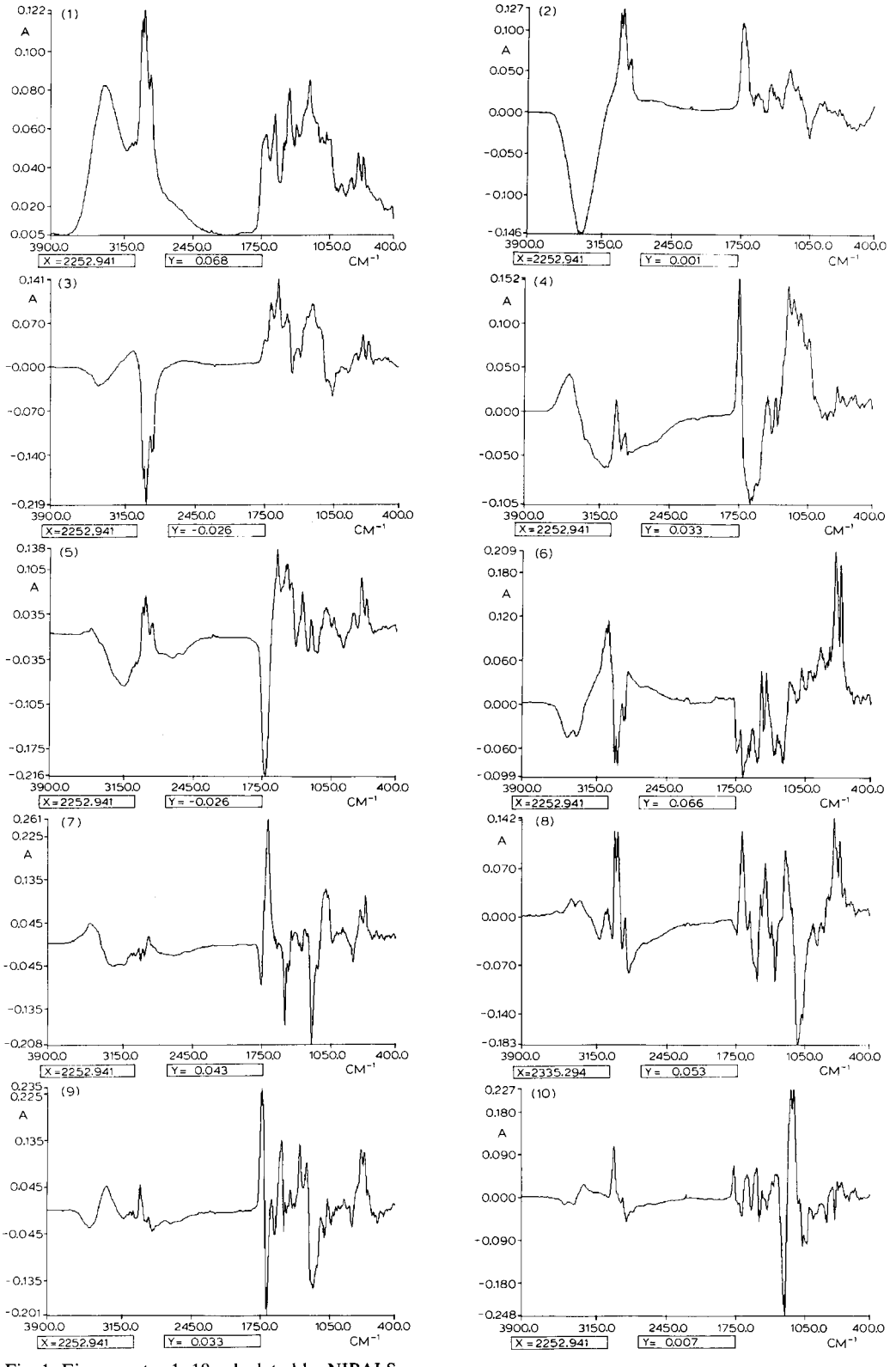

Fig. 1. Eigenspectra 1–10 calculated by NIPALS.

TABLE 2

Output errors of trained network

	Number of scores			
	4	6	8	10
Output error (absolute)	218.75	139.15	94.50	69.68
Output error (%)	2.4	1.5	1.03	0.76

functional groups the recognizing ability increases more or less continuously with the number of input elements of the network (e.g., alcohols, amines and carboxylic acids) whereas for some other functionalities the performance decreases or stagnates (e.g., esters, aldehydes and amides). The reason for the different behavior of functional groups is the distribution of spectral information in the eigenspectra obtained by PCA. If the total information of a spectral feature (corresponding to a certain functional group) is distributed more evenly to all eigenspectra, the performance of network learning will improve with increasing numbers of input elements. For the opposite case, if the spectral information related to a substructure can be focussed by PCA into one or only a few eigenspectra, the recognizing ability of the network may alternate to become better or worse with increasing numbers of input elements. The special performance behavior of some of these functional groups will be discussed below.

In the case of the ketone functionality using 4 input elements only 28% were recognized by the network. This indicates, that only a small part of characteristic spectral information is involved in the first four eigenspectra. The increase of the number of input elements to 6 causes a strong improvement of "true" recognized ketones up to 70%, which means that the main part of spectral information characteristic for ketones is concentrated in the fifth and sixth eigenspectrum. Switching to 8 input elements, the performance increases slightly to 85% and remains constant also for 10 input elements.

Another interesting example is the ester functionality. The performance is already high with 4 input elements (93% "true") and gets better with 6 (95% "true") and 8 (100% true) input elements. But the expansion of input elements up to 10 leads to a decrease of recognizing performance down to 89%. How can this behavior be interpreted? The main part of specific spectral information for the ester functionality is located in the first four eigenspectra, but also in the next eigenspectra (5–8) some useful information is contained. The use of additional scores (corresponding to eigenspectrum 9 and 10) as network input does not improve but reduces the recognizing ability, because this information is non-relevant for the ester functionality or in conflict with the assignment to other substructures containing a carboxylic group (e.g., ketones, aldehydes, carboxylic acids). In other words, the specific information attributed to the ester functionality becomes more fuzzy with expansion of score numbers up to ten.

A third type of dependence of functional group recognition from the number of scores can be observed for the sulfo group. The performance improves with increasing numbers of scores, but even with 10 score values the recognizing ability is relatively poor (68%). This indicates that the number of principal components used for the network training is too low (some specific information is involved in further principal components) or the spectral feature of a functional group is not clearly correlated to a distinct substructure.

Prediction step

After the training step it was tried to classify a set of unknown spectra (represented by their NIPALS scores as described above) by the neural network. The results of the prediction of functional groups using also 4, 6, 8 and 10 score values as network input are shown in Table 4. It can be seen that, of course, the prediction ability is close correlated with the performance of the training for the different functional groups. Functionalities which were recognized very well in the training step can also be predicted very well whereas the prediction performance for some other functional groups with wrong training results is relative poor. In average (for all used substructures and all numbers of scores) the level of "true" prediction is lower than the level of

TABLE 3

Network performance using the training set (recognizing ability)

No.	Structural pattern	Number of scores as network input											
		4			6			8			10		
		True (%)	False − (%)	False + (%)	True (%)	False − (%)	False + (%)	True (%)	False − (%)	False + (%)	True (%)	False − (%)	False (%)
1	Alcohol	86	14	2	90	10	2	92	8	1	96	4	0
2	Amine	62	38	1	84	16	1	93	7	0	95	5	0
3	Ketone	28	72	0	70	30	0	85	15	0	85	15	0
4	Ester	93	7	0	95	5	0	100	0	0	89	11	0
5	Aldehyde	52	48	0	80	20	0	80	20	0	56	44	0
6	Carboxylic acid	74	26	1	97	3	0	99	1	0	100	0	0
7	Amide	69	31	1	82	18	0	74	26	0	90	10	0
8	C–Halogen group	57	43	5	68	32	8	66	34	1	80	20	1
9	Nitro group	48	52	1	77	23	0	93	7	0	97	3	0
10	Sulfo group	44	56	0	60	40	0	60	40	0	68	32	0
11	Ether	75	25	1	77	23	0	82	18	0	85	15	0
12	Aromatic C–H group	94	6	19	98	2	5	97	3	4	100	0	4
13	Aliphatic C–H group	92	8	26	96	4	9	97	3	5	99	1	3
	Total	79.6	20.4	2.5	89.6	10.4	1.5	91.8	8.2	0.6	94.4	5.6	0.4

TABLE 4

Network performance using the prediction set (prediction ability)

No.	Structural pattern	Number of scores as network input											
		4			6			8			10		
		True (%)	False − (%)	False + (%)	True (%)	False − (%)	False + (%)	True (%)	False − (%)	False + (%)	True (%)	False − (%)	False + (%)
1	Alcohol	80	20	7	79	21	3	81	19	6	83	17	3
2	Amine	25	75	2	56	44	4	44	56	7	69	31	4
3	Ketone	27	73	1	48	52	4	64	36	3	59	41	3
4	Ester	92	8	2	90	10	2	86	14	2	74	26	1
5	Aldehyde	36	64	1	21	79	3	36	64	1	21	79	1
6	Carboxylic acid	72	28	3	100	0	3	100	0	3	94	6	3
7	Amide	31	69	1	41	59	1	21	79	0	64	36	1
8	C–Halogen group	45	55	9	53	47	16	46	54	5	57	43	9
9	Nitro group	31	69	1	69	31	1	69	31	1	85	15	1
10	Sulfo group	0	100	0	11	89	1	56	44	2	0	100	3
11	Ether	45	55	4	57	43	1	55	45	2	60	40	2
12	Aromatic C–H group	88	12	25	81	19	23	80	20	21	91	9	20
13	Aliphatic C–H group	93	7	47	89	11	41	94	6	35	92	8	30
	Total	71.6	28.4	4.2	72.0	28.0	4.9	75.0	25.0	4.2	78.9	21.11	4.0

true recognition in the training step, but in some cases the prediction behavior as function of the number of scores is unexpected or obscure. For example, for the aldehydes the "true" value for the training using 4 scores is 52%, the corresponding prediction value is 36%. Switching to 6 scores the values are 80% and 21%, respectively. The recognizing ability increases but the prediction performance decreases. There are some possible reasons for such a behavior. One reason can be a different distribution of types of aldehydes (aromatic, aliphatic or heterocyclic) in the training set and in the prediction set. Another possible explanation is the different certainty of recognition or prediction of a functionality for changing numbers of scores. Because the threshold of "true" assignment is simply set to 0.5 without further differentiation of the quality of assignment for all values climbing over this threshold the distribution of these "true" values can variously affect the performance of the network for different numbers of scores. This fact should be illustrated by the histograms of the output values of the network for the training and prediction step (Fig. 2). It can be seen that in the case of 4 scores the general feature of the histograms (distribution) for the training step and the prediction step is more or less similar apart from a slight shift to lower output values for the prediction. If 6 scores are used as network input the percentage of output values > 0.5 becomes relatively high (80%) for the training set but the distribution of these values is very broadly smeared between 0.5 and 1.0. This feature of the training set histogram may be the reason for the bad prediction performance (21%) which is in accordance to the shown histogram for the prediction set.

Whereas the percentage of "false +" assignments in the training step is very low (with exception of the aromatic and aliphatic C–H functionality with 4 scores as network input), in the prediction step the part of additional functional groups found, which are not present in the substance, became higher, but it is apparent that this effect is more marked for functionalities, which are more general and not so specialized, e.g., the aromatic or aliphatic C–H or the C–halogen group, respectively.

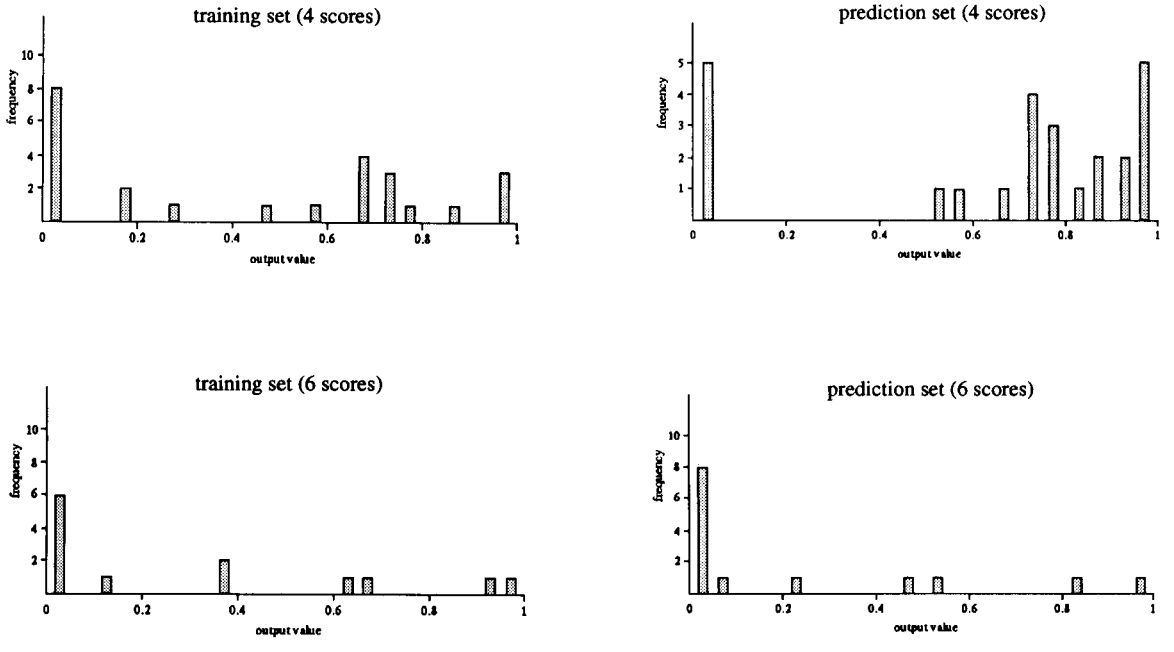

Fig. 2. Histograms of network output values for the aldehyde functionality.

Another typical effect which is often found in neural network studies is the phenomenon of overtraining. Such a behavior can be observed in our investigation especially for the ester and the carboxylic acid functionality. In both cases the network can be trained so that it recognizes all present substructures in the training set ("true" = 100%) if the available spectroscopic information (number of used eigenspectra or scores, respectively) is sufficient. For esters 8, and for carboxylic acids 10 scores are needed for this behavior, but using the same number of scores for the prediction step the performance for these learned functional groups was wrong in contrast to the case that the training was performed with a lower number of scores, where the recognition rate is in a region between 95 and 100%. An explanation for this is that if too much specialized information for a distinct functional group is included in the data of the training set the network is not able to tolerate possible variations in the spectral data of the prediction set. Therefore a little loss of information in the training set makes the network more flexible and can enhance the performance in the prediction step.

Conclusions

The goal of our studies presented in this paper was to find out what is the minimal amount of spectral information for classifying infrared spectra by an artificial neural network. The use of PCA for the reduction of spectral data is very favorable for a selective extraction of the specific information correlated with the functional groups of the compounds. It has been shown that in most of the cases a number between 4 and 10 scores obtained by the NIPALS procedure is sufficient to classify structural unknown substances by a neural network into the 13 defined substructures. With respect to the fact that most of the compounds of the training and the prediction set are multifunctional substances (average value = 2.5 functional groups per compound), the performance of the network operating with such extremely reduced spectral data is surprisingly good. It has been shown that the combined application of PCA and neural networks is a powerful tool for a quick structural classification.

REFERENCES

1 J. Zupan and J. Gasteiger, Anal. Chim. Acta, 248 (1991) 1.
2 K. Tanabe, T. Tamura and H. Uesaka, Appl. Spectrosc., 46 (1992) 807.
3 L.S. Anker and P.C. Jurs, Anal. Chem., 64 (1992) 1157.
4 C. Borggaard and H.H. Thodberg, Anal. Chem., 64 (1992) 545.
5 M. Meyer and T. Weigelt, Anal. Chim. Acta, 265 (1992) 183.
6 M. Meyer, I. Weber, R. Sieler and H. Hobert, Jena Rev., 35 (1990) 16.
7 H. Martens and T. Naes, Multivariate Calibration, Wiley, Chichester, 1989.
8 K. Varmuza, Pattern Recognition in Chemistry, Springer, New York, 1980.

Analytica Chimica Acta, 282 (1993) 417–422
Elsevier Science Publishers B.V., Amsterdam

Hypertext tools for the selection of dissolution methods prior to the atomic absorption analysis of pharmaca

W. Penninckx, J. Smeyers-Verbeke and D.L. Massart,
Vrije Universiteit Brussel, Laarbeeklaan 103, 1090 Brussels (Belgium)

L.G.C.W. Spanjers and F.A. Maris
AKZO Pharma group, Organon International BV, P.O. Box 20, 5340 BH Oss (Netherlands)

(Received 1st June 1993)

Abstract

A hypertext system for the selection of dissolution methods prior to the atomic absorption analysis of pharmaca was developed. The knowledge about dissolution methods, available in an industrial quality assurance laboratory, was first structured in a decision tree. The tree was implemented in a knowledge-based computer system using Toolbook software, an object oriented language for the personal computer. Beside its user-friendliness and possibility to build an attractive user-interface, this language permits the extension of the system with some important options, which would be difficult or impossible to create with other tools. The most important options are: (a) a partial maintainability of the system that is given to the user, (b) the visualization of the strategy of the decision making by displaying the structure of the tree in combination with a list of consulted pages, and (c) a database which ensures the completeness of the presented information and can easily be separately consulted.

Keywords: Atomic absorption spectrometry; Dissolution methods; Knowledge-based systems; Pharmaca

The selection of a dissolution step prior to the analysis is found to be one of the major problems in the development of atomic absorption spectrometric methods for pharmaceutical purposes [1]. In practice a wide variety of dissolution methods is used, which frequently differ from matrix to matrix and from element to element. Industrial quality control laboratories often develop specific methods for the analysis of their own products and materials. In this project we tried to structure the knowledge about this problem, available in an analytical industrial laboratory, and to present it in a clear and complete way to the analyst. First the knowledge was structured in a number of rules which were transformed into a decision tree. Different tools have been investigated to implement the tree in a knowledge-based computer system, which assists the analyst in the selection of dissolution methods [2]. Among them an expert system shell, analog to the one that was used by Browett et al. [3] to implement "ACmethods", the analytical methods selection module of the "ACexpert" system for automated atomic absorption spectrometry. The fact that the knowledge was structured in a decision tree is, however, in contradiction with the concept of a rule-based expert system, where the system itself should decide which parts of the information are used and how these parts are linked to each

Correspondence to: D.L. Massart, Vrije Universiteit Brussel, Laarbeeklaan 103, 1090 Brussels (Belgium).

other. Moreover the unattractive user-interface and the poor maintainability were seen as additional disadvantages. Toolbook software, which is considered as one of the best object oriented languages for the PC [4], was found to be the most suitable tool [2]. A prototype of the system was developed and evaluated on the accuracy of the information it contains, its user-friendliness and its didactic value. Subsequently, the possibility to attach a database to it was investigated.

Instrumentation

An IBM Model 55 SX personal computer was used for all programming. All programmes that were used run under Microsoft Windows. Toolbook 1.0 software (Asymetrix Co., Belleville, IL) was used since it is recommended as object oriented language for the PC [4]. Superbase 4 (Software Products International, San Diego, CA) was selected as database package. It was shown to be one of the best Windows packages [5]. A graphical representation of the decision tree was made with ABC flowcharter (Roykore, San Francisco, CA) and, subsequently, pasted into the Toolbook application.

Knowledge acquisition and structuring

An analytical industrial laboratory, charged with the quality control of pharmaca, provided the knowledge that was necessary for this work. The strategy that was followed for the knowledge acquisition and structuring was discussed earlier [2]. All validated analyses that are performed in the quality control laboratory were subdivided in a number of sets and subsets according to the nature of the sample, since this was found to be the principal parameter in the selection of dissolution methods. For each set and subset a simple first-guess method was sought, as well as a more powerful method which can be used if the first-guess method fails in practice. In some situations, the use of different dissolution methods in one set or subset of related sample types could only be explained by taking into consideration the type of the analyte, the concentration level of the analyte or the purpose of the analysis. The primary rules were corrected and refined by submitting them to new examples. The refined rules were transformed into a decision tree. In this tree the user is guided through a certain path by the answers he gives on a number of questions. Eventually, a dissolution method is selected.

Description of the knowledge-based system

For the implementation of the decision tree in a computer system Toolbook software, an object-oriented language for the PC, was found to be the most suitable tool [2]. The system can be looked at as an electronic book. Some pages contain questions on the matrix, the type of analyte or the concentration level of the analyte with a number of possible answers. The user can select one of these answers by clicking a button on the screen with the mouse. The small script (or program) that is attached to this button is then activated and the user is navigated to another page, depending on the selected answer. This can be a page with a new question to the user or a page where a dissolution method is proposed. In general the user is guided through a number of question pages before a dissolution method is proposed. Information pages are included since an inexperienced user can have problems with the understanding of some concepts that are used in the system. This information is displayed when the concept that has to be explained is clicked with the mouse. Afterwards, the consultation can be continued. The working of the system is explained by an example in Fig. 1. A dissolution method that can be used prior to the determination of a number of heavy metals (Cd, Pb, Zn, etc.) in allylestrenol is selected. At the start of the consultation a different path will be followed by a user who works for the first time with the system and by a more experienced user. The former will be guided through a number of pages with specific information, while the latter is immediately guided to page number 3, where he is reminded to check if a dissolution method for the product is described in the Pharmacopea. He is also informed on a number of analyses for which specific dissolution methods are used. Since none of these are relevant for the given example the "Continue" button has been selected which is linked to page 15. There the matrix type must be specified. If the user has problems with the con-

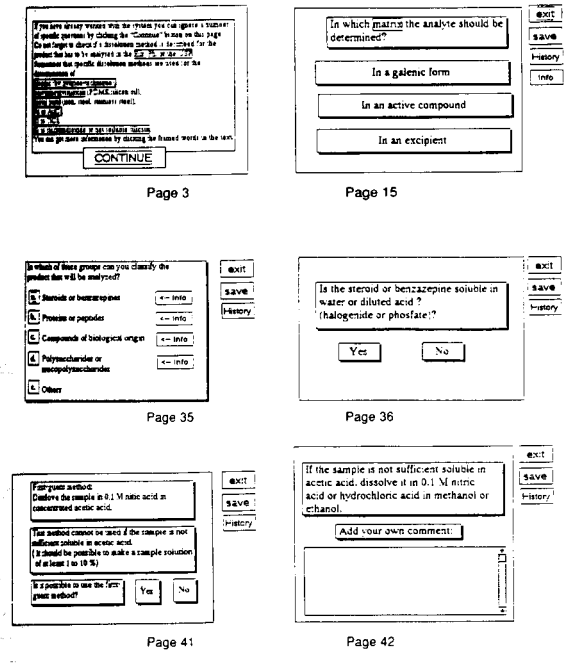

Fig. 1. Screens of the knowledge-based system the user is guided through when selecting a dissolution method for allylestrenol.

cepts "galenic form", "active component" or "excipient", a short explanation can be displayed by selecting the "Info" button. From the information page the consultation can be continued by selecting the "Back" button. Subsequently, the type of the active compound should be defined. Information screens are provided if any problems with the selection would occur. Since a dissolution method for allylestrenol is looked for, the "Steroids" button is selected. Page 36 mentions that only halogenide and phosphate salts of steroids are soluble in water so that the question on this page will be answered with "no". Finally, a dissolution in 0.1 M nitric acid in concentrated acetic acid will be proposed (page 41). However, this method cannot be used if no sample solution of 1–10% can be made, due to the low solubility of the matrix in acetic acid. If no information about the solubility of allylestrenol in acetic acid is available this can be investigated by a small experiment. In practice the first-guess method is found to be unsuitable and the question on page 41 is answered with "no". The system reacts by proposing a dissolution in 0.1 M nitric acid in methanol or ethanol (on page 42), which was indeed found suitable. The user can leave the system at any moment of the consultation by selecting the "exit" button. The use of the "save" and "history" button is explained further.

Validation and evaluation of the system

The system's advice was asked for 60 sample types which were used for the building of the primary rules and 70 sample types were used for the correction and refining. Little discrepancies were found between the method suggested by the system and the one that was found suitable in practice. Small differences could easily be corrected by making small changes in the information that is displayed in the system. For 30 new samples that were investigated some problems occurred with sample types for which a specific dissolution method should be used. In general these specific analyses were mentioned too late in the system which could lead to a wrong system's advise. The detection of metal parts (iron, steel, stainless steel), for example, requires the use of a specific and powerful method, where the sample is digested in a mixture of concentrated nitric acid and hydrochloric acid with heat supply. In the analyses that were evaluated to build the system, metal parts were only traced in tablets and the information was incorporated in this part of the tree. Consequently, if the system's advise on the detection of metal parts in another matrix was asked, a wrong suggestion was obtained.

These problems were corrected by making small changes to the structure of the tree and the linking of the pages. Note that the system that is described in Fig. 1 is already corrected, as can be seen on page 3.

A student, with good theoretical background but little practical experience, who evaluated the prototype of the system experienced only small problems with the working of the system. The main problem occurred with the understanding of some concepts so that it was found useful to extend the number of information pages. Overall, it can be concluded that since the didactical possibilities of the system are very good, inexperi-

enced people can effectively learn the reasoning behind the selection of dissolution methods.

Options

The use of a hypertext language permits the incorporation of some important options which contribute to the maintainability, didactic value, user-friendliness and completeness of information of the system. It would be impossible or very difficult to create these when another tool, such as an expert shell, was used.

Maintainability. The maintainability is one of the main problems for most expert- and knowledge-based systems. While the expertise in many domains changes frequently, most systems cannot be updated by the user. Moreover, it is not possible to correct defaults or gaps which are detected during the use of the system. Generally, changes of the system can only be made by the programmer, after re-evaluation of the knowledge and discussion with the expert. This is especially the case for rule-based expert systems where small changes in the rules can change the working of the whole system. The use of Toolbook software permitted us to give a partial maintainability to the user. Therefore empty text fields are provided on pages where dissolution methods are proposed, as can be seen on page 42 of Fig. 1. In these fields the user can add his personal comments on the system's advise or propose an alternative dissolution method. These comments are displayed in later consultations and can also be used as background material for updating of the tree. A more complete maintainability by the user, where the complete information of the system can be changed, was not found beneficial. If different users all change the information in the system a completely different system will be created of which the exact content is known by nobody, and that would lead to confusion.

History function. In practice it was found that to achieve a better understanding of the strategy of the selection of dissolution methods, it is beneficial to use the system in combination with a representation of the decision tree. Consequently the system was extended with a number of pages where such a representation of the tree is given, as can be seen in Fig. 2. The user can navigate to

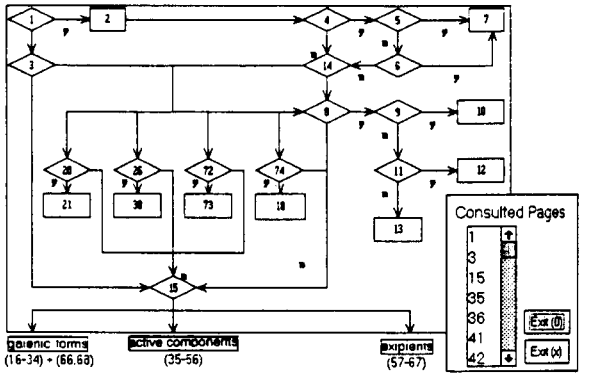

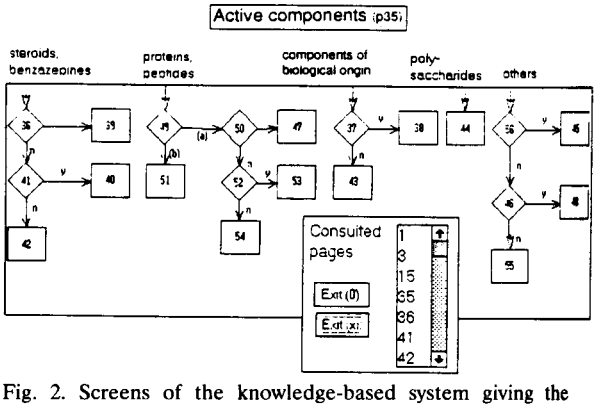

Fig. 2. Screens of the knowledge-based system giving the history of the consultation.

these pages at any time of the consultation. There, he is also informed about the screens of the system he has been guided through, which must demonstrate the strategy of the decision making to the inexperienced analyst. From the representation of the tree the user can navigate to the different pages of the system by clicking their number in the tree. This can be useful if somewhere a wrong choice was made or when dissolution methods are selected for several similar matrices, with the information in the same part of the tree. Moreover the information on the consulted pages can be saved so that the user can exit the system, perform an experiment, and continue his consultation. If, for example, the user has selected a dissolution method for allylestre-

nol (see Fig. 1) and clicks the "History" button, the first screen of Fig. 2 will be displayed. Note that the information pages are not mentioned in the "consulted pages" list, since these have no influence on the selection of the dissolution step. On the flow-chart it can be seen that a short way was followed to page 15 were the type of matrix was specified. Subsequently all pages consulted can be found in the part of the tree about active components. By clicking the "active component" button this part of the tree will be displayed (Screen 2 of Fig. 2). When the user wants to leave the system or to start a new consultation, he can save the information on the consulted pages by selecting the "Exit(o)" button, or clear this information by selecting the "Exit(x)" button.

The database. An extension of the system with a database that contains information on the analyses that are performed in the laboratory was found essential to guarantee the completeness of the presented information. The combination of database and knowledge-based system prevents the use of the computer system as a black box: while the database gives information on the method that was used in practice, the knowledge-based system can be used to investigate how this method was selected Moreover, this permits the detection and evaluation of system advises which are different from the methods used in practice. However, since the database is also consulted by more experienced analysts it should also be possible to use it without the knowledge system.

To permit a complete interaction we tried to build the database in the same tool as the knowledge system. A Toolbook application was built where every page was considered as a database record and contained information on a single analysis. The user is asked for the matrix of interest and is navigated to the page that gives this information. It was possible to build a system with a nice user-interface which gives very specific information. However, as the amount of information stored increases, it becomes very slow. Another possibility is to run an existing database programme from a Toolbook application. We selected Superbase software since this is recommended as the best database package for a Windows environment [5]. The programme can easily be started from Toolbook and the search for information is very quick. Although the programme has many advantages on user-friendliness over the conventional database programmes it still requires some expertise to handle. Eventually we succeeded to combine the user-friendliness of the Toolbook application with the speed of the database programme. Toolbook provides several Dynamic Link Libraries (DLL), including one that can be used to access dBASE III + compatible databases. Consequently the user-interface was built in a Toolbook environment while the information is stored and consulted in a dBASE III file. A small Toolbook system, containing 11 pages was built for the communication with the user. The working of the system is

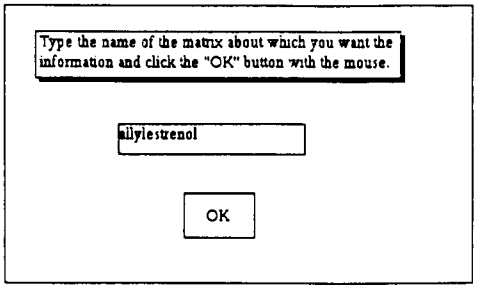

Page 2

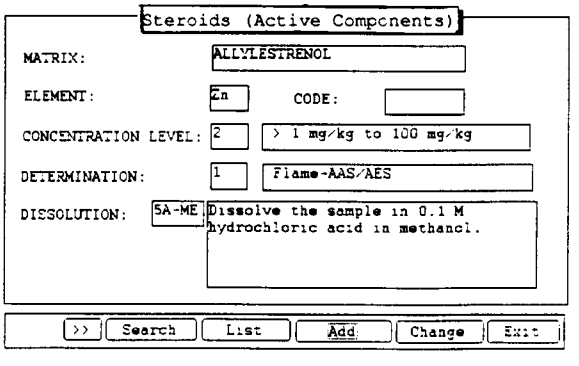

Page 3

Fig. 3. Screens of the Toolbook system linked to the dBASE III + file.

demonstrated in Fig. 3 by an example. To retrieve information on the analysis of a certain product, first page 2 of the system should be displayed. This is possible by clicking the "search" button on one of the other pages. On this page the user can enter the name of the matrix, for example allylestrenol. When the "OK" button is selected the information on allylestrenol will be searched in the dBASE file and displayed on page 3 of the Toolbook system. Information that is stored in the dBASE file as a code is decoded here. The system knows, for example, that concentration level 2 corresponds with a concentration of the analyte between 1 mg kg^{-1} and 100 mg kg^{-1}. If the analyst needs more general information, for example about all analyses of steroids where the concentration of the analyte is situated between 1 mg kg^{-1} and 100 mg kg^{-1}, he should select the "List" button. Moreover, information can be added to or changed in the dBASE file from the Toolbook application. Therefore a password was build in, so that information in the database can only be added or changed by more experienced analysts.

Conclusion

It can be concluded that Toolbook is a good tool for the implementation of a decision tree into a knowledge-based computer system. The main advantages to other tools, such as rule-based expert systems, are the attractive user-interface, the possibility to add personal comments, the easy implementation and the possibility to obtain an overview of the consulted information. This is especially interesting if it is used in combination with a representation of the decision tree, as implemented by us within the system. The dynamic import and export of data from other programmes such as dBASE III + makes it possible to extend the knowledge system with a user-friendly database. The combination of the knowledge system and a database in one tool must prevent the use of the system as a black box, since the inexperienced analyst can investigate how the method that was used in practice was selected. Moreover, after the addition of the database, the system is also frequently used by the experts, which is an additional stimulant for the inexperienced analysts to consult the system.

REFERENCES

1 P. Greber, C. Heppler, C. Hodel, H.R. Lang, R. Maurer, J.B. Reust and H.D. Selner, Swiss Pharma, 12 (1990) 17.
2 W. Penninckx, J. Smeyers-Verbeke, D.L. Massart, L.G.C.W. Spanjers and F. Maris, Chemom. Intell. Lab. Syst. Laboratory Information Management, 17 (1992) 193.
3 W.R. Browett and M.J. Stillman, Prog. Anal. Spectrosc., 12 (1989) 73.
4 L. Wood, Byte, April (1991) 244.
5 R. Grehan and S. Diehl, Byte, January (1992) 226.

Analytica Chimica Acta, 282 (1993) 423–431
Elsevier Science Publishers B.V., Amsterdam

Optimization by mathematical procedures of two dynamic headspace techniques for quantifying virgin olive oil volatiles

Maria Teresa Morales and Ramon Aparicio

Instituto de la Grasa y sus Derivados, Avda Padre García Tejero, 4, 41012 Seville (Spain)

(Received 2nd December 1992; revised manuscript received 11th May 1993)

Abstract

Two dynamic headspace techniques, using activated charcoal with on-column injection and Tenax TA with thermal desorption and cold trap injection, were studied and applied to Spanish virgin olive oil samples. Optimum responses taking into account an overall desirability function were detected by Simplex method and response surfaces were built. Isobutyl acetate, among three considered, was the best standard for both techniques. Finally, the number of trials and injections (testing schemes) for both techniques were studied considering the variance and laboratory expenses and time as factors to decide the optimum.

Keywords: Chromatography; Headspace techniques; Virgin olive oil volatiles; Olive oil

The success of the food industry depends on the quality of the products. Sensory analysis is the most widespread method used to measure quality and it is well-known that volatiles are responsible for the attributes evaluated by sensory trials.

Several methods have been used to determine volatiles though there is a trend towards the use of dynamic headspace (DHS) rather than direct injection or static headspace [1]. The latter techniques have been progressively abandoned because they do not perform any concentration of volatiles and so they lack sensitivity, making them inadequate for the trace analysis that requires at least an enrichment step.

The objective of this paper is the comparison of two kinds of DHS, which use different kind of adsorbents (Tenax TA and activated charcoal) and desorption methods (thermal or solvent), using as application the quantification of virgin olive oil volatiles. To carry out this comparison it is necessary to link more than one scientifical subject; (i) the optimization of variables that have some influence in the process by Simplex techniques [2], (ii) the response surface methods [3,4] that should allow us to check if the optimum values of variables do not belong to a relative maximum in the response surface at all, (iii) classical multivariate statistical methods of analysis of variance [5] that should be used to choose the best standard for each procedure and study the repeatability of each DHS, and (iv) testing schemes [6] that should finally help us to select the number of trials, with and without repetition of injections, for both DHS. Figure 1 displays the process followed in this work, remarking some noticeables alternatives, for example fuzzy algorithms for evaluating the desired response that optimize the processes and a new kind of testing scheme.

Correspondence to: R. Aparicio, Instituto de la Grasa y sus Derivados, Avda Padre García Tejero, 4, 41012 Seville (Spain).

EXPERIMENTAL

Equipment and reagents

A preliminary step of pre-concentration is required for headspace volatiles in order to trap the analytes in an ideal medium and allow an ideal injection into the gas chromatograph. Nuñez et al. [7] have described many preconcentration methods that eliminate the disadvantages of direct injection. In the work described here the preconcentration has been carried out using the instrument designed by Zlatkis et al. [8], as improved by Cert and Bahima [9], in which a stream of gas (nitrogen) sweeps the surface of virgin olive oil and volatiles are stripped in an open trap.

The traps consisted of activated charcoal tubes (SCK Inc., Pennsylvania), with two fractions, and adsorption traps filled with Tenax TA (Chrompack) which had been adequately conditioned prior to use.

A Hewlett-Packard 5890 series II gas chromatograph was used with a FID detector and Hewlett-Packard 3396A integrator. Helium was used as the carrier and make-up gas. A fused silica Supelcowax 10 column [60 m × 0.32 mm i.d., 0.5 μm film thickness (FT)] was employed. A Chrompack thermal desorption cold trap injector (TCT) was coupled to the gas chromatograph. The oven temperature was held at 40°C for four minutes and programmed to rise at 4°C/min to a final temperature of 240°C where it was held for 10 min.

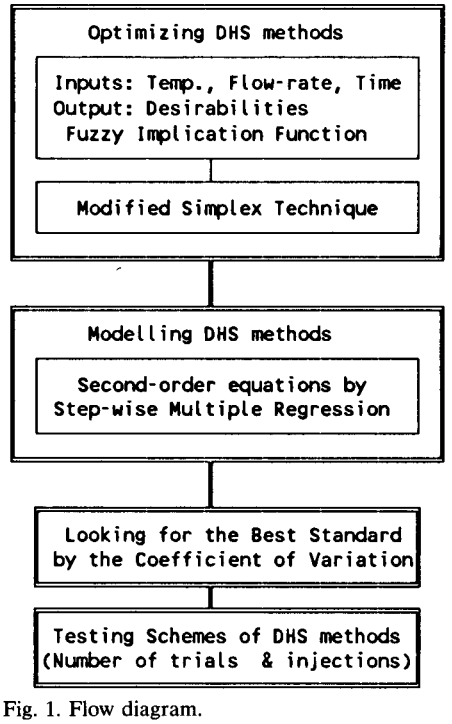

Fig. 1. Flow diagram.

Three internal standards were added to each sample at a concentration of 2500 ppb. They were isobutyl acetate, methyl nonanoate (PolyScience Co., analytical standards) and Dioxane (Carlo Erba). The solvent was S_2C (reagent grade, Merck).

The following procedures were performed after optimizing the conditions.

Dynamic headspace 1 (DHS1)

50 g of Spanish virgin olive oil were heated at 80°C, stirred and swept with N_2 (1500 ml/min) for 120 min in a concentrating device [9]. Volatiles were collected on a trap containing activated charcoal and subsequently each fraction was desorbed with S_2C (0.5 ml). 1 μl of this solution was injected into the chromatograph by on-column injection.

Dynamic headspace 2 (DHS2)

0.5 g of Spanish virgin olive oil were heated at 40°C and swept with N_2 (200 ml/min) for 15 min, in a similar concentrator device as that used in DHS1 but of smaller dimensions. Tenax TA was used as the trap. Volatiles were thermally desorbed at 220°C onto a fused silica trap cooled at −110°C for 5 min. When cold this trap was flushed by heating at 170°C for 5 min. The volatiles that had condensed within the trap were transferred onto a capillary column.

Chromatograms were held in a relational database. From Fig. 2, which displays one of each DHS, the differences between both techniques can be seen. The GC integrator was linked to a 80386 computer and the chromatograms were held in a SQL database.

Mathematical procedures and software facilities

Mathematically speaking, four different subjects have been applied in the work, (i) non-linear optimization techniques, (ii) response surface

methods, (iii) multivariate statistics and (iv) a small application of fuzzy logic algorithms. This mixture of different subjects implies that only a brief overview of each one will be given here but wide details of these subjects and more interesting applications are reported in the references.

Statistical analyses have been carried out using SPSS [10] and BMDP [11] libraries whilts the other algorithms have been programmed by the authors. The graphical representations have been made by AutoCAD package [12].

RESULTS AND DISCUSSION

Optimization of the pre-concentration of headspace volatiles

The optimization of this process involves determining the experimental conditions that allow us to achieve the best selected response by programming experiences or search methods. Modified simplex [2] is a nonlinear optimization technique that has become increasingly popular to optimize processes because it allows an easy implementation. Basically, a simplex only needs the input variables, which will be optimized, and an output variable that will be minimized or maximized.

Numerous input variables have a possible influence upon the DHS response though most of them are insignificant or non-pertinent and are rejected. In this work, sample size, temperature, time and flow were identified as the most significant variables though sample size was fixed at the values used in previous works [13,14]. Thus only the latter three parameters were really used for the optimization procedure.

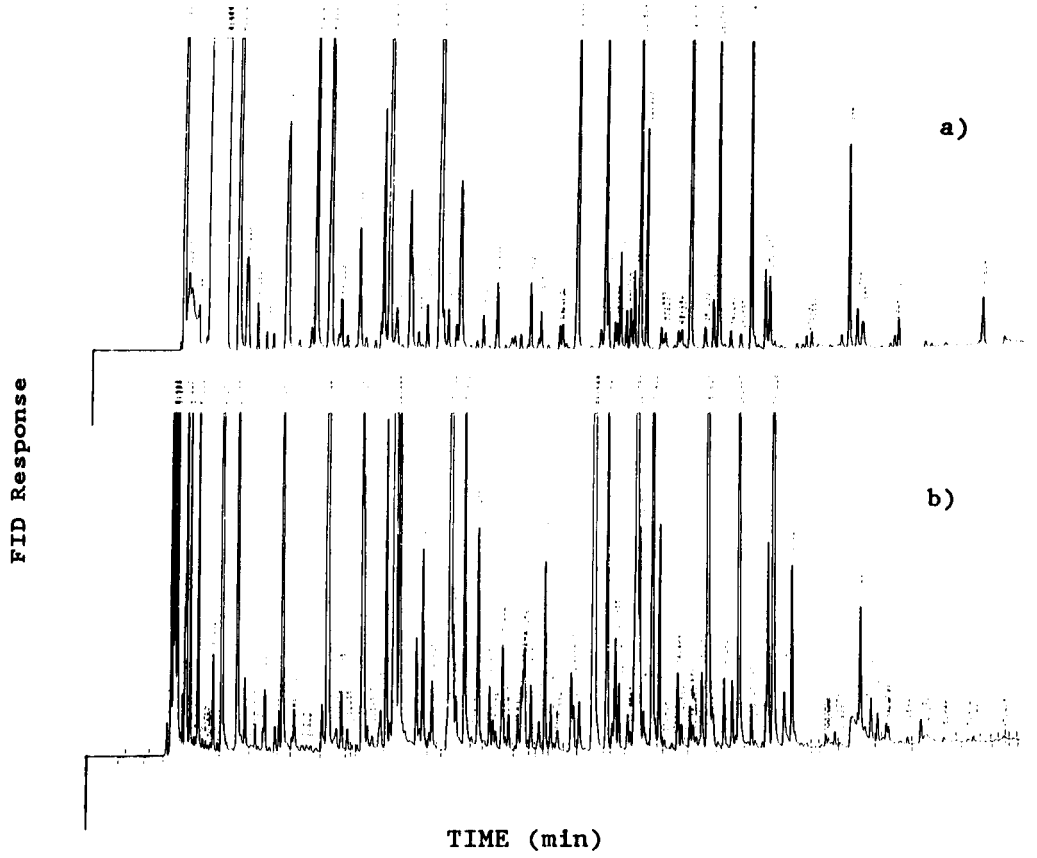

Fig. 2. Chromatograms obtained from the same virgin olive oil: (a) using DHS1, (b) using DHS2.

The selected factors are not naturally limited but there is a region of interest for each factor. The upper temperature was fixed at 90°C because beyond this there is a degradation in volatiles whereas a temperature lower than 20°C did not permit the majority of the volatiles to be stripped. Technical reasons also limited the flow-rate boundaries. The upper flow-rate was fixed at 2500 ml/min and the lower at 50 ml/min, while the time limits were from 15 to 240 min. These are the maximum boundaries of each factor for both DHS.

Optimizing also implies to select the output variable or response to be minimized or maximized. The chromatograms contain enough information for this purpose. The sum of areas of peaks for all standards or some selected peaks are usually the responses to be optimized [15]. However, these responses cannot always be used to optimize the whole process because they do not calculate the rate between the large and small peaks, or only optimize the part of the chromatogram where the selected peaks are placed. In fact, the optimization is quite often a compromise among several variables, sometimes acting in opposition to each other, that helps to the suppresion of undesirable side-results as these just described above.

A large experience in evaluating chromatograms has been used to decide which are the characteristics that should have a chromatogram measuring the quality of a preconcentration process. These characteristics, experts' subjective opinions, are called desirabilities [16] and they can be the output variables, or process responses, that should be maximized.

Three desirabilities were evaluated by experts: chromatographic balance, stripping quality and standard recovery. The chromatographic balance measures the rate between the large and small peaks taking into account the chromatographic resolution of these peaks. If the ratio is very high there will be many unresolved large peaks but if it is small there will be many unresolved small peaks, well-understood that the perfect balance is attained when the number of unresolved peaks, either large or small, is minimum. The stripping quality evaluates the total number of peaks in the chromatogram. A small number of peaks means that the process conditions were unadequate to strip volatiles, due to low temperature and/or flow-rate for instance, whilts a large number also means the same though now due to a degradation occurred during the process. The standard recovery is the third desirability function and it describes how the standards were recovered after the process.

The desirability functions are characterized by possibility distributions and hence their response assumes values between 0 and 1 (minimum and maximum). These functions are graphically represented by different non-linear equations that are defined by two parameters: the peak-point and the bandwidth. The peak-point is a point at which the desirability function is fully satisfactory (maximum). The bandwidth is defined as the distance between the cross-over points, where the desirability function reaches its poorest values (minimum).

The values of the desirability functions are computed by the following pattern Eqns. 1–5,

$$z_i = \underset{i=1,2,3}{\mathrm{D}(x) = 0}$$

$$\text{for } x \le p - \beta_1 \text{ or } x \ge p + \beta_2 \tag{1}$$

and

$$z_i = \frac{2}{\beta_1^2}(x - p + \beta_1)^2$$

$$\text{for } p - \beta_1 \le x \le p - 0.5\beta_1 \tag{2}$$

$$= 1 - \frac{2}{\beta_1^2}(x - p)^2$$

$$\text{for } p - 0.5\beta_1 \le x \le p \tag{3}$$

$$= 1 - \frac{2}{\beta_2^2}(x - p)^2$$

$$\text{for } p \le x \le p + 0.5\beta_2 \tag{4}$$

$$= \frac{2}{\beta_2^2}(x - p - \beta_2)^2$$

$$\text{for } p + 0.5\beta_2 \le x \le p + \beta_2 \tag{5}$$

where D is the desirability function, x is the variable being $x, E\ (-\infty, \infty)$, z is the result after

applying the equation to x, β is the bandwidth, in symmetrical functions $\beta_1 = \beta_2$, and p is the peak-point. Since we have three desirability functions, we are analysing the same process from three different criteria. However, we are interested in building one unique response and hence we should join the three criteria in a single function (implication function) that generates the overall desirability.

Although the peak-point and bandwidth of each one of these desirability functions depend on experts who have a large knowledge of the process, there is some subjetiveness on the evaluations which involves a certain grade of uncertain reasoning and fuzzyness. Thus, it seems reasonable that the implication function that links the desirability functions to calculate the overall desirability should belong to the fuzzy logic rather than classical arithmetic [17]. A fuzzy algorithm, Luckasiewicz $T_{1.5}$-conorm [18,19], was selected instead of the geometric mean proposed by Clementi et al. [20] that could be considered rather inappropriate to express the vagueness concept.

The selected implication function (6), Luckasiewicz $T_{1.5}$-conorm, is formulated as

$$T_{1.5}(w_i, w_j) = w_i w_j / [2 - (w_i + w_j - w_i w_j)] \quad (6)$$

where w_i and w_j are the values associated with two desirabilities. This is an AND-function that truthfully shows the overall desirability meaning; for example, the best overall desirability will be obtained when we obtain the best "chromatographic balance" *and* the best "stripping quality" *and* the best "standard recovery". Concerning the values, this algorithm is not as optimistic as geometric mean is.

Once the response to be maximized was formulated, through the implication function, the vertices of initial simplex were calculated by strictly applying the criteria given by Yarbro and Deming [21].

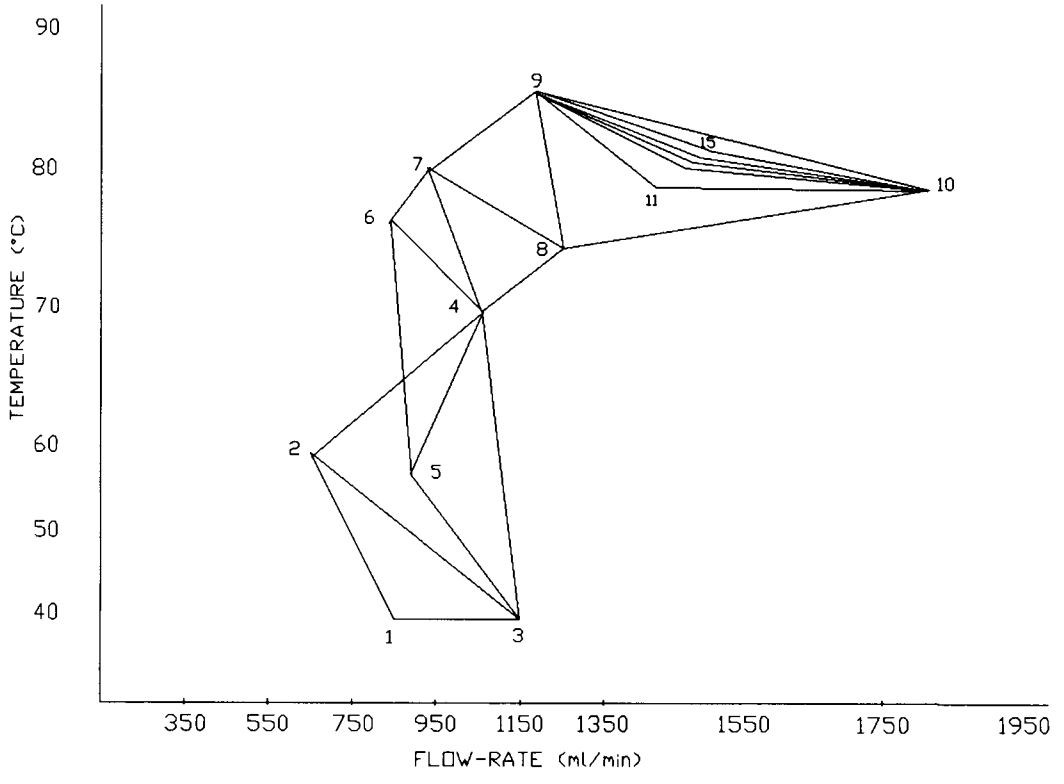

Fig. 3. Development of the simplex method for DHS1. Time = 120 min.

TABLE 1

Characteristics and conditions of dynamic headspace techniques

Method	DHS1	DHS2
Conditions	80°C, 1500 ml/min, 120 min	40°C, 200 ml/min, 15 min
Sample	50 g	0.5 g
Trap	Activated charcoal	Tenax TA
Desorption	S_2C	Thermal
Injection	on column	TCT
Injector Temp.	43°C	175°C
Detector Temp.	275°C	275°C

Column Supelcowax 10, 60 m × 0.32 mm i.d., 0.5 μm FT
Oven Temp. 40°C (4 min) – 4°C/min – 240°C (10 min)

The two-dimensional Fig. 3 shows the different experiments done during the development of the modified simplex applied to DHS1, time being fixed at 120'. The step sizes have been $\alpha = 1$ (reflection), $\beta = 0.5$ (contraction) and $\gamma = 2$ (expansion). After successive expansions and contractions, there were massive contractions in the vicinity of the optimum as four experiments were required to reach the optimum; experiments 12, 13 and 14 are not labelled in Fig. 3 the axes of which (numbers 8 to 15) have different scales to amplify the last experiments. The final values were 80°C and 1500 ml/min which are close to their highest values.

A similar process was applied to DHS2 giving results of 40°C, 15 min and 200 ml/min which are close to the lowest values of each factor, in contrast to DHS1. This disparity can be understood by analysing the processes (Table 1). For instance DHS2 uses thermal desorption so that it has no need of a high temperature nor a high flow-rate of the stripping gas in the pre-concentration procedure in order to strip 95% of the solute.

Surface response

The Simplex procedure does not provide a response surface so that different methods have been proposed to model results [4]. Zupan and Rius [22] designed a program in which the users can choose the equation that better fits to the results, but unfortunately this procedure needs previous studies or a predefined model.

Alternatives can be found using multiple regression analysis [3] or partial least squares [20] but these procedures do not evaluate the contribution of each variable to the equation because they use all variables to calculate the coefficients. Thus, if there is not any test that evaluates the contribution of each variable to the final equation, it is impossible to know whether the variable trusthfully contributes to the final result or merely brings noise to the equation, or helps to produce a satisfactory conclusion by chance [23].

Therefore, we opted for a stepwise multiple regression analysis (SMRA). SMRA was applied to a set of factors constituted by the combination of variables (temperature, flow-rate and time) up to the second-order. These extra "artificial" factors (T^2, Tt, etc) represent non-linear transformations of the original ones [4] and allow to model nonlinear responses. Concerning the statistical procedure, a criterion based on F-distribution was used to select the best variable at each step of the regression process [5]. At the end of the stepwise process the following Eqn. 7 was obtained which relates the overall desirability values (obtained from the implication function) to the flow-rate, time and temperature parameters,

$$D(x) = aT + bT^2 + cT^2F + dF^2T + eT^2t + \alpha \quad (7)$$

where $D(x)$ is the overall desirability, T the temperature, F the flow-rate and t the time. The values of the different coefficients were: $a = 1.66 \times 10^{-2}$, $b = -2.057 \times 10^{-4}$, $c = 7.998 \times 10^{-8}$, $d = -7.476 \times 10^{-9}$, $e = 2.33 \times 10^{-8}$ and $\alpha = -0.397$. The analysis of variance gave 0.516 for the mean square of regression equation and 0.0452 for residual, with an F-ratio 11.42.

The values of the coefficients indicate the high importance of the temperature factor. This conclusion, is logical given that DHS sweeps the olive oil surface and works with volatile compounds, and is in accordance with the conclusions of Bertsch et al. [24]. It is also interesting to note the low influence of variable time in the equation. This is probably due to the fact that the flow and the product flow × time can be considered to be very similar.

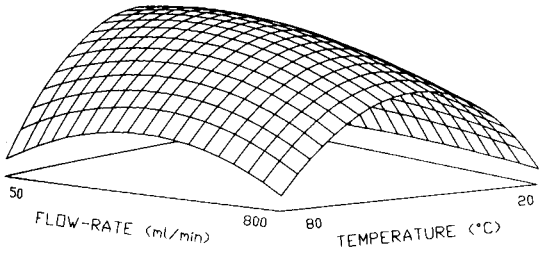

Fig. 4. Response surface for DHS2. Time = 15 min.

Figure 4 shows the response surface for DHS2 made by AUTOCAD [12] at time 15'. It can be seen that the response improves as the temperature and flow-rate increase from their minimum values and worsens as a result of significant degradation in volatiles when they reach high values. The response does not change at any flow-rate when the temperature is low because no volatile is stripped whilst, above a certain maximum value, the response does not improve further and even worsens when the flow is increased due to the trap circuit being open [8,9].

A similar response surface was obtained for DHS1 confirming the results attained by Simplex.

Looking for the best standard

Once the best conditions were calculated for both methods, the next objective was to look for the best standard for both DHS methods. Twelve trials on DHS2 and ten on DHS1 procedure were performed with the same Spanish virgin olive oil. We must notice that solvent desorption (DSH1) allows more than one injection of the same concentrated volatiles but thermal desorption (DHS2) does not. Therefore, we can distinguish two sources of errors on DHS1, pre-concentration and quantification, whilts DHS2 only allows analysing the whole process error (pre-concentration + quantification). Trials were characterized by 56 peaks (DHS1) and 45 peaks (DHS2), the number of peaks suggested a multivariate statistical analysis for identifying the outliers and selecting the best standard.

A cluster analysis showed there was a great similarity between injections in the DHS1 procedure though trial number four was different to the others. Mahalanobis distance, evaluated as

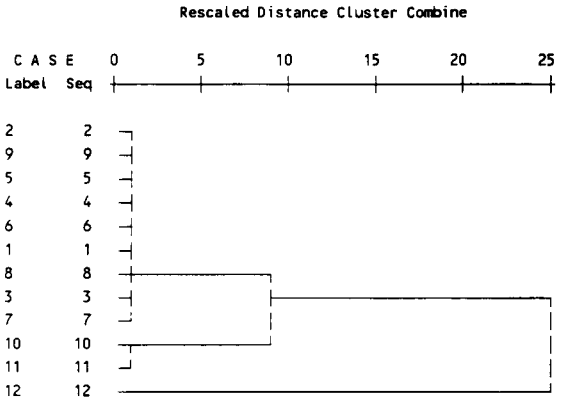

Fig. 5. Cluster analysis for DHS2 showing the outlier.

chi-squared, was used to identify possible outliers with respect to the solution and among cases [5] but no outliers were detected. In relation to DHS2, the cluster analysis, displayed in Fig. 5, shows that sample number 12 is very dissimilar to the others. This sample was judged aberrant (outlier) and was removed from the subsequent statistical studies. This decision was taken due to the clearness with which the outlier was detected.

Once the outlier was removed, the next step was to select the best standard among the three used. Table 2 shows the univariate statistics associated with each standard. From the values of coefficients of variation, kurtosis and skewness, the best standard appeared to be isobutyl acetate

TABLE 2

Standards used in the study, statistical results

Standard	Kurtosis	Skewness	Coefficients of variation
DHS1			
Isobutyl acetate	0.253	0.384	0.0856
Dioxane	0.716	0.821	0.0888
Methyl nonanoate	4.721	−2.229	0.1682
DHS2			
Isobutyl acetate	−0.177	−0.644	0.0476
Dioxane	−0.852	0.775	0.5505
Methyl nonanoate	0.062	0.748	0.1373

for both methods though dioxane is not an unacceptable standard for DHS1.

On the other hand the place of a peak in a chromatogram can have some influence over its resolution quality. Peaks situated at the front and rear of the chromatograms are always more affected by random variables and their values can change in the repetitions. The use of standards allows to normalize the chromatograms dividing the peak areas by the standard and so removing the influence of many random variables. Therefore, we also can choose the best standard by a different way. Thus, the coefficient of variation of this rate (peak area/standard area) can be used as measure of repeatability. Table 3 shows that the isobutyl acetate has more peaks with a coefficient of variation lower than 20% whilst methyl nonanoate is the least suitable for DHS1 and dioxane for DHS2, in accordance with the results obtained by the other method.

TABLE 3

Number of peaks grouped by their coefficient of variation for both kinds of traps after divided by the three standards

Traps	Coeffient of variation	Standard		
		Isobutyl acetate	Dioxane	Methyl nonanoate
Activated charcoal	< 0.1	15	13	10
	< 0.2	31	31	20
	< 0.3	2	4	17
	< 0.4	3	2	5
	< 0.5	2	3	1
	> 0.5	0	0	0
Tenax TA	< 0.1	17	0	13
	< 0.2	15	0	22
	< 0.3	9	0	0
	< 0.4	0	6	6
	< 0.5	0	32	0
	> 0.5	1	4	1

Optimum analytical scheme

Factorial design has been widely used to determine the analytical errors and choice the optimum scheme, number of analysis (trials plus injections), of an instrumental method. The analysis of variance allows calculating the method error and so deciding which is the optimum number of analysis [6]. However, there is no pattern that enables to make a decision properly because it is always best to do as many analysis as possible. Actually, although the variance is taken into account, the cost (laboratory expenses and time) will be which finally limits the number of analysis. Therefore, the cross-point between the cost and variance curves can be used in deciding the optimum number of analysis, so avoiding subjective decisions.

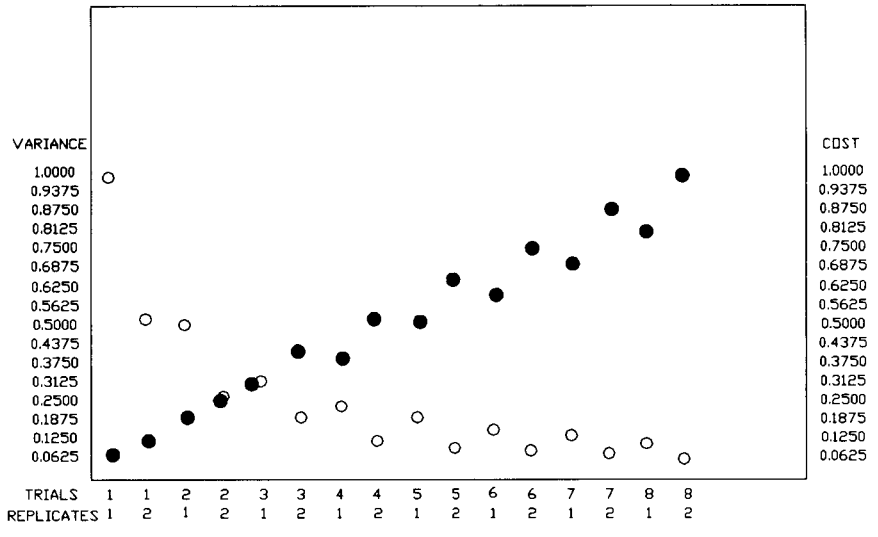

Fig. 6. Cost analysis for DHS1.

The analysis of variance was calculated reducing the independent variables (peaks) to only three applying principal components analysis, the three eigenvectors explain more than 87% of variance for both methods. The cost analysis (laboratory expenses, traps, solvents and time) was carried out for each DHS. The most important factor in DHS1 was time due to the long time required for each analysis whilst the maximum variance, 0.80, corresponds to one trial with only one injection and the minimun, 0.21, to 10 trials with two injections.

Figure 6 displays the results of DHS1. The values of variance and cost were scaled, between zero (minimum) and one (maximum), in order to use the same *Y* axis. The crosspoint between both curves corresponds to four analysis, two trials and two injections, with variance of 0.42. Concerning DHS2, the point of intersection corresponded to two analysis, two trials, with variance of 0.15.

The results suggest that there are no great differences between these techniques, though time, random variables and progress suggest that TCT (DHS2) is the technique most likely to be useful in the future.

The authors would like to acknowledge their indebtedness to Dr. Cert for his contribution in solving many experimental problems. This work has been supported by CICYT-SPAIN ALI-91-0786.

REFERENCES

1 M.T. Morales, R. Aparicio and F. Gutierrez, Grasas y Aceites, 43 (1992) 164.
2 P.B. Ryan, L.B. Barr and H.D. Todd, Anal. Chem., 52 (1980) 1460.
3 L. Vuataz, in J. R. Pigott (Eds.), Methods in Statistical Procedures in Food Research, Elsevier, London, 1986, pp. 101–124
4 H. Martens and T.M. Naes, Multivariate Calibration, Wiley, Chichester, 1989.
5 B. G. Tabachnick and L.S. Fidell, Using Multivariate Statistics, Harper & Row, New York, 1983.
6 F. Gutiérrez, M.A. Albi, R. Palma, J.J Ríos and J.M Olías, J. Food Sci., 54 (1989) 68.
7 A.J. Núñez, L.F. González and J.J Janák, J. Chromatogr., 380 (1984) 127.
8 A. Zlatkis, H.A. Lichtenstein and A. Tishbee, Chromatographia, 6 (1973) 67.
9 A. Cert and J.J. Bahima, J. Chromatogr. Sci., 22 (1984) 7.
10 SPSS User's Guide, McGraw Hill, New York, 1986.
11 BMDP Statistical Software, University of California, Los Angeles, 1981.
12 N. Johnson, AutoCAD: The Complete Reference, McGraw Hill, New York, 1989.
13 D.M. Wyatt, J. Chromatogr. Sci., 25 (1987) 257.
14 M. Solinas, F. Angerosa and V. Marsilio, Riv. Ital. Sostanze Grasse, 65 (1988) 361.
15 R.M. Marce, M. Calull, J.C. Olucha, F. Borrull and F.X. Rius, Anal. Chim. Acta, 242 (1991) 25.
16 G. Derriger and R. Suich, J. Qual. Technol., 12 (1980) 214.
17 A. Kandel, Fuzzy Mathematical Techniques with Applications, Addison Wesley, Reading, MA,1986.
18 W. Bandler and L.J. Kohout, in E.H. Mandami and B.R. Gaines (Eds.), Fuzzy Reasoning and its implications, Academic Press, London, 1987, pp. 219–246.
19 L.I. Godo, R. López de Mántaras, C. Sierra and A. Verdaguer, Proc. 7th Int. Workshop on Expert Systems and their Applications, Edited by EC2, France, Vol. 1, 1987, pp. 571–596.
20 S. Clementi, G. Cruciani, G. Giulietti, M. Bertuccioli and I. Rosi, Food Qual. Preference, 2 (1990) 1.
21 L.A. Yarbro and S.N. Deming, Anal. Chim. Acta, 73 (1974) 391.
22 J. Zupan and F.X. Rius, Anal. Chim. Acta, 239 (1990) 311.
23 R. Aparicio, F. Gutierrez and J. Rodriguez, J. Sci. Food Agric., 58 (1992) 555.
24 W. Bertsch, E. Anderson and G. Holzer, J. Chromatogr., 112 (1975) 701.

Analytica Chimica Acta, 282 (1993) 433–436
Elsevier Science Publishers B.V., Amsterdam

Use of hydrogen in electrothermal atomic absorption spectrometry to decrease the background signal arising from environmental slurry samples

Les Ebdon, Andrew S. Fisher and Steve J. Hill

Plymouth Analytical Chemistry Research Unit, University of Plymouth, Drake Circus, Plymouth PL4 8AA (UK)

(Received 3rd March 1993; revised manuscript received 4th June 1993)

Abstract

The use of hydrogen in electrothermal atomic absorption spectrometry (ETAAS) to reduce the effects arising from smoke and other non-specific absorption interference has been investigated. Introduction of the hydrogen as a 10% (v/v) mixture in argon during the cool down and autozero stage just prior to atomisation led to a very much reduced background signal for environmental samples such as soil and a sewage sludge. For many of the samples in the absence of hydrogen, the background correction system was incapable of removing the interference and unreliable results were obtained. The method was validated using certified reference materials Canmet SO-2 soil and BCR 145 sewage sludge. Reasonable agreement with the certified values was obtained.

Keywords: Atomic absorption spectrometry; Environmental slurry sample analysis; Interference reduction

Hydrogen was first used in electrothermal atomic absorption spectrometry (ETAAS) by Amos et al. [1] who produced a hydrogen diffusion flame above a graphite rod. This resulted in reduced interferences. It has since been used by several workers. Ohta and co-workers [2–9] have reported increased sensitivity for many analytes when hydrogen was introduced to various metal tube analysers. The hydrogen had the effect of protecting the atomiser against oxidative attack by residual oxygen, reducing the analyte oxide to analyte atoms, e.g.,

$$GeO_2 + 2H_2 \rightarrow Ge + 2H_2O$$

and preventing atom loss by recombination, e.g, by atmospheric oxygen. Increases in sensitivity have also been reported by other workers [10,11].

Correspondence to: L. Edon, Plymouth Analytical Chemistry Research Unit, University of Plymouth, Drake Circus, Plymouth PL4 8AA (UK).

Hydrogen has been used in graphite atomisers to reduce the spectral interference of calcium oxide molecular band emission on the determination of barium, and strontium band emission on lithium determinations [12]. Chloride interferences on lead determinations have also been eliminated by the addition of hydrogen [13,14]. Other workers, however, have reported that hydrogen does not overcome this interference [15,16]. These inconsistent results have been attributed to the use of different types of atomiser and by working under different experimental conditions.

The introduction of hydrogen has been used before to decrease the background signal obtained during molybdenum determinations [17]. The background arose because of the very high atomisation temperature required for molybdenum volatilising carbon particles from the surface of the atomiser into the light beam. The reduction of background signal on the addition of the

hydrogen was attributed to the removal of these particles via the formation of hydrocarbons. It therefore seemed feasible that, by the same type of mechanism, hydrogen could be used to reduce the background signal from samples with carbonaceous or refractory matrices.

In graphite atomisers, hydrogen has been used primarily to overcome chemical and spectral interferences. In this study, the list of interferences that are diminished by the use of hydrogen has been extended.

EXPERIMENTAL

Reagents and standards

High purity water was obtained by using reverse osmosis (Milli-R04; Millipore, Harrow, UK) followed by adsorption, deionisation and ultrafiltration (Millipore, Milli-Q system). Standards (1000 μg ml^{-1}) of lead, manganese and chromium were obtained from Merck (Spectrosol, Merck, Poole, UK). Working standards were produced from these stock standards by serial dilution on a daily basis.

Instrumentation

All analyses were performed using an atomic absorption spectrometer (PU 9100x, Unicam, Cambridge, UK) fitted with an electrothermal atomiser (PU9390x, Unicam) and a data station (PU9178x, Unicam). This instrument is fitted with a continuum source (deuterium lamp), to allow the measurement and correction of background absorption. Gas mixtures were achieved, where necessary, by using a gas blender (Series 800, Signal Instrument, Camberley, UK). Pyrolytic carbon coated tubes were used throughout, and in-house fabricated pyrolytic carbon coated platforms were used for some analyses. Samples were introduced to the atomiser by a hand-held precision micropipette (Gilson, Villiers-Le-Bel, France).

Sample preparation

Certified reference materials BCR 145 sewage sludge (European Community, Bureau of Community Reference, Brussels, Belgium) and CANMET SO-2 (Canada Centre For Mineral Energy Technology, Ottawa, Canada) were slurried using the bottle and bead method. Sample (approximately 0.2500 g) was weighed accurately into a 30-ml capacity polypropylene bottle. Zirconia beads (10 g) and deionised water (3 ml) were added, and the bottle placed on a mechanical flask shaker (Gallenkamp, Loughborough, UK) and shaken for 2 h. After shaking the slurry was diluted to 25 ml by the addition of more deionised water. No dispersant was necessary. Blanks were prepared in a similar fashion, but omitting the sample.

Procedure

It is important to note that before any experiment using hydrogen at high temperature was performed, the instrumentation and gas lines were flushed with hydrogen at a low temperature to expel any air present. Failure to do this may result in a relatively small, but potentially damaging explosion.

The instrumentation used in this study incorporated a cool-down period as an integral part of every furnace programme just prior to auto-zero and atomisation. The introduction of hydrogen during this stage ensured that its effects would appear during atomisation, but with less dilution effects observed when atomisation without gas stop is used.

RESULTS AND DISCUSSION

Certified reference materials BCR 145 sewage sludge and CANMET SO-2 soil were chosen to validate the method because the levels of the analytes present in these samples required the use of analytical atomic lines above 330 nm. Above 330 nm the deuterium background correction system is outside its optimal range, and hence any particulate or matrix material entering the light beam would not be properly corrected for. It was therefore necessary to remove this matter by some other means. The use of hydrogen (10%, v/v) introduced just prior to the atomisation stage was compared with normal operation and with air

TABLE 1

Operating conditions used for the analysis of certified reference material slurries (injection volume = 20 μl)

Analyte	Lamp current (mA)	Bandpass (nm)	Wavelength (nm)
Chromium	5	0.5	429.0
Manganese	5	0.5	403.0
Lead	5	0.5	368.4

ashing. Air or oxygen ashing has been used numerous times previously to destroy organic matrices [18–20], and should therefore exhibit similar matrix destruction properties as hydrogen. The certified reference materials were analysed for lead, manganese and chromium content using the operating conditions described in Table 1 and the furnace programmes detailed in Table 2. For the air ash analyses, a second ash stage at the same temperature was required to remove air from the tube before atomisation, and hence prevent tube oxidation and destruction. The results of the analyses are shown in Table 3. The results are in reasonable agreement with the certificate values for all analyses except chromium in soil. This analysis was found to yield results double the expected value for both normal operation and air ashing. This was presumably due to the particulate matter or smoke not being destroyed before it entered the light beam and therefore causing false atomic signals. The use of 10% (v/v) hydrogen successfully eliminated this problem and the result for this analysis was in agreement with the certificate value. This indicates that hydrogen is more efficient in removing some interferences than the more commonly used air ashing procedure.

TABLE 2

Furnace programmes used for the analysis of certified reference material slurries (F.P. = full power. For the air ash analyses, a second ash stage at the same temperature was required to remove air from the tube before atomisation)

Analyte	Stage	Temperature (°C)	Hold time (s)	Ramp (°C s^{-1})
Cr	Dry	110	35	20
	Ash	800	30	100
	Atomise	2500	3	F.P.
	Clean	2600	3	F.P.
Mn	Dry	110	35	20
	Ash	800	30	50
	Atomise	2400	3	F.P.
	Clean	2500	3	F.P.
Pb	Dry	110	35	20
	Ash	500	30	50
	Atomise	1800	3	F.P.
	Clean	2200	3	F.P.

In addition, the presence of the hydrogen improved the peak shape of the analytes when platform atomisation was used. This was because the extremely high specific heat capacity and thermal conductivity of the hydrogen caused cooling of the gas atmosphere inside the graphite tube and also ensured that the hydrogen diffused from the tube faster. These two effects combined to ensure that the analyte signal returned to the baseline, i.e., atoms were removed from the light beam, more rapidly.

Conclusions

Samples with carbonaceous or refractory matrices produce nonspecific absorbance interference that can prevent reliable data acquisition.

TABLE 3

Results obtained for the analysis of slurries of certified reference materials [$n = 5$] ( ) = reference value. Results expressed as $\pm 2\sigma_{n-1}$.

Material	Analyte	Certified value (μg g^{-1})	Result obtained with		
			Argon (μg g^{-1})	10% (v/v) H_2 (μg g^{-1})	Air ash (μg g^{-1})
BCR 145	Cr	(105)	131 ± 10	125 ± 8	131 ± 14
sewage sludge	Mn	241 ± 12	212 ± 8	241 ± 12	235 ± 10
Canmet SO-2	Cr	16 ± 2	38 ± 10	18 ± 2	35 ± 2
soil	Pb	21 ± 4	16 ± 1	22 ± 4	18 ± 2

Hydrogen (10%, v/v) has been used in the cool-down and autozero stage just prior to atomisation to eliminate this interference. The method was compared with air ashing and was found to be more efficient. The method was validated by the analysis of certified reference materials. Reasonable agreement with the certificate values was obtained.

The authors acknowledge support for one of us (A.S.F.) by the Science and Engineering Research council (SERC) and Unicam under the Co-operative Award in Science and Engineering (CASE) scheme.

REFERENCES

1 M.D. Amos, P.A. Bennett, K.G. Brodie, P.W.Y. Lung and J.P. Matousek, Anal. Chem., 44 (1971) 211.
2 K. Ohta and M. Suzuki, Anal. Chim. Acta, 96 (1978) 77.
3 K. Ohta and M. Suzuki, Anal. Chim. Acta, 104 (1979) 293.
4 K. Ohta and M. Suzuki, Anal. Chim. Acta, 107 (1979) 245.
5 M. Suzuki and K. Ohta, Fresenius' Z. Anal. Chem., 322 (1985) 480.
6 K. Ohta and T. Mizuno, Microchem. J., 37 (1988) 203.
7 K. Ohta, W. Aoki and T. Mizuno, J. Anal. At. Spectrom., 3 (1988) 1027.
8 K. Ohta and T. Mizuno, Anal. Chim. Acta, 217 (1989) 377.
9 K. Ohta, T. Sugiyama and T. Mizuno, Analyst, 115 (1990) 279.
10 W. Frech and A. Cedergren, Anal. Chim. Acta, 82 (1976) 83.
11 M.W. Routh, Anal. Chem., 52 (1980) 182.
12 J.M. Ottaway and R.C. Hutton, Analyst, 102 (1977) 785.
13 W. Frech and A. Cedergren, Anal. Chim. Acta, 82 (1976) 93.
14 Z.M. Ni, H.B. Han and X.C. Le, J. Anal. At. Spectrom., 1 (1986) 131.
15 K.C. Thompson, K. Wagstaff and K.C. Wheatstone, Analyst, 102 (1977) 310.
16 W. Frech and A. Cedergren, Anal. Chim. Acta, 88 (1977) 57.
17 D.J. Johnson, T.S. West and R.M. Dagnall, Anal. Chim. Acta, 66 (1973) 171.
18 M.W. Hinds and K.W. Jackson, J. Anal. At. Spectrom., 3 (1988) 997.
19 L. Ebdon and H.G.M. Parry, J. Anal. At. Spectrom., 3 (1988) 131.
20 L. Ebdon, A.S. Fisher, H.G.M. Parry and A.A. Brown, J. Anal. At. Spectrom., 5 (1990) 321.

Analytica Chimica Acta, 282 (1993) 437–443
Elsevier Science Publishers B.V., Amsterdam

Determination of trace metal ions in water samples by on-line preconcentration and inductively coupled plasma mass spectrometry

Hueih-Jen Yang, Kuang-Shie Huang, Shiuh-Jen Jiang, Cheng-Chang Wu and Chin-Hsing Chou

Department of Chemistry, National Sun Yat-Sen University, Kaohsiung 804 (Taiwan)

(Received 17th March 1993; revised manuscript received 12th May 1993)

Abstract

An on-line sample pretreatment method was developed to preconcentrate trace metal ions from water samples. Complexes of metal ions with butane-2,3-dione bis(*N*-pyridinoacetyl hydrazone) were retained on a column packed with Amberlite XAD-4 resin at pH 8–9. The metal complexes were removed from the column with an acidic eluent and detected by inductively coupled plasma mass spectrometry. The metal ions studied were Cu, Cd, Co, Ni and Pb. The detection limits were in low ng l^{-1} range for the elements studied. The method was applied to the determination of various trace metals in the riverine reference material SLRS-2.

Keywords: Inductively coupled plasma MS; Metal ions; Preconcentration; Trace metals; Waters

The determination of metal ions in samples from uncontaminated areas requires powerful techniques to detect extremely low concentrations of analytes, and few techniques have sufficient sensitivity. Inductively coupled plasma mass spectrometry (ICP-MS) is applicable to trace multi-elemental and isotopic analysis of solutions [1–4]. This technique combines the characteristics of the ICP for atomizing and ionizing injected material with the sensitivity of mass spectrometry. It is applicable to a wide range of materials, although highly saline samples can cause both spectral interferences and matrix effects [5,6].

In order to achieve accurate, reliable and sensitive results, preconcentration and separations are needed when the concentrations of analyte elements in the original material or the prepared solution are too low to be determined directly by mass spectrometry or when matrix elements interfere with the determination. Several matrix–analyte separation and preconcentration techniques have been adapted to ICP-MS analysis [7–17]. Plantz et al. [11] used bis(carboxymethyl) dithiocarbamate to complex V, Cr, Ni, Co, Pt and Cu and successfully separated them from matrix interferents. Main and Fritz [18] applied 2,6-diacetylpyridine bis(quaternary ammonium hydrazone) to complex with Ti, V, U, Th and Fe and separated the complexes by liquid chromatography.

This work involved the retention of analyte metals with the use of the complexing agent butane-2,3-dione bis(*N*-pyridinoacetyl hydrazone) (H_2bdpa). This water-soluble reagent complexes a large number of transition metals over a wide pH range. At a suitable pH the metal complexes are readily adsorbed on a polystyrene–divinylbenzene resin bed. Interfering matrix ions (anions and metals of Groups IA and IIA) are weakly or

Correspondence to: S.-J. Jiang, Department of Chemistry, National Sun Yat-Sen University, Kaohsiung 804 (Taiwan).

not complexed and are washed through the column during the loading procedure. During this step, the liquid flow containing the matrix is diverted from the nebulizer. The metal complexes adsorbed on the resin are then washed with acidic solution, which displaces the complexes from the non-polar resin. This column effluent is introduced into the nebulizer for multi-elemental analysis by ICP-MS. No organic solvent is needed for removing the metal complexes from the resin. Moreover, mild elution conditions are adequate to remove the complexes completely. These two characteristics are advantageous for ICP-MS analysis. The method was applied to the determination of various metals in the riverine reference material SLRS-2.

EXPERIMENTAL

ICP-MS device and conditions

The inductively coupled plasma mass spectrometer used was an ELAN 5000 (Perkin-Elmer SCIEX, Thornhill, ON, Canada) with a single-channel mass-flow controller to regulate the nebulizer gas flow-rate. Samples were introduced with a cross-flow nebulizer. The plasma and sampling conditions were optimized daily to obtain the best response across a wide mass range. This was performed by continuously introducing a solution composed of 10 μg l^{-1} each of Mg, Cu, Cd, Rh and Pb. The indicated parameters were adjusted so that the five ion count rates were maximized as much as possible at the same time. This method provided reasonable sensitivity and allowed for multi-element analysis under one set of conditions. The gas flow-rates were set to 14 l min^{-1} for the plasma gas, 0.9 l min^{-1} for the auxiliary gas and 0.85 l min^{-1} for nebulizer gas (r.f. power 1000 W). These were the optimized parameters for the elution flow-rate. Detailed descriptions of the instrumental system and conditions are given in Table 1. The element elution peaks were recorded in real time and stored on hard disk with "graphic" software. Under various combinations of the mass spectrometer parameter sets, normally a data point could be obtained for each isotope every 1 s.

TABLE 1

ICP-MS equipment and operating conditions

ICP-MS instrument	Perkin-Elmer SCIEX ELAN 5000
ICP system:	
Outer gas flow-rate	14 l min^{-1}
Auxiliary gas flow-rate	0.9 l min^{-1}
Nebulizer gas flow-rate	0.85 l min^{-1}
R.f. power	1.0 kW
Mass spectrometer:	
Sampler cone orifice	1.14 mm
Skimmer cone orifice	0.89 mm
Lens voltages:	
Photon stop (S2)	−6.04 V
Bessel box barrel (B)	+12.04 V
Einzel lenses 1 and 3 (E1)	+1.97 V
Bessel box end lens (P)	−65.9 V

Preconcentration system

A TraceCon preconcentration instrument (Knapp Logistik Automation) was used for analyte–matrix separation and preconcentration in combination with an ELAN 5000 ICP-MS system. Detailed descriptions of TraceCon were published previously [16,17]. During this study a mini-column (20 mm × 5 mm i.d.) packed with XAD-4 resin (170 mg) was used. At a suitable pH, the complexing agent H_2bdpa complexes a large number of transition metals. These metal complexes are readily adsorbed on a polystyrene–divinylbenzene resin bed. Commonly encountered matrix components such as alkali and alkaline earth elements do not form stable complexes or to a lesser extent and are not retained on the resin. This matrix separation strongly reduces matrix interference effects and helps to obtain uniform samples and standard solutions. The operating procedures for TraceCon are given in Table 2. For on-line studies, the elution tube was connected directly to the cross-flow nebulizer of the ICP with PTFE tubing. The standard peristaltic pump was not used during the preconcentration process.

Reagents and materials

The polystyrene–divinylbenzene resin used was Amberlite XAD-4 (Rohm and Haas, Philadelphia, PA). The resin was ground, cleaned, dried and sieved. Resin fines were removed and the 100–200-mesh fraction was syringe-packed in the column. In order to remove trace metallic contaminants, the resin was washed successively with water, 1 M HNO_3, 1 M NaOH and water.

Stock standard metal solutions (1000 mg l^{-1}) were obtained from SPEX. The displacing eluent was 1.0 M HNO_3 in 1% methanol. All buffers and eluents were prepared with high-purity deionized water (Milli-Q reagent water system; Millipore). All other reagents were of analytical-reagent grade. The buffers used were ammonium acetate–acetic acid for pH 4–7 and ammonium acetate–ammonia solution for pH 7–10. Buffer solutions were purified by passing the solutions through an SO_3–oxine CM-cellulose column twice [17].

Synthesis of butane-2,3-dione bis(N-pyridinoacetyl hydrazone) (H_2bdpa)

A 0.01 mol amount of butane-2,3-dione and 0.02 mol of 1-pyridinoacetyl hydrazine chloride (Girard's Reagent P; Aldrich) were mixed in 40 ml of absolute ethanol. This mixture was refluxed for 5 h and the resulting white precipitate was collected. The product, butane-2,3-dione bis(*N*-pyridinoacetyl hydrazone) dichloride, was then recrystallized from ethanol–water (85 + 15). This chelating reagent is stable in water, so an aqueous solution of H_2bdpd could be prepared in advance and added to sample solutions in suitable amounts.

TABLE 2

Operating conditions of TraceCon preconcentration system

Preconcentration device		TraceCon, Knapp Logistic Automation		
Flow-rates of pumps:				
Pump 1 (sample)		2.71 ml min^{-1}		
Pump 2 (buffer)		3.10 ml min^{-1}		
Pump 3 (eluent)		3.40 ml min^{-1}		
Preconcentration method				
Step No.	Pump in operation	Valve in open position	Solution volume (ml)	Duration (s)
1	P-2	V-2	2.0	22
2	P-2	V-3	3.0	33
3	P-1	V-2	1.0	12
4	P-1	V-3	20.0	242
5	P-2	V-3	1.0	11
6	P-3	V-3	1.0	21
7	P-3	V-1	7.5	161
8	P-2	V-2	1.0	11
9	P-2	V-3	2.0	22

TABLE 3

Characterization of H_2bdpa

Melting range (°C)	IR (cm^{-1})	Major mass spectral line m/z (relative intensity, %)	NMR Proton chemical shift (ppm) (integration)
> 300	3526	390 (6.09)	8.92–8.80 (3.34)
	3399	354 (57.8)	8.71–8.62 (1.63)
	3055	261 (15.6)	8.18–8.11 (3.34)
	2867	203 (10.9)	6.10–6.00 (2.62)
	1694	154 (59.1)	5.78–5.70 (1)
	1634	136 (62.9)	2.32–2.17 (5.17)
	1486	120 (41.0)	
	1419	107 (25.2)	
	1374	93 (100)	
	1265	77 (42.2)	
	1142		
	1100		

Characterization of butane-2,3-dione bis(N-pyridinoacetyl hydrazone)

H_2bdpa was characterized by the following procedures. The infrared spectrum was measured on a Perkin-Elmer Model 1330 infrared spectrophotometer. The ^{1}H NMR spectrum was measured with a Varian VXR-300 NMR spectrometer using D_2O as the solvent and chemical shift standard. The mass spectrum of the sample was recorded with a VB QUATTRO 5022 spectrometer employing fast atom bombardment (FAB). The physical characteristics for H_2bdpa are given in Table 3 and the structural formula is shown in Fig. 1. The UV–visible spectrophotometer used to obtain absorption spectra and evaluate the degree of cadmium complex formulation was a Varian DMS-100 equipped with quartz cells of path length 1.0 cm.

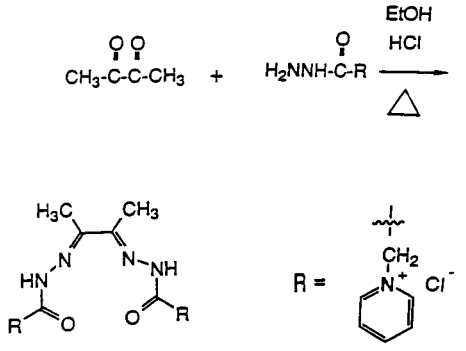

Fig. 1. Synthesis of H_2bdpa.

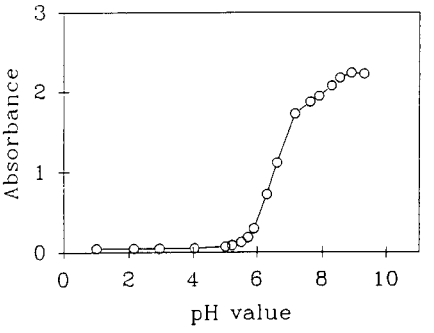

Fig. 2. Effect of pH on the absorbance of the cadmium complex. $[Cd^{2+}] = 3.9 \times 10^{-4}$ M; $[Cd^{2+}]/(H_2bdpa] = 1$.

Evaluation of retention

The effect of the loading eluent pH on the adsorption of the metal complexes was studied with the TraceCon preconcentration system in an off-line mode. A known amount of metal mixture buffered to suitable pH values and a 20-fold excess of the complexing agent were added and mixed to form the metal complexes. This mixture was then "loaded" on the XAD-4 resin at a flow-rate of 2.7 ml min^{-1}. Finally, any retained metal complexes were eluted with 5 ml of 1.0 M HNO_3 in 1% methanol into a 10 ml volumetric flask and diluted to volume with water. The concentrations of metals were determined by ICP-MS. Recoveries were calculated against the theoretical concentrations.

Sample preparation

Riverine reference material SLRS-2 (National Research Council of Canada, Ottawa) was analysed to demonstrate the applicability of the method to real samples. A 75-ml volume of the acidified sample was adjusted to pH 8.7 with 20 ml of 0.2 M purified ammonium acetate–ammonia buffer solution, an excess H_2bdpa reagent was added and the mixture was diluted to 100 ml with deionized, distilled water.

RESULTS AND DISCUSSION

Effect of pH on retention

In order to optimize the chromatographic conditions for retention of the metal complexes, the degree of Cd complex formation was monitored spectrophotometrically while changing the pH of the solution. The wavelength was adjusted to 348 nm. The metal complex of Cd with H_2bpda showed a strong absorbance at 348 nm. The result is shown in Fig. 2. The dependence of the recovery on the pH of the loading solution was similar to that of absorbance on pH, as shown in Fig. 3.

Figures 2 and 3 indicate that higher recoveries were obtained at pH values that favoured the formation of the complexes. This phenomenon is understandable, as the retention of metal ions is due to the physical adsorption of the metal complexes on the XAD-4 resin. Figure 3 shows that no retention occurs at pH < 7, whereas at pH ca. 8–9 the recoveries are 60–100%. The reproducibility of the recoveries is shown in Table 4. According to these results, the optimum pH for retention of these metal ions was 8.7. For multi-

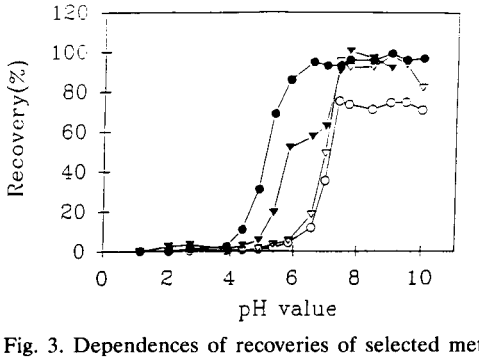

Fig. 3. Dependences of recoveries of selected metal ions on pH of loading solutions. ▽ = Ni; ● = Cu; ○ = Cd; ▼ = Pb.

TABLE 4

Recovery at pH 8.5 and relative standard deviations for standard solutions using the optimized preconcentration procedure

Element	Mean recovery (%) [a]	R.S.D. (%)
Co	74.7	3.7
Ni	92.2	0.7
Cu	99.3	1.4
Cd	71.2	0.5
Pb	90.3	1.3

[a] Calculated from five replicate preconcentrations.

element analysis a solution pH between 8.5 and 9.0 should be chosen, as this will result in the largest number of metals being complexed by H_2bdpa and being sorbed on the XAD-4 resin. The recoveries of commonly encountered matrix components such as Na, K, Mg and Ca were less than 1% in this pH range.

In order to form the metal complexes completely, the mole ratio of ligand to metal (L/M) is critical. Figure 4 shows that stable recoveries could be obtained when the L/M ratios were > 10. Cd is the only metal that shows a great dependence on the L/M ratio. This result is understandable, as Cd needs more ligand to form complexes kinetically. Longer columns and smaller resin particles could improve retention, but this would increase the preconcentration time and back-pressure of the column.

The results in Fig. 3 indicate that the concentration of acid in the eluent is not critical as long as the pH is below 5. In practice, the concentration of HNO_3 used to elute the complexes affects the heights of the elution peaks. The HNO_3 concentration should be at least 0.1 M to elute the complexes completely; 1.0 M HNO_3 in 1% methanol was used as the eluent in subsequent experiments.

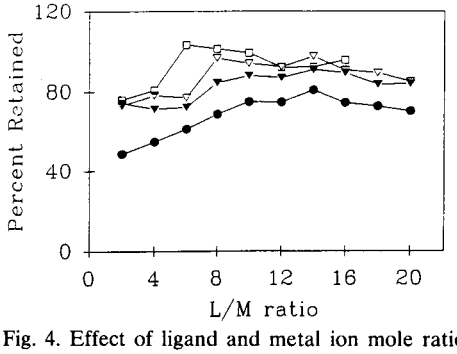

Fig. 4. Effect of ligand and metal ion mole ratios (L/M) on the percentage of metal retained by the column. ▼ = Ni; ▽ = Cu; ● = Cd; □ = Pb.

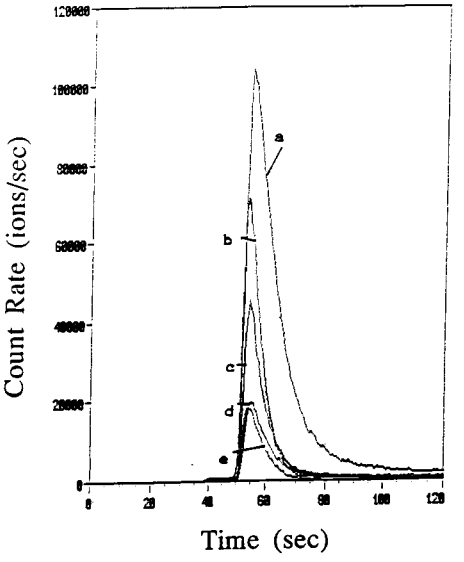

Fig. 5. Typical elution peaks for (a) Rh , (b) Pb, (c) Cu, (d) Ni and (e) Cd. Each metal ion was present at 1 $\mu g\ l^{-1}$ in 20 ml of loaded sample.

Separation of transition metals

Typical elution peaks for several elements (20 ng each) are illustrated in Fig. 5. All the metal ions elute at the same time (in 60 s). The peak heights for this 20-ml sample were 50–100 times higher than for continuous introduction of the same solution at the same flow-rate. Higher eluent flow-rates will lead to higher elution peak heights. A higher eluent flow-rate would also decrease the nebulization efficiency, which would cause the ion signal to decrease. Therefore, a compromise eluent flow-rate of 3.40 ml min^{-1} was adopted.

The trace-metal grade HNO_3 used for elution never produced any noticeable blank values, because the contaminants therein (if any) did not undergo preconcentration, whereas the contaminants in the chelating reagent were preconcentrated with the sample solution. Therefore, a

blank solution with same amount of chelating reagent should be run to correct for the contaminants in the chelating reagent. Reagent blanks for the elements studies are given in Table 5.

Linearity and detection limits

The peak height varied linearly with analyte concentration over several orders of magnitude. The calibration graphs for Cu, Cd, Pb and Ni were linear with correlation coefficients of 0.996–1.000 at levels near the detection limits up to at least 10 $\mu g\ l^{-1}$, as shown in Table 5. Detection limits for the several elements are reported in Table 5, based on the concentration of analyte yielding a net signal equivalent to three times the standard deviation of the background signal. These values are better than those obtained with direct introduction of aqueous samples in the absence of a matrix. It is important to note that these values were obtained with a 20-ml sample and at average sensitivities for all the masses. Better detection limits are to be expected with larger samples and instrument conditions optimized for one element or a restricted mass range.

Matrix effect and spectral interferences

In order to evaluate the possibility of the selective recovery of a metal ion in the presence of Ca, Mg and Na ions, the procedure was carried out with a solution containing 10 mg l^{-1} each of Ca, Mg and Na. The recoveries for Ca, Mg and Na were less than 1%. It should be mentioned that the low recoveries for Ca, Mg and Na are helpful in the determination of heavy metals at trace levels in natural waters. The low recoveries of Ca, Mg and Na did not create any problem of saturation of the resin and they did not cause interferences in the determination of trace heavy metals.

TABLE 5

Calibration parameters for metal ions

Parameter	Cu	Ni	Cd	Pb
S [a]	1.17×10^4	1.34×10^4	1.46×10^4	4.53×10^4
r [b]	0.996	0.998	1.000	1.000
DL [c]	3	10	2	3
RB [d]	32	17	5	25

[a] Sensitivity (counts per $\mu g\ l^{-1}$). [b] Regression coefficient. [c] Detection limits (ng l^{-1}). Defined as the concentration of analyte that gives a response equivalent to three times the standard deviation of the background, based on a 20-ml sample. [d] Typical reagent blanks (ng l^{-1}). Concentrations may vary for different amounts of reagent added.

TABLE 6

ICP-MS analysis of the reference material SLRS-2

Element	ICP-MS result ($\mu g\ ml^{-1}$) [a]	Certificate value ($\mu g\ ml^{-1}$)
Co	0.057 ± 0.004	0.063 ± 0.013
Ni	$1.02\ \pm0.14$	$1.03\ \pm0.10$
Cu	$2.78\ \pm0.58$	$2.72\ \pm0.17$
Cd	0.029 ± 0.004	0.028 ± 0.004
Pb	0.198 ± 0.048	0.129 ± 0.011

[a] Mean of five measurements ± standard deviation.

Determination of trace metals in water samples

The results of ICP-MS analysis of the riverine reference material SLRS-2 by external calibration were compared with the accepted values. The ICP-MS results (Table 6) are blank-corrected means based on five separate analyses with precision expressed as standard deviations. The agreement with the accepted values is good, with the exception of the result for Pb, which appears to be too high. A possible explanation is that the reagents were contaminated with lead. The standard deviations of the results were higher for Cu and Pb. These two elements are common contaminants in the reagent and solutions.

This work was supported by the National Science Council of the Republic of China.

REFERENCES

1 R.S. Houk, V.A. Fassel, G.D. Flesch, H.J. Svec, A.L. Gray and C.E. Taylor, Anal. Chem., 52 (1980) 2283.
2 R.S. Houk and J.J. Thompson, Mass Spectrom. Rev., 7 (1988) 425.
3 R.S. Houk, Anal. Chem., 58 (1986) 97A.
4 D.J. Douglas and R.S. Houk, Prog. Anal. At. Spectrosc., 8 (1985) 1.
5 S.H. Tan and G. Horlick, Appl. Spectrosc., 40 (1986) 445.
6 S.H. Tan and G. Horlick, J. Anal. At. Spectrom., 2 (1987) 745.

7 J.W. McLaren, A.P. Mykytiuk, S.N. Willie and S.S. Berman, Anal. Chem., 57 (1985) 2907.
8 D. Beauchemin, J.W. McLaren, A.P. Mykytiuk and S.S. Berman, J. Anal. At . Spectrom., 3 (1988) 305.
9 J.W. McLaren, D. Beauchemin and S.S. Berman, J. Anal. At. Spectrom., 2 (1987) 227.
10 E.M. Heithmar, T.A. Hinners, J.T. Rowan and J.M. Riviello, Anal. Chem., 62 (1990) 857.
11 M.R. Plantz, J.S. Fritz, F.G. Smith and R.S. Houk, Anal. Chem., 61 (1989) 149.
12 D. Beauchemin and S.S. Berman, Anal. Chem., 61 (1989) 1857.
13 V. Porta, C. Sarzanini and O. Abollino, Anal. Chim. Acta, 258 (1992) 237.
14 H. Bukowsky, E. Uhlemann, K. Gloe and P. Muhl, Anal. Chim. Acta, 257 (1992) 105.
15 M.A. Vaughan and D.M. Templeton, Appl. Spectrosc., 44 (1990) 1685.
16 P. Schramel, L.Q. Xu, G. Knapp and M. Michaelis, Mikrochim. Acta, 106 (1992) 191.
17 K.-S. Huang and S.-J. Jiang, Fresenius' J. Anal. Chem., (1993) in press.
18 M.V. Main and J.S. Fritz, Anal. Chem., 61 (1989) 1272.

Analytica Chimica Acta, 282 (1993) 445–449
Elsevier Science Publishers B.V., Amsterdam

Determination of morestan residues in waters by solid-phase spectrofluorimetry

José Luis Vilchez, Ramiro Avidad, Jamal Rohand, Alberto Navalón and Luis Fermín Capitán-Vallvey

Department of Analytical Chemistry, University of Granada, E-18071 Granada (Spain)

(Received 19th February 1993; revised manuscript received 12th May 1993)

Abstract

Morestan in solution in a neutral medium shows native fluorescence. A method for the determination of trace amounts of morestan in waters by solid-phase spectrofluorimetry is described. Morestan is fixed on C-18 silica-gel, packed in a 1-mm silica cell and measured directly with a solid-surface attachment giving fluorescence at λ_{em} = 392 nm for wavelength of excitation λ_{ex} = 370 nm. The applicable concentration range is 1.0–7.0 ng ml^{-1} with a relative standard deviation of 1.9% and a detection limit of 0.15 ng ml^{-1}. The influence of the presence of other pesticides and chemical species has also been studied. The method is found to be more sensitive and selective than other methods proposed in the literature. It was applied to the determination of morestan in natural waters. Recoveries were from 95 to 105%.

Keywords: Fluorimetry; Morestan; Pesticides; Waters

Quinomethionate (6-methyl-2,3-quinoxalinediyl cyclic S,S-dithiocarbonate) commercially known as morestan is an insecticide widely used for the control of mites present in many crops including potatoes, apples and pears [1,2]. Also, it is a fungicide specific to powdery mildew on fruits, ornamental plants and vegetables [3].

It is reported as practically insoluble in water [3], but as, in spite of that, trace amounts of morestan can be present in water coming from agricultural manipulation its determination might be worthwhile.

Natural fluorescence of morestan enables its direct determination. This fluorescence is enhanced if the morestan is previously fixed in silica-gel. This led Mallet et al. [4] to propose a method based on the use of thin-layer chromatography and direct measurement of the fluorescence for its determination in water.

It can be determined, too, by other techniques such as colorimetry [5], gas–liquid chromatography (GLC) using an electron capture detector [6–9], polarography with a previous separation by thin-layer chromatography (TLC) [10] using "in situ" fluorescence on a silica-gel plate for TLC [11,12] or on aluminium oxide layers as solid-phase for the fixation of the pesticides [13].

In previous papers we have used the solid-phase spectrofluorimetry (SPSF) as a powerful technique appropriate for the determination of ionic species [14–20] and organic pesticides [21–23] at trace level in waters.

Detection limits, selectivity and sensitivity are dramatically increased by this improved SPSF which small amounts (250 mg) of a suitable solid support (e.g. an ion exchanger or a dextran type resin) to preconcentrate the analyte. The analyte might be intrinsically fluorescent or induced to

Correspondence to: L.F. Capitán-Vallvey, Department of Analytical Chemistry, University of Granada, E-18071 Granada (Spain).

fluorescence by the use of an appropriate derivation reaction followed by fluorescent detection. Here, fluorescence measured is the diffuse transmitted in all cases, as the signal intensity is higher than in the diffuse reflected fluorescence methods. Other bonuses on the deal are: simplicity, low interference level, low detection limits, high selectivity and the use of conventional instrumentation.

Here, the detection of morestan residues in waters of diverse nature such as natural, waste and tap water near drinkable sources as well as the presence of ion species and other fluorescent pesticides has been investigated.

EXPERIMENTAL

Apparatus

All the spectrofluorimetric measurements were conducted with a Perkin-Elmer LS-5 luminescence spectrometer as described earlier [17].

The measurements of relative fluorescence intensity vs. angle were carried out with a variable-angle surface accessory designed and constructed by the authors [23].

The LS-5 spectrometer was interfaced to an IBM PS/2 30–286 microcomputer using RS 232C connections for spectral acquisition and subsequent treatment of data [24].

Further, a Braun Melsungen Thermomix 1441 thermostatic water-bath circulator for temperature control, a Crison 501 digital pH meter with a combined glass-saturated calomel electrode and an Agitaser 2000 rotating agitator were used.

Reagents

All reagents were of analytical-reagent grade unless stated otherwise.

Morestan stock solution, 0.1 mg ml^{-1}, was prepared by exact weighing of the reagent (Lab. Dr. Ehrenstorfer) and dissolution in ethanol (98%, v/v). This solution was stable for at least two weeks. Working solutions were obtained by appropriate dilutions with doubly distilled water.

C-18 silica-gel (Sigma, HPLC sorbent) was used without pre-treatment.

Buffer solution: $H_2PO_4^-/HPO_4^{2-}$ (pH = 7.1) was prepared from sodium hydroxide (Merck) 0.2 M and NaH_2PO_4 (Merck) 0.2 M solutions.

Fluorescence measurements

The measured relative fluorescence intensity (RFI) of the gel beads containing the fluorescent compound and packed in a 1-mm silica cell was the diffuse transmitted fluorescence emitted from the gel at the unirradiated face to the cell. The optimum angle between the cell plane and the excitation beam was 45° in all instances [25].

Basic procedure

An appropriate volume of water sample containing between 0.5 and 3.5 μg of morestan and 4 ml of phosphate buffer solution (pH 7.1) were placed into a 500-ml calibrated flask. The mixture was diluted to the mark with doubly distilled water and then transferred into a 1-litre glass bottle (Scott). When 250 mg of C-18 gel were added the mixture was shaken mechanically at 50 rpm for 10 min after which the gel beads were collected by filtration and dried at room temperature under suction. Then the gel-system was packed in a 1-mm silica cell with the aid of a microspatula. A blank solution containing all the reagents except morestan was prepared and treated in the same way as described for the sample.

The RFI of the sample and blank were always measured at $\lambda_{em} = 392$ nm with a $\lambda_{ex} = 370$ nm.

A calibration graph was constructed in the same way using solutions of morestan of known concentration.

Procedure for waters

The above-mentioned reagents were added to a volume of water sample containing an adequate amount of morestan and were treated as described under 'Basic Procedure'. The standard additions method was used for calibration.

Sample treatment

Water samples were filtered through a filter-paper with a pore size of 0.45 μm (Millipore), collected in a glass bottle that had been cleaned carefully with hydrochloric acid and stored at 4°C

until analysis. The usual precautions were taken to avoid contamination [26]. Analyses were performed with the least possible delay.

RESULTS AND DISCUSSION

Spectral characteristics

Morestan in the presence of C-18 gel is fixed at neutral pH. The peak wavelengths for excitation and emission are 370 and 392 nm, respectively, for solid-phase gel while 362 and 398 nm are observed in solution, no doubt due to the change of environments.

From a study of the half-life of the excited state of the system in the morestan–C-18 gel at different temperatures (0–60°C) it was concluded that the luminescence process was fluorescence ($t < 5 \times 10^{-6}$ s).

Effect of experimental variables

The effect of pH was studied using NaOH and HCl solutions for adjustment. The optimum pH value for the fixation of the morestan in the gel was found to be within the range 2.3–8.0 (Fig. 1). In solution the optimum pH range was 4.0–7.8.

Different buffer solutions (acetate, hydrogen phthalate and dihydrogen phosphate) were tested. Monohydrogen phosphate/dihydrogen phosphate (pH = 7.1) was found to be the most useful, because the RFI measured was higher than with the other buffers.

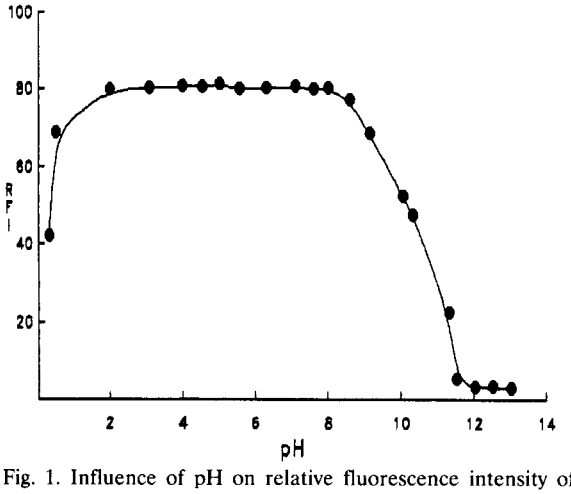

Fig. 1. Influence of pH on relative fluorescence intensity of morestan in gel-phase.

The fluorescence is independent of ionic strength, adjusted with the buffer solution, NaCl or $NaClO_4$ up to 1 M solutions.

The dependence of the relative fluorescence intensity on the morestan concentration is linear in the range 1.0–7.0 ng ml^{-1} and a quenching effect is observed at higher morestan concentrations. This effect is probably due to re-absorption by the solid matrix.

The effect of temperature on the fluorescence emission was studied in the range 0–60°C. A decrease of the RFI was observed when the temperature of the system increases, the effect being totally reversible. The decrease in the RFI is 0.7% at 10°C, 2.4% at 20°C, 8.5% at 40°C and 11.2% at 60°C. All measurements of RFI reported here were made at 20.0 ± 0.5°C in the instrument compartment of the cell.

The fixation of morestan was carried out at room temperature, because this process was independent of temperature in the range 0–40°C.

The stirring time necessary for maximum RFI development was 10 min for 100-, 200- and 500-ml sample volumes. The effect of the stirring speed on the RFI was studied in the range from 20 to 80 rpm, which showed there was no effect on the emission intensity.

The order of addition of the reactants did not affect the results obtained. The order used was: morestan, buffer and gel.

The amount of gel was 250 mg in all instances, the amount required to fill the cell. As the use of amounts of gel higher than 250 mg lowers the RFI, precisely the adequate amount is used. The fluorescence for the compound developed immediately, remaining constant for at least 2 h after equilibration.

Increases in sensitivity in solid-phase spectrofluorimetry are expected with increasing volume of the samples trapped on C-18 gel with different volumes of solutions containing the same concentration of morestan and proportional amounts of other reagents. A linear dependence of RFI vs. sample volume in the range 100–500 ml was observed. If the sample volume is higher than 500 ml the dependence of RFI is not linear,

the optimum sample volume being 500 ml because the detection limit is lower than in other cases.

Analytical parameters

The calibration graphs for samples treated according to the procedure described above are linear for the concentration range 3.0–30.0 ng ml^{-1} for a 100-ml sample volume, 2.0–20.0 ng ml^{-1} for a 200-ml and 1.0–7.0 ng ml^{-1} for a 500-ml sample volume.

The reproducibility of the proposed method was checked with a series of ten samples having a morestan concentration of 5.0 ng ml^{-1}; the relative standard deviations (RSDs) ($P = 0.05$, $n = 10$) were 1.2%, 1.4% and 1.9% for 100, 200 and 500 ml of sample respectively. The precision (RSD) of the packing operation, calculated from ten measurements, was 1.9% for the morestan fixed on the gel, 1.3% for the gel blank (gel with buffer solution) and 1.1% for the gel only. The detection limits ($k = 3$) according to IUPAC [27] and the quantification limits ($k = 10$) [28] were calculated for 100-, 200- and 500-ml sample volumes. The 500-ml sample volume was selected as optimum because the calibration graph shows a major slope which permits a higher sensitivity. The analytical parameters are summarized in Table 1.

We have found in a search in the open literature only three methods for determination of morestan in waters using solid-phase fluorescence spectrometry [11] and gas chromatography [29,30]. In all cases the procedures are quite laborious and the detection limits are reported as higher than 0.5 $\mu g\ l^{-1}$.

TABLE 1

Analytical parameters

Parameters	Sample volume (ml)		
	100	200	500
Intercept	−0.10	−0.23	0.80
Slope	2.83	3.16	6.40
LDR [a] (ng ml^{-1})	3.0–30.0	2.0–20.0	1.0–7.0
Correlation coefficient	0.999	0.999	0.998
Detection limit (ng ml^{-1})	0.37	0.21	0.15
QL [b] (ng ml^{-1})	1.20	0.70	0.50
RSD [c] (%)	1.2	1.4	1.9

[a] Linear dynamic range. [b] Quantification limit. [c] Relative standard deviation.

TABLE 2

Effect of foreign ions or species on the determination of 5 ng ml^{-1} of morestan

Foreign ion or species	Tolerance level (ng ml^{-1})
F^-, Cl^-, Br^-, I^-, ClO_4^-, CO_3^{2-}, SO_4^{2-}, NO_3^-, EDTA, $C_2H_3O_2^-$, Li^+, Na^+, K^+, NH_4^+, Zn^{2+}, Cd^{2+}, Mg^{2+}, Ca^{2+}, Al^{3+}, Fe^{3+}, Cu^{2+}, Be^{2+}	20000
Carbendazim	4000
Carbaryl	3000
o-Phenylphenol	2000
Folpet	1200
Humic acid	1060
Thiabendazole	250
Captan	200

Effect of foreign species

A systematic study of the effect of foreign species (ions and other pesticides) on the determination of morestan at the 5 ng ml^{-1} level was undertaken. A 20 mg l^{-1} level of each potentially interfering fluorescent and non-fluorescent species was tested first. If the interference occurred, the ratio was progressively reduced till interference ceased. Tolerance was defined as the amount of foreign species that produced an error not exceeding ±5% in the determination of the analyte. All interferences observed are negatives. Table 2 shows the results obtained.

The most serious interferences were those from thiabendazole and captan for concentrations equal or higher than 250 and 200 ng ml^{-1} respectively.

The benomyl is not included in Table 3 because in aqueous solution and neutral pH this pesticide undergoes a degradation process to give carbendazim [31].

Applications of the method

To check the accuracy of the proposed method a recovery study was carried out on several sample waters. Genil river and Quentar Dam waters were analyzed after adequate additions of

TABLE 3

Recovery study of morestan in water

Sample	Taken (ng ml^{-1})	Found [a] (ng ml^{-1})	% Recovery
Raw water [b]	6.0	6.2	103.5
	4.0	4.2	105.0
	2.0	2.1	105.0
Tap water [c]	6.0	6.1	101.7
	4.0	3.9	97.5
	2.0	2.0	100.0
Spring water [d]	6.0	6.0	100.0
	4.0	3.9	97.5
	2.0	1.9	95.0

[a] Data are the average value of three determinations. [b] From Genil River. [c] From Granada City. [d] From Lanjarón (Granada).

morestan in order to check plausible future contaminations.

The volume used was 500 ml in all instances. The standard addition method was applied. Table 3 shows the results obtained.

Conclusion

This paper provides a simple and practical application of the solid-phase spectrofluorimetry technique to the determination of morestan at residue levels in waters menaced by unproper contamination coming from agricultural manipulations.

REFERENCES

1 C. de Liñan, Vademecum de Productos Fitosanitarios y Nutricionales, Ed. Embajadores, Madrid, 1990.
2 E.Y. Spencer, Guide to the Chemicals Used in Crop Protection, Publ. 1093, Canada Department of Agriculture, Ottawa, Canada, 5th edn., 1968.
3 The Pesticide Manual, Ed. C.R. Worthing, 7th edn., 1983.
4 V.N. Mallet, C. LeBel and D.P. Surette, Analusis, 9 (1974) 643.
5 R. Haves, J.M. Adams and C.A. Anderson, J. Agric. Food Chem., 12 (1964) 247.
6 H. Tietz, M. Osmon, H. Frehse and H. Niessen, Pflanzenschuznachr. Bayer, 15 (1967) 170.
7 H. Vogler and H. Niessen, Pflanzenschuznachr. Bayer, 20 (1967) 550.
8 C.A. Anderson, in G. Zweig (Ed.), Analytical Methods for Pesticides, Plant Growth Regulator and Food Additives, Vol. 5. Academic Press, New York, 1967.
9 G.H. Tjan and T. Konter, J. Assoc. Off. Anal. Chem., 54 (1971) 11222.
10 F.E. Hearth, D.E. Otl and G.A. Gunther, J. Assoc. Off. Anal. Chem., 49 (1966) 774.
11 Y. Francouer and V. Mallet, J. Assoc. Off. Anal. Chem., 59 (1976) 172.
12 V. Mallet, D. Surette and L. Brun, J. Chromatogr., 79 (1973) 217.
13 G.E. Caissie and V.N. Mallet, J. Chromatogr., 117 (1976) 129.
14 F. Capitán, E. Manzano, J.L. Vilchez and L.F. Capitán-Vallvey, Anal. Sci., 5 (1989) 549.
15 F. Capitán, E. Manzano, A. Navalón, J.L. Vilchez and L.F. Capitán-Vallvey, Analyst, 114 (1989) 969.
16 F. Capitán, A. Navalón, J.L. Vilchez and L.F. Capitán-Vallvey, Talanta, 37 (1990) 193.
17 F. Capitán, J.P. de Gracia, A. Navalón, L.F. Capitán-Vallvey and J.L. Vilchez, Analyst, 115 (1990) 849.
18 F. Capitán, A. Navalón, E. Manzano, J.P. de Gracia, L.F. Capitán-Vallvey and J.L. Vilchez, Analusis, 19 (1991) 132.
19 F. Capitán, E. Manzano, A. Navalón, J.L. Vilchez and L.F. Capitán-Vallvey, Talanta, 39 (1992) 21.
20 F. Capitán, G. Sánchez-Palencia, A. Navalón, L.F. Capitán-Vallvey and J.L. Vilchez, Anal. Chim. Acta, 259 (1992) 345.
21 J.L. Vilchez, R. Avidad, A. Navalón, J. Rohand and L.F. Capitán-Vallvey, Int. J. Environ. Anal. Chem. (in press).
22 J.L. Vilchez, A. Navalón, R. Avidad, J. Rohand and L.F. Capitán-Vallvey, Fresenius' J. Anal. Chem., 345 (1993) 716.
23 F. Capitán, E.J. Alonso, R. Avidad, L.F. Capitán-Vallvey and J.L. Vilchez, Anal Chem., 65 (1993) 1336.
24 M.T. Oms, V. Cerda, F. García-Sánchez and A.L. Ramos, Talanta, 35 (1988) 671.
25 E. Manzano, PhD. Thesis, University of Granada, 1989.
26 APHA-AWWA-WPCF, Métodos Normalizados para el Análisis de Aguas Potables y Residuales, Ed. Díaz de Santos S.A., Madrid, 1992.
27 IUPAC, Nomenclature, Symbols, Units and Their Usage in Spectrochemical Analysis, Pure Appl. Chem., 45 (1976) 105.
28 Guidelines for Data Acquisition and Data Quality Evaluation in Environmental Chemistry, Anal. Chem., 52 (1980) 2242.
29 A. Malin, T. Lena and S. Anders, Waar Foeda, 42 (1990) 236.
30 R. Brennecke and K. Vogeler, Pflanzenschutz Nachr., 37 (1984) 46.
31 R.P. Singh, C.H. Marvin and I.D. Brindle, J. Agric. Food Chem., 40 (1991) 1304.

Analytica Chimica Acta, 282 (1993) 451–458
Elsevier Science Publishers B.V., Amsterdam

Solvent venting technique for gas chromatography with microwave-induced plasma atomic emission spectroscopy

M. Eileen Birch

U.S. Department of Health and Human Services, Public Health Service, Centers for Disease Control and Prevention, National Institute for Occupational Safety and Health, Division of Physical Sciences and Engineering, 4676 Columbia Parkway, Cincinnati, OH 45226 (USA)

(Received 15th February 1993; revised manuscript received 21st May 1993)

Abstract

A solvent-venting interface for gas chromatography with microwave plasma emission detection was developed. Solvent venting is necessary to avoid the deleterious effects that can occur when solvent is permitted to enter the plasma. During venting, the flow of plasma supply gas through the discharge tube is reversed. The reversed gas flow directs the solvent away from the plasma to vent through resistively heated stainless steel tubing. Gas flow direction is controlled by a 6-port valve. After venting, the valve is switched to the analysis mode, and the supply gas and column effluent flow in the forward direction to the plasma for analyte determination. Vent operation does not appear to affect plasma stability. Although a change in background is observed during solvent venting, the background quickly returns to its original level when the vent is switched back to the analysis mode. The interface is a low dead volume design that allows placement of the column 2–3 mm from the plasma. Because a transfer line or other components are not required, active sites in the interface are avoided. A modified commercial instrument (Applied Chromatography Systems MPD 850) was used for this research. Performance of the modified instrument was improved relative to that of the original system. Interface design and analytical results are reported.

Keywords: Gas chromatography; Atomic emission spectrometry; Solvent venting technique

Gas chromatography–microwave-induced plasma (GC–MIP) atomic emission spectroscopy has become a widely accepted analytical method. The widespread application of plasma emission spectroscopy for element-selective detection is related to the superior analytical performance afforded by this technique relative to traditional arc/spark and flame methods. Element-selective detection can be especially useful in reducing chromatographic resolution requirements for analysis of species in complex sample matrices when the analyte of interest contains an element not present in coeluting components. In addition, a qualitative knowledge of elemental composition can greatly simplify interpretation of mass and infrared spectra, and enable confirmation of library search results. Applications of GC–MIP atomic emission spectroscopy have been reviewed in the literature [1–3].

Correspondence to: M.E. Birch, U.S. Department of Health and Human Services, Public Health Service, Centers for Disease Control and Prevention, National Institute for Occupational Safety and Health, Division of Physical Sciences and Engineering, 4676 Columbia Parkway, Cincinnati, OH 45226 (USA).

Various GC–MIP interface designs have been developed, with specific interface requirements being dependent on instrument configuration. In cases where the plasma can survive solvent introduction without extinguishment, the GC column

has been inserted directly into the discharge tube; however, deposition of solvent-source elemental carbon on the tube wall can result in shortened tube life. To avoid this problem, the plasma has been initiated after the solvent has passed through the discharge tube [4], but results were reportedly compromised by this approach because analyte response depended on the time passed since plasma initiation [4].

To avoid the deleterious effects (i.e., plasma extinguishment, carbon deposition) that can occur when solvent is permitted to enter the plasma, solvent venting is necessary. Most often, the column end has been connected to a high-temperature valve located within the GC oven, or in a separate oven, which enables redirection of the column effluent to a vent [5]. Problems with this arrangement include valve-heating requirements (to prevent condensation), lack of inertness in the valve's interior, and loss of chromatographic resolution.

A solvent-venting approach involving a chemically deactivated, low dead volume, heated interface based on a fluid logic gas-switching network has been described [6]. Drawbacks to this approach include its general complexity and a heated stainless steel transfer line, which introduces some dead volume and requires deactivation. In addition, the significant changes in helium flow that result during venting could affect analyte response. Other solvent-venting schemes have been reported [7,8]; however, these also have required use of heated transfer lines and additional helium flow.

A solvent-venting design based on fluid logic within the plasma containment tube recently has been described [9]. This design required no transfer line and plasma stability was reportedly unaffected by activation of the vent. However, placement of the column end 3 mm from the end of a stainless steel tube located within the quartz discharge tube was necessary for vent operation. Ideally, the column end and plasma should be as close to each other as possible to avoid potential contact with active surfaces and loss of chromatographic resolution.

In this paper, a GC–MIP interface that effects solvent-venting by reversal of the gas flow through the plasma discharge tube is described. The interface design permits placement of the GC column end 2–3 mm from the plasma. A similar approach was employed in an instrument recently introduced by Hewlett-Packard [10]; however, a specialized re-entrant cavity was used. In contrast, the interface described here is relatively simple to construct and can be adapted to many of the GC–MIP instruments currently in use. Interface design and analytical results are reported.

EXPERIMENTAL [a]

Plasma emission detector system

A modified Applied Chromatography Systems plasma emission detector, the MPD 850, was used in this research. The original MPD 850 comprised a 2450-MHz microwave generator (200 W maximum output power), 1/4-λ Evenson microwave cavity, heated transfer line and stainless steel plasma head unit, fused silica plasma containment tube (i.e., discharge tube), vacuum pump for reduced-pressure operation, gas control unit, and a 0.75-m spectrometer. The MPD's generator is equipped with reflected current and overload latching circuits for automatic disconnection of power to the magnetron should severe cavity/generator mismatch (i.e., high reflected power) occur, which would normally result in generator damage. The spectrometer incorporates a 960 grooves/mm grating with a reciprocal dispersion of 1.39 nm/mm (first order) and has a wavelength range of 380–800 nm (first order). It is equipped with slits and photomultiplier tubes (PMTs) for monitoring atomic emission from the following twelve species: C, H, F, Cl, Br, I, O, S, N, P, Si, and D. Limits of detection specified [11] for most elements are from 0.1–1.0 ng/s. A total of 14 PMTs and twelve amplifiers can be used with the instrument, enabling simultaneous determination of up to twelve elements.

[a] Mention of company names or products does not constitute endorsement by the Centers for Disease Control and Prevention.

The background correction scheme featured on the MPD-850 system involves hardware attenuation of nonelemental signals, called ghosts, arising from carbon continuum emission. Although the magnitude of the ghost signal varies from element to element, all ghost responses are proportional to the amount of carbon present in the plasma. This proportionality is the basis of the ghost correction method. In this method, a small portion of the carbon signal is fed into each elemental channel. The amount of correction applied is adjusted by the appropriate potentiometer and is equal to the continuum contribution to the channel. Because each photomultiplier tube is linked to a separate amplifier that monitors and subtracts the adjusted portion of the carbon signal, elimination of the ghost response from carbon continuum is achieved.

A schematic diagram of the modified instrument is shown in Fig. 1. Modifications to the original instrument were made to enable atmospheric-pressure operation. Advantages of atmospheric-pressure operation include the elimination of cumbersome vacuum equipment, enhanced sensitivity for most elements, and the ability to view the plasma emission axially (end-on) instead of radially (transversely) through the wall of the quartz discharge tube. Radial viewing is undesirable because the optical emission window (i.e., the tube wall) continually undergoes changes due to devitrification, and metal oxide and elemental carbon deposition. These factors result in day-to-day reproducibility problems [12]. Modifications included replacement of the Evenson cavity with a Beenakker TM_{010} [13], construction of a new GC–plasma interface, and replacement of the gas-flow control unit with mass flow controllers and plumbing associated with the solvent-venting technique detailed in this paper. Further details regarding instrument modification and evaluation can be found elsewhere [14].

Six Hewlett-Packard A/D converters (Model 18652A) operated at 4 Hz and an HP3357 Laboratory Automation System were used for data

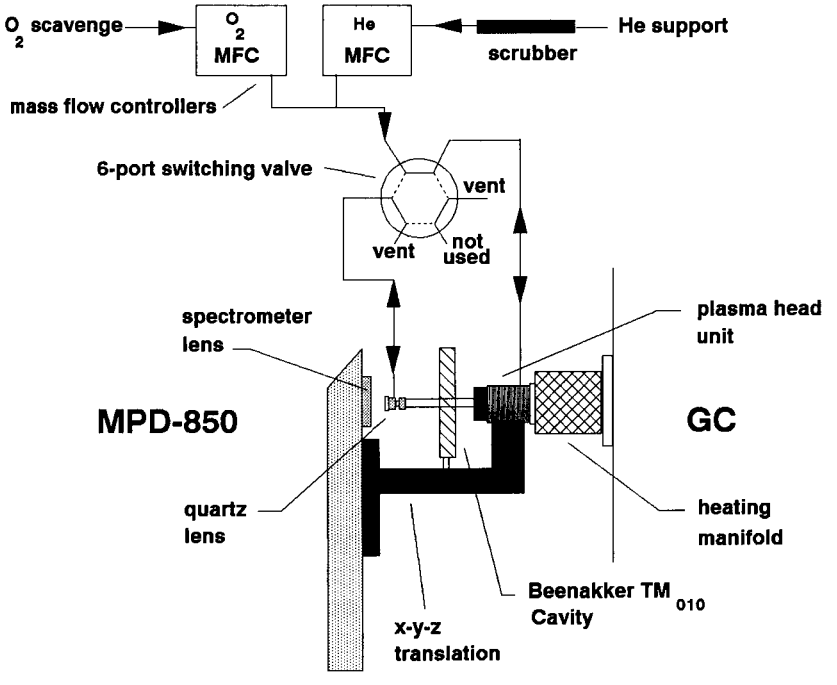

Fig. 1. Schematic diagram of modified GC–MIP system. Six-port valve shows gas flow direction during analysis (solid lines) and solvent venting (dashed lines).

collection. The A/D J4 remote start lines were connected to VALVE 10 on the valve controller board of a Hewlett-Packard (HP) 5880A to provide a +5 V signal for A/D activation. A/D on-off control was achieved during run time by including VALVE 10 OFF/ON commands in the Run Table (i.e., program) entered at the GC terminal. Coaxial cable was used for all connections.

GC–plasma interface and gas flow control

A hole was drilled in the outer left wall of the HP5880A GC to accommodate an aluminum transfer tube flanged at one end, and a heating manifold that fits snugly around the tube (Fig. 1). The flanged end of the transfer tube was mounted to the outside wall of the GC. The capillary column and heating manifold's associated thermocouple sensor (HP No. 19301-60600) were inserted through two small holes drilled into the GC oven wall. The sensor was connected to the AUX 1 heating zone on the GC and the heating manifold (HP5792 Interface Heater, HP No. 0854-0301) was connected to 115 V ac on the GC's duct board edge connector. The manifold extends just beyond the end of the transfer tube and butts against the plasma head unit, which is a resistively heated stainless steel block with gas ports and a knurled-nut fitting for attachment of a quartz discharge tube. Fused quartz tubing (Quartz Scientific) was used as the discharge tube material. Tubing (1 mm i.d., 6 mm o.d.) was scored and broken to the desired length (about 10 cm).

To protect against minor air leaks at the tube/plasma-head seal, a helium purge is provided around the seal. The column (J and W Scientific DB-5, 30 m × 0.32 mm i.d., 0.25-μm film thickness) was connected to the plasma block using a 0.4-mm 40% graphite/vespel ferrule and 1/16″ nut. To minimize mixing between plasma gases and column effluent, and prevent contact between the effluent and metal block interior, the capillary column was inserted completely through the plasma head block and into the discharge tube to within 2–3 mm of the plasma. The column must not be inserted too close to the plasma to avoid fusing the column end.

Use of high-purity helium and a leak-free gas flow control system is essential for achieving the lowest possible detection limits. The MPD's flow control unit comprised pressure controllers, flow meters, and restrictors. Because this unit was leakage prone and tedious to use, it was not employed. Instead, two electronic mass flow controllers (Tylan) were used for control of the O_2 scavenge gas and helium flow rates. House helium, which is passed through a getter located in an adjacent lab, was used. An H_2O/O_2 scrubber (OMI-1, Supelco) connected near the back of the GC also was used to remove any water and/or oxygen that may have entered the gas lines after the getter. The scavenge gas, which prevents deposition of elemental carbon on the tube wall, is selected via a 3-port ball valve.

Solvent vent

To enable solvent venting by reversal of the system gas flow direction, a quartz-window assembly was connected to the end of the discharge tube opposite the plasma head unit. Silicone rubber (Silastic® 732 RTV, Dow Corning) was used to attach the window to a 1/4″ stainless steel cap fitting with a hole in its end for plasma viewing. The cap/window assembly was swage-fitted to the discharge tube. Graphitized vespel (40% graphite) ferrules were used with fittings at both ends of the tube. A piece of 1/16″ stainless steel tubing was silver soldered to the side of the cap. At the end of this tubing, a 1/16″ nut and union were used for coupling to 1/4″ tubing (stainless) connected to a 6-port, air-actuated switching valve (Valco) that controls the gas flow direction. The 6-port valve was actuated by two 3-port solenoid valves (Skinner Electric, Model MBD002, 24 V dc), which allowed its pressurization and depressurization. Power to the 3-port valves was provided by the VALVE 1 circuit on the HP5880A valve control circuit board, and the valves were activated through use of VALVE 1 ON/OFF commands in the Run Table.

In the analysis mode, plasma gases flow from the 6-port valve and enter the plasma head unit and discharge tube. The column effluent is swept into the plasma by the forward flow of plasma gases. In the solvent-vent mode, the 6-port valve

Fig. 2. Carbon background response during solvent-vent valve switching.

redirects the plasma-gas flow such that it enters the discharge tube at its quartz-window end. In this mode, the solvent is backflushed through the plasma head unit and exits through resistively heated stainless steel tubing to vent. Because the plasma continues to receive supply gases, it is sustained during venting. After venting, the 6-port valve is switched to the analysis mode position, and the plasma gases and column effluent flow in the forward direction again.

A strip chart recording of the carbon channel's response during solvent-vent valve switching is shown in Fig. 2. In the vent-on position (i.e., gas flows in reverse direction), a lower baseline was obtained. When the solvent vent was switched off, a spike occurred. The spike was followed by a peak that exponentially decayed to baseline within about 30 s. No change in the plasma's appearance was observed during vent operation.

Analysis

The GC (HP5880A) oven temperature was held at 35°C for 5 min, ramped at 10°C/min for 5 min, and then at 20°C/min to a final tempera-

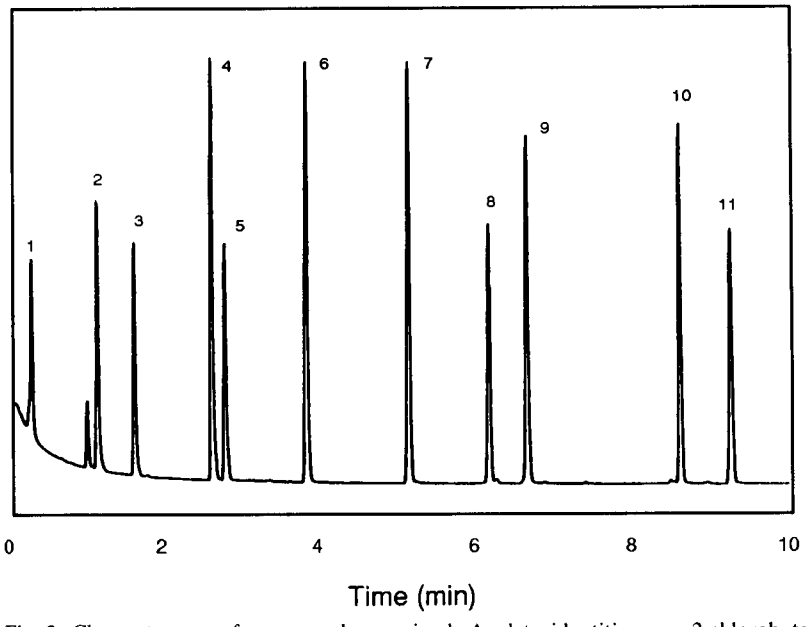

Fig. 3. Chromatogram of compounds examined. Analyte identities are: 2-chlorobutane (1), fluorobenzene (2), α,α,α,-trifluorotoluene (3), toluene (4), 2-iodobutane (5), chlorobenzene (6), bromobenzene (7), 1,5-dichloropentane (8), iodobenzene (9), dodecane (10), and 1,2-dibromocyclohexane (11).

ture of 250°C. The injector temperature was set at 250°C. Helium flow through the column was 1.5 ml/min. The aluminum transfer tube and plasma head unit were maintained at 250°C.

Analytes used to evaluate the performance of the modified instrument are listed in the legend of Fig. 3. Compounds were purchased from Aldrich and were $\geq 99\%$ pure except for iodobenzene, which was 98% pure. The stock solution was prepared by adding 10 μl of each compound except 2-chlorobutane, where 15 μl was used, to a 10-ml volumetric flask and diluting with CS_2. Four additional solutions were prepared through serial dilution of 2-ml aliquots with CS_2 in 10-ml volumetrics. A sixth solution, which was not used for serial dilutions, also was prepared by diluting 5 ml of stock to a 10-ml volume with CS_2. The six solutions covered a range from 0.11–131 nanomoles (1.32–1572 ng) of analyte carbon per injection. All injections were splitless and were 2 μl in volume. The plasma was operated at a tube current of 70 mA (0.1 mA reflected current) and a helium flow of 70 ml/min except where noted. Carbon emission was monitored at 247.9 nm.

RESULTS AND DISCUSSION

Compound structure and response

The effect of compound structure on carbon response was investigated. The chromatogram resulting from a 2-μl injection of a solution containing eleven different compounds is shown in Fig. 3. In the figure, time zero indicates the time when data collection began, which was 4.5 min after sample injection. The response observed on the carbon channel during solvent vent use is not seen in the figure because the vent was switched back to the analysis mode prior to data collection. The sloping baseline at the beginning of the chromatogram is due to residual solvent, which entered the plasma because the venting time used was less than that required for complete solvent venting. Incomplete venting was deliberate in this

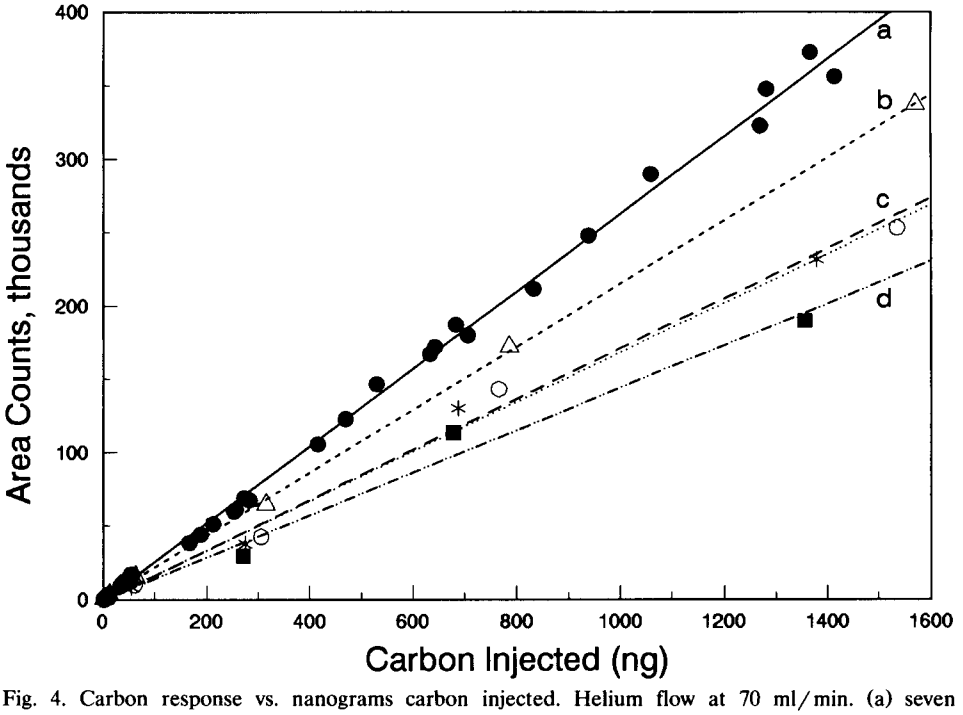

Fig. 4. Carbon response vs. nanograms carbon injected. Helium flow at 70 ml/min. (a) seven compounds: 2-iodobutane, chlorobenzene, bromobenzene, 1,5-dichloropentane, iodobenzene, dodecane, 1,2-dibromocyclohexane; (b) toluene; (c) fluorobenzene and α,α,α-trifluorotoluene; (d) 2-chlorobutane.

TABLE 1

Linear regression results

Parameter	Analytes 5–11	Toluene	Fluoro-benzene	Trifluoro-toluene	2-Chloro-butane
Slope (area counts/ng C)	263	215	169	172	144
Standard error of slope	2	2	6	7	25
Intercept (area counts)	−517	440	−143	−727	−68
Standard error of intercept	1088	1306	4571	4265	22143
Standard error of y estimate	55339	2488	8712	8128	19289
r^2	0.998	0.999	0.994	0.994	0.970
n	42	6	6	6	3

case to allow determination of chlorobutane, which eluted on the solvent tail. Two additional compounds, 2-bromopropane and 1-bromo-3-chloropropane, were initially selected, but were not used because of co-elution with the solvent and chlorobenzene, respectively.

For seven of the compounds examined (analytes 5–11), carbon response did not appear to be compound-dependent when a helium flow of 70 ml/min was employed. Plots of carbon response (area counts) versus nanograms carbon injected (2-μl injections) are given in Fig. 4. The uppermost line (solid circles) was obtained for analytes 5–11. Linear regression results for these analytes and for the other analytes examined are given in Table 1. A correlation coefficient (r^2) of 0.998 was obtained for the pooled results for analytes 5–11. On any given day, the percent relative standard deviation (%R.S.D.) of the area-count averages ($n = 3$) was under 5% for all concentration levels examined except for the lowest level, where the %R.S.D. was usually $\leqslant 10\%$. Day-to-day precision was better than 10%, provided that the discharge tube was not severely eroded, which occurred after about three weeks of use (8–10 h/day).

Carbon responses for toluene, fluorobenzene, α,α,α-trifluorotoluene, and 2-chlorobutane were lower than those observed for the other seven compounds examined. Lower responses were expected for the fluorinated compounds, which reportedly interact with the quartz discharge tube wall [15], but not for toluene and 2-chlorobutane. The lower response for 2-chlorobutane may be related to its presence on the solvent tail.

At flows less than about 50 ml/min, a significant increase in response per unit decrease in flow rate was obtained. Calibration data also were collected at 30 ml/min and the structure/response relationship was again examined. Because significantly increased scatter in response was observed relative to results obtained at 70 ml/min, operation at 70 ml/min is preferable. Results obtained at 70 ml/min were used for calculation of the limit of detection (LOD). These results are discussed in the following section.

TABLE 2

Calibration results and estimated LOD for carbon

Analyte	Mass range examined (ng C)	Slope[a], SE[b]	Intercept, SE	SE of y estimate	r^2	LOD (pg/s)	
						Specified	Calc. [c], %R.S.D.
Nonane	–	–	–	–	–	250	–
Iodobutane	1.32–835	254, 3	−537, 975	1857	0.999	–	64, 11
Dodecane	2.04–1273	255, 3	194, 2007	3827	0.999	–	63, 13

[a] Area counts/ng C. [b] Standard error, $n = 6$. [c] Mean value, $n = 4$. Calculated with results of injections of 6.67 and 10.14 ng carbon from iodobutane and dodecane, respectively.

LOD calculation

To compare LODs specified [11] for the original system with those obtained with the modified instrument, LODs for elements were calculated by the definition given by the instrument manufacturer [11]. This definition can be expressed by the following equation:

$$\mathrm{LOD} = \{[2VDd(AW_t)snA_n]/(MW)t_hRA_s\}$$

where parameters are defined as: V = sample volume (ml); D = dilution ratio (ml compound/ml solution); d = compound density; AW_t = total atomic weight in molecule of element being determined; s = split ratio; n = peak-to-peak noise (mV); A_n = amplifier attenuation during noise measurement; A_s = amplifier attenuation during signal measurement; MW = molecular weight; t_h = half peak height width (s); R = element response (mV).

To estimate the LOD for carbon, a mean LOD was calculated from the results of multiple injections of 2-iodobutane and dodecane. Two injections of each compound were made on two different days, giving a total of eight injections. Calculated LODs and their %R.S.D. values are given in Table 2. The carbon mass range examined, results of linear regression of the calibration data (area counts versus nanograms carbon injected), and the carbon LOD specified for the original system also are listed in the table. The calculated carbon LOD was about 25% of that originally specified for the unmodified system.

Conclusions

The solvent-venting interface developed allows for sensitive carbon determination and its use does not appear to affect plasma stability. The interface is easy to assemble and has a low dead volume design, which is important in preserving chromatographic resolution. When comparing chromatograms obtained with the GC–MIP system to those obtained with the same column and a flame ionization detector (FID), no differences in peak shape were discernable.

Overall performance of the modified instrument was superior to that of the original MPD-850 reduced-pressure system. Carbon response for seven of the compounds examined in this study did not appear to be compound dependent when a helium flow of 70 ml/min was employed. When comparing regression results for three compounds used in both the evaluation of the original instrument and the modified instrument, the mean slope obtained with the original instrument was lower (173 area counts/ng C versus 260 for the modified system) and had a much higher %R.S.D. than that obtained with the modified instrument (48% versus less than 4% for the modified system).

REFERENCES

1 L. Ebdon, S. Hill and R.W. Ward, Analyst, 111 (1986) 1113.
2 P.C. Uden, Y. Yoo, T. Wang and Z. Cheng, J. Chromatogr., 468 (1989) 319.
3 J.S. Marhevka, D.F. Hagen and J.W. Miller, in P.C. Uden (Ed.), Element-Specific Chromatographic Detection by Atomic Emission Spectroscopy (ACS Symposium Series 479), American Chemical Society, Washington, DC, 1992, p. 117.
4 D.T. Bostick and Y. Talmi, J. Chromatogr. Sci., 15 (1977) 164.
5 B.D. Quimby, P.C. Uden and R.M. Barnes, Anal. Chem., 50 (1978) 2112.
6 S.A. Estes, P.C. Uden and R.M. Barnes, Anal. Chem., 53 (1981) 1336.
7 D.L. Haas and J.A. Caruso, Anal. Chem., 57 (1985) 846.
8 C.S. Cerbus and S.J. Gluck, Spectrochim. Acta, 38B (1983) 387.
9 L. Zhang, J.W. Carnahan, R.E. Winans and P.H. Neill, Anal. Chim. Acta, 233 (1990) 149.
10 B.D. Quimby and J.J. Sullivan, Anal. Chem., 62 (1990) 1027.
11 MPD 850 Organic Analyser Instruction Manual, Applied Chromatography Systems, Luton.
12 S.A. Estes, P.C. Uden and R.M. Barnes, Anal. Chem., 53 (1981) 1829.
13 C.I.M. Beenakker, Spectrochim. Acta, 31B (1976) 483.
14 M.E. Birch, National Technical Information Service (NTIS), Publication No. PB-92-217-959.
15 D.F. Hagen, J. Belisle and J.S. Marhevka, Spectrochim. Acta, 38B (1/2) (1983) 377.
16 Y.T. Gagnon, NIOSH, Cincinnati, OH, unpublished results.

PUBLICATION SCHEDULE FOR 1994

	S'93	O'93	N'93	D'93	J	F						
Analytica Chimica Acta	281/1 281/2 281/3	282/1 282/2 282/3	283/1 283/2	283/3 284/1 284/2	284/3 285/1 285/2	285/3 286/1 286/2						
Vibrational Spectroscopy		6/1			6/2							

INFORMATION FOR AUTHORS

Detailed "Instructions to Authors" for *Analytica Chimica Acta* was published in Volume 256, No. 2, pp. 373–376. Free reprints of the "Instructions to Authors" of *Analytica Chimica Acta* and *Vibrational Spectroscopy* are available from the Editors or from: Elsevier Science Publishers B.V., P.O. Box 330, 1000 AH Amsterdam, The Netherlands. Telefax: (+31-20) 5862845.

Manuscripts. The language of the journal is English. English linguistic improvement is provided as part of the normal editorial processing. Authors should submit three copies of the manuscript in clear double-spaced typing on one side of the paper only. *Vibrational Spectroscopy* also accepts papers in English only.

Abstract. All papers and reviews begin with an Abstract (50–250 words) which should comprise a factual account of the contents of the paper, with emphasis on new information.

Figures. Figures should be prepared in black waterproof drawing ink on drawing or tracing paper of the same size as that on which the manuscript is typed. One original (or sharp glossy print) and two photostat (or other) copies are required. Attention should be given to line thickness, lettering (which should be kept to a minimum) and spacing on axes of graphs, to ensure suitability for reduction in size on printing. Axes of a graph should be clearly labelled, along the axes, outside the graph itself. All figures should be numbered with Arabic numerals, and require descriptive legends which should be typed on a separate sheet of paper. Simple straight-line graphs are not acceptable, because they can readily be described in the text by means of an equation or a sentence. Claims of linearity should be supported by regression data that include slope, intercept, standard deviations of the slope and intercept, standard error and the number of data points; correlation coefficients are optional.

Photographs should be glossy prints and be as rich in contrast as possible; colour photographs cannot be accepted. Line diagrams are generally preferred to photographs of equipment.

Computer outputs for reproduction as figures must be good quality on blank paper, and should preferably be submitted as glossy prints.

Nomenclature, abbreviations and symbols. In general, the recommendations of the International Union of Pure and Applied Chemistry (IUPAC) should be followed, and attention should be given to the recommendations of the Analytical Chemistry Division in the journal *Pure and Applied Chemistry* (see also *IUPAC Compendium of Analytical Nomenclature, Definitive Rules*, 1987).

References. The references should be collected at the end of the paper, numbered in the order of their appearance in the text (*not* alphabetically) and typed on a separate sheet.

Reprints. Fifty reprints will be supplied free of charge. Additional reprints (minimum 100) can be ordered. An order form containing price quotations will be sent to the authors together with the proofs of their article.

Papers dealing with vibrational spectroscopy should be sent to: Dr J.G. Grasselli, 150 Greentree Road, Chagrin Falls, OH 44022, U.S.A. Telefax: (+1-216) 2473360 (Americas, Canada, Australia and New Zealand) or Dr J.H. van der Maas, Department of Analytical Molecule Spectrometry, Faculty of Chemistry, University of Utrecht, P.O. Box 80083, 3508 TB Utrecht, The Netherlands. Telefax: (+31-30) 518219 (all other countries).

0003-2670/93/$06.00

This issue is printed on acid-free paper.

PRINTED IN THE NETHERLANDS

Vibrational Spectra and Structure

A Series of Advances

Volume 20

edited by **J.R. Durig**, College of Science and Mathematics, University of South Carolina, Columbia, SC, USA

The current volume comprises five chapters, three of which address recent advances in experimental techniques for providing information on biomolecular reaction paths, for determining linewidth and small frequency shifts, and for applying the microwave Fourier transform technique to experiments of static gases in waveguide cells. Chapters 4 and 5 consider *ab initio* calculations for both inorganic and organic systems.

Contents:

1. Applications of Matrix Infrared Spectroscopy to Mapping of Bimolecular Reaction Paths *(H. Frei)*. Introduction. Oxygen Transfer Reactions. Hydrogen Transfer Reactions. Concluding Remarks.

2. Vibrational Line Profile and Frequency Shift Studies by Raman Spectroscopy *(B.P. Asthana, W. Kiefer)*. Introduction. Deconvolution of Raman Line Profile. Determination of Frequency Shifts by Raman Difference Spectroscopy (RDS). Study of Linewidth Changes by RDS. Experimental Techniques. Applications. Summary.

3. Microwave Fourier Transform Spectroscopy *(A. Bauder)*. Introduction. Experimental. Rotational Spectra.

4. *Ab Initio* Quality of SCMEH-MO Calculations of Complex Inorganic Systems *(E.A. Boudreaux)*. Introduction. Theoretical Foundation. Applications and Results. Comments, Conclusions and Acknowledgments.

5. Calculated and Experimental Vibrational Spectra and Force Fields of Isolated Pyrimidine Bases *(W.B. Person, K. Szczepaniak)*. Introduction. Methods for Study of Isolated Molecules. Stabilities, Structures, and Dipole Moments of Isolated Pyrimidine Bases. Comparison of Experimental and Calculated Infrared Spectra for Pyrimidine Bases. Basis Set Dependence of Calculated Infrared Spectra and Vibrational Parameters for Uracil. Comparison of Spectra Calculated for Uracil, Thymine, Cytosine, and 1-Methylcytosine. Comparison and Transferability of Bond Force Constants from Thymine, Uracil, Cytosine, and 1-Methylcytosine. Comparison and Transferability of Bond Dipole Derivatives from Uracil, Thymine, Cytosine, and 1-Methylcytosine. Concluding Remarks. Author Index. Subject Index.

"Each volume in this excellent series is eagerly awaited and the general reader is never disappointed."

Journal of Molecular Structure

1993 xx + 352 pages
Price: US $ 231.50 / Dfl. 370.00
ISBN 0-444-89865-4

ORDER INFORMATION

For USA and Canada
ELSEVIER SCIENCE PUBLISHERS
Judy Weislogel
P.O. Box 945
Madison Square Station,
New York, NY 10160-0757
Tel: (212) 989 5800
Fax: (212) 633 3880

In all other countries
ELSEVIER SCIENCE PUBLISHERS
P.O. Box 211
1000 AE Amsterdam
The Netherlands
Tel: (+31-20) 5803 753
Fax: (+31-20) 5803 705

US$ prices are valid only for the USA & Canada and are subject to exchange rate fluctuations; in all other countries the Dutch guilder price (Dfl.) is definitive. Books are sent postfree if prepaid.

ELSEVIER
SCIENCE PUBLISHERS

711/414\140\0001-00

0003-2670(19931020)282:2;1-F